

Electronic Thesis and Dissertation Repository

12-16-2020 1:00 PM

Biodegradability Of Cellulose And Its Impact On Oxygen Transfer Efficiency And Biological Nutrients Removal

Ahmed Shawki Ahmed, *The University of Western Ontario*

Supervisor: Nakhla, George, *The University of Western Ontario*

A thesis submitted in partial fulfillment of the requirements for the Doctor of Philosophy degree in Civil and Environmental Engineering

© Ahmed Shawki Ahmed 2020

Follow this and additional works at: <https://ir.lib.uwo.ca/etd>



Part of the [Environmental Engineering Commons](#)

Recommended Citation

Ahmed, Ahmed Shawki, "Biodegradability Of Cellulose And Its Impact On Oxygen Transfer Efficiency And Biological Nutrients Removal" (2020). *Electronic Thesis and Dissertation Repository*. 7556.
<https://ir.lib.uwo.ca/etd/7556>

This Dissertation/Thesis is brought to you for free and open access by Scholarship@Western. It has been accepted for inclusion in Electronic Thesis and Dissertation Repository by an authorized administrator of Scholarship@Western. For more information, please contact wlsadmin@uwo.ca.

Abstract

Cellulose from toilet paper is a significant fraction of particulate organics, which is recoverable. For the first time, comprehensive mapping and tracking the fate of cellulose across various unit processes at full-scale in two water resource recovery facilities located in North America and Europe was undertaken. The influent cellulose content accounted for approximately one-third of the total suspended solids (TSS). More than 80% of the raw wastewater cellulose was captured in primary treatment. The high cellulose content of the primary sludge accounting for 17%-35% of the TSS facilitates cellulose recovery. Cellulose biodegradation efficiency varied between 70%-90% of the primary effluent, confirming that cellulose recovery from primary treatment is beneficial to reduce oxygen demand.

Aeration is a major contributor to the high energy demand in municipal wastewater treatment plants. Thus, it is important to understand the dynamic impact of wastewater characteristics on oxygen transfer efficiency to develop suitable control strategies for minimizing energy consumption since aeration efficiency is influenced by the biodegradation of pollutants in the influent. The real-time impact of acetate as a readily biodegradable substrate and cellulose as a slowly biodegradable substrate were studied at different operational conditions. At an ambient DO of 2 mg l⁻¹ and air flow of 1.02 m³ h⁻¹ (0.6 SCFM), the α -factor was more sensitive to readily biodegradable substrates than to cellulose. On average, α -factor decreased by 48% and 19% due to the addition of acetate and cellulose, respectively. At a DO of 4 mg l⁻¹ and air flow of 1.7 m³ h⁻¹ (1 SCFM), α -factor remained constant irrespective of cellulose and acetate concentrations. An inverse correlation between the α -factor and reactor sCOD was defined and incorporated into a dynamic model to estimate the real-time airflow rates associated with the improvement of the oxygen transfer efficiency due to biodegradation.

The effect of bioreactor configurations on the dynamics of oxygen demand and aeration performance was assessed by conducting an advanced calibration study of a newly developed aeration model against experimental data during a pilot SBR study, and by utilizing the validated aeration model to assess different bioreactor configurations. Three different correlations to estimate α -factor were applied in the study. The first correlation which estimated the α -factor based on the operating reactor sCOD was able to predict the temporal

measured air flow rate change in the SBRs pilot. The second correlation which estimated the α -factor based on the influent COD overestimated the air flow rates as it considered the impact of the influent loading rates on the α -factor and overlooked the improvement in α -factor due to biodegradation. The third correlation which estimated the α -factor based on an MLSS underestimated the air flow rates as it overlooked the impact of the influent loading rates on the α -factor. Results indicated that a completely mixed stirred reactor (CSTR) showed an aeration energy reduction of 56%-67% when compared to the plug flow model. The model-based analysis showed that the step-feed plug-flow reactor achieved a 15 % reduction in aeration energy relative to the plug-flow reactor. However, both systems had equivalent aeration energy when denitrification was considered. In a plug flow reactor and CSTR, denitrification reduced the aeration energy by 30% and 11%, respectively.

Cellulose hydrolysis rate constants under both anoxic and aerobic conditions were estimated using a calibrated batch model based on experimental measurements. The aerobic cellulose hydrolysis rate constant was $3.74 \pm 0.33 \text{ d}^{-1}$, and the anoxic hydrolysis rate was $0.7 \pm 0.31 \text{ d}^{-1}$. The estimated hydrolysis rate constants were then incorporated into a calibrated SBR model to estimate cellulose fraction in the influent wastewater. Influent cellulose accounted for 21% of influent total COD and 35% of influent TSS.

The addition of the fermented primary sludge at different SRTs to the SBR increased the efficiency of nitrogen and phosphorus removal by up to 92% and 98% when compared to the feed with RBF effluent only. The fermented primary sludge, however, had a marginal impact on α -factor, α SOTE, and OUR. The addition of the fermented primary sludge increased aeration energy by 25%-36% compared to the case of RBF effluent.

Keywords

Cellulose; Wastewater; Rotating Belt Filter; Primary Clarifier; Biodegradation; Aeration; Activated Sludge; Oxygen Transfer; α -Factor; Off-Gas Test; Fermentation.

Summary for Lay Audience

Cellulose in municipal wastewater originates from the use of toilet paper. It represents a large fraction of the influent organic contaminants in wastewater. Biological wastewater treatment is one of the most economical approaches to the treatment of municipal wastewater using active bacteria (biomass) that are present in the influent wastewater. Active biomass biodegrades organic contaminants, including cellulose. To keep biomass functioning, oxygen is needed for respiration, and for this reason, there is a major step in any biological wastewater treatment plant known as aeration where the air is supplied to help the growth of bacteria. Aeration is designed to provide oxygen to active biomass so that it can decompose and biodegrade organic contaminants such as cellulose. According to the literature, aeration consumes more than half of the total energy of the treatment plant.

Cellulose is a particulate matter that can be removed by any solid separation technique, such as primary clarification, where the particles are removed by settling or rotating belt filters, where the particles are removed by sieving. Removing cellulose from influent wastewater reduces aeration energy and can be further treated with other discarded solids to produce energy or soluble organic compounds that can be used to improve the biological treatment process.

In this Ph.D. thesis, the fate of cellulose in the municipal wastewater treatment plant using data from two different full-scale treatment plants in two different regions; Europe and North America has been tracked and shown that more than 80% of the influent cellulose can be removed through primary solid separation. In addition, a pilot study was conducted to thoroughly investigate the impact of cellulose and other organic contaminants on aeration efficiency. Modeling was also used to understand the theoretical impact of organic biodegradation on aeration efficiency. The results of the study showed that the removal of cellulose through the primary solid separation step reduced the aeration energy by 25%. It also showed that aeration efficiency improved with the time of reaction due to biodegradation and therefore a mathematical relationship between aeration efficiency and organic biodegradation was developed to be used as a new design tool for aeration tanks.

Co-Authorship Statement

The content of this Ph.D. thesis is either published, under review, or in preparation for submission in peer-reviewed journals as listed below:

Chapter 3: Fate of Cellulose in Primary and Secondary Treatment at Municipal Water Resource Recovery Facilities

Authors: Ahmed Shawki Ahmed, Gholamreza Bahreini, Dang Ho, Ganesh Sridhar, Medhavi Gupta, Coos Wessels, Pim Marcelis, Elsayed Elbeshbishy, Diego Rosso, Domenico Santoro, George Nakhla

Authors contribution:

Ahmed Shawki Ahmed and Gholamreza Bahreini are equally-contributing first authors. Both performed all the experimental analysis, data collection, data analysis, and interpretation, as well as drafted the manuscript.

Domenico Santoro and George Nakhla were involved in the conception, and design of the study, data interpretation, and evaluating the manuscript critically.

Dang Ho helped and supported the logistics of sampling in Europe .

Ganesh Sridhar, and Medhavi Gupta, were operating the lab-scale SBRs.

Coos Wessels and, Pim Marcelis provided the required operational data for the European case study.

Elsayed Elbeshbishy, and Diego Rosso were also involved in data interpretation and evaluating the manuscript critically for novelty and scientific contribution.

Status: published

Reference: Ahmed, A.S., Bahreini, G., Ho, D., Sridhar, G., Gupta, M., Wessels, C., Marcelis, P., Elbeshbishy, E., Rosso, D., Santoro, D., Nakhla, G., 2019. Fate of cellulose in primary and secondary treatment at municipal water resource recovery facilities. *Water Environ. Res.* 91, 1479–1489. <https://doi.org/10.1002/wer.1145>

Chapter 4: Dynamic Impact of Cellulose and Readily Biodegradable Substrate on Oxygen Transfer Efficiency in Sequencing Batch Reactors

Authors: Ahmed Shawki Ahmed, Ahmed Khalil, Yuichi Ito, Mark C.M. van Loosdrecht, Domenico Santoro, Diego Rosso, George Nakhla

Authors contribution:

Ahmed Shawki Ahmed performed all the experimental analysis, data analysis, and interpretation, combined the model equations as well as drafted the manuscript.

George Nakhla and Diego Rosso were involved in the conception and design of the study, data interpretation, and evaluating the manuscript critically for novelty and scientific contribution.

Ahmed Khalil helped and supported the model setup by incorporating the aeration model equations using MATLAB software.

Yuichi Ito supported the pilot plant set up by providing high-quality ammonia sensors through HORIBA.

Mark C.M. van Loosdrecht and Domenico Santoro were also involved in data interpretation and evaluating the manuscript critically for novelty and scientific contribution.

Status: published.

Reference: Ahmed, A.S., Khalil, A., Ito, Y., van Loosdrecht, M.C.M., Santoro, D., Rosso, D., Nakhla, G., 2020. Dynamic Impact of Cellulose and Readily Biodegradable Substrate on Oxygen Transfer Efficiency in Sequencing Batch Reactors. *Water Research* 116724.

<https://doi.org/10.1016/j.watres.2020.116724>

Chapter 5: Influence of Bioreactor Configurations on the Dynamics of Oxygen Demand and Aeration Performance in Activated sludge Processes

Authors: Ahmed Shawki Ahmed, Domenico Santoro, Diego Rosso, George Nakhla,

Authors contribution:

Ahmed Shawki Ahmed performed all the activated sludge modeling, data analysis, and interpretation, as well as drafted the manuscript.

George Nakhla was involved in the conception and design of the study, data interpretation, and evaluating the manuscript critically for novelty and scientific contribution.

Diego Rosso and Domenico Santoro were also involved in data interpretation and evaluating the manuscript critically for novelty and scientific contribution.

Status: Under review at *Water Research*.

Chapter 6: Performance Assessment of Anoxic And Aerobic Biodegradation Of Cellulose in SBRs.

Authors: Ahmed Shawki Ahmed, Gholamreza Bahreini, Domenico Santoro, Diego Rosso, George Nakhla,

Authors contribution:

Ahmed Shawki Ahmed performed all the experimental analysis, data analysis, and interpretation, as well as drafted the manuscript.

George Nakhla was involved in the conception and design of the study, data interpretation, and evaluating the manuscript critically for novelty and scientific contribution.

Gholamreza Bahreini was responsible for operating the three pilot fermenters that fed the pilot-scale SBRs.

Diego Rosso and Domenico Santoro were also involved in data interpretation and evaluating the manuscript critically for novelty and scientific contribution.

Status: In preparation for submission to Water Environment Research.

Acknowledgments

First of all, I would like to express my special and deep gratitude to my supervisor, Dr. George Nakhla, for his excellent mentorship as well as continuing encouragement and support throughout my Ph.D. All I learned about wastewater treatment was because of him. He has helped me a lot in improving my skills, such as learning skills, research skills, teaching skills, and writing skills. I am really glad to be one of his students.

I would also like to sincerely thank Dr. Diego Rosso (UCI) for his help and support during my Ph.D. We did some experimental measurements in the field together, but I learned a lot from him about how to calculate oxygen transfer parameters and how to understand and analyze the results. Given the fact that he is living in the US, he has always been available via emails and virtual meetings to provide assistance, support, and advice.

I would also like to thank Dr. Domenico Santoro (USP) for his help and support, along with excellent guidance and encouragement through my Ph.D. research. I was lucky enough to do two industrial internships with him where we worked closely together, and I learned a lot from him during those two internships.

Special thanks to the research team of Trojans; Dr. Siva Sarathy, Dr. Vahid Ghodsi, and Dr. Pankaj Chowdhury for their outstanding continuous assistance during the operation of the Greenway Treatment Pilot. I would also like to sincerely thank Kirby Oudekerk (Greenway treatment facility) for being very responsive and helpful during the pilot and start-up during the operation. Special thanks to Chris Mckenzie, the plant supervisor, who was always available to help whenever there was an emergency during the operation. I would also like to thank Brian High, the plant chief operator, for his support whenever we need his help.

I would like to thank my colleagues that I had the pleasure to work with at Western, Gholamreza Bahreini, Ahmed Khalil, Medhavi Gupta, Peyman Dalaei, Dr. Dang Ho Dr. Basem Haroun, Dr. Min Gu Kim, Xiaoguang Liu, Masuduz Zaman, Mohammad Chowdhury, Ganesh Ram Dutt Sridhar, Moustafa Elbahrawi, Mariam Abdulazeez, Emmanuel Tepari, Niema Afroze, Amr Ismail, and Federica Piras. I really enjoyed working with you all.

To my lovely parents, Shawki Badawi, and Manal Kassab, I would like to express my special and profound gratitude for their constant love and spiritual support throughout my life. I wish I could return some of the countless things that you have been giving me. I would also like to thank my lovely siblings Mohamed, Sara, and Nehal for their spiritual support and prayers.

Last but not the least, I would like to especially thank my lovely and beautiful wife Ola for her endless love and support during my busy and stressful time and for keeping me happy and focused over the past few months.

Table of Contents

Abstract	i
Summary for Lay Audience	iii
Co-Authorship Statement.....	iv
Acknowledgments.....	vii
Table of Contents	ix
List of Tables	xiv
List of Figures	xvi
List of Appendices	xx
List of abbreviations	xxi
Chapter 1	1
1 Introduction	1
1.1 Rationale	1
1.2 Research objectives.....	2
1.3 Thesis Organization	3
1.4 Thesis Format.....	4
References	5
Chapter 2.....	8
2 Literature review	8
2.1 Municipal wastewater characteristics.	8
2.1.1 Organics	8
2.1.2 Solids.....	8
2.1.3 Nitrogen	10
2.1.4 Phosphorous.....	11

2.2	Cellulose in municipal wastewater	12
2.2.1	Cellulose measurement	12
2.2.2	Cellulose removal by primary treatment.....	13
2.2.3	Cellulose biodegradability	14
2.3	Oxygen transfer efficiency and aeration energy	16
2.3.1	Measurement methods for OTE.....	17
2.3.2	Environmental factors affecting OTE.....	22
2.3.3	Process conditions affecting OTE.....	23
2.3.4	Design parameters affecting OTE.....	36
2.3.5	Aeration modeling	38
2.4	Volatile fatty acids (VFA) production and impact on the BNR	39
2.5	Synopsis of the literature	40
2.6	Knowledge Gaps.....	42
	References	44
	Chapter 3.....	57
3	Fate of Cellulose in Primary and Secondary Treatment at Municipal Water Resource Recovery Facilities.....	57
3.1	Introduction.....	57
3.2	Methodology.....	62
3.2.1	Laboratory-scale sequencing batch reactors study	62
3.2.2	Full-scale wastewater treatment plants studies	62
3.2.3	Analytical methods	65
3.3	Results and discussion	65
3.3.1	Laboratory-scale sequencing batch reactor study	65
3.3.2	North American full-scale study (London Ontario, Canada WWTP)	67

3.3.3	European full-scale study (Aarle Rixtel, the Netherlands WWTP).....	70
3.3.4	Role of water temperature.....	75
3.3.5	Operational Cost Implications of Cellulose Removal in Primary Treatment	78
3.4	Summary and Conclusions	79
	References	80
Chapter 4.....		83
4	Dynamic Impact of Cellulose and Readily Biodegradable Substrate on Oxygen Transfer Efficiency in Sequencing Batch Reactors.	83
4.1	Introduction.....	83
4.2	Methodology	86
4.2.1	Sequencing batch pilot reactors design.....	86
4.2.2	Oxygen transfer efficiency testing	88
4.2.3	Oxygen transfer efficiency measurements.....	90
4.2.4	Wastewater characterization	91
4.2.5	Model structure	92
4.3	Results and Discussion	97
4.3.1	Pilot SBRs performance.....	97
4.3.2	Oxygen transfer studies.....	97
4.3.3	Aeration model results	109
4.4	Summary and Conclusions	115
	References	117
Chapter 5.....		123
5	Influence of Bioreactor Configurations on the Dynamics of Oxygen Demand and Aeration Performance in Activated sludge Processes.....	123
5.1	Introduction.....	123

5.2	Material and methods.....	127
5.2.1	Sequencing batch reactors pilot	127
5.2.2	Wastewater characterization	128
5.2.3	Model setup.....	128
5.2.4	Dynamic α -factor estimation	132
5.3	Results and discussion	132
5.3.1	SBRs performance	132
5.3.2	Model calibration and validation	133
5.3.3	Aeration Performance in Continuous-flow Activated Sludge Processes	138
5.3.4	Impact of Pre-denitrification on Aeration Performance	145
5.4	Discussion	148
5.5	Summary and Conclusions	155
	References	157
Chapter 6	164
6	Performance Assessment of Anoxic And Aerobic Biodegradation Of Cellulose.....	164
6.1	Introduction.....	164
6.2	Material and methods.....	167
6.2.1	Sequencing batch reactors pilot	167
6.2.2	Hydrolysis of cellulose	167
6.2.3	Cellulose hydrolysis model development	167
6.2.4	Pilot Fermenters	168
6.2.5	Testing stages for the addition of the fermented primary sludge.....	169
6.2.6	Oxygen transfer efficiency measurements	170
6.2.7	Wastewater characterization	170
6.3	Results and discussion	172

6.3.1	Anoxic and aerobic hydrolysis rate constant of cellulose.....	172
6.3.2	Impact of the fermented primary sludge on the SBR performance	180
6.4	Summary and Conclusions	190
	References	192
Chapter 7	195
7	Conclusions and recommendations for future work.	195
7.1	Conclusions.....	195
7.2	Recommendations for future research	198
Appendices	199
Curriculum Vitae	240

List of Tables

Table 3-1. A literature review of cellulose degradation efficiencies	60
Table 3-2. Operational parameters and cycle time break up for both SBRs.....	63
Table 3-3. TSS concentrations, cellulose concentrations, TSS masses, and cellulose masses for both SBRs.....	66
Table 3-4. TSS concentrations, cellulose concentrations, loading rates, and flow rates for the North American case study (summer samples)	68
Table 3-5. TSS and cellulose concentrations, loading rates, and flow rates (European case study).....	72
Table 3-6. TSS and cellulose concentrations, loading rates, and flow rates for the North American case study (Winter samples a).....	76
Table 3-7. TSS and cellulose concentrations, loading rates, and flow rates for the North American case study (Winter samples b).....	77
Table 4-1. Aeration testing scenarios.....	90
Table 4-2. Oxygen transfer parameters at different testing scenarios and different acetate loading rates with active biomass	102
Table 4-3. Oxygen transfer parameters at different testing scenarios and different cellulose loading rates	105
Table 4-4. Impact of RBF screening on the oxygen transfer efficiency	106
Table 4-5. Oxygen transfer parameters at different testing scenarios and different acetate and cellulose loading rates without active biomass	108
Table 4-6. The average α -factor, required airflow, and energy consumption for the modeled scenarios.....	115

Table 5-1. Estimated α -factor and aeration energy for the modeled scenarios using typical wastewater characteristics.....	152
Table 5-2. Measured α -factor in plug flow reactors	153
Table 5-3. Measured α -factor in CSTRs.....	154
Table 5-4. Measured α -factor in MBRs	154
Table 6-1. Stoichiometry and kinetics for ASM1CL2.....	171
Table 6-2. Influent and effluent characteristics for the SBR receiving raw wastewater.	172
Table 6-3. Aerobic and anoxic hydrolysis constant using surface limited reaction rate equation.....	176
Table 6-4. Calibrated state variables for the influent using both models ASM1 and ASM1CL2.....	177
Table 6-5. Calibration results of the particulate COD fractions in the SBR using both models ASM1 and ASM1CL2	178
Table 6-6. Fermented primary sludge characteristics	181
Table 6-7. Influent, effluent and mixed liquor characteristics at each stage	182
Table 6-8. COD/N and COD/P ratios at the different stages	186
Table 6-9. Impact of the fermented primary sludge on the oxygen transfer efficiency.....	189

List of Figures

Figure 2-1: COD fractions in wastewater (Metcalf & Eddy, 2014)	9
Figure 2-2. Solids fractions in wastewater (Metcalf & Eddy, 2014)	9
Figure 2-3. Nitrogen fractions in wastewater (Metcalf & Eddy, 2014).....	10
Figure 2-4. Phosphorus fractions in wastewater (Metcalf & Eddy, 2014)	11
Figure 2-5. RBF Schematic diagram (Behera et al., 2018).....	14
Figure 2-6. A scheme with a comparison of the energy intensity of treatment processes of a wastewater treatment plant (Henze et al., 2015).....	17
Figure 2-7. Gas-phase mass balance (Redmon et al., 1983).....	18
Figure 2-8. Schematic diagram illustrating the main components of the off-gas analyzer	20
Figure 2-9. The correlation between α -factor and MLSS in systems with high MLSS concentrations (Krampe and Krauth, 2003).....	26
Figure 2-10. The impact of MLSS on α -factor in MBR systems (Cornel et al., 2003)	26
Figure 2-11. The impact of MLSS on α -factor in MBR systems (Germain et al., 2007).....	27
Figure 2-12. Linear correlation between α -factor and MLSS at SRT>20days (Henkel et al., 2011).....	28
Figure 2-13. Correlation between α -factor and MLSS within the range between 0.5 g/L to 30 g/L (Baquero-Rodríguez et al., 2018).	29
Figure 2-14. The biofilm development on the fine pore diffuser's surface, with micrographs screening the diffuser material and organic and inorganic coating details (Garrido-Baserba et al., 2016).	33
Figure 2-15. The correlation between α -factor and the influent COD (Jiang et al., 2017).....	39

Figure 3-1. Treatment process layout and sampling scheme for the London Ontario facility	64
Figure 3-2. Treatment process layout and sampling scheme for The Netherlands facility	64
Figure 3-3. TSS and cellulose concentrations for the London Ontario WRRF	67
Figure 3-4. Cellulose mass balance around the secondary treatment (London ON WRRF)..	69
Figure 3-5. TSS and cellulose concentrations for the Aarle-Rixtel WRRF (in green: train 1 with RBF as primary treatment; in brown: train 2 with no primary treatment).....	71
Figure 3-6. Cellulose mass balance around the secondary treatment of Train 1	73
Figure 3-7. Cellulose mass balance around the secondary treatment of Train 2	73
Figure 4-1. Schematic representation of one of the two identical SBRs.	88
Figure 4-2. Testing scenarios for the aeration efficiency with and without active biomass...	89
Figure 4-3. Model structure.	96
Figure 4-4. Impact of acetate and cellulose on α -factor, OUR and α SOTE. (80% fill ratio). .	99
Figure 4-5. Impact of anionic surface-active agents (SAA) on the α -factor (80% fill ratio).100	
Figure 4-6. Ammonia and airflow profiles showing the nitrification rate change while controlling the airflow rates.	103
Figure 4-7. The α -factor improvement due to the biosorption impact.....	109
Figure 4-8. Correlation between sCOD and α -factor.....	111
Figure 4-9. The change in the measured and modeled α -factor with the time due to the biodegradation of the organic loadings in both SBRs.	112
Figure 4-10. The temporal variation in the measured and modeled (30 mins moving average) air flow rates for both SBRs. ϵ is the percent error ((measured-modeled) *100/measured). 113	

Figure 5-1. Treatment scheme for the modelled scenario with a plug flow reactor.	131
Figure 5-2. Treatment scheme for the modeled scenario with a step feed plug flow reactors.	131
Figure 5-3. a) sCOD predicted by the model and measured sCOD after calibration. b) Ammonia predicted by the model and measured Ammonia after calibration	135
Figure 5-4. a-top) Measured and modeled air flow rates using the three different correlations to estimate α -factor (SBR1). b-bottom) Measured and modelled air flow rates using the three different correlations to estimate α -factor (SBR2).	137
Figure 5-5. a) Estimated α -factor in each compartment using the three correlations (Nitrification only). b) Estimated air flow rates in each compartment using the three correlations (Nitrification only).	141
Figure 5-6. The change in aeration energy over a day due to the changes in the influent concentrations using the three correlations.	142
Figure 5-7. The change in aeration energy over a day due to the change in the influent concentrations using the three correlations (CSTR).	142
Figure 5-8. Air flow rates estimated in the four plug flow bioreactors using the three correlations.	143
Figure 5-9. The daily change in aeration energy in the aerobic bioreactor due to the change in the influent concentrations using the three correlations (MBR-Nitrification only).	146
Figure 6-1. Process diagram for the three fermenters.	169
Figure 6-2. Cellulose hydrolysis rates estimated by the model to best match measured values under aerobic conditions (overall average percent error=8%).	174
Figure 6-3. Cellulose hydrolysis rates estimated by the model to best match measured values under anoxic conditions (overall average percent error=1%).	175

Figure 6-4. COD fractions in the influent raw wastewater using both models; ASM1 and ASM1CL2.....	178
Figure 6-5. Calibrated MLSS and MLVSS for the modeled SBR using ASM1CL2 model (average absolute error for MLSS was 3.6% and for MLVSS was 5.5%)	179
Figure 6-6. Cellulose concentration change with the time	180
Figure 6-7. Influent and effluent COD during the different stages.....	184
Figure 6-8. Influent and effluent TN during the different stages.....	184
Figure 6-9. Influent and effluent TP during the different stages	185
Figure 6-10. The cumulative MLVSS production and cumulative COD removed to estimate the observed yield after mixing the RBF effluent with the fermented primary sludge	186
Figure 6-11. α - factor improvement due to the MLVSS increase	189
Figure 6-12. α - factor change during the aeration cycle for the three different stages	190

List of Appendices

Appendix A: Supplementary information for Chapter 3	199
Appendix B: Supplementary information for Chapter 4.....	208
Appendix C: Supplementary information for Chapter 5.....	223

List of abbreviations

Abbreviation	Description
WWTP	Wastewater treatment plant
PC	Primary clarification
SBR	Sequencing batch reactor
RBF	Rotating belt filter
DO	Dissolved oxygen
SCFM	Standard cubic feet per minutes
COD	Chemical oxygen demand
OTE	Oxygen transfer efficiency
SRT	Solids retention time
HRT	Hydraulic retention time
TSS	Total suspended solids
VSS	Volatile suspended solids
TDS	total dissolved solids
BOD	Biochemical oxygen demand
MLSS	Mixed liquor suspended solids
MLVSS	Mixed liquor volatile suspended solids
MBR	Membrane bioreactors
OTE	Oxygen transfer efficiency at field conditions
OTR	Oxygen transfer rates at field conditions
SOTR	Standard oxygen transfer rates
SOTE	Standard oxygen transfer efficiency in clean water
SAE	standard aeration efficiency
αSOTE	Standard oxygen transfer efficiency in process water
α-factor	Wastewater correction factor, the ratio of process water to clean water SOTE
EPDM	The ethylene propylene diene monomer
PU	polyurethane

DWP	Dynamic wet pressure
BRV	bubble release vacuum
ASM1	Activated sludge model No. 1
ASM1CL	Activated sludge model No. 1 extended by cellulose conversion (first-order)
ASM1CL2	Activated sludge model No. 1 extended by cellulose conversion (Contois model)
ASM3	Activated sludge model No. 3
EPDM	Ethylene propylene diene monomer
SF	SALSNES filter
ORP	Oxidation-reduction potential
OUR	Oxygen uptake rate
OTR	Oxygen transfer rate
TN	Total nitrogen
SN	Soluble nitrogen
TP	Total phosphorus
SP	Soluble phosphorus
ThOD	Theoretical oxygen demand
HRT	Hydraulic retention time
EBPR	Enhanced biological phosphorus removal
NOUR	nitrogenous oxygen uptake rate
sCOD	Soluble COD
rbCOD	Readily biodegradable COD
CSTR	Completely stirred mixed reactor
FS	Fermented sludge
VFA	volatile fatty acids

Chapter 1

1 Introduction

1.1 Rationale

The majority (45% to 75%) of the wastewater treatment plant's energy is consumed by the aeration process, essentially for the biodegradation of organics and nutrients (Reardon, 1995; Tao and Chengwen, 2012). Oxygen transfer efficiency is impacted by many factors, including, wastewater characteristics (e.g surfactants, and organic substrates), solids retention time (SRT), primary treatment efficiency, diffusers fouling, diffusers types (i.e fine vs. coarse bubble diffusers), operation and design parameters (e.g. mechanical equipment and geometrical tanks design), and other variables (e.g. temperature and sewer network length) (Garrido-Baserba et al., 2017, 2016; Gori et al., 2013, 2011; Rosso et al., 2011, 2006; Rosso and Stenstrom, 2006, 2005).

Cellulose originating from the direct discharge of toilet paper represents a significant fraction of particulate organic substrates in raw municipal wastewater (Hurwitz et al., 1961; Ruiken et al., 2013). Cellulose can be biodegraded under both anaerobic and aerobic conditions (Hurwitz et al., 1961; Reijken et al., 2018; Ruiken et al., 2013). Thus, the degradation of cellulose may consume a large amount of oxygen and hence energy (Hofsten and Edberg, 1972). In addition, the influent cellulose can be recovered from biosolids generated by primary treatment such as primary clarification and rotating belt filters (RBF) (Ruiken et al., 2013).

Primary clarification removes some of the influent particulate biodegradable substrates reducing the energy required for aeration (Gori et al., 2013, 2011). The RBF is a primary treatment technology, utilizing fine mesh, rotating belts, that effectively removes the total suspended solids (TSS) and biochemical oxygen demand (BOD) by up to 50%, and 20% respectively (Chakraborty, 2015; Franchi et al., 2015). In addition, RBFs remove cellulose in the influent wastewater producing a cellulose-rich sludge (Ruiken et al., 2013). Reducing the cellulose loading rates to the biological treatment positively impacts the oxygen transfer efficiency and reduces aeration energy. Also, the recovered cellulose can be converted into biogas (Ghasimi et al., 2016) or utilized as a resource for different industries such as

biofuels, and additives in building materials and asphalt (Boztas, 2017; Honda et al., 2000). Furthermore, research to convert the recycled cellulose into energy, bio-plastics bottles, and other products is well underway (Boztas, 2017).

This study was originally inspired by the limited and contradictory information on the fate of cellulose in WWTP. In addition, despite the fact that the dynamic impact of wastewater characteristics on oxygen transfer efficiency (OTE) is known, the theoretical relationship between OTE and organic loadings including cellulose is not well established. The current approach to design aeration tanks relies on estimating the theoretical oxygen demand and constant values for OTE parameters. This design approach overlooks a variety of essential factors, such as aeration tank configuration, operating conditions, the temporal change of organics as well as biomass concentrations inside the aeration tank, and the treatment goals with respect to nitrogen removal (i.e. conventional treatment, nitrification, or nitrification/denitrification).

1.2 Research objectives

Based on the known knowledge gaps and the ongoing paradigm shift towards energy saving and resource recovery, the main objectives of this Ph.D. thesis are:

- 1- Mapping cellulose fate, removal efficiency, and degradability across water resource recovery facilities (WRRF).
- 2- Evaluating the impact of cellulose, organic loading rates, and biomass on the oxygen transfer efficiency; to develop a dynamic aeration model incorporating OTE parameters (α -factor) as a function of readily and slowly biodegradable substrates.
- 3- Evaluating the impact of activated sludge reactor type on aeration energy, using dynamic α -factor, and assessing the impact of pre-denitrification on dynamic α -factors and aeration performance.
- 4- Estimation of the cellulose hydrolysis rate constants under both anoxic and aerobic conditions

- 5- Assessment of the impact of primary sludge fermentation, which solubilizes cellulose, on nutrients removal efficiency, solids production, and oxygen transfer efficiency.

1.3 Thesis Organization

Chapter 1 provides a concise overview and motivation of this Ph.D. thesis. It briefly discusses the important pertinent literature and knowledge gaps and emphasizes the need for this research.

Chapter 2 includes a comprehensive literature review of wastewater cellulose and its biodegradability in activated sludge systems. It also discusses the fundamentals of oxygen transfer efficiency and the different factors that have an impact on aeration performance, emphasizing the current knowledge gaps and the scope for this research.

Chapter 3 is a published research paper in *Water Environment Research*, entitled “Fate of Cellulose in Primary and Secondary Treatment at Municipal Water Resource Recovery Facilities”. This study aimed at tracking cellulose fate, elimination efficiency, and biodegradability through wastewater treatment plants using data from two full-scale case studies in North America and Europe, one using a conventional primary clarification and the other using the RBF technology.

Chapter 4 is a published research paper in *Water Research*, entitled “Dynamic Impact of Cellulose and Readily Biodegradable Substrate on Oxygen Transfer Efficiency in Sequencing Batch Reactors”. This study aimed to delineate the real-time impact of acetate as a readily biodegradable substrate and cellulose as a slowly biodegradable substrate on oxygen transfer efficiency under different operating conditions.

Chapter 5 is a research paper under review in *Water Research*, entitled “Influence of Bioreactor Configurations on the Dynamics of Oxygen Demand and Aeration Performance in Activated sludge Processes”, In this study, the effect of bioreactor configurations on oxygen demand dynamics and aeration performance was assessed by calibrating a newly developed aeration model using experimental data from an SBR pilot, and using the

aeration model to evaluate the impact of different bioreactor configurations on aeration energy dynamics.

Chapter 6 is a research paper entitled “Performance assessment of anoxic and aerobic biodegradation”. Cellulose in wastewater is a large fraction of the influent organic substrates that can be either removed by primary treatment or biodegraded in secondary treatment. The objective of this study was to estimate the cellulose hydrolysis rate constants under both anoxic and aerobic conditions and to evaluate the impact of fermented primary sludge on nutrient removal efficiency, solid production, and oxygen transfer efficiency in sequencing batch reactors (SBRs).

Chapter 7 summarizes the major contribution of this research and includes recommendations for future research.

1.4 Thesis Format

This thesis was prepared in an integrated article format following the requirements given by the School of Graduate and Postdoctoral Studies (SGPS), Western University. Chapter 3 has been published in *Water Environment Research*. Chapter 4 has been published in *Water Research*. Chapter 5 is under peer review in *Water Research*. Chapter 6 will be submitted to *Water Environment Research*.

References

- Boztas, S., 2017. The ick factor: Dutch project making bike lanes and bottles from used loo roll. *The Guardian*.
- Chakraborty, T., 2015. Evaluation of Filtration Performance of a Rotating Belt Filter for Different Primary Wastewater Influent. MSc., The University of Western Ontario.
- Franchi, A., Williams, K., Lyng, T.O., Lem, W., Santoro, D., 2015. Rotating Belt Filters as Enabling Technology for Energy-Neutral Wastewater Treatment Plants: Current Status and Applications. *Proc. Water Environ. Fed.* 2015, 1743–1749. <https://doi.org/10.2175/193864715819540847>
- Garrido-Baserba, M., Asvapathanagul, P., McCarthy, G.W., Gocke, T.E., Olson, B.H., Park, H.-D., Al-Omari, A., Murthy, S., Bott, C.B., Wett, B., Smeraldi, J.D., Shaw, A.R., Rosso, D., 2016. Linking biofilm growth to fouling and aeration performance of fine-pore diffuser in activated sludge. *Water Res.* 90, 317–328. <https://doi.org/10.1016/j.watres.2015.12.011>
- Garrido-Baserba, M., Sobhani, R., Asvapathanagul, P., McCarthy, G.W., Olson, B.H., Odize, V., Al-Omari, A., Murthy, S., Nifong, A., Godwin, J., Bott, C.B., Stenstrom, M.K., Shaw, A.R., Rosso, D., 2017. Modelling the link amongst fine-pore diffuser fouling, oxygen transfer efficiency, and aeration energy intensity. *Water Res.* 111, 127–139. <https://doi.org/10.1016/j.watres.2016.12.027>
- Ghasimi, D.S.M., Zandvoort, M.H., Adriaanse, M., van Lier, J.B., de Kreuk, M., 2016. Comparative analysis of the digestibility of sewage fine sieved fraction and hygiene paper produced from virgin fibers and recycled fibers. *Waste Manag.* 53, 156–164. <https://doi.org/10.1016/j.wasman.2016.04.034>

- Gori, R., Giaccherini, F., Jiang, L.-M., Sobhani, R., Rosso, D., 2013. Role of primary sedimentation on plant-wide energy recovery and carbon footprint. *Water Sci. Technol.* 68, 870. <https://doi.org/10.2166/wst.2013.270>
- Gori, R., Jiang, L.-M., Sobhani, R., Rosso, D., 2011. Effects of soluble and particulate substrate on the carbon and energy footprint of wastewater treatment processes. *Water Res.* 45, 5858–5872. <https://doi.org/10.1016/j.watres.2011.08.036>
- Hofsten, B.V., Edberg, N., 1972. Estimating the Rate of Degradation of Cellulose Fibers in Water. *Oikos* 23, 29. <https://doi.org/10.2307/3543924>
- Honda, S., Miyata, N., Iwahori, K., 2000. A Survey of Cellulose Profiles in Actual Wastewater Treatment Plants. *Jpn. J. Water Treat. Biol.* 36, 9–14. <https://doi.org/10.2521/jswtb.36.9>
- Hurwitz, E., Beck, A.J., Sakellariou, E., Krup, M., 1961. Degradation of Cellulose by Activated Sludge Treatment. *J. Water Pollut. Control Fed.* 33, 1070–1075.
- Reardon, D.J., 1995. Turning down the power. *Civ. Eng.* 65, 54–56.
- Reijken, C., Giorgi, S., Hurkmans, C., Pérez, J., van Loosdrecht, M.C.M., 2018. Incorporating the influent cellulose fraction in activated sludge modelling. *Water Res.* 144, 104–111. <https://doi.org/10.1016/j.watres.2018.07.013>
- Rosso, D., Huo, D.L., Stenstrom, M.K., 2006. Effects of interfacial surfactant contamination on bubble gas transfer. *Chem. Eng. Sci.* 61, 5500–5514. <https://doi.org/10.1016/j.ces.2006.04.018>
- Rosso, D., Lothman, S.E., Jeung, M.K., Pitt, P., Gellner, W.J., Stone, A.L., Howard, D., 2011. Oxygen transfer and uptake, nutrient removal, and energy footprint of parallel full-scale IFAS and activated sludge processes. *Water Res.* 45, 5987–5996. <https://doi.org/10.1016/j.watres.2011.08.060>

- Rosso, D., Stenstrom, M.K., 2006. Surfactant effects on α -factors in aeration systems. *Water Res.* 40, 1397–1404. <https://doi.org/10.1016/j.watres.2006.01.044>
- Rosso, D., Stenstrom, M.K., 2005. Comparative economic analysis of the impacts of mean cell retention time and denitrification on aeration systems. *Water Res.* 39, 3773–3780. <https://doi.org/10.1016/j.watres.2005.07.002>
- Ruiken, C.J., Breuer, G., Klaversma, E., Santiago, T., van Loosdrecht, M.C.M., 2013. Sieving wastewater – Cellulose recovery, economic and energy evaluation. *Water Res.* 47, 43–48. <https://doi.org/10.1016/j.watres.2012.08.023>
- Tao, X., Chengwen, W., 2012. Energy consumption in wastewater treatment plants in China. Unpubl. Manusc. Retrieved [Httpwww Res. NetprofileTaoXie11publication266146909Energy Consum. Pdf](http://www.Res.NetprofileTaoXie11publication266146909Energy%20Consum.Pdf).

Chapter 2

2 Literature review

2.1 Municipal wastewater characteristics.

2.1.1 Organics

Organic constituents of municipal wastewater generally include proteins, carbohydrates, oils, fats, and urea, as well as various synthetic organics. Figure 2-1 shows the various fractions of chemical oxygen demand (COD), which is the quantity of oxygen used to oxidize organics. The biodegradable organic matter is determined by the biochemical oxygen requirement (BOD) (Metcalf & Eddy, 2014). Total COD has both biodegradable and nonbiodegradable fractions. Each of them is present in wastewater in both particulate and soluble forms. In the biological wastewater treatment plant, non-biodegradable soluble fractions typically leave the plant untreated, while the non-biodegradable particle fraction accumulates in biosolids. Readily biodegradable COD (rbCOD) is typically soluble and is rapidly assimilated into new biomass. Slowly biodegradable particulate COD (sbCOD) must first be solubilized, resulting in slower biodegradation rates. The rbCOD consists of complex COD that can be fermented to volatile fatty acids (VFAs). The typical BOD/COD ratio for municipal wastewater ranged from 0.3 to 0.8 (Henze et al., 2000; Metcalf & Eddy, 2014). Biodegradable COD fraction varied between 0.75 to 0.85 and nonbiodegradable COD fraction varied between 0.15-0.25 (Henze et al., 2000)

2.1.2 Solids

The most important physical parameter to characterize wastewater is the total solids (TS) which consist of total suspended solids (TSS) and total dissolved solids (TDS) (Fig. 2-2). TSS is usually the portion of the TS retained on a filter paper of specific pore size (usually 1.2 μm) after being dried at 105°C. The solids contained in the filtrate that passes through the filter paper consists of dissolved and colloidal solids. The solids contained in wastewater are either fixed or volatile. The volatile fraction contributes to BOD, organic nitrogen (which is converted to ammonia through ammonification), and organic

phosphorous. The typical VSS/TSS ratio in the influent wastewater is 0.6-0.8 (Metcalf & Eddy, 2014).

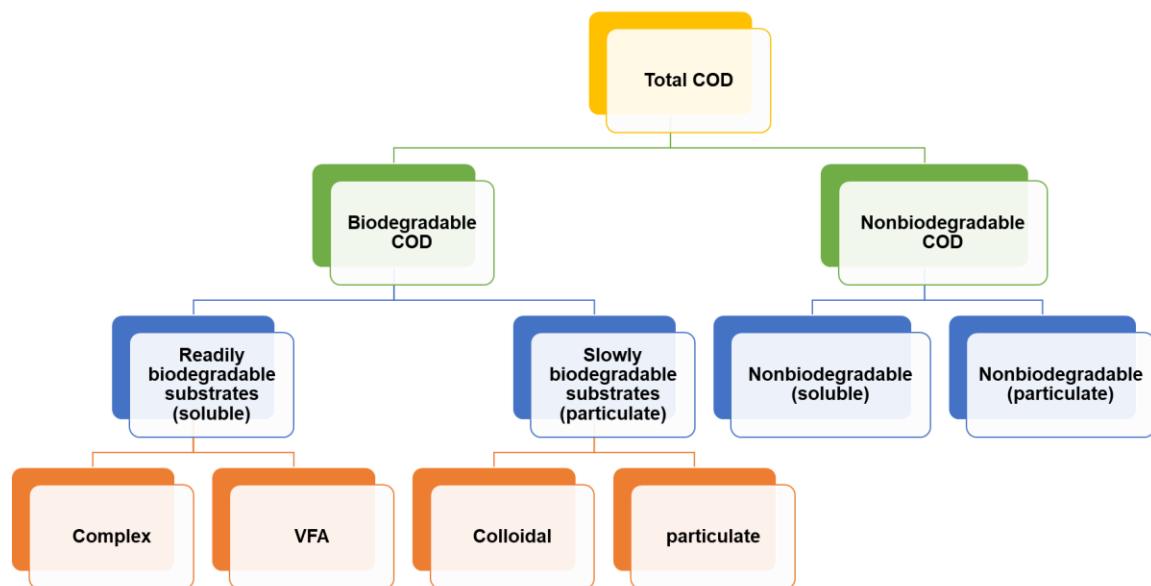


Figure 2-1: COD fractions in wastewater (Metcalf & Eddy, 2014)

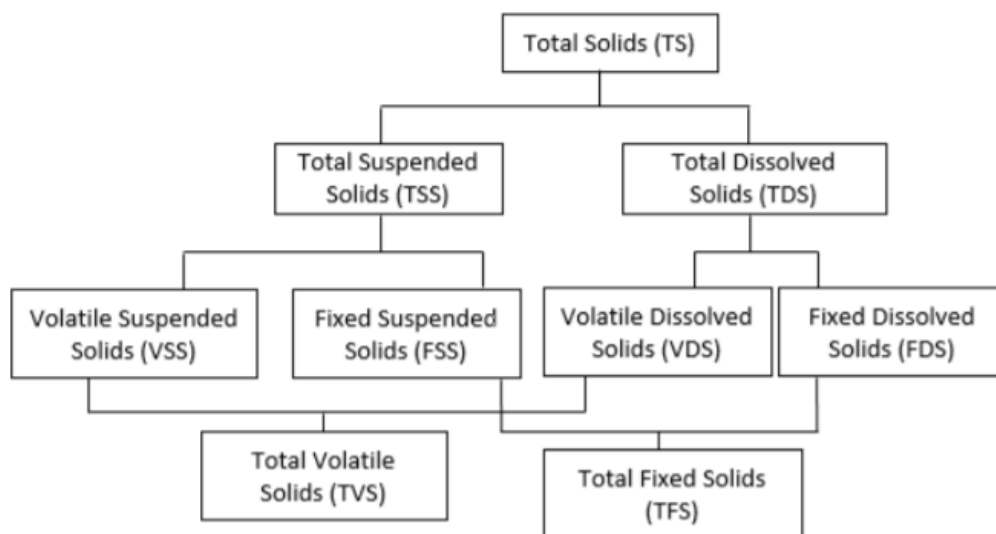


Figure 2-2. Solids fractions in wastewater (Metcalf & Eddy, 2014)

2.1.3 Nitrogen

Nitrogen and phosphorous are essential for microorganisms' growth, commonly referred to as nutrients or biostimulants. The most important forms of nitrogen in wastewater are ammonia (NH_3), ammonium (NH_4^+), nitrogen gas (N_2), nitrite ion (NO_2^-), nitrate ion (NO_3^-), and organic nitrogen (Metcalf & Eddy, 2014). Figure 2-3 shows the fractionation of nitrogen in wastewater.

Wastewater treatment plants receive nitrogen in the form of total Kjeldahl nitrogen (TKN), of which 60% is ammonia ($\text{NH}_4\text{-N}$) and 40% is organic. Biodegradable particulate nitrogen is composed of amino acids and proteins that are hydrolyzed biologically to ammonium by ammonification. The microorganisms can easily assimilate biodegradable soluble nitrogen. Non-biodegradable organic nitrogen is present in soluble (SON), colloidal (CON), and particulate matter (PON) forms, where SON and CON leave the effluent plant, while PON ends up in the sludge (Gupta, 2018; Henze et al., 2000; Metcalf & Eddy, 2014).

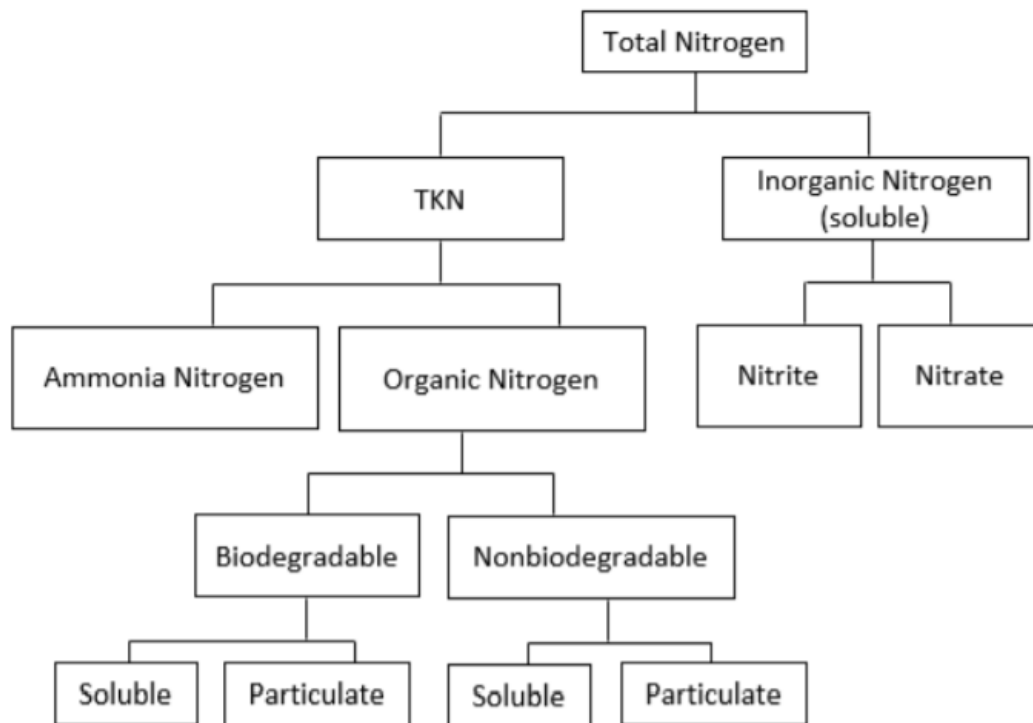


Figure 2-3. Nitrogen fractions in wastewater (Metcalf & Eddy, 2014)

2.1.4 Phosphorous

Phosphorus is an essential nutrient for microorganisms and most forms of phosphorus are inorganic orthophosphates (PO_4^{3-} , HPO_4^{2-} , H_2PO_4^- , H_3PO_4), polyphosphate (condensed phosphates), and organic phosphate (phospholipids and nucleotides) (Metcalf & Eddy, 2014). Figure 2-4 shows the different forms of phosphorus in municipal wastewater. Inorganic phosphorus forms are orthophosphate (also known as reactive phosphorous) and polyphosphates (also known as acid hydrolyzable phosphorous). Orthophosphate, 70%-90 % of the total phosphorus (TP) in raw municipal wastewater, is readily assimilated by microorganisms without further decomposition. Organic particulate phosphorous, including biodegradable and nonbiodegradable fractions, is usually precipitated and removed in sludge. Organic soluble biodegradable phosphorous is hydrolyzed into orthophosphates (Gupta, 2018; Henze et al., 2000; Metcalf & Eddy, 2014).

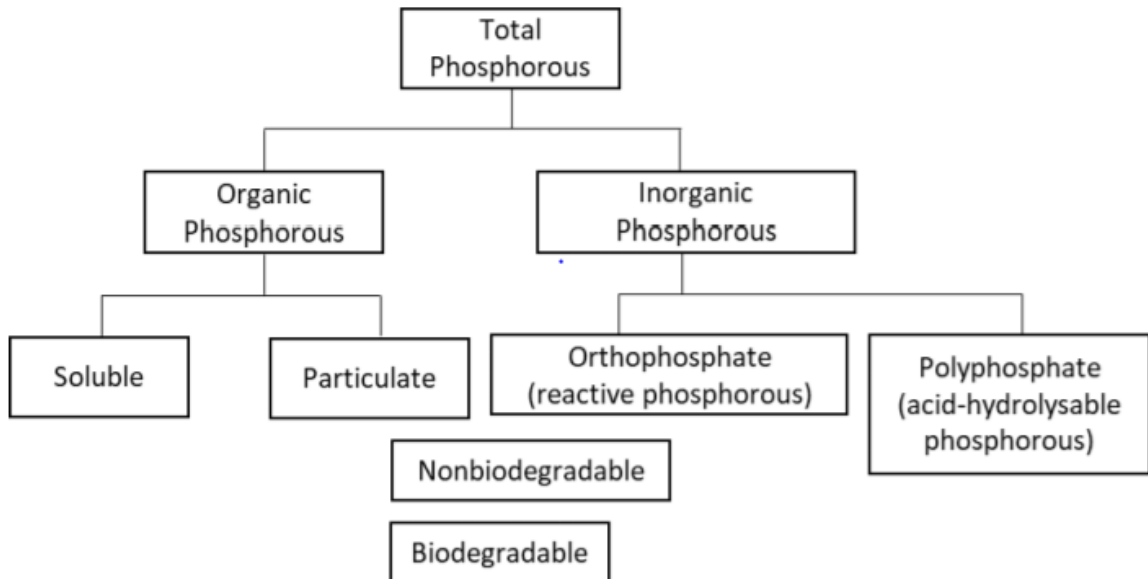


Figure 2-4. Phosphorus fractions in wastewater (Metcalf & Eddy, 2014)

2.2 Cellulose in municipal wastewater

Cellulose originating from toilet paper represents a large portion of raw wastewater particulate organics (Ramasamy et al., 1981; Ruiken et al., 2013). Cellulose is the world's main organic polymer and is closely related to many facets of human existence such as fuel, clothes, food, and paper (Bauer and Ibáñez, 2014; Gupta et al., 2018; Harris et al., 2010; Olsson and Westman, 2013). Cellulose is very similar to starch as a complex carbohydrate and a linear polymer with β -1,4- glycosidic bond paired with β -D-glucose units (Olsson and Westman, 2013).

The average annual consumption of toilet paper is 23 kg/capita in North America and 14 kg/capita in western Europe (www.worldwatch.org/node/5142). Theoretically, the estimated influent cellulose to wastewater treatment plants in western Europe is 40% of the influent total suspended solids (TSS) and 25%-30% of the influent COD (Ruiken et al., 2013). Similarly, using the per capita annual toilet paper consumption of 23 kg/day in North America (www.worldwatch.org/node/5142), and per capita, water consumption of 400 L/d, the estimated influent toilet paper is 158 mg/L, representing approximately 46% of the influent solids mass. Cellulose, in combination with hemicellulose and lignin, may account for almost half of the organic matter entering wastewater treatment plants (WWTP) (Verachtert et al., 1982). The cellulose content of raw municipal wastewater varied between 4.5% to 40% of TSS while in settled sludge it varied between 2% to 10% of the TSS (Honda et al., 2000; Hurwitz et al., 1961; Ruiken et al., 2013). The cellulose content of waste activated sludge (WAS) ranged between 1% and 3.55% confirming that cellulose is biodegradable (Hurwitz et al., 1961).

2.2.1 Cellulose measurement

Over the past years, several methods have been developed to separate cellulose from the wastewater samples. Hurwitz et al., 1961 was the first to measure cellulose in wastewater and sludges gravimetrically using the Schweitzer reagent (copper ammonium hydroxide) as a solvent for cellulose. This method was originally invented by (Waksman and Heukelekian, 1924) to determine cellulose in soils. Hofsten and Edberg, 1972 measured

cellulose and hemicellulose contents using the enthrone method after hydrolysis with an H_2SO_4 solution. Honda et al., 2000 determined cellulose in wastewater samples using the phenol-sulphuric acid method (DuBois et al., 1956) after treatment with NaOH, and H_2SO_4 solutions. Another method was developed by (Honda et al., 2002) to separate cellulose from wastewater sludge by hydrolysis using diluted sulfuric acid, followed by conventional autoclaving treatment. Other studies (Honda et al., 2000; Ruiken et al., 2013), determined cellulose microscopically using polarized light; however, both studies claimed that due to lack of the method accuracy neither removal efficiencies by primary treatment nor biodegradation were estimated accurately.

Gupta et al., 2018, compared four measurement methods for cellulose detection in wastewater and sludge: acid hydrolysis (sulfuric acid), enzymatic hydrolysis, NREL (National Renewable Energy Laboratory), and the Schweitzer methods and concluded that the Schweitzer method was the most reliable and accurate technique to measure cellulose content in municipal wastewater and sludges. Additionally, the authors highlighted that the Schweitzer method does not rely on the hydrolysis of cellulose into glucose that not only requires a long time but also shows a temperature-dependent conversion efficiency, reliability, and reproducibility.

2.2.2 Cellulose removal by primary treatment

Primary treatment processes such as primary clarification and RBF (commercially known as Salsnes filter, Fig. 2-5) efficiently remove cellulose from wastewater (Hurwitz et al., 1961; Ruiken et al., 2013). Removed cellulose through primary treatment can be either converted to biogas by digestion (Ghasimi et al., 2016) or utilized as a resource for different industries such as biofuels, additives in building materials, and asphalt (Boztas, 2017; Honda et al., 2000).

The primary clarification is a commonly used technology with TSS and BOD removal efficiencies of 50%-70% and 25%-40%, respectively (Metcalf & Eddy, 2014). RBF is an alternative primary treatment method with a smaller footprint when compared to primary clarification with TSS removal efficiencies ranging from 30% to 60% (Chakraborty, 2015;

Franchi et al., 2015; Ruiken et al., 2013). RBF with a fine mesh of <0.35 mm has been widely used in Norway in coastal applications where further biological treatment is not required (Odegaard, 1998; Rusten and Odegaard, 2006). Furthermore, the RBF was used in combination with membrane bioreactors (MBR) to enhance the membrane performance and reduce the operational problems, using a larger mesh size of 0.8-2 mm (Schier et al., 2009). The cellulose content was measured microscopically and was found to be 79% of the total solids mass content in the RBF-sieved sludge and between 25% to 32% in the primary clarification sludge (Ruiken et al., 2013).

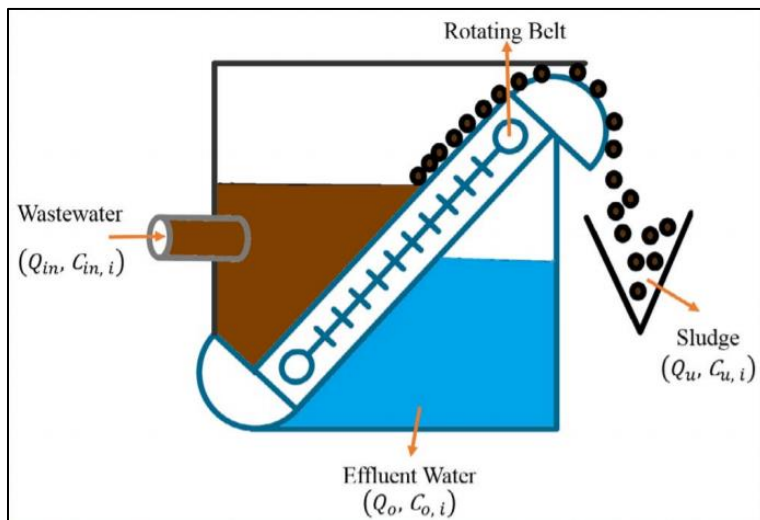


Figure 2-5. RBF Schematic diagram (Behera et al., 2018)

2.2.3 Cellulose biodegradability

Cellulolytic microorganisms, in combination with non-cellulolytic species, can achieve complete degradation of cellulose (Edberg and Hofsten, 1975; O’Sullivan et al., 2007; Pérez et al., 2002). Cellulose can be biodegraded under both aerobic and anaerobic conditions, releasing carbon dioxide and water in aerobic conditions, carbon dioxide, methane, and water under anaerobic conditions (Edberg and Hofsten, 1975; O’Sullivan et al., 2007; Pérez et al., 2002). In environments where cellulolytic bacteria can not multiply due to growth limiting factors, which are usually the available amount of nitrogen and the slow intrinsic hydrolysis rate, cellulose biodegradation is very slow (Hofsten and Edberg,

1972). Hurwitz et al., 1961 studied the aerobic degradation of cellulose using laboratory batch experiments and showed that 6.7 % of the cellulose was degraded at a temperature of 12 to 13 °C compared to 87 % at 23 °C within a contact time of 72 hrs. The study also, showed that at 12 to 13 °C, increasing the contact time to 96 hrs, increased the biodegradation efficiency to 20%, which indicates that the cellulose biodegradation is temperature-dependent. Cellulose biodegradation rates have also been reported to increase in proportion to the concentration of mixed liquor suspended solids (MLSS), suggesting that the cellulose biodegradation rate is proportional to the solids retention time (SRT). Edberg and Hofsten, 1975 studied cellulose biodegradation under anaerobic conditions using nylon bags and showed that 70% of the cellulose was biodegraded in 30 days. Verachtert et al., 1982 using nylon bags showed that 50% of the cellulose was biodegraded aerobically while 60% was biodegraded anaerobically at a contact time of 15 days. Ruiken et al., 2013, determined cellulose biodegradability under anaerobic conditions using batch experiments and showed that 10% of cellulose was biodegraded in 20 days at 9 °C while complete biodegradation was observed within 12 days at 24 °C. Alvarez et al., 2009 determined the aerobic biodegradation of the tissue paper and showed a biodegradation efficiency of 50%. Ghasimi et al., 2016 showed that anaerobic biodegradation efficiencies of the cellulose-rich sieved sludge (fine mesh <0.35 mm) were 57% and 62% under mesophilic and thermophilic conditions, respectively.

To conclude, cellulose biodegradation efficiency under aerobic conditions as reported in the aforementioned studies widely varied between 50% and 87% at room temperature and between 6.7% and 60% for temperatures lower than 13%. Additionally, cellulose biodegradation under anaerobic conditions varied between 50% and 100%.

Cellulose biodegradation can be modeled using either first order (Weimer, 1992), or using the surface limited reaction rate (Henze et al., 2000). Benneouala et al., 2017, using respirometry, studied the role of biomass in the biodegradation of slowly biodegradable substrates using toilet paper and pure cellulose under aerobic conditions. ASM1 model was used to better understand the role of biomass in hydrolysis. Results showed that cellulose and toilet papers can be biodegraded within 10 days and showed that a small portion of the

active biomass was responsible for the hydrolysis of the toilet papers and cellulose among other slowly biodegradable particles. Behera et al., 2018 studied the effect of cellulose biodegradability and digestibility on the plant-wide energy balance using BSM2. In this study, cellulose was assumed to account for 30% of the influent TCOD. Results showed that cellulose can play a very important role in plant-wide energy balance (i.e energy consumption in aeration versus energy production through digestion). Reijken et al., 2018 integrated cellulose into the ASM1 model as a separate state variable assuming that cellulose hydrolysis follows first-order hydrolysis kinetics. The cellulose fraction as well as cellulose hydrolysis rate were calibrated using typical COD and solids characteristics from a full-scale treatment plant. The study clearly demonstrated that cellulose as a separate state variable constitutes a significant fraction of the influent particulate organic matters; however, it was argued that cellulose hydrolysis is not clearly understood and hence a simplified first-order kinetic reaction model was proposed.

2.3 Oxygen transfer efficiency and aeration energy

Water is profoundly entangled with energy. Although energy demand decrease is known as one of the major contributors to the mitigation of global climate change, it is of the utmost importance to consider the relation between water and energy. Firstly, energy uses for water delivery and wastewater treatment are estimated to be about 2% of the world's total energy consumption and to be 20% of the municipal energy sector (Pasini, 2019).

Aeration systems, as an important part of the wastewater treatment, were basically engineered to provide the oxygen needed to promote aerobic biokinetics. Aeration systems perform two roles in the activated sludge systems: (1) To satisfy the process requirement of oxygen; and (2) To provide adequate mixing to ensure the suspension of the solids (Baquero-Rodríguez et al., 2018). Energy demand for biological wastewater treatment plants varies between 0.2 to 2 kWh/m³ and might reach up to 8.33 kWh/m³ depending on influent wastewater characteristics, treatment plant capacity, used technology, and disposal standards (Gude, 2015; Singh et al., 2016; Tao and Chengwen, 2012). The majority of the treatment plant's energy is consumed through aeration (Rosso et al., 2011). The energy required for aeration represents about 45 to 75% of the treatment plant's net power demand

(Reardon, 1995; Rieth et al., 1990; Rosso and Stenstrom, 2006). Figure 2-6 shows a qualitative energy density diagram of a typical wastewater treatment plant. Thus, it is important to quantify the OTE precisely and understand the key factors that affect the OTE in order to optimize the energy needed for aeration.

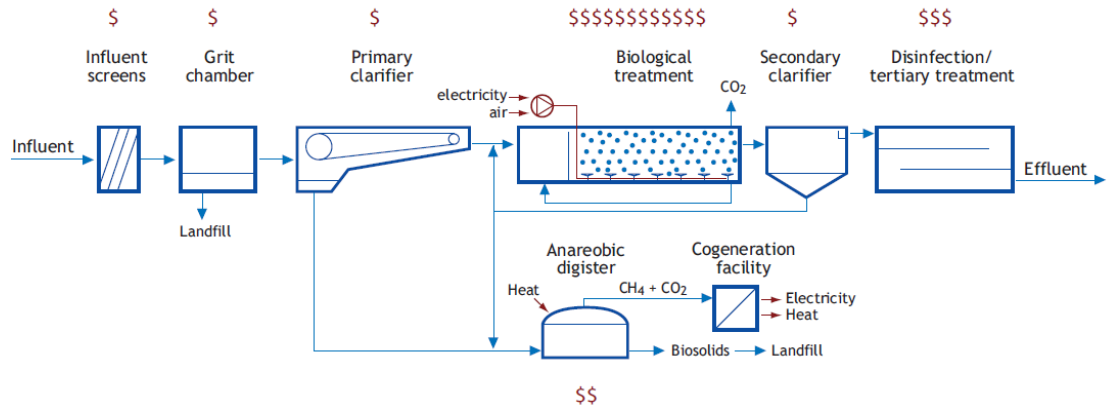


Figure 2-6. A scheme with a comparison of the energy intensity of treatment processes of a wastewater treatment plant (Henze et al., 2015)

2.3.1 Measurement methods for OTE

Three main methods are commonly used for oxygen transfer efficiency testing under process conditions; the non-steady-state, tracers, and the off-gas methods (Zhou et al., 2013). The non-steady-state method is used under process conditions where the changes in oxygen concentration are monitored by modifying power levels, adding hydrogen peroxide, or aerating with pure oxygen (Mahendraker et al., 2005b, 2005a; Pratt et al., 2004). In the tracer method, inert gaseous tracers are used with radioactive isotopes to measure the gas transfer rates (ASCE, 1997).

The non-steady-state method is commonly used to test the oxygen transfer efficiency in clean water where the dissolved oxygen is removed either chemically (i.e., using sodium sulfite and cobalt chloride) or physically via nitrogen stripping (ASCE, 1993). While reoxygenation, the dissolved oxygen concentrations are monitored, and parameters such as the k_{la} and C_{∞}^* can be estimated using the oxygen transfer mass balance (ASCE, 1993; Hwang and Stenstrom, 1985).

The off-gas method developed by (Redmon et al., 1983) has been proven to be the most reliable and robust method for measuring the oxygen transfer rates in process conditions. The main advantage of using the off-gas method is that it gives an accurate oxygen transfer efficiency for diffused aeration systems, without interfering with the DO concentrations and oxygen uptake rate (OUR) in the reactor (Krause et al., 2003; Redmon et al., 1983; Rosso and Stenstrom, 2005). Furthermore, neither the trace nor non-steady-state tests could accurately estimate the real-time OUR under process conditions in continuous flow systems.

The off-gas is the gas emitted from the surface of the liquid volume being aerated. In the off-gas approach, A gas-phase mass balance over the aerated volume can be used to estimate the oxygen transfer capacity of a submerged air device based on the following assumptions (Fig. 2-7, Eq. 2-1):

- 1- Conservative interts.
- 2- Constant air flow rate and barometric pressure in the tested location.
- 3- The off-gas humidity equal to the saturated value at mixed liquor temperature.
- 4- No oxygen transfer is taking place at the liquid surface.

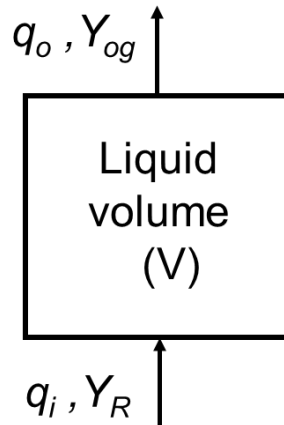


Figure 2-7. Gas-phase mass balance (Redmon et al., 1983)

$$V\rho \frac{dY}{dt} = \rho q_i Y_R - \rho q_o Y_{og} - k_{La}(C_{\infty}^* - C)V \quad (2 - 1)$$

Where: ρ air density x %O₂ in the air by mass; q_i , q_o are the air flow rates; V is the aeration test volume; Y_R , Y_{og} are the molar ratios of inlet and outlet oxygen gas fractions, respectively; C_{∞}^* and C are the oxygen saturated concentration achieved at the infinite time and the average oxygen concentration in the bioreactor, respectively; k_{La} = overall oxygen mass transfer coefficient.

At steady-state conditions when the change in the DO concentrations is negligible, the OTE % is calculated from the measured molar ratios of the inlet and outlet gas fractions in the aeration tank following gas-phase mass balance (Eq.2-2). The product of the gas flow rate and the gas transfer efficiency yields the OTR. The oxygen uptake rate (OUR) is then calculated by dividing the OTR by the volume of the liquid phase (Eq.2-3).

$$\text{OTE (\%)} = \frac{\text{mass O}_2 \text{ in } (\rho q_i Y_R) - \text{mass O}_2 \text{ out } (\rho q_o Y_{og})}{\text{mass O}_2 \text{ in } (\rho q_i Y_R)} \times 100 \quad (2 - 2)$$

$$\text{OUR} = \frac{q_o \times \rho \times \text{OTE}}{V \times 100} \quad (2 - 3)$$

The off-gas is captured using a hood that covers a small portion of the aeration tank (Fig. 2-8a). Sampling numbers or locations should cover at least 2% of the total aerated surface area to be representative. The captured off-gas goes through the off-gas analyzer (Fig. 2-8b). The off-gas analyzer consists of the oxygen gas sensor, desiccant (Drierite) to remove moisture, and CO₂ adsorber (NaOH) for gas pre-treatment, air flow meter, and diaphragm suction pump. In addition, an air flow meter is used to monitor the air flow rates, and DO probe is used to measure the DO in the mixed liquor.

To compare different systems OTE is normalized using the temperature correction (Eq. 2-4). Then the oxygen transfer efficiency in process water at standard conditions (α SOTE) is then calculated (Eq. 2-5).

$$OTE_{sp20} = \frac{OTE}{(C_{\infty}^* - C)} \times 1.024^{(20-T)} \quad (2-4)$$

$$\alpha SOTE = OTE_{sp20} \times C_{\infty,20}^* \times \beta \quad (2-5)$$

Where, β is the correction factor for salinity and dissolved solids, the ratio of C_{∞}^* in wastewater to clean water

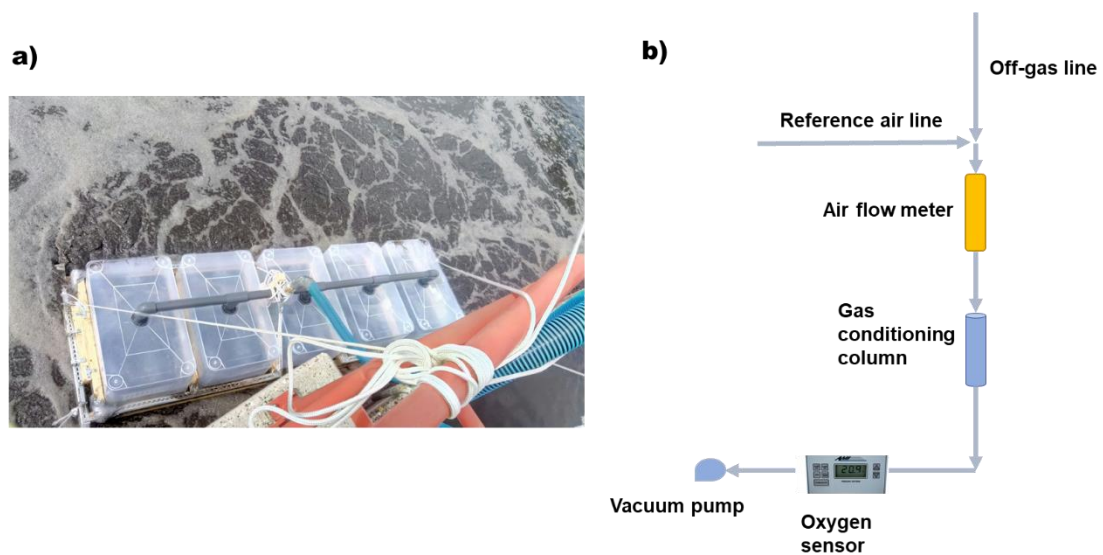


Figure 2-8. Schematic diagram illustrating the main components of the off-gas analyzer

To prevent inconsistencies due to site-specific environmental conditions and process conditions, standard conditions are applied and specified as zero DO, zero salinity, 20°C, and 1 atm. Standardized parameters are typically used to compare performances of different plants, including standard oxygen transfer efficiency (SOTE), standard oxygen transfer rate (SOTR), or standard aeration efficiency (SAE) (Henze et al., 2015).

The oxygen transfer rate reduction due to the organic loading rate in wastewater can be evaluated using the α -factor. The α -factor is a function of the sludge age, and tank geometry

(diffusers submergence, numbers, and surface area). It could be calculated either by using the ratio of process water to clean water mass transfer coefficients (Eq. 2-6) or using the ratio between the oxygen transfer efficiency in standard conditions for clean water to process water (Eq.2-7) (Baquero-Rodríguez et al., 2018; Henze et al., 2015)

$$\alpha = \frac{(k_{la}) \text{ process water}}{(k_{la}) \text{ clean water}} \quad (2 - 6)$$

$$\alpha = \frac{SOTE}{\alpha SOTE} \quad (2 - 7)$$

Where

SOTE is the oxygen transfer efficiency at standard conditions (%).

Fine bubble diffusers were reported to enhance wastewater treatment efficiency by 20% and decrease energy demand by 40% when compared with coarse bubble diffusers (Hansen et al., 2004). Fine bubbles have a rise velocity of 0.2 m/s when compared to the coarse bubbles with a velocity of 1.5 m/s which increases the fine bubbles residence time and increases the surfactant accumulation rate (Baquero-Rodríguez et al., 2018; Rosso and Stenstrom, 2006).

The α -factor for fine bubble diffusers varies between 0.3 to 0.85 (Baquero-Rodríguez et al., 2018). Fine bubbles' diameter is 2 to 5 mm depending on the airflow rate. Bigger bubbles are linked with high air flow rates. The reduction in the bubble size increases the k_{la} and the standard oxygen transfer rate through the increased surface area per unit volume and increased contact time. The airflow rate also affects the bubble shape and velocity and the turbulence of the system.

Coarse bubbles are usually produced by 6 mm orifices and can be as big as 50 mm in diameter. Rising coarse bubbles have large interfacial gas-liquid velocity gradients and can be bundled as high-flow regime interfaces, while fine bubbles have low interfacial velocity gradients and can be bundled as low-flow regime interfaces indicating that fine bubbles are

associated with low α -factor and coarse bubbles are characterized by high α -factor (Rosso and Stenstrom, 2006).

2.3.2 Environmental factors affecting OTE

Environmental conditions affect the OTE regardless of the operating conditions. Water temperature change is a very important factor in designing and testing aeration systems. At high water temperature, oxygen solubility decreases, and hence the oxygen saturation concentration (C^*_∞) decreases (Baquero-Rodríguez et al., 2018).

Barometric pressure is another important factor. The efficiency of the blowers is inversely proportional to the height at which the blowers are installed due to the influence of height on atmospheric pressure and air density (Baquero-Rodríguez et al., 2018).

Three factors reduce air density: a rise in air temperature, a reduction in atmospheric pressure, and an increase in relative humidity.

Estimation of the energy requirements depends on working conditions, control techniques, and type of blower (Baquero-Rodríguez et al., 2018). Any change in the temperature and the barometric pressure of the inlet air changes the density of the compressed air and therefore the performance of the blower. The rise in gas density increases the barometric pressure and higher power is therefore required. Blowers must be chosen to have sufficient capacity for a hot summer's day and with drivers with sufficient power during the coldest winter weather. The blowers power requirements for adiabatic compression were estimated using Eq. 2-8 (Metcalf & Eddy, 2014).

$$BHP = \frac{wRT_1}{29.7 n e} \left[\left(\frac{p_2}{p_1} \right)^n - 1 \right] \quad (2 - 8)$$

Where: BHP = blower break horse power (kW); w= ponderal air flow (kg s⁻¹); R = gas constant (8.314 J mol⁻¹ K⁻¹); T₁= absolute inlet temperature (K), p₁= absolute inlet pressure (Pa), p₂= absolute discharge pressure (Pa), n= 0.283 for air (-), e= blower efficiency (-).

Oxygen saturation concentration is another important factor that represents the maximum amount of dissolved oxygen in water (Jenkins, 2013). The oxygen saturation concentration is directly impacted by the atmospheric pressure and significantly decreases with the increase of temperature and salinity (Baquero-Rodríguez et al., 2018).

2.3.3 Process conditions affecting OTE

2.3.3.1 Surface active agents (surfactant)

Surfactants accumulation on the bubble interfaces phenomenon is characterized by the hydrophilic heads accumulation at the gas-liquid interface, and the hydrophobic tails arrangement inside the bubble volume, happening by chemical segregation (Rosso et al., 2006). Once the bubble is detached from the diffusers, it starts to accelerate vertically until the drag force F_d equals the buoyancy force F_b (Eq.2-9) (Suñol and González-Cinca, 2019).

$$\frac{1}{2} \rho v_T^2 C_d \frac{\pi d^2}{4} = \Delta \rho g \frac{\pi d^3}{6} \quad (2-9)$$

Where: v_T is the terminal velocity; C_d is the drag coefficient; g is the gravity level; d is the bubble equivalent diameter

Accumulated surfactants increase surface stiffness and the bubble drag coefficient, resulting in diminished terminal velocity (Alves et al., 2005). Besides, the existence of hydrophobic tails inside the bubble hinders the internal gas circulation, which decreases the gas-side mass transfer film renewal rate (Garner and Hammerton, 1954). Rosso et al., 2006 studied the impact of surfactant on the aeration efficiency for the fine bubbles using sodium lauryl sulfate with a high molecular weight of 288 g/mol, and iso-amyl alcohol with a low molecular weight of 88 g/mol and high diffusivity. The results showed that OTE was reduced by 30%-70% of the clean water value because of the accumulation of surfactants on the bubble interface reducing surface tension, gas-liquid interfacial renewal, and gas diffusivity into the liquid. Another related study by Rosso and Stenstrom, 2006 measured the surfactant impact on α -factor under two operational conditions; high and low

interfacial velocities (i.e coarse and fine bubble aeration). In the case of a low flow regime, surfactants migrate, with time, to the gas-liquid interface hindering the interfacial renewal process, reducing α -factor. On the other hand, increasing the flow regime from laminar to turbulent flow increased the surface renewal rate and sheared surfactants off the bubble surface, increasing α -factor. Although high turbulence associated with coarse bubble diffusers improved mass transfer rates, the required energy to produce coarse bubbles is much higher compared to fine bubble diffusers. Furthermore, the authors' experiment showed that Reynold number (Re) and high energy intensity were independent, and therefore, inconsistent mass transfer rates were produced (i.e. Re increase was not proportional to α -factor increase).

2.3.3.2 The impact of process design selectors

The anaerobic or anoxic biological selector is a tank, in which influent wastewater and returned active sludge are mixed. Selectors are usually placed before the aeration tanks and are primarily designed to enhance biological nutrient removal, promote the production of floc-forming bacteria, and to avoid the spread of filamentous bacteria. In addition to enhancing settling and improving nutrient removal, selectors have a beneficial impact on OTE since they degrade rbCOD and surface-active agents (Henze et al., 2015; Metcalf & Eddy, 2014).

Rosso and Stenstrom, 2005 using the off-gas results of 22 treatment plants, the estimated oxygen for a treatment capacity of 2000 m³/day were 3800, 5034, and 3469 kg O₂/day for conventional, nitrification, and nitrification and denitrification (NDN) treatment plants respectively, proving that upgrading conventional treatment plants to remove nitrogen reduces oxygen requirements which, consequently, reduces the energy cost. The measured oxygen transfer efficiency at the field for conventional, nitrification, and nitrification and denitrification (NDN) treatment plants were 15.3%, 17.6%, and 18.8%, respectively. This observed improvement was due to the anoxic removal of the organic substrates which reduced organic loading rates to the aeration tank (Fisher and Boyle, 1999; Rosso and Stenstrom, 2006). Also, high α -factor was found to be due to the efficient removal of

biodegradable organic carbons, and anthropogenic compounds such as pharmaceuticals in the anoxic tank (Khan et al., 1998; Soliman et al., 2004). In addition, in the nitrification process, used oxygen is partially recovered by producing nitrate which, alternatively, serves as an electron acceptor (Rosso and Stenstrom, 2005). Rosso et al., 2008 compared the α -factors from different activated sludge process configurations and observed that α -factor increases from 0.37 to 0.48 to 0.59 for conventional, nitrifying, and nitrification/denitrification systems, respectively.

2.3.3.3 The impact of solids retention time (SRT) and mixed liquor suspended solids (MLSS) Concentrations

Systems with high SRT are characterized by their high solids concentration and high oxygen requirements. At high SRT, surfactants that are contained in the rbCOD can be removed, enhancing the OTE and α -factor (Baquero-Rodríguez et al., 2018; Henkel et al., 2011; Rosso et al., 2008a). The physical presence of solids has a detrimental impact on the OTE due to their accumulation on the bubble surface (Baquero-Rodríguez et al., 2018).

Krampe and Krauth, 2003 showed that MLSS concentrations are inversely correlated with α -factor in systems with high MLSS concentrations ranging from 2 g/L to 30 g/L (Fig. 2-9). The same observation was made by Cornel et al., 2003 in membrane bioreactors (MBR) for MLSS concentrations more than 5 g/L (Fig. 2-10).

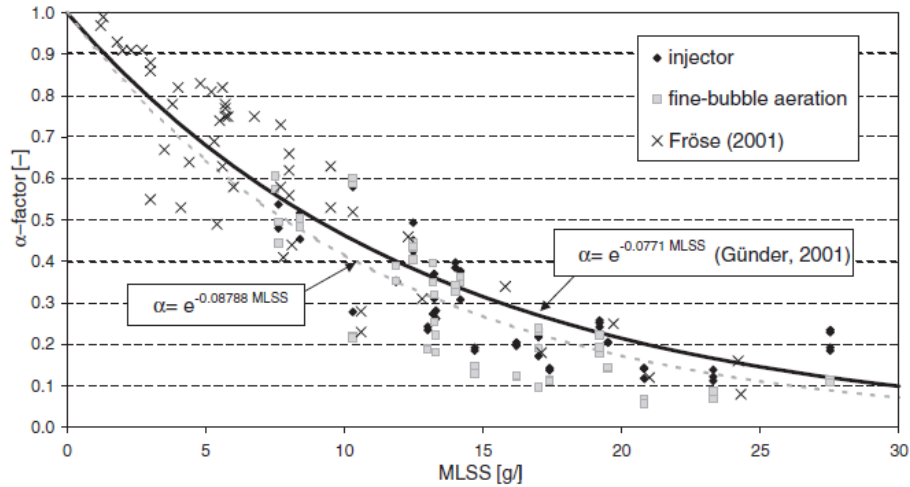


Figure 2-9. The correlation between α -factor and MLSS in systems with high MLSS concentrations (Krampe and Krauth, 2003)

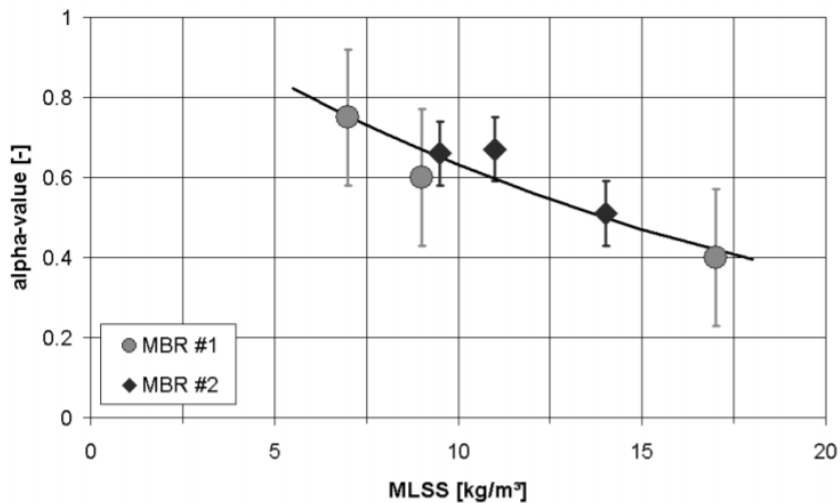


Figure 2-10. The impact of MLSS on α -factor in MBR systems (Cornel et al., 2003)

Germain et al., 2007 studied the biomass impact on α -factor and showed that α -factor decreased exponentially with the MLSS increase (Fig. 2-11). Henkel et al., 2011, using data from the aforementioned studies, showed a negative linear correlation between MLSS

and α -factor in activated sludge systems at MLSS concentrations ranging from 2 g/L to 14 g/L (Fig. 2-12).

Contrary to the observations of Krampe and Krauth, 2003, and Henkel et al., 2011 that the α -factor decreased with the increase in MLSS concentrations in the range of 1-4 g/L, Rosso et al., 2005, using oxygen transfer efficiency measurements from 26 treatment plants over fifteen years, showed that for MLSS concentrations between 1-4 g/L (SRT varying between 2-18 days), α -factor increases with the SRT increase, and hence MLSS concentrations increase. Gillot and Héduit, 2008 also confirmed that α -factor improves with the SRT increase up to 30 days. The fact that the SRT of the activated sludge plant, is also correlated with MLSS, and for plants with MLSS concentrations varying between 1-4 g/L, low MLSS is associated with low SRT and hence low α -factors associated with low biodegradation efficiency.

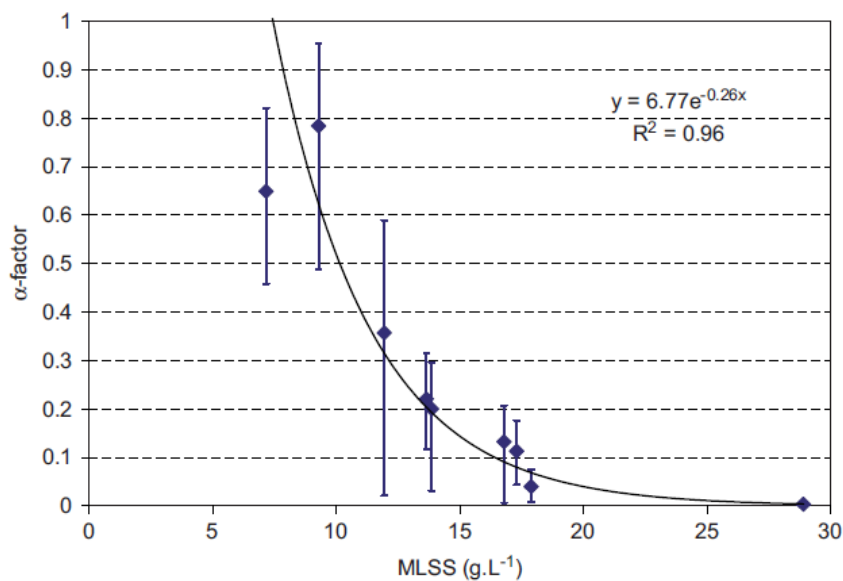


Figure 2-11. The impact of MLSS on α -factor in MBR systems (Germain et al., 2007)

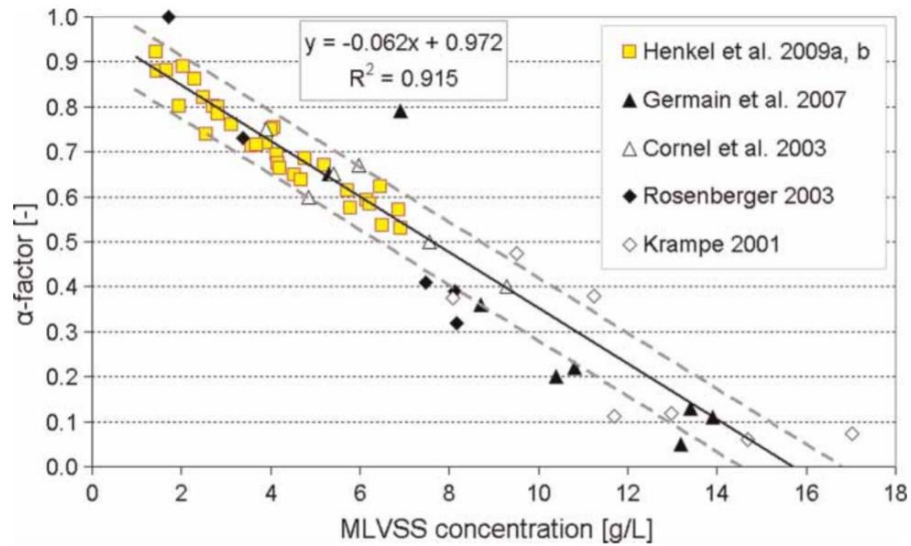


Figure 2-12. Linear correlation between α -factor and MLSS at SRT>20days (Henkel et al., 2011)

Baquero-Rodríguez et al., 2018 combined the data from the aforementioned studies and plotted a correlation between α -factor and MLSS. As shown in figure 2-13 a double exponential correlation was defined. At MLSS concentrations below 4 g/L, MLSS increase impacted the α -factor beneficially, due to the increased biosorption provided by the biomass. However, MLSS concentrations more than 6 g/L are associated with a dramatic decrease in α -factor due to the shear-thinning nature of the solid suspension that increases bubble coalescence and decreases the gas transfer interfacial area when compared to clean water. The gap between 4 g/L and 6 g/L is where clarifiers are solids limited and the use of MBR is not economically preferred.

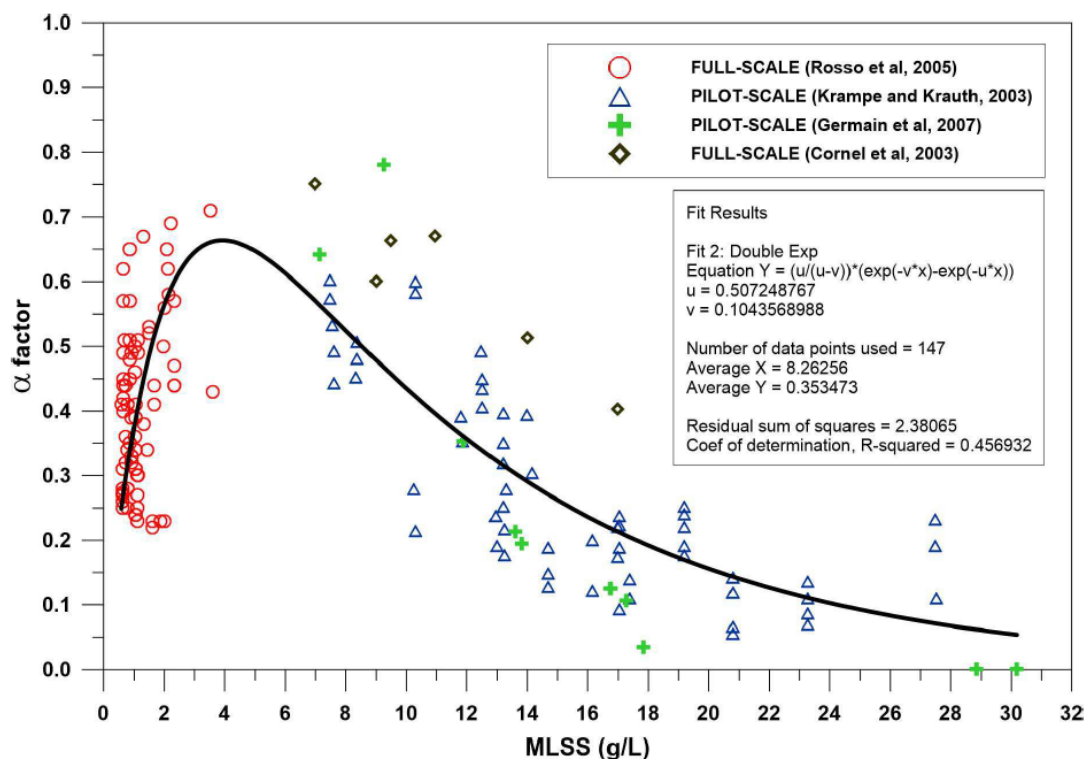


Figure 2-13. Correlation between α -factor and MLSS within the range between 0.5 g/L to 30 g/L (Baquero-Rodríguez et al., 2018).

2.3.3.4 Extracellular Polymeric Substances (EPS) and soluble microbial products (SMP)

Germain et al., 2007, using statistical analysis, identified the impact of different biomass characteristics including the microbial aggregates, EPS, and SMP on OTE for the MLSS concentrations ranging between 7 g/L and 30 g/L. Only the EPS carbohydrate fraction was found to impact OTE. This fraction contributes to the basic structure of the EPS matrix, facilitating cell aggregation and the formation of large flocs which possess higher porosities and diffusivity when compared to small flocs (Wingender et al., 1999). Study results showed that oxygen transfer parameters including k_{la} and α -factor increased with the EPS carbohydrate fraction increase. SMP_{COD} fractionation was found to impact OTE; although, carbohydrate and protein SMP fractions did not impact OTE. Surfactants are organic molecules and COD measurements partly account for the presence of the surfactants in the

biomass. Surfactants directly impact k_{la} , by reducing the liquid film mass transfer coefficient, k_l , and by increasing the surface area (a). Study results showed that SMP_{COD} reduced k_{la} and α -factor due to the presence of surfactants, indicating that k_l was more impacted by SMP_{COD} than the surface area (a).

2.3.3.5 Primary treatment

Primary treatment impacts the aeration energy in two different ways. First, it reduces the energy required for aeration as it removes part of influent particulate biodegradable substrates and secondly, reduces fouling propensity due to the removal of particulate non-biodegradable substrates. Additionally, it increases the solids discharged to the digesters, enhancing the biogas energy recovery (Gori et al., 2013, 2011).

Flores-Alsina et al., 2014, 2012 used BSM2 to model the impact of primary clarifications on treatment energy and GHG emissions. Results showed that TSS removal efficiency of 50% was enough to balance the energy consumption and production. TSS removal efficiency of 66% produced more energy than the energy consumed; however, it negatively impacted the BNR process due to the inadequate C/N ratio. TSS removal efficiency of 33% increased energy consumption, reduced energy production, and overloaded the bioreactors, reducing the overall treatment efficiency. Gori et al., 2011 modeled the impact of COD and solids fractions on carbon and energy footprints. The results showed the impact of variable ratios of particulate pCOD/VSS and soluble sCOD/COD on energy footprint and energy recovery due to carbon emissions. Increasing pCOD/VSS ratio increased the active biosolids discharged to the digester which, consequently, increases the energy recovery. On the other hand, increasing the sCOD/COD ratio increased the energy required for the aeration and the emissions from the processed carbon. In a similar study, Gori et al., 2013 used ASM3 combined with ADM1 to quantify energy and carbon footprints using data from two municipal wastewater treatment plants in two different regions; Europe and North America. The primary sedimentation process reduced the overall energy demand by 3.9%-4.4% and increased the energy recovery by 17% to 55% depending on the pCOD/VSS ratio in the influent raw wastewater. Although using coagulants was recommended by the

authors to enhance the primary treatment, additional sources of carbon in the form of readily biodegradable rbCOD would be required for the denitrification process.

2.3.3.6 Diffusers fouling

Depending on the physical and chemical properties of different types of diffusers, bacteria in liquid adhere to the diffuser's material forming a biofilm (Fletcher, 1996) and, as time progresses, the bacteria in the two microhabitats (i.e. suspended bacteria and the biofilm) separate in both diversity and bacterial abundance (Besemer et al., 2012). The ethylene propylene diene monomer (EPDM) and polyurethane (PU) diffusers are composed of organic compounds that could be utilized as a carbon source for bacteria while the silicone diffusers consist of inorganic materials (Hansen et al., 2004; Wagner and von Hoessle, 2004). Noble et al., 2016 studied the biofilm community composition, function, and diversity change with the time in the two microhabitats liquid and the biofilm. Three diffusers substrates were tested; EPDM, PU, and silicone. Since MLSS are responsible for colonizing the diffusers' surface and biofilm formation, biofilm development for each diffuser was measured two times after three and nine months and compared with the bacteria in the MLSS. The physical and chemical properties of the diffusers played a great role in changing the bacterial diversity between the suspended bacteria and the biofilm. After three months, bacterial communities in the EPDM and the silicone biofilms were observed to be similar to bacterial communities in the MLSS; however, bacterial communities in the polyurethane biofilm were dissimilar to those in the liquid. In contrast, after nine months, bacterial communities in the EPDM and the silicone biofilms were different from bacterial communities in the liquid, and bacterial communities in the polyurethane biofilm were similar to those communities in the MLSS. This was explained by the diffusers' selectivity due to local factors, including, diffusers' chemical properties, and bacterial interactions. The increase in diversity of the EPDM and silicone diffusers was presumed to be due to a transition from mid- to late-stage biofilm development which suggested that some of the increased diversity could be due to the recruitment of secondary colonizers from the suspended bacteria. Alternatively, the decrease in bacterial diversity for the polyurethane biofilms was due to a transition from early to mid-stage biofilm

development, reflecting slower biofilm development on polyurethane diffusers than the other diffusers substrates.

Fine pore diffusers' performance deteriorates with time due to inorganic and organic compounds that lead to scaling and biofouling (Rosso and Stenstrom, 2006). The organic biofouling consists of bacterial flocs, protozoa, soluble microbial products, and extracellular polymeric substances, as well as the particulate and soluble substrate in the influent wastewater. Inorganic scaling consists of inorganic salts precipitation such as carbonate, sulfate, and silica that impact the diffusers' material properties. The combined effect of organic and inorganic foulants and material aging was defined as fouling (Fig. 2-14) (Garrido-Baserba et al., 2016). The existence of organic foulants changes the air bubbles character by increasing the bubble size and reducing their surface area (Rieth et al., 1990). Practically, coarse bubbles were observed in the influent zone where the organic loading rate is relatively high (Rieth et al., 1990; Rosso et al., 2008b). The diffusers' surface is a convenient environment for biofilm to form due to oxygen and substrates availability, surface biocompatibility for adhesion, and convective flows to transport bacterial cells from the suspended mixed liquor to the diffuser surface. In addition to the influent substrates, the soluble microbial products (SMP) produced by the planktonic biomass serve as a substrate for the sessile microbial community (Garrido-Baserba et al., 2016). Fouling was linked to low airflow, and low DO as it primarily occurred due to the existence of high soluble organic loading rates. (Rieth et al., 1990).

To account for fouling, the fouling factor (F) is calculated using the ratio of α -factor after a particular time to the initial α -factor ($F=\alpha(t)/\alpha(0)$) (Garrido-Baserba et al., 2016, 2017). In addition, other measurements can be performed to understand the diffusers deformation with time. Rieth et al., 1990 used the dynamic wet pressure (DWP) and bubble release vacuum (BRV) to evaluate the impact of diffusers' fouling on the aeration efficiency. The BRV test is performed by applying pressure on a small localized area on the surface of the diffuser to determine the effective pores diameter as well as the uniformity of the pore, which makes it more sensitive than DWP to fouling. Also, the ratio of DWP to BRV shows the fraction of active pores in the diffuser's surface area. Results showed that oxygen

transfer efficiency reduction correlated with the decrease of the ratio of DWP to BRV. Kim and Boyle, 1993 studied the fouling mechanisms using three types of foulants; organics, inorganics, and a combination of organic and inorganic compounds. Results showed that inorganic compounds such as CaCO_3 , or sand have a more significant impact on the diffuser's performance compared to organic biomass; however, diffusers were colonized primarily with the biomass due to their watery and viscous properties.

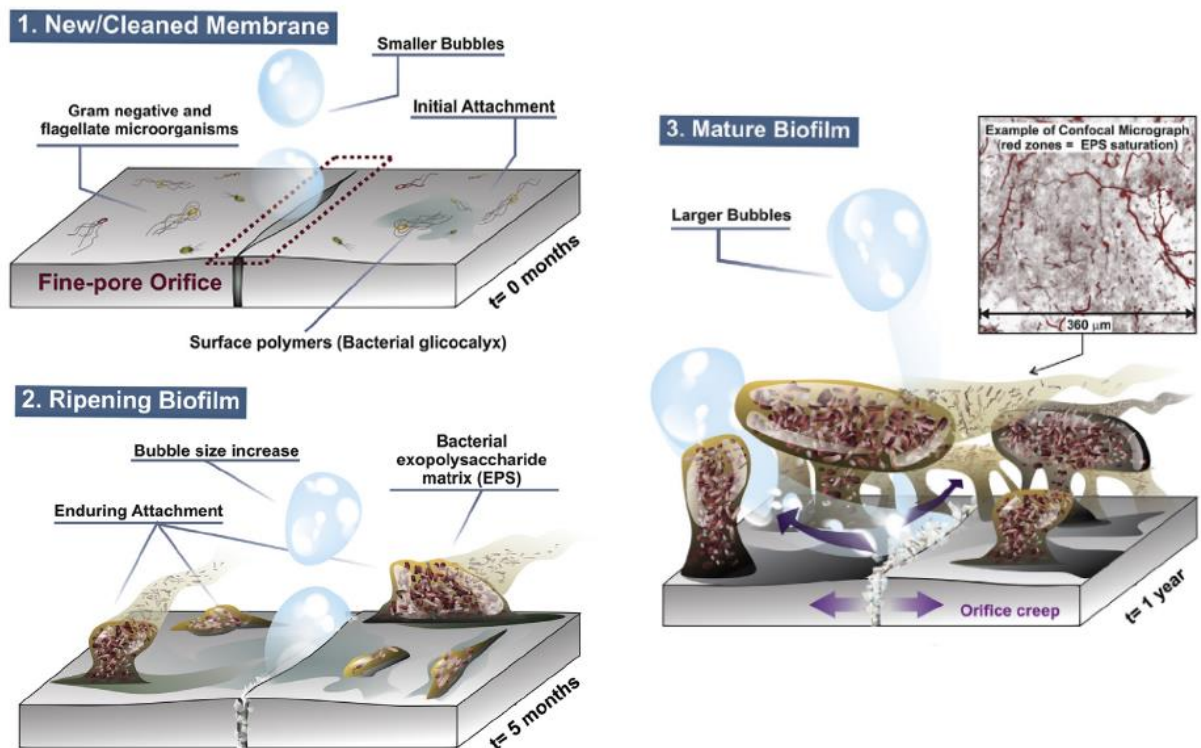


Figure 2-14. The biofilm development on the fine pore diffuser's surface, with micrographs screening the diffuser material and organic and inorganic coating details (Garrido-Baserba et al., 2016).

Kaliman et al., 2008 studied membrane aging using different types of membranes EPDM, and PU by subjecting them to a static load while being submerged in chemical solutions to speed up aging. Periodic testing including Young's modulus, hardness, and orifice creep was performed to test the membrane deformation with the time. Polymeric membranes have additives such as plasticizers in their composition to enhance their mechanical and

chemical properties. The biofilm formation biodegrades some of these additives, changing the membrane properties, and hence performance. Study results showed that Yong's modulus and hardness along with the DWP build-up measurements were not enough to evaluate the membrane deformation as they showed a slow change with time. Orifice creeps using an optical microscope showed more rapid detection of the membrane change with time. In addition, it showed the differences in the performance of the same membrane material subjected to different chemical cycles. Also, applying this test does not require sacrificing the tested membrane which means that this method can be used to monitor the membrane performance during service.

Leu et al., 2009 used the off-gas approach for real-time monitoring to study the impact of the diffusers cleaning on the aeration efficiency over time. Results showed that after five months OTE decreased from 18.3% to 16.3%, increasing the aeration energy by 21% due to the DWP increase associated with the air distribution head losses increase. Also, diffusers cleaning helped to recover the α SOTE from 16.1% to 18.6%, reducing the energy demand by 18%, reflecting that cleaning frequency could be calculated by balancing the cost of the cumulatively wasted power with the cleaning cost.

Garrido-Baserba et al., 2016 studied the biofilm characteristics and compared the aeration performance of different types of fine pore diffusers to link between the biofilm formation and the aeration efficiency deterioration. Different types of diffusers were installed: membrane tubes (EPDM, PU, and silicone SI 50 mm), and discs (EPDM, and ceramic). Off-gas tests were used to measure oxygen transfer efficiencies, and the DNA measurements were used to quantify the biofilm growth. The fouling factor decreased with time and stabilized after 24 months at 50% of the initial value. DNA measurements and extracellular polymeric substances (EPS) analysis were performed to quantify the biological growth and monitor their color, texture, and membrane dimensions changes. Energy-dispersive X-ray spectroscopy (EDX) was used to characterize the diffusers' surface to compare the elemental compositions of the used membranes with the new membranes. These analyses showed that 85%-90% of the attached materials were organics, and 10%-15% were inorganics. Also, the deterioration of aeration efficiency with DNA

increase showed that an average increase of 2-log in DNA concentration decreased F by 20%, 3-log increase reduced F by 30%, and 4-log increase diminished F by 40%-45%, after stabilization. The agglomeration parameter ($\alpha F = \alpha(t)$) was used to link the aeration efficiency deterioration with the (F) factor. Although the study's results showed that the EPDM disc had the highest DNA concentration, it had better performance in terms of the αF than the membrane tubes, which was attributed to the additive effect of both changes in the diffuser's mechanical properties due to the time-dependent degradation of the diffuser's material as well as microbial fouling. Furthermore, the aeration efficiency deterioration at high, and low loading rates were evaluated after 5 and 12 months. Diffusers running at high loading rates (i.e. low SRT, and high MLSS) exhibited higher DNA concentrations than at a low rate. After 12 months DNA was shown to be proportionally larger than DNA detected after five months which indicated that the biofilm matured during the operation. Also, the differences in DNA between high and low rates after five months were greater than the difference after 12 months which is potentially due to the initial colonization.

Garrido-Baserba et al., 2017 modeled the link between aeration efficiency deterioration due to diffusers fouling and aeration energy demand. Different types of diffusers including, membrane tubes (EPDM, polyurethane, and silicone) and discs (EPDM, and ceramic) were installed at a treatment plant, operating at a low organic loading rate (influent COD= 295 ± 39 mg/L; SRT; 8 ± 2.7 d; MLSS: 2500 ± 400 mg/L; OUR: 80-90 mg/L.h), and located in a warm climate. Another set consisting of six diffusers were installed in another pilot treatment process located in an area with four seasons. This treatment pilot was running at high loading rate for carbon removal only (influent COD= 2500 ± 1500 mg/L; SRT: 2.5 ± 0.4 d; MLSS; 7000 ± 1400 mg/L; OUR: 50-60 mg/L.h). Oxygen transfer efficiency under process conditions was measured using the off-gas approach. The results showed that aeration efficiency decreased for both installed systems; however, diffusers in the high loading rate pilot showed a steeper decrease in the aeration efficiency than in the low rate plant. This steep decline was due to the high loading rates of COD, and surfactants that hindered the oxygen transfer process which consequently, reduced α -factor. After 15-months of operation, α -factor decreased by $27 \pm 8\%$ at low rate conditions, and $37 \pm 5\%$ at high rate conditions increasing the energy demand by 32%, and 42% respectively. After

24 months, (αF) decreased to around 0.4, and 0.5 for the high, and low rate conditions, respectively. Diffusers types affected energy demand including, primary energy consumption, and power consumption increase due to fouling. For instance, SI 50mm diffusers demonstrated a higher power consumption (123 kWh/1000m³) than 75 mm EPDM diffusers (95 kWh/1000m³), however, SI 50mm diffusers showed stable performance with the time which reduces the operating costs and cleaning frequency.

2.3.4 Design parameters affecting OTE

2.3.4.1 Diffusers density

Diffusers' density represents the area covered by diffusers relative to the total area of the aeration tanks floor. Typically, increasing diffusers' density improves OTE. There is a maximum value for the diffuser density, where the increase in SOTE is minimal, depending on the diffusers' size, airflow rates, and the space between the diffusers (Baquero-Rodríguez et al., 2018).

2.3.4.2 Bioreactor configuration

Aerobic reactors can be designed as plug-flow reactors (PFR) or completely mixed stirred reactors (CSTR). Each design has a set of conditions that impact the treatment performance as well as oxygen transfer efficiency (Baquero-Rodríguez et al., 2018).

In a plug flow reactor, the fluid flow through the reactor parallels to the reactor axis as plugs with no longitudinal mixing. All fluid particles have the same residence time in the reactor. The concentrations of various contaminants and the oxygen demand change spatially (Jenkins, 2013, Rosso, 2018). Plug flow reactors have low α -factor at the inlet but increase due to biodegradation. Therefore, tapered aeration is preferred for plug flow reactors to provide high air flow rates at the inlet and low air flow rates at the exit. (Brade and Shahid, 1993; Garrido-Baserba et al., 2020; Mueller et al., 2000). In plug flow reactors, pre-anoxic denitrification improves the α -factor and reduces the aeration energy by 12%-27% (Mueller et al., 2000, Rosso and Stenstrom, 2005).

CSTRs are used mostly at low or atmospheric pressures for liquid-phase reactions. In CSTR, the reactant flows into the reactor continuously, the product effluent flows out continuously and the contents of the reactor are mixed continuously. The concentrations of various contaminants are uniform within the tank (Jenkins, 2013). In CSTR, uniform and high α -factors were observed when compared to plug flow reactors due to the uniform distribution of the pollutants (Baquero-Rodríguez et al., 2018; Brade and Shahid, 1993; Jenkins, 2013). Practically, in CSTRs the stirrers are the main gas dispersing devices that provide mixing and aeration, and their speed and size have a detrimental effect on oxygen transfer (Garcia-Garcia et al., 2011). Zhu et al., (2001) showed that using radial flow impellers increased the oxygen mass transfer by 17% when compared to axial flow impellers. Also, Puthli et al. (2005) found that oxygen transfer efficiency and energy consumption were significantly improved with a triple impeller system.

2.3.4.3 Aeration tank depth

The bubble size and surface area change with depth due to pressure reduction, bubble splitting and coalescence, and oxygen and nitrogen mass transfer to and from the bubble. Current OTE measurement methods assume a constant k_1 value over depth that should be reasonably acceptable if plume turbulence does not differ significantly with depth. (DeMoyer et al., 2003).

Typically, aeration tanks' depth varies between 3m to 12m depending on the available surface area (Wagner and Pöpel, 1998). The OTE of the aerobic reactor increases with the depth increase due to the increase of the residence time of the bubbles, and the greater partial oxygen pressure at the time of bubble formation. The operating pressure also increases for the blower as the partial pressure increases with the diffusers' depth. The standard aeration efficiency (SAE) (kgO_2/kWh), however, remains constant since depth increase is associated with energy consumption increase (Baquero-Rodríguez et al., 2018). Aeration energy increases linearly with the depth increase and therefore, balancing energy consumption and oxygen transfer efficiency while designing aeration tanks is necessary. (Eckenfelder, 1952).

2.3.5 Aeration modeling

Historically, process models for activated sludge systems relied on the constant α -factor inputs (Henze et al., 1987; Jiang et al., 2017; Metcalf & Eddy, 2014; Henze et al., 2015). In fact, the α -factor is sensitive to several parameters including the dynamic change in the influent wastewater characteristics, and operating conditions (e.g., SRT, the temporal change in the concentrations of the organic inside the bioreactor due to biodegradation) (Leu et al., 2009). Ignoring these variables while assuming constant α -factor leads to either overestimating or underestimating the aeration energy requirements.

Wagner and Pöpel, 1998 were the first to improve aeration modeling as they correlated oxygen transfer efficiency parameters including SOTR and k_{La} to airflow rate and diffusers submergence. Rosso et al., 2005 normalized the SRT, air flow rate, diffuser, and tank geometry, to reduce process data and create empirical correlations for α SOTE and α -factors. Gillot et al., 2005 tried to minimize uncertainty in-process data by conducting dimensional analysis and generating correlations that depended on different entities, such as surface gas velocity and dynamic surface tension. Gillot and Héduit, 2008 have specified a new composite variable (Equivalent Contact Time) that is a function of the SRT, kLa , and air flow rates to predict the α -factor in fine pore aeration systems. Pittoors et al., 2014 developed a mathematical model for the oxygen transfer efficiency in both clean and process water using experimental measurements from a cylindrical batch reactor (2.7-9.3 L). The model correlates k_{La} to nine operating variables including reactor volume, height, diameter, surface area, airflow rate, diffusers surface area and depth, bubble size, and dynamic viscosity. Jiang et al., 2017 developed a dynamic aeration model that described the change in oxygen transfer efficiency due to the change in the influent COD. Their results showed that the α -factor decreased exponentially with the influent total COD to the secondary treatment (Fig. 2-15).

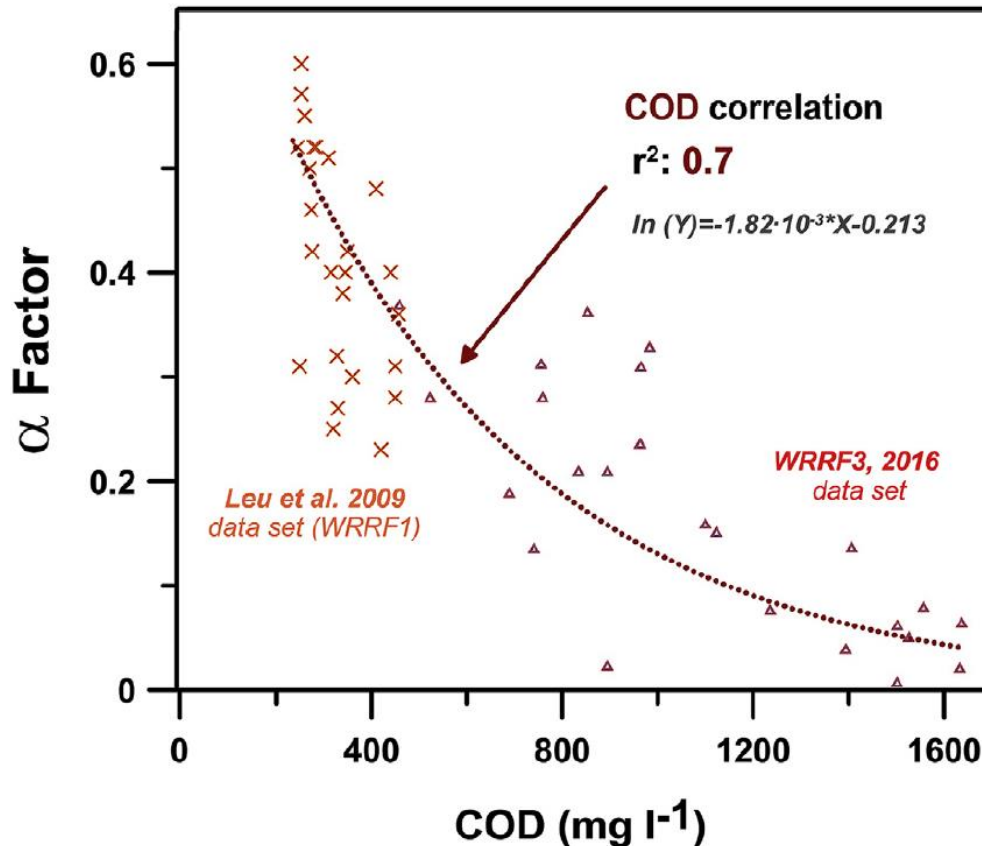


Figure 2-15. The correlation between α -factor and the influent COD (Jiang et al., 2017)

2.4 Volatile fatty acids (VFA) production and impact on the BNR

Biological nutrient removal (BNR) is commonly applied in municipal wastewater treatment plants (WWTPs) to remove phosphorus and nitrogen. However, the lack of organic substrates in domestic wastewater is a major obstacle to BNR systems, whereas significant amounts of waste activated sludge (WAS) are invariably generated in WWTPs and the associated treatment processes are expensive (Liu et al., 2017). VFA is a carbon source that can efficiently enhance the BNR process and can be generated through the fermentation of primary sludge, waste activated sludge (WAS), or a mixture of both

(Liu et al., 2017; Yuan et al., 2016, 2016; Zheng et al., 2010). The carbon source is important to balance nutrients ratio and stabilize the BNR process. The practical carbon to nitrogen ratio for the nitrification/denitrification process ranges from 5 to 10 mg COD/mg N (Lee et al., 2014). To achieve phosphorus removal, 7.5-10.7 mg of COD is required to remove 1 mg of phosphorus (Lee et al., 2014). Tong and Chen, 2007 who studied the impact of WAS-derived VFA and acetate on the removal efficiency of phosphorus showed that WAS-derived VFA achieved higher phosphorus removal (99%) than acetate (71%). Zheng et al., 2010 studied the impact of WAS derived VFA and synthetic acetate on phosphorus and nitrogen removal and showed that WAS derived VFA achieved higher removal efficiencies of 82% and 95% for nitrogen and phosphorus, respectively compared to 74% and 87% achieved by acetate. Liu et al., 2016 studied the impact of methanol, acetic acid, propionate, glucose, and fermented primary sludge on the denitrification rate. At a total nitrogen concentration of 45 mg/L, methanol achieved a removal efficiency of 81% while other carbon sources achieved complete removal of nitrogen. At an initial total nitrogen concentration of 70 mg/L, glucose and fermented primary sludge showed the highest denitrification rates of 0.2 and 0.17 mg NO₃-N/mg MLSS.d, respectively. Acetic acid, propionate, and methanol showed denitrification rates of 0.105, 0.092, and 0.086 mg NO₃-N/mg MLSS.d, respectively. Wang et al. (Wang et al., 2016) used the fermented WAS as a carbon source. Results showed that 95% of nitrate was converted to nitrogen.

2.5 Synopsis of the literature

Cellulose fibers in municipal wastewater originating from toilet paper represent a significant fraction of the influent particulate organics that could be recovered with a primary solids separation (Honda et al., 2000; Ruiken et al., 2013). Cellulose can be biodegraded to carbon dioxide and water under aerobic conditions, and carbon dioxide, methane, and water under anaerobic conditions (Edberg and Hofsten, 1975; O'Sullivan et al., 2007; Pérez et al., 2002) reflecting that under certain environmental conditions, cellulose degradation may consume a substantial amount of oxygen (Hofsten and Edberg, 1972).

The secondary treatment process is the most intensive part of the WWTPs in terms of energy consumption. The aeration process consumes 45% -75% of the treatment plant's net energy requirement (Reardon, 1995). To assess the energy required for the aeration process, OTE parameters should be accurately quantified. There are three main methods to measure OTE parameters: steady-state, non-steady-state, and off-gas methods. The off-gas technique is classified as the most powerful tool in measuring OTE under process conditions. Likewise, it does not require modifying DO concentrations as required for the non-steady method, which makes it an economical testing technique for operating WWTPs (Leu et al., 2009).

Many factors were observed to influence the OTE, including, wastewater quality, (SRT), primary treatment efficiency, diffusers fouling, diffusers types, diffusers substrates types, operation, and design parameters, and other temporal variabilities (e.g. temperature and sewer network length) (Baquero-Rodríguez et al., 2018). Wastewater characteristics have a significant impact on OTE. The existence of the surfactants in the influent wastewater reduces the OTE as they migrate to the bubble surface, reducing surface tension, gas-liquid interfacial renewal rate, and gas diffusivity and circulation (Rosso and Stenstrom, 2006). Additionally, high concentrations of biodegradable substrates increase the required aeration and, consequently, increase the energy demand. Thus, improving the aerobic bioreactor influent water quality causes a substantial reduction in aeration energy. SRT is a key design and operational parameter in the biological treatment process design. Increasing SRT for the nitrification process was observed to increase the oxygen demand, and energy consumption; however, increasing SRT associated with nitrification/denitrification processes enhanced the oxygen transfer efficiency, reducing the energy required for the aeration process (Rosso et al., 2005).

Primary treatment impacts both wastewater and sludge treatment processes. In reality, preclarified wastewater exerts low oxygen demand, which, consequently, leads to lower energy consumption. Besides, primary treatment reduces the inert particulate COD and mineral (TSS) discharged to the biological process and redirects the removed solids to the digesters, improving the biogas energy recovery process. Primary treatment processes

could be enhanced chemically using coagulants or polymers, which reduces the rbCOD available for denitrification. In this case, an additional carbon source will be required to balance the COD/N ratio (Lee et al., 2014).

VFA produced by primary sludge and WAS fermentation can be used as a carbon source for the BNR enhancement, reducing the overall treatment cost. Also, the literature showed that sludge derived VFA has a superior impact on the BNR than other commercial carbon sources. WAS derived VFA showed removal efficiencies of 83%-89% for nitrogen and 95%-99% for phosphorus. Primary sludge derived VFA showed complete removal of nitrogen.

2.6 Knowledge Gaps

Given that most of the methods developed to measure cellulose in wastewater were published in the 1970s and 1980s, and since then have not been further validated, cellulose removal efficiency across treatment processes in all the studies reviewed is a clear knowledge gap. Additionally, it is noticeable that the estimated cellulose degradation efficiencies in all the abovementioned studies were established under controlled conditions (i.e. lab-scale or nylon bags). Only a few studies measured cellulose in full-scale treatment plants (e.g. (Honda et al., 2000), and (Ruiken et al., 2013)); however, biodegradation efficiencies, as well as physical removal efficiency through treatment processes, have not been accurately estimated due to neglecting the effect of cellulose accumulation in the biological systems which can only be considered using mass balance calculations. Despite the significant experimental attempts to estimate cellulose biodegradation efficiency under aerobic and anaerobic conditions, only two studies modeled the cellulose biodegradation process under aerobic conditions, assuming that cellulose biodegradation rates under both anoxic and aerobic conditions were identical. (Benneouala et al., 2017; Reijken et al., 2018).

The impact of influent organic loading rates on aeration efficiency has been addressed experimentally in several studies (e.g., Gori et al., 2011; Jiang et al., 2017; Leu et al., 2009; Rosso et al., 2005). However, the real-time impact of biodegradation of these organics on

the OTE during the aeration process is a clear knowledge gap. While all commercial softwares allow the use of dynamic alpha factors, none of the existing models captures the time-dependency of the alpha factor on substrate biodegradation kinetics. In addition, the impact of cellulose on aeration efficiency has never been studied before. Furthermore, the role of biomass in oxygen transfer is not completely understood. According to the literature, all studies by (Campbell et al., 2019; Cornel et al., 2003; Germain et al., 2007; Henkel et al., 2011; Krampe and Krauth, 2003) were implemented in MBR systems where α -factor is negatively impacted by MLSS concentrations. Apparently, produced correlations between α -factor and MLSS from those studies were primarily driven by the high MLSS concentrations (> 7 g/L) and high SRT. Rosso et al., 2005 was the only study to correlate α -factor and MLSS at relatively low MLSS concentrations between 1-4 g/L, showing that α -factor improved with the MLSS increase.

Additionally, due to the knowledge gap in estimating the dynamic α -factor, the influence of the bioreactor configuration as well as the pre-denitrification process on the dynamics of aeration energy is another important knowledge gap.

Diverting cellulose from the mainstream to the biosolids stream through primary treatment is beneficial to enhance BNR as a result of primary sludge fermentation. The impact of the recovered VFA through fermentation on the aeration energy as well as oxygen transfer efficiency is a clear knowledge gap.

References

- Alvarez, J.V.L., Larrucea, M.A., Bermúdez, P.A., Chicote, B.L., 2009. Biodegradation of paper waste under controlled composting conditions. *Waste Manag.*, First international conference on environmental management, engineering, planning and economics 29, 1514–1519. <https://doi.org/10.1016/j.wasman.2008.11.025>
- Alves, S.S., Orvalho, S.P., Vasconcelos, J.M.T., 2005. Effect of bubble contamination on rise velocity and mass transfer. *Chem. Eng. Sci.* 60, 1–9. <https://doi.org/10.1016/j.ces.2004.07.053>
- ASCE (Ed.), 1997. Standard guidelines for in-process oxygen transfer testing, ASCE standard. American Society of Civil Engineers, New York.
- ASCE, 1993. *Measurement of Oxygen Transfer in Clean Water*, 2nd ed. American Society of Civil Engineers, New York, NY. <https://doi.org/10.1061/9780872628854>
- Baquero-Rodríguez, G.A., Lara-Borrero, J.A., Nolasco, D., Rosso, D., 2018. A Critical Review of the Factors Affecting Modeling Oxygen Transfer by Fine-Pore Diffusers in Activated Sludge. *Water Environ. Res.* 90, 431–441. <https://doi.org/10.2175/106143017X15131012152988>
- Bauer, S., Ibáñez, A.B., 2014. Rapid determination of cellulose. *Biotechnol. Bioeng.* 111, 2355–2357. <https://doi.org/10.1002/bit.25276>
- Behera, C.R., Santoro, D., Gernaey, K.V., Sin, G., 2018. Organic carbon recovery modeling for a rotating belt filter and its impact assessment on a plant-wide scale. *Chem. Eng. J.* 334, 1965–1976. <https://doi.org/10.1016/j.cej.2017.11.091>
- Benneouala, M., Bareha, Y., Mengelle, E., Bounouba, M., Sperandio, M., Bessiere, Y., Paul, E., 2017. Hydrolysis of particulate settleable solids (PSS) in activated sludge is determined by the bacteria initially adsorbed in the sewage. *Water Res.* 125, 400–409. <https://doi.org/10.1016/j.watres.2017.08.058>

- Besemer, K., Peter, H., Logue, J.B., Langenheder, S., Lindström, E.S., Tranvik, L.J., Battin, T.J., 2012. Unraveling assembly of stream biofilm communities. *ISME J.* 6, 1459–1468.
- Boztas, S., 2017. The ick factor: Dutch project making bike lanes and bottles from used loo roll. *The Guardian*.
- Brade, C.E., Shahid, K., 1993. Advances in the Design of Fine Bubble Aeration Plants. *Water Sci. Technol.* 28, 343–350. <https://doi.org/10.2166/wst.1993.0252>
- Campbell, K., Wang, J., Liu, G., Daigger, G., 2019. Activated sludge morphology significantly impacts oxygen transfer at the air–liquid boundary. *Water Environ. Res.* 91, 500–509. <https://doi.org/10.1002/wer.1066>
- Chakraborty, T., 2015. Evaluation of Filtration Performance of a Rotating Belt Filter for Different Primary Wastewater Influent. MSc., The University of Western Ontario.
- Cornel, P., Wagner, M., Krause, S., 2003. Investigation of oxygen transfer rates in full scale membrane bioreactors. *Water Sci. Technol. J. Int. Assoc. Water Pollut. Res.* 47, 313–319.
- DeMoyer, C.D., Schierholz, E.L., Gulliver, J.S., Wilhelms, S.C., 2003. Impact of bubble and free surface oxygen transfer on diffused aeration systems. *Water Res.* 37, 1890–1904. [https://doi.org/10.1016/S0043-1354\(02\)00566-3](https://doi.org/10.1016/S0043-1354(02)00566-3)
- DuBois, Michel., Gilles, K.A., Hamilton, J.K., Rebers, P.A., Smith, Fred., 1956. Colorimetric Method for Determination of Sugars and Related Substances. *Anal. Chem.* 28, 350–356. <https://doi.org/10.1021/ac60111a017>
- Eckenfelder, W.W., 1952. Aeration Efficiency and Design: I. Measurement of Oxygen Transfer Efficiency. *Sew. Ind. Wastes* 24, 1221–1228.

- Edberg, N., Hofsten, B. v., 1975. Cellulose Degradation in Wastewater Treatment. *J. Water Pollut. Control Fed.* 47, 1012–1020.
- Fisher, M.J., Boyle, W.C., 1999. Effect of anaerobic and anoxic selectors on oxygen transfer in wastewater. *Water Environ. Res.* 71, 84–93.
- Fletcher, M. (Ed.), 1996. Bacterial adhesion: molecular and ecological diversity, Wiley series in ecological and applied microbiology. John Wiley & Sons, New York.
- Flores-Alsina, X., Arnell, M., Amerlinck, Y., Corominas, L., Gernaey, K.V., Guo, L., Lindblom, E., Nopens, I., Porro, J., Shaw, A., 2012. A dynamic modelling approach to evaluate GHG emissions from wastewater treatment plants, in: *World Congress on Water, Climate and Energy*. pp. 2012–18.
- Flores-Alsina, X., Arnell, M., Amerlinck, Y., Corominas, L., Gernaey, K.V., Guo, L., Lindblom, E., Nopens, I., Porro, J., Shaw, A., Snip, L., Vanrolleghem, P.A., Jeppsson, U., 2014. Balancing effluent quality, economic cost and greenhouse gas emissions during the evaluation of (plant-wide) control/operational strategies in WWTPs. *Sci. Total Environ.* 466–467, 616–624.
<https://doi.org/10.1016/j.scitotenv.2013.07.046>
- Franchi, A., Williams, K., Lyng, T.O., Lem, W., Santoro, D., 2015. Rotating Belt Filters as Enabling Technology for Energy-Neutral Wastewater Treatment Plants: Current Status and Applications. *Proc. Water Environ. Fed.* 2015, 1743–1749.
<https://doi.org/10.2175/193864715819540847>
- Garcia-Garcia, E., Pun, J., Perez-Estrada, L.A., Din, M.G.-E., Smith, D.W., Martin, J.W., Belosevic, M., 2011. Commercial naphthenic acids and the organic fraction of oil sands process water downregulate pro-inflammatory gene expression and macrophage antimicrobial responses. *Toxicol. Lett.* 203, 62–73.
<https://doi.org/10.1016/j.toxlet.2011.03.005>

- Garner, F.H., Hammerton, D., 1954. Circulation inside gas bubbles. *Chem. Eng. Sci.* 3, 1–11. [https://doi.org/10.1016/0009-2509\(54\)80001-7](https://doi.org/10.1016/0009-2509(54)80001-7)
- Garrido-Baserba, M., Asvapathanagul, P., McCarthy, G.W., Gocke, T.E., Olson, B.H., Park, H.-D., Al-Omari, A., Murthy, S., Bott, C.B., Wett, B., Smeraldi, J.D., Shaw, A.R., Rosso, D., 2016. Linking biofilm growth to fouling and aeration performance of fine-pore diffuser in activated sludge. *Water Res.* 90, 317–328. <https://doi.org/10.1016/j.watres.2015.12.011>
- Garrido-Baserba, M., Rosso, D., Odize, V., Rahman, A., Van Winckel, T., Novak, J.T., Al-Omari, A., Murthy, S., Stenstrom, M.K., De Clippeleir, H., 2020. Increasing oxygen transfer efficiency through sorption enhancing strategies. *Water Res.* 116086. <https://doi.org/10.1016/j.watres.2020.116086>
- Garrido-Baserba, M., Sobhani, R., Asvapathanagul, P., McCarthy, G.W., Olson, B.H., Odize, V., Al-Omari, A., Murthy, S., Nifong, A., Godwin, J., Bott, C.B., Stenstrom, M.K., Shaw, A.R., Rosso, D., 2017. Modelling the link amongst fine-pore diffuser fouling, oxygen transfer efficiency, and aeration energy intensity. *Water Res.* 111, 127–139. <https://doi.org/10.1016/j.watres.2016.12.027>
- Germain, E., Nelles, F., Drews, A., Pearce, P., Kraume, M., Reid, E., Judd, S.J., Stephenson, T., 2007. Biomass effects on oxygen transfer in membrane bioreactors. *Water Res.* 41, 1038–1044. <https://doi.org/10.1016/j.watres.2006.10.020>
- Ghasimi, D.S.M., Zandvoort, M.H., Adriaanse, M., van Lier, J.B., de Kreuk, M., 2016. Comparative analysis of the digestibility of sewage fine sieved fraction and hygiene paper produced from virgin fibers and recycled fibers. *Waste Manag.* 53, 156–164. <https://doi.org/10.1016/j.wasman.2016.04.034>
- Gillot, S., Héduit, A., 2008. Prediction of alpha factor values for fine pore aeration systems. *Water Sci. Technol.* 57, 1265–1269. <https://doi.org/10.2166/wst.2008.222>

- Gillot, S., Kies, F., Amiel, C., Roustan, M., Héduit, A., 2005. Application of the off-gas method to the measurement of oxygen transfer in biofilters. *Chem. Eng. Sci.*, 7th International Conference on Gas-Liquid and Gas-Liquid-Solid Reactor Engineering 60, 6336–6345. <https://doi.org/10.1016/j.ces.2005.04.056>
- Gori, R., Giaccherini, F., Jiang, L.-M., Sobhani, R., Rosso, D., 2013. Role of primary sedimentation on plant-wide energy recovery and carbon footprint. *Water Sci. Technol.* 68, 870. <https://doi.org/10.2166/wst.2013.270>
- Gori, R., Jiang, L.-M., Sobhani, R., Rosso, D., 2011. Effects of soluble and particulate substrate on the carbon and energy footprint of wastewater treatment processes. *Water Res.* 45, 5858–5872. <https://doi.org/10.1016/j.watres.2011.08.036>
- Gude, V.G., 2015. Energy and water autarky of wastewater treatment and power generation systems. *Renew. Sustain. Energy Rev.* 45, 52–68. <https://doi.org/10.1016/j.rser.2015.01.055>
- Gupta, M., 2018. Microsieving as a Primary Treatment for Biological Nitrogen Removal from Municipal Wastewater. *Electron. Thesis Diss. Repos.*
- Gupta, M., Ho, D., Santoro, D., Torfs, E., Doucet, J., Vanrolleghem, P.A., Nakhla, G., 2018. Experimental assessment and validation of quantification methods for cellulose content in municipal wastewater and sludge. *Environ. Sci. Pollut. Res.* <https://doi.org/10.1007/s11356-018-1807-7>
- Hansen, E.J., Estevez, M.A., Es-Said, O.S., 2004. On the shrinking and hardening of EPDM rubber membranes in water sanitation filtration tanks. *Eng. Fail. Anal.* 11, 361–367.
- Harris, D., Bulone, V., Ding, S.-Y., DeBolt, S., 2010. Tools for Cellulose Analysis in Plant Cell Walls. *Plant Physiol.* 153, 420–426. <https://doi.org/10.1104/pp.110.154203>

- Henkel, J., Cornel, P., Wagner, M., 2011. Oxygen transfer in activated sludge – new insights and potentials for cost saving. *Water Sci. Technol.* 63, 3034–3038. <https://doi.org/10.2166/wst.2011.607>
- Henze, M., Grady, C.P.L., Gujer, W., Marais, G.V.R., Matsuo, T., 1987. A general model for single-sludge wastewater treatment systems. *Water Res.* 21, 505–515. [https://doi.org/10.1016/0043-1354\(87\)90058-3](https://doi.org/10.1016/0043-1354(87)90058-3)
- Henze, M., Gujer, W., Mino, T., Loosdrecht, M.C.M. van, 2000. *Activated sludge models ASM1, ASM2, ASM2d and ASM3*. IWA Publishing.
- Henze, M., van Loosdrecht, M.C.M., Ekama, G.A., Brdjanovic, D., 2015. *Biological Wastewater Treatment: Principles, Modelling and Design*. *Water Intell. Online* 7, 9781780401867–9781780401867. <https://doi.org/10.2166/9781780401867>
- Hofsten, B.V., Edberg, N., 1972. Estimating the Rate of Degradation of Cellulose Fibers in Water. *Oikos* 23, 29. <https://doi.org/10.2307/3543924>
- Honda, S., Miyata, N., Iwahori, K., 2002. Recovery of biomass cellulose from waste sewage sludge. *J. Mater. Cycles Waste Manag.* 4, 46–50.
- Honda, S., Miyata, N., Iwahori, K., 2000. A Survey of Cellulose Profiles in Actual Wastewater Treatment Plants. *Jpn. J. Water Treat. Biol.* 36, 9–14. <https://doi.org/10.2521/jswtb.36.9>
- Hurwitz, E., Beck, A.J., Sakellariou, E., Krup, M., 1961. Degradation of Cellulose by Activated Sludge Treatment. *J. Water Pollut. Control Fed.* 33, 1070–1075.
- Hwang, H.J., Stenstrom, M.K., 1985. Evaluation of fine-bubble alpha factors in near full-scale equipment 11.
- Jenkins, T.E., 2013. *Aeration Control System Design: A Practical Guide to Energy and Process Optimization*. John Wiley & Sons, Incorporated, Somerset, UNITED STATES.

- Jiang, L., Garrido-Baserba, M., Nolasco, D., Al-Omari, A., DeClippeleir, H., Murthy, S., Rosso, D., 2017. Modelling oxygen transfer using dynamic alpha factors. *Water Res.* 124, 139–148. <https://doi.org/10.1016/j.watres.2017.07.032>
- Kaliman, A., Rosso, D., Leu, S.-Y., Stenstrom, M.K., 2008. Fine-pore aeration diffusers: Accelerated membrane ageing studies. *Water Res.* 42, 467–475. <https://doi.org/10.1016/j.watres.2007.07.039>
- Khan, E., Babcock, R.W., Suffet, I.H., Stenstrom, M.K., 1998. Method development for measuring biodegradable organic carbon in reclaimed and treated wastewaters. *Water Environ. Res.* 70, 1025–1032.
- Kim, Y.-K., Boyle, W.C., 1993. Mechanisms of fouling in fine-pore diffuser aeration. *J. Environ. Eng.* 119, 1119–1138.
- Krampe, J., Krauth, K., 2003. Oxygen transfer into activated sludge with high MLSS concentrations. *Water Sci. Technol.* 47, 297–303. <https://doi.org/10.2166/wst.2003.0618>
- Krause, S., Cornel, P., Wagner, M., 2003. Comparison of different oxygen transfer testing procedures in full-scale membrane bioreactors. *Water Sci. Technol.* 47, 169–176.
- Lee, W.S., Chua, A.S.M., Yeoh, H.K., Ngoh, G.C., 2014. A review of the production and applications of waste-derived volatile fatty acids. *Chem. Eng. J.* 235, 83–99. <https://doi.org/10.1016/j.cej.2013.09.002>
- Leu, S.Y., Rosso, D., Larson, L.E., Stenstrom, M.K., 2009. Real-Time Aeration Efficiency Monitoring in the Activated Sludge Process and Methods to Reduce Energy Consumption and Operating Costs. *Water Environ. Res.* 81, 2471–2481. <https://doi.org/10.2175/106143009X425906>
- Liu, F., Tian, Y., Ding, Y., Li, Z., 2016. The use of fermentation liquid of wastewater primary sedimentation sludge as supplemental carbon source for denitrification

based on enhanced anaerobic fermentation. *Bioresour. Technol.* 219, 6–13.
<https://doi.org/10.1016/j.biortech.2016.07.030>

Liu, J., Yuan, Y., Li, B., Zhang, Q., Wu, L., Li, X., Peng, Y., 2017. Enhanced nitrogen and phosphorus removal from municipal wastewater in an anaerobic-aerobic-anoxic sequencing batch reactor with sludge fermentation products as carbon source. *Bioresour. Technol.* 244, 1158–1165.
<https://doi.org/10.1016/j.biortech.2017.08.055>

Mahendraker, V., Mavinic, D.S., Hall, K.J., 2005a. Comparison of oxygen transfer parameters determined from the steady state oxygen uptake rate and the non-steady-state changing power level methods. *J. Environ. Eng.* 131, 692–701.

Mahendraker, V., Mavinic, D.S., Rabinowitz, B., 2005b. Comparison of oxygen transfer parameters from four testing methods in three activated sludge processes. *Water Qual. Res. J. Can.* 40, 164–176.

Matters of Scale - Into the Toilet | Worldwatch Institute [WWW Document], n.d. URL <http://www.worldwatch.org/node/5142> (accessed 2.9.18).

Metcalf & Eddy, 2014. *Wastewater engineering: treatment and resource recovery*, Fifth edition / revised by George Tchobanoglous, H. David Stensel, Ryujiro Tsuchihashi, Franklin Burton ; contributing authors, Mohammad Abu-Orf, Gregory Bowden, William Pfrang. ed. McGraw-Hill Education, New York, NY.

Mueller, J.A., Kim, Y.-K., Krupa, J.J., Shkreli, F., Nasr, S., Fitzpatrick, B., 2000. Full-Scale Demonstration of Improvement in Aeration Efficiency. *J. Environ. Eng.* 126, 549–555. [https://doi.org/10.1061/\(ASCE\)0733-9372\(2000\)126:6\(549\)](https://doi.org/10.1061/(ASCE)0733-9372(2000)126:6(549))

Noble, P.A., Park, H.-D., Olson, B.H., Asvapathanagul, P., Hunter, M.C., Garrido-Baserba, M., Lee, S.-H., Rosso, D., 2016. A survey of biofilms on wastewater aeration diffusers suggests bacterial community composition and function vary by

- substrate type and time. *Appl. Microbiol. Biotechnol.* 100, 6361–6373.
<https://doi.org/10.1007/s00253-016-7604-7>
- Odegaard, H., 1998. Optimised particle separation in the primary step of wastewater treatment. *Water Sci. Technol., Pretreatment for Separation* 37, 43–53.
[https://doi.org/10.1016/S0273-1223\(98\)00297-2](https://doi.org/10.1016/S0273-1223(98)00297-2)
- Olsson, C., Westman, G., 2013. Direct Dissolution of Cellulose: Background, Means and Applications. *Cellul. - Fundam. Asp.* <https://doi.org/10.5772/52144>
- O’Sullivan, C., Burrell, P.C., Clarke, W.P., Blackall, L.L., 2007. A survey of the relative abundance of specific groups of cellulose degrading bacteria in anaerobic environments using fluorescence in situ hybridization. *J. Appl. Microbiol.* 103, 1332–1343. <https://doi.org/10.1111/j.1365-2672.2007.03362.x>
- Pasini, F., 2019. Energy Optimization of Secondary Treatment in WRRFs via Off-Gas and Respirometric Measurements (Ph.D.). University of California, Irvine, United States -- California.
- Pérez, J., Muñoz-Dorado, J., de la Rubia, T., Martínez, J., 2002. Biodegradation and biological treatments of cellulose, hemicellulose and lignin: an overview. *Int. Microbiol.* 5, 53–63. <https://doi.org/10.1007/s10123-002-0062-3>
- Pittoors, E., Guo, Y., Van Hulle, S.W.H., 2014. Oxygen transfer model development based on activated sludge and clean water in diffused aerated cylindrical tanks. *Chem. Eng. J.* 243, 51–59. <https://doi.org/10.1016/j.cej.2013.12.069>
- Pratt, S., Zeng, R., Yuan, Z., Keller, J., 2004. Comparison of methods for the determination of KLaO2 for respirometric measurements. *Water Sci. Technol.* 50, 153–161.
- Puthli, M.S., Rathod, V.K., Pandit, A.B., 2005. Gas–liquid mass transfer studies with triple impeller system on a laboratory scale bioreactor. *Biochem. Eng. J.* 23, 25–30. <https://doi.org/10.1016/j.bej.2004.10.006>

- Ramasamy, K., Meyers, M., Bevers, J., Verachtert, H., 1981. Isolation and characterization of cellulolytic bacteria from activated sludge. *J. Appl. Microbiol.* 51, 475–481.
- Reardon, D.J., 1995. Turning down the power. *Civ. Eng.* 65, 54–56.
- Redmon, D., Boyle, W.C., Ewing, L., 1983. Oxygen transfer efficiency measurements in mixed liquor using off-gas techniques. *J. Water Pollut. Control Fed.* 1338–1347.
- Reijken, C., Giorgi, S., Hurkmans, C., Pérez, J., van Loosdrecht, M.C.M., 2018. Incorporating the influent cellulose fraction in activated sludge modelling. *Water Res.* 144, 104–111. <https://doi.org/10.1016/j.watres.2018.07.013>
- Rieth, M.G., Boyle, W.C., Ewing, L., 1990. Effects of selected design parameters on the fouling characteristics of ceramic diffusers. *Res. J. Water Pollut. Control Fed.* 877–886.
- Rosso, D., 2018. *Aeration, Mixing, and Energy: Bubbles and Sparks*. IWA Publishing. <https://doi.org/10.2166/9781780407845>
- Rosso, D., Huo, D.L., Stenstrom, M.K., 2006. Effects of interfacial surfactant contamination on bubble gas transfer. *Chem. Eng. Sci.* 61, 5500–5514. <https://doi.org/10.1016/j.ces.2006.04.018>
- Rosso, D., Iranpour, R., Stenstrom, M.K., 2005. Fifteen years of offgas transfer efficiency measurements on fine-pore aerators: key role of sludge age and normalized air flux. *Water Environ. Res.* 77, 266–273.
- Rosso, D., Larson, L.E., Stenstrom, M.K., 2008a. Aeration of large-scale municipal wastewater treatment plants: state of the art. *Water Sci. Technol.* 57, 973–978. <https://doi.org/10.2166/wst.2008.218>

- Rosso, D., Libra, J.A., Wiehe, W., Stenstrom, M.K., 2008b. Membrane properties change in fine-pore aeration diffusers: Full-scale variations of transfer efficiency and headloss. *Water Res.* 42, 2640–2648. <https://doi.org/10.1016/j.watres.2008.01.014>
- Rosso, D., Lothman, S.E., Jeung, M.K., Pitt, P., Gellner, W.J., Stone, A.L., Howard, D., 2011. Oxygen transfer and uptake, nutrient removal, and energy footprint of parallel full-scale IFAS and activated sludge processes. *Water Res.* 45, 5987–5996. <https://doi.org/10.1016/j.watres.2011.08.060>
- Rosso, D., Stenstrom, M.K., 2006. Surfactant effects on α -factors in aeration systems. *Water Res.* 40, 1397–1404. <https://doi.org/10.1016/j.watres.2006.01.044>
- Rosso, D., Stenstrom, M.K., 2005. Comparative economic analysis of the impacts of mean cell retention time and denitrification on aeration systems. *Water Res.* 39, 3773–3780. <https://doi.org/10.1016/j.watres.2005.07.002>
- Ruiken, C.J., Breuer, G., Klaversma, E., Santiago, T., van Loosdrecht, M.C.M., 2013. Sieving wastewater – Cellulose recovery, economic and energy evaluation. *Water Res.* 47, 43–48. <https://doi.org/10.1016/j.watres.2012.08.023>
- Rusten, B., Odegaard, H., 2006. Evaluation and testing of fine mesh sieve technologies for primary treatment of municipal wastewater. *Water Sci. Technol.* 54, 31–38. <https://doi.org/10.2166/wst.2006.710>
- Schier, W., Frechen, F.-B., Fischer, St., 2009. Efficiency of mechanical pre-treatment on European MBR plants. *Desalination, International Membrane Science and Technology Conference 2007* 236, 85–93. <https://doi.org/10.1016/j.desal.2007.10.054>
- Singh, P., Kansal, A., Carliell-Marquet, C., 2016. Energy and carbon footprints of sewage treatment methods. *J. Environ. Manage.* 165, 22–30. <https://doi.org/10.1016/j.jenvman.2015.09.017>

- Soliman, M.A., Pedersen, J.A., Suffet, I.H. (Mel), 2004. Rapid gas chromatography–mass spectrometry screening method for human pharmaceuticals, hormones, antioxidants and plasticizers in water. *J. Chromatogr. A* 1029, 223–237.
<https://doi.org/10.1016/j.chroma.2003.11.098>
- Suñol, F., González-Cinca, R., 2019. Effects of gravity level on bubble detachment, rise, and bouncing with a free surface. *Int. J. Multiph. Flow* 113, 191–198.
<https://doi.org/10.1016/j.ijmultiphaseflow.2019.01.016>
- Tao, X., Chengwen, W., 2012. Energy consumption in wastewater treatment plants in China. Unpubl. Manuscr. Retrieved Httpwww Res.
NetprofileTaoXie11publication266146909Energy Consum. Pdf.
- Tong, J., Chen, Y., 2007. Enhanced Biological Phosphorus Removal Driven by Short-Chain Fatty Acids Produced from Waste Activated Sludge Alkaline Fermentation. *Environ. Sci. Technol.* 41, 7126–7130. <https://doi.org/10.1021/es071002n>
- Verachtert, H., Ramasamy, K., Meyers, M., Bevers, J., 1982. Investigations on cellulose biodegradation in activated sludge plants. *J. Appl. Microbiol.* 52, 185–190.
- Wagner, M., Pöpel, H.J., 1998. Oxygen transfer and aeration efficiency - influence of diffuser submergence, diffuser density, and blower type. *Water Sci. Technol.* 38, 1–6. <https://doi.org/10.2166/wst.1998.0163>
- Wagner, M., von Hoessle, R., 2004. Biological coating of EPDM-membranes of fine bubble diffusers. *Water Sci. Technol. J. Int. Assoc. Water Pollut. Res.* 50, 79–85.
- Waksman, S.A., Heukelekian, O., 1924. Microbiological analysis of soil as an index of soil fertility: VIII. Decomposition of cellulose. *Soil Sci.* 17, 275–292.
- Wang, X., Zhang, Y., Zhang, T., Zhou, J., Chen, M., 2016. Waste activated sludge fermentation liquid as carbon source for biological treatment of sulfide and nitrate in microaerobic conditions. *Chem. Eng. J.* 283, 167–174.
<https://doi.org/10.1016/j.cej.2015.07.062>

- Weimer, P.J., 1992. Cellulose Degradation by Ruminant Microorganisms. *Crit. Rev. Biotechnol.* 12, 189–223. <https://doi.org/10.3109/07388559209069192>
- Wingender, J., Neu, T.R., Flemming, H.-C., 1999. What are Bacterial Extracellular Polymeric Substances?, in: Wingender, J., Neu, T.R., Flemming, H.-C. (Eds.), *Microbial Extracellular Polymeric Substances: Characterization, Structure and Function*. Springer, Berlin, Heidelberg, pp. 1–19. https://doi.org/10.1007/978-3-642-60147-7_1
- Yuan, Y., Liu, J., Ma, B., Liu, Y., Wang, B., Peng, Y., 2016. Improving municipal wastewater nitrogen and phosphorous removal by feeding sludge fermentation products to sequencing batch reactor (SBR). *Bioresour. Technol.* 222, 326–334. <https://doi.org/10.1016/j.biortech.2016.09.103>
- Zheng, X., Yinguang, C., Chenchen, L., 2010. Waste activated sludge alkaline fermentation liquid as carbon source for biological nutrients removal in anaerobic followed by alternating aerobic-anoxic sequencing batch reactors. *Chin. J. Chem. Eng.* 18, 478–485.
- Zhou, X., Wu, Y., Shi, H., Song, Y., 2013. Evaluation of oxygen transfer parameters of fine-bubble aeration system in plug flow aeration tank of wastewater treatment plant. *J. Environ. Sci.* 25, 295–301. [https://doi.org/10.1016/S1001-0742\(12\)60062-X](https://doi.org/10.1016/S1001-0742(12)60062-X)
- Zhu, Y., Bandopadhyay, P.C., Wu, J., 2001. Measurement of Gas-Liquid Mass Transfer in an Agitated Vessel. A Comparison between Different Impellers. *J. Chem. Eng. Jpn.* 34, 579–584. <https://doi.org/10.1252/jcej.34.579>

Chapter 3

3 Fate of Cellulose in Primary and Secondary Treatment at Municipal Water Resource Recovery Facilities

3.1 Introduction

Cellulose has been indicated as a major component (25%-30%) of the particulate fraction of municipal wastewater due to the direct discharge of toilet paper (Ramasamy, Meyers, Bevers, & Verachtert, 1981; Ruiken, Breuer, Klaversma, Santiago, & van Loosdrecht, 2013). Theoretical estimation of the influent cellulose using the per capita annual toilet paper consumption in western Europe (14 kg/capita) indicated that cellulose is 40% of the influent solid mass (Ruiken et al., 2013). Similarly, using the per capita annual toilet paper consumption of 23 kg/capita in North America (<http://www.worldwatch.org/node/5142>), and per capita water consumption of 400 L/d, the estimated influent toilet paper is 158 mg/L, representing approximately 50% of the typical raw municipal wastewater (Metcalf & Eddy, Tchobanoglous, Burton, & Stensel, 2002).

In order to understand the fate of cellulose in wastewater treatment, reliable quantification of cellulose is needed. To quantify cellulose in wastewater, and understand its fate in different treatment processes, several methods have been developed. Hurwitz, Beck, Sakellariou, & Krup, 1961 determined the cellulose content in the wastewater sludges gravimetrically using the Schweitzer reagent (copper ammonium hydroxide) as a solvent for cellulose and showed that the cellulose content in raw wastewater and primary sludge varied from 4.5% to 13.5%, and 2% to 10% of the total TSS, respectively. In addition, the cellulose content of the waste activated sludge (WAS) dry solids ranged between 1% in summer, and 3.55% in winter (Hurwitz et al., 1961). Hofsten & Edberg, 1972 determined cellulose (including hemicellulose) contents using the anthrone method after hydrolysis with H₂SO₄ solution. Honda, Miyata, & Iwahori, 2000 determined cellulose in the wastewater samples using the phenol-sulphuric acid method (DuBois, Gilles, Hamilton, Rebers, & Smith, 1956) after treatment with NaOH, and H₂SO₄ solutions. The cellulose contents in both raw wastewater and primary sludge were 17% and 7% of the TSS for separate and combined sewer systems, respectively while in the biological sludge it was

1% of the TSS (Honda et al., 2000). Another method developed by (Honda, Miyata, & Iwahori, 2002) aimed at separating cellulose fractions from wastewater sludge by hydrolysis of the sludge with diluted sulfuric acid, followed by conventional autoclaving treatment. The phenol-sulphuric acid method was used to estimate the purity of the separated cellulose. Results showed that cellulose purity was impacted by the cellulose percentage in the sample (i.e. samples with low cellulose contents (less than 5% of dry mass) had a purity of 9.2% to 34%, while samples with a high content (more than 20%) had a purity higher than 70% (Honda et al., 2002). Moreover, other studies (Honda et al., 2000; Ruiken et al., 2013), determined cellulose microscopically using polarized light; however, removal efficiency could not be estimated accurately due to the method uncertainty. The cellulose content of the rotating belt filter (RBF) sludge, examined microscopically by (Ruiken et al., 2013), showed that cellulose content in the RBF sludge was 79% of the total solids mass, as compared to between 25% to 32% in the primary clarifier sludge.

The widely disparate values reported for the cellulose content of raw wastewater by (Honda et al., 2000; Hurwitz et al., 1961; Ruiken et al., 2013) may suggest that the different analytical methods could be inadequate for accurate quantification of cellulose in heterogeneous matrices such as wastewater and sludge. Furthermore, most of the developed methods were published in the 70's and 80's, and since then they have not been further validated.

Recently, (Gupta et al., 2018) compared four measurement methods for cellulose detection in wastewater and sludge: acid hydrolysis (sulfuric acid), enzymatic hydrolysis, NREL (National Renewable Energy Laboratory), and the Schweitzer methods. The aforementioned authors concluded that the Schweitzer method was the most reliable and accurate technique for measuring cellulose content in municipal wastewater and sludge, as it does not rely on the hydrolysis of cellulose into glucose which not only requires a long time but also shows a temperature-dependent conversion efficiency, reliability, and reproducibility.

Table 3-1 summarizes the cellulose degradation efficiencies reported in the literature by various authors. (Hurwitz et al., 1961) studied the aerobic degradation of cellulose using laboratory batch experiments. Results showed that after 72 hours, only 6.7 % of the cellulose was degraded at a temperature of 12 to 13 °C compared with 87 % at 23 °C. Increasing the contact time to 96 hours at 12 to 13 °C increased the cellulose degradation efficiency to 20 %, reflecting that the temperature impact could be partially outweighed by the contact time increase. Also, cellulose degradation rates were reported to increase proportionally to the mixed liquor suspended solids (MLSS) concentration, and therefore, the biodegradation rate is proportional to the solids retention time (SRT). (Edberg & Hofsten, 1975) studied the cellulose degradation under anaerobic conditions using nylon bags. Results showed that 70% of the cellulose was biodegraded in 30 days. In a similar study, (Verachtert, Ramasamy, Meyers, & Bevers, 1982) used nylon bags to determine cellulose degradation under aerobic and anaerobic conditions and showed that 50% of the cellulose was degraded aerobically while 60% was degraded anaerobically at a contact time of 15 days. (Ruiken et al., 2013), using batch experiments, showed that cellulose degradation under anaerobic conditions was affected by temperature (i.e., 10% of cellulose was degraded in 20 days during winter (9 °C) while complete removal was observed within 12 days during summer (24 °C)). Aerobic biodegradation of tissue paper was examined by (Alvarez, Larrucea, Bermúdez, & Chicote, 2009) and showed a biodegradation rate of 50%. (Ghasimi, Zandvoort, Adriaanse, van Lier, & de Kreuk, 2016) showed that anaerobic biodegradation rates of the cellulose-rich sieved sludge (fine mesh <0.35 mm) were 57% and 62% under mesophilic and thermophilic conditions, respectively.

Previous studies have also confirmed the important role of cellulose in the formation of the filtration cake that effectively enhances the separation in RBFs. In this regard, RBFs is a primary treatment method that, while allowing the selective capture of fibers and cellulose, can achieve (without chemical pre-treatment) TSS removal efficiency ranging from 30% to 60% (Franchi, Williams, Lyng, Lem, & Santoro, 2015; Ruiken et al., 2013). In the absence of cellulosic fibers in the raw wastewater influent, the RBF would function only as a sieve, with reduced TSS removal efficiencies. Therefore, the harvest of cellulose in primary filtration with RBF is associated with the dual advantage of removing the cellulose

from the secondary treatment load and enhancing the solids separation in primary treatment, with the concomitant enhancement in biogas production in the digesters.

Table 3-1. A literature review of cellulose degradation efficiencies

No.	Reference	Measurement method	Treatment conditions	Contact time (d)	Temperature	Degradation efficiency
1	(Hurwitz et al., 1961)	The Schweitzer method	Aerobic (Laboratory scale)	3	12-13 °C	6.7%
					23 °C	87%
				4	12-13 °C	20%
2	(Edberg & Hofsten, 1975)	The anthrone method after H ₂ SO ₄ hydrolysis	Anaerobic (nylon bag)	30	30 °C	70%
3	(Verachtert et al., 1982)	The anthrone method after H ₂ SO ₄ hydrolysis	Aerobic (nylon bag)	21-35	n/a	60%
			Anaerobic (nylon bag)	n/a	n/a	50-60%
4	(Alvarez et al., 2009)	Evaluated against visual disappearance of fibers ^a	Aerobic (Laboratory scale)	45	Room temperature	50%
5	(Ruiken et al., 2013)	Microscopically using polarized light	Anaerobic (Laboratory scale)	20	9 °C	10%
				12	24 °C	100%
6	(Ghasimi et al., 2016)	Evaluated against visual disappearance of fibers ^a	Anaerobic (Laboratory scale)	15	Mesophilic	57%
				15	Thermophilic	62%

^aChromatographic cellulose with a particle size of less than 0.02 mm was estimated using microcrystalline cellulose as a reference material. For this method, it was assumed that maximum degradation was achieved when no cellulose fibers exist (i.e. existing cellulose is only in the form of microcrystalline cellulose)

Behera, Santoro, Gernaey, & Sin, 2018 modeled the impact of organic carbon recovery (including cellulose) using RBF on methane gas production and aeration energy assuming that cellulose fraction in the influent varies from 25% to 40% of the influent COD. Furthermore, cellulose anaerobic and aerobic biodegradability were assumed to be between 50%-70%, and 15%-35%, respectively. Results showed that cellulose recovery by RBF with thick mat formation increased methane production by about 10% while reducing energy demand in the activated sludge systems by 8% when compared to primary

clarification. On the other hand, RBF without mat formation showed less methane production (about 20% less) and aeration energy (about 2% less) than primary clarification.

Reijken, Giorgi, Hurkmans, Pérez, & van Loosdrecht, 2018 incorporated the cellulose into activated sludge model (ASM1) to model the impact of cellulose sieving on the plant performance. The model considered cellulose as a separate state variable at 20% of the total COD. Results showed that cellulose recovery had a negligible impact on nitrogen removal since most of the cellulose can be degraded aerobically at a solids retention time of 16 days, and part of the remaining cellulose is not hydrolyzed (i.e. 15% to 5% of the cellulose was found in the produced excess sludge at hydrolysis coefficient of more than 0.2 day^{-1})

As shown in Table 3-1, the reported degradation rates, as well as cellulose contents in the wastewater and sludge samples, varied considerably. The lack of mass balance data on cellulose conversion in water resource recovery facilities (WRRF) is a clear knowledge gap. It should also be noted that, with the exception of (Honda et al., 2000), the estimated degradation efficiencies for cellulose were established under controlled conditions (i.e. laboratory scale or nylon bags). Therefore, there is a clear need for full-scale studies, supported by laboratory observations, and detailed mass-balance calculations. Such information will also be useful to elucidate the cellulose fate in WRRF, also in consideration of the central role played by cellulose in the ongoing paradigm of WRRFs. Moreover, plant-wide benefits could be expected by removing fibrous material from the wastewater influent, as the former represents a large fraction of very slowly biodegradable COD. Captured cellulose can be either converted to biogas by co-digestion with biosolids (Ghasimi et al., 2016) or utilized as a resource for different industries such as biofuels, additives in building materials, and asphalt (Boztas, 2017; Honda et al., 2000). Furthermore, research to convert the recycled cellulose into energy, bio-plastics bottles, and other products is well underway (Boztas, 2017).

Thus, the main objective of this study was to track the fate of cellulose in primary and secondary treatment processes under-representative, full-scale conditions and controlled SBR experiments. This study was also motivated by the discrepancy in cellulose

biodegradation efficiency and the lack of validated methods used in previous studies for cellulose quantification in wastewater and sludge, which is now available (Gupta et al., 2018). Finally, an accurate survey of cellulose content and fiber-like material across various processes would also provide crucial information for assessing the plant-wide benefits of RBFs in water resource recovery facilities.

3.2 Methodology

3.2.1 Laboratory-scale sequencing batch reactors study

Two SBRs with a capacity of 2 L were set up in the laboratory to treat raw wastewater and RBF effluent, at room temperature (22 °C- 24 °C). Raw wastewater was collected from water resource recovery facility (A), London, Ontario. RBF effluent was collected from an RBF pilot that was being operated at the same treatment plant. The SBR receiving raw wastewater was set up with a fill ratio of 0.35 and a treatment capacity of 2.8 L/d. The other SBR receiving RBF effluent wastewater was set up with a fill ratio of 0.5 and a treatment capacity of 5 L/d. Table 3-2 summarizes the operational parameters for both SBRs. SRT of 10 days was manually controlled by wasting sludge at 200 mL/d from both SBRs. Both SBRs were dosed with 10 mg/L FeCl₃ to achieve an effluent TP of less than 1 mg/L. At steady-state conditions, samples of the raw wastewater, RBF effluent, as well as mixed liquor, and effluent of both SBRs were analyzed for TSS, COD, total nitrogen (TN), ammonia (NH₄⁺-N), total phosphorus (TP), and cellulose.

3.2.2 Full-scale wastewater treatment plants studies

The North American facility (B) selected for this study is located in London Ontario (Canada). It has an annual average flow rate of 117,000 m³/day and three treatment trains comprising primary clarification and conventional biological treatment (aeration tanks + secondary clarifiers). In summer, alum is used as a coagulant to enhance primary clarification and partially remove phosphorus. The average SRT was 7 days.

Table 3-2. Operational parameters and cycle time break up for both SBRs

Operational parameters	Unit	Raw wastewater (RWW)-SBR	RBF-SBR
Fill ratio	–	0.35	0.5
Number of cycles	Cycles/day	4	5
SRT	Day	10	10
Treatment capacity	L/day	2.8	5
Volume of reactor	L	2	2
Cycle time breakup			
Fill period	Hour	0.25	0.15
Anoxic period	Hour	1	0.75
Aerobic period	Hour	3.5	3
Settle period	Hour	1	0.75
Decant period	Hour	0.25	0.15
		6 hours/cycle	4.8 hours/cycle

Cellulose characterization measurements were conducted by collecting samples during the summer period ($T=24.8\text{ }^{\circ}\text{C}$) from one of the three trains treating a flow rate of $28,000\text{ m}^3/\text{d}$ or 24% of the whole treatment plant. The overall process layout is reported in Fig. 3-1. Grab samples were collected twice a day, in the morning and in the afternoon, at seven plant locations as illustrated in Fig. 3-1. The measurements were extended over three days, for a total number of 42 samples. The experimental campaign was repeated at the end of the winter season ($T=13.7\text{ }^{\circ}\text{C}$), in order to study the possible impact of temperature, with another two sets of samples (14 samples) collected and analyzed for cellulose content and other standard water quality parameters.

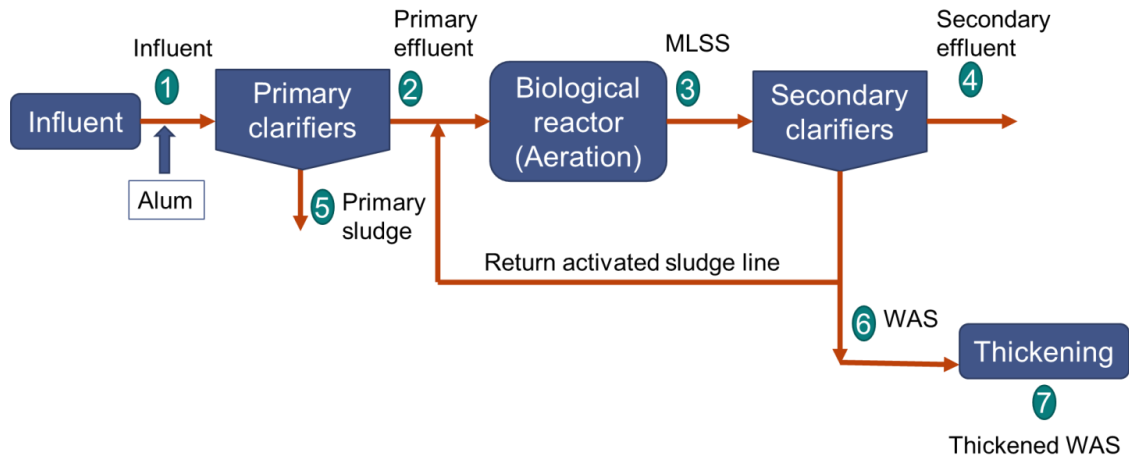


Figure 3-1. Treatment process layout and sampling scheme for the London Ontario facility

The European treatment plant selected for this study is located in Aarle-Rixtel (The Netherlands). It consists of two identical modified University of Cape Town (m-UCT) treatment trains, with the process schematic reported in Fig. 3-2. Each train operates with an average SRT of 14 days and treats an annual average flow of 65,000 m³/day.

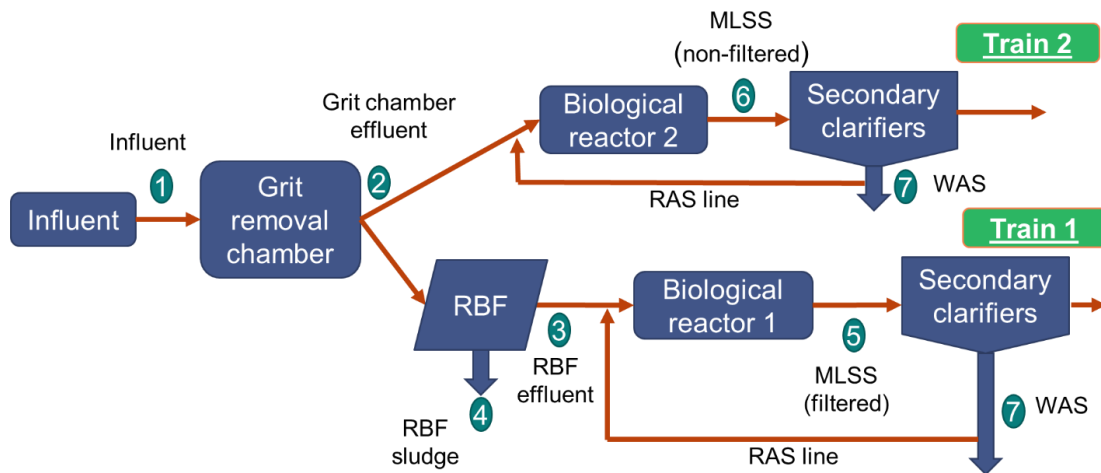


Figure 3-2. Treatment process layout and sampling scheme for The Netherlands facility

The first train is preceded by an RBF, while the second train does not have primary treatment; thus, raw wastewater is directly fed into the biological process after grit and fate removal. By design, the raw wastewater was divided equally, with 50% of the flow directed to the RBF train and followed by biological treatment, while the remaining 50% bypasses primary treatment and biologically treated directly by the MUCT process, followed by the secondary clarifiers. The sludge lines from the two parallel trains were independently operated, thereby making these two trains *de facto* isolated treatment plants fed by the same raw wastewater. During the plant survey conducted at the end of the summer (water temperature =20.5 °C), seven composite samples from the locations illustrated in Fig. 3-2 were collected every day for five days (i.e., the total number of samples was 35) and analyzed for cellulose content and other standard water quality parameters.

3.2.3 Analytical methods

TSS and cellulose were measured for the collected samples from both treatment plants. TSS was measured following Standard Methods (American Public Health Association, 2005). Cellulose was measured following the method (Gupta et al., 2018), using the Schweitzer reagent as a solvent for cellulose, following which cellulose is determined gravimetrically. The method consists of several steps to ensure that only cellulose is selectively separated from a variety of organics and inorganics in the solution. The required chemicals for this analysis include the Schweitzer reagent, concentrated sodium hydroxide (50%), ethyl alcohol (80%), and hydrochloric acid (1.25%). It must be asserted however the aforementioned method was verified for α -cellulose and cellulose concentrations of 500 to 8000 mg/L. However, no detection limit was proposed and verified in the aforementioned study and hence its reliability for low cellulose concentrations has yet to be verified.

3.3 Results and discussion

3.3.1 Laboratory-scale sequencing batch reactor study

Table 3-3 summarizes the TSS concentrations, cellulose concentrations, TSS masses, and cellulose masses for both SBRs. At steady-state conditions, both SBRs achieved COD, TN,

ammonia, and total phosphorous removal efficiencies of 88%, 52%, 93%, and 77% respectively (Tables S1a, and S1b).

Table 3-3. TSS concentrations, cellulose concentrations, TSS masses, and cellulose masses for both SBRs

No.	Sample name	TSS concentration (mg/L) ^a	Cellulose concentration (mg/L) ^a	TSS loading rate (mg/day)	Cellulose loading rate (mg/day)
1	Raw wastewater (RWW)	145±2	42±5	407±4	118±13
2	RBF effluent	95±3	10±2	475±15	50±10
3	RWW-SBR effluent	9±2	2±0	23±5	6±1
4	RBF-SBR effluent	9±2	3 ±0	43±10	15±2
5	RWW-SBR waste	2,410±58	54±4	482±12	11±1
6	RBF-SBR waste	2,120±17	19±6	424±3	4±1

^a Values represent the average ±standard deviation of three samples

Cellulose content in the raw wastewater was 29% of the TSS. RBF showed a cellulose removal efficiency of 76%±2% and TSS removal efficiency of 35%±2%. Cellulose biodegradability in both SBRs was calculated from cellulose mass balances around the SBRs.

For the SBR fed by raw wastewater, the influent cellulose loading rate was 118±13 mg/day while the effluent cellulose loading rate (SBR effluent+ SBR waste) was 17±2 mg/day, showing a degradation efficiency of 86±2%. Cellulose concentration in the secondary SBR effluent was in the range of 2-3 mg /L.

For the second SBR fed by RBF-filtered wastewater, the influent cellulose loading rate was 50±10 mg/day while the effluent cellulose loading rate was 19±3 mg/day, showing a degradation efficiency of 62±2%. Also, in this case, cellulose concentration in the secondary SBR effluent was in the range of 2-3 mg /L. This reflects the presence of a non-

settleable and non-biodegradable cellulose in the wastewater. Also, the experimental evidence that both SBRs produced a cellulose effluent concentration in the same range may indicate that the cellulose biodegradability could be slightly underestimated due to insufficient, yet realistic, cellulose content in the real wastewater used in this study. The cellulose content in the activated sludge varied between 1 to 2% of the TSS, reflecting that cellulose was biodegraded in both SBRs.

3.3.2 North American full-scale study (London Ontario, Canada WWTP)

Figure 3-3 shows the treatment flow diagram with the TSS and cellulose concentrations as measured at the various sampling locations. The same data are reported in a numeric format in Table 3-4.

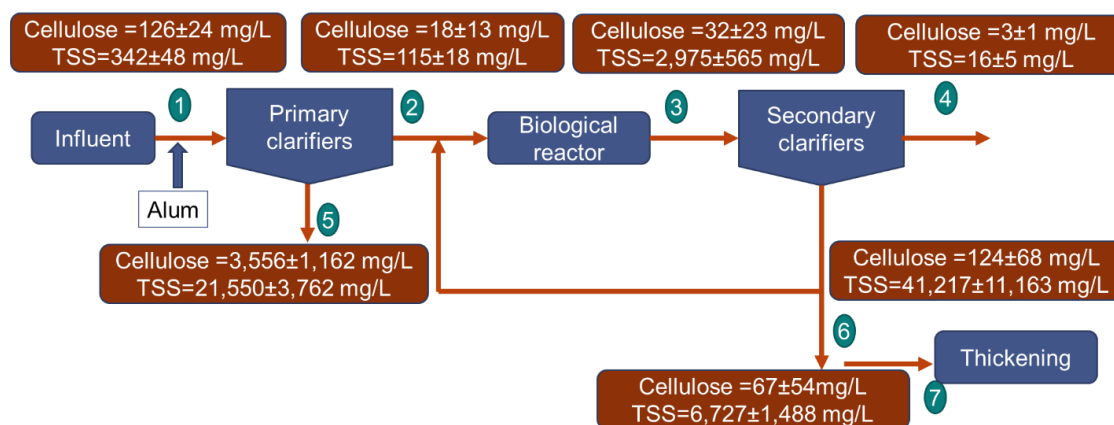


Figure 3-3. TSS and cellulose concentrations for the London Ontario WRRF

Average cellulose concentrations in the influent and primary effluent were 126 ± 24 mg/L, and 18 ± 13 mg/L, respectively, corresponding to a cellulose removal efficiency of 86% while clarifier TSS removal efficiency was 67%. In order to estimate the cellulose biodegradability, two approaches were used. The first entailed the use of mass balance around the biological system (Fig. 3-4). In order to perform mass balances for cellulose, daily flow rates (as observed during the days of the sampling campaign) were obtained from the plant flow meters for influent, WAS, and RAS (Table 3-4). The influent cellulose loading rate to the secondary treatment was 334 ± 244 kg/day, while the effluent (combining

both liquid and WAS) was 104 ± 40 kg/day, implying that 276 ± 206 kg/d of the cellulose was biodegraded through the secondary treatment (i.e., $70\pm 10\%$ of the primary effluent cellulose was biodegraded).

Table 3-4. TSS concentrations, cellulose concentrations, loading rates, and flow rates for the North American case study (summer samples)

Sample locations	TSS concentration ^a	Cellulose concentration ^a	Flow ^b	TSS loading rates	Cellulose loading rates
Unit	mg/L	mg/L	m ³ /day	kg/day	kg/day
1- Influent	342±48 (6)	126±24 (6)	18,838±2,543	6,483±1,497	2,384 ±602
2- Primary Effluent	115±18 (6)	18±13 (6)	18,630±2,472	2,158±478	334±244
3- Aeration Effluent (MLSS)	2,975±565 (6)	32±23 (6)	32,235±3,408	96,837±25,723	1,032±779
4- Secondary Effluent	16±5 (6)	3±1 (6)	17,988±2,581	279±84	61±18
5- Primary sludge	21,550±3,762 (6)	3,556±1,162 (6)	208±81	4,324±1,060	699±194
6- Waste activated sludge (WAS)	6,727±1,488 (6)	67±54 (6)	642±110	4,223±610	42±35
7- Thickened activated sludge (TWAS)	41,217±11,163 (6)	124±68 (4)	–	–	–

^a Values represent average±standard deviation, and numbers within parenthesis are the number of samples.

^b Influent, WAS, RAS average daily flow rates, for the measurement days, were obtained from the treatment plant flow meters. Primary sludge flow rate was calculated based on TSS mass balance for the primary clarifier.

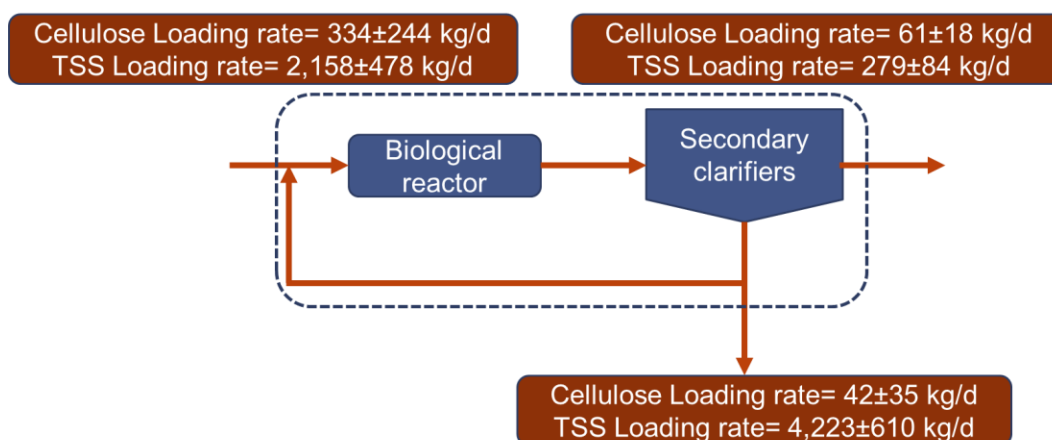


Figure 3-4. Cellulose mass balance around the secondary treatment (London ON WRRF)

The second approach for estimating cellulose biodegradability was based on a comparison of its concentration in the mixed liquor with the theoretical concentration that a hypothetical substrate with 0% biodegradability (or, 100% non-biodegradability) would have had. According to a theoretical mass balance for a non-biodegradable substrate, excluding the rate of non-biodegradable volatile suspended solids (nbVSS) production from the cell debris, any non-biodegradable substrate would accumulate in a biological system by a factor of SRT/HRT (Metcalf & Eddy et al., 2002). Thus, using an SRT of 7 days and an HRT of 8.6 hours for the biological reactor (as recorded during the sampling period), the estimated theoretical concentration of cellulose (assumed to be 100% non-biodegradable) in the aeration tank would have been 345 ± 248 mg/L. When compared with the actual concentration of 32 ± 23 mg/L measured in the mixed liquor, this indicates a biodegradation efficiency of $90 \pm 4\%$. It should be noted that both approaches used to estimate cellulose biodegradability produce an estimate in good agreement with each other. Moreover, the estimated cellulose biodegradability correlates well with the results obtained in the SBR experiments reported in the previous section. As shown in Table 3-4, the non-settleable and non-biodegradable cellulose concentration was around 3 mg/L or 2.4% of the raw wastewater cellulose, a value that is in excellent agreement with the laboratory studies described in the previous section.

To better understand the fate of cellulose in the primary treatment process, batch settling tests were conducted using a 3.65 m high, 0.15 m internal diameter settling column with a working volume of 65 L (Fig. S1). Results showed that 43% of the influent cellulose was neither in the effluent nor in the primary sludge (Table S2). It must be asserted that the TSS removal efficiency by primary treatment in the full-scale plant averaging ~ 67% was consistent with the 70% observed in the column test, although the full-scale cellulose removal efficiency of 85% was slightly lower than that observed in the settling column (96%). Column test results indicated that the cellulose in the effluent and primary settled sludge accounted for only 57% of the raw cellulose, with the remaining 43% accumulated in the central portion of the column (representing the middle part of a primary clarifier). This poor settleability of cellulose fibers emphasized by the column test, in combination with potentially unsteady operations of the primary clarification unit due to variability in influent flowrate and intermittent underflow pumping, could explain why the cellulose mass balance around the primary clarifier did not close, with the primary sludge and primary effluent cellulose loading accounting for only 43% of the influent cellulose.

The correlation between TSS and cellulose loading rates for the influent, primary effluent, and primary sludge samples showed regression with a correlation coefficient of an R^2 of 0.75, and a slope of 0.31, implying that cellulose accounts for 31% of the influent TSS (Fig. S2a). On the other hand, the regression between TSS and cellulose loading rates for the MLSS and WAS samples showed regression with an R^2 of 0.81 and a slope of 0.014, implying that the cellulose content of the biological solids was 1.4% by weight (Fig. S2b).

3.3.3 European full-scale study (Aarle Rixtel, the Netherlands WWTP)

Figure 3-5 shows the treatment flow diagram with the TSS and cellulose concentrations as measured at the various sampling locations. The same data are reported in a numeric format in Table 3-5.

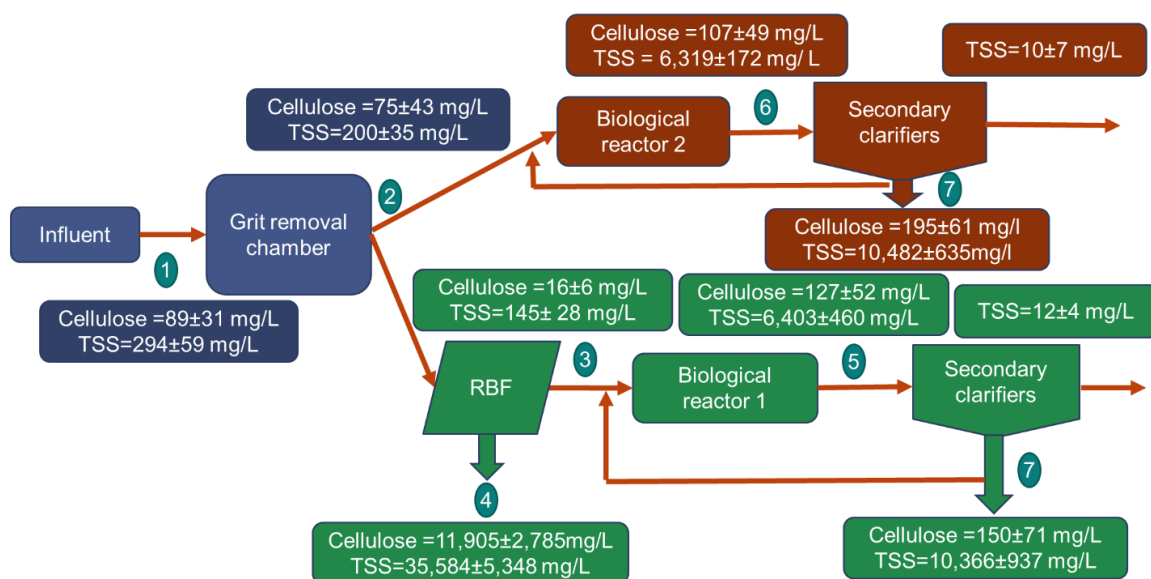


Figure 3-5. TSS and cellulose concentrations for the Aarle-Rixtel WRRF (in green: train 1 with RBF as primary treatment; in brown: train 2 with no primary treatment)

Average cellulose concentrations in the influent and primary effluent (in this case, for the line operating with micro screening by RBF) were 89 ± 31 mg/L, and 16 ± 6 mg/L, respectively, corresponding to a cellulose removal efficiency of 79% while TSS removal efficiency was 28%. This confirms the highly selective removal of cellulose of the RBF reported by (Ruiken et al., 2013). RBF historical data showed removal efficiencies of 11%, 7%, and 7% for sCOD, TN, and TP respectively.

By comparing the primary sludge characteristics produced by the RBF at the European plant with the primary sludge produced by primary clarifiers at the North American plant, the RBF sludge was more than double the cellulose content per unit mass of TSS compared to the primary clarifier sludge (35% vs. 17%, respectively). Furthermore, the extent of variability in the cellulose contents displayed by the primary sludge produced by primary clarification was much higher than the one associated with RBF sludge.

Table 3-5. TSS and cellulose concentrations, loading rates, and flow rates (European case study)

Sample location	TSS concentration^a	Cellulose concentration^a	Flow^b	TSS loading rates	Cellulose loading rates
Unit	mg/L	mg/L	m³/day	kg/day	kg/day
1- Raw	294±59 (4)	89±31(5)	51,546±9,401	15,320±5,464	4,671±2,302
2- Grit effluent	200±35 (4)	75±43 (5)	51,546±9,401	10,158±1,890	3,737±2,041
2- 1st train influent	200±35 (4)	75±43 (5)	25,029±4,274	4,937±901	1,818±995
2- 2nd train influent	200±35 (4)	75±43 (5)	26,518±5,129	5,221±993	1,919±1,047
3- RBF effluent	145±28 (4)	16±6 (4)	24,987±4,264	3,525±385	373±112
4- RBF sludge	35,584±5,348 (4)	11,905±2,785 (5)	41±14	1,411±573	495±192
5- Biological reactor 1	6,403±460 (5)	107±49 (4)	61,734±7,693	396,084±61,691	6,596±3,057
6- Biological reactor 2	6,319±172 (5)	118±37 (5)	63,265±8,560	400,118±57,446	7,500±2,492
7- WAS 1	10,366±937 (5)	150±71 (4)	1,259±283	13,069±3,440	208±127
7- WAS 2	10,482±635 (5)	195±61 (5)	1,242±254	12,937±2,328	246±109
Secondary effluent 1	12±4 (5)	2.7±0.9 ^c	23,728±4,454	296±150	65±33 ^c
Secondary effluent 2	10±7 (5)	2.1±1.6 ^c	25,276±5,294	249 ±191	55 ±42 ^c

^a Values represent average ±standard deviation, and numbers within parenthesis are the number of samples.

^b Influent, WAS, RAS average daily flow rates, for the measurement days, were obtained from the treatment plant flow meters. Primary sludge flow rate was calculated based on TSS mass balance for the primary clarifier.

^c The secondary effluent cellulose concentrations and loading rates were estimated to be equal to 22% of the TSS loading rates as obtained by the column test .

Similar calculation approaches as previously described for the North American case study were applied to estimate the cellulose biodegradability in the European case. The daily flow rates, reported in Table 3-3, for influent, WAS, and RAS, on the days of measurements, were taken from the plant flow meters while the RBF sludge flow rate was calculated based on the TSS mass balance around the RBF.

The average cellulose concentration in the influent (measured in the grit chamber effluent) feeding the two parallel treatment trains was 75 ± 43 mg/L. Figures 3-6 and 3-7 show the mass balances around secondary treatment trains 1 and 2.

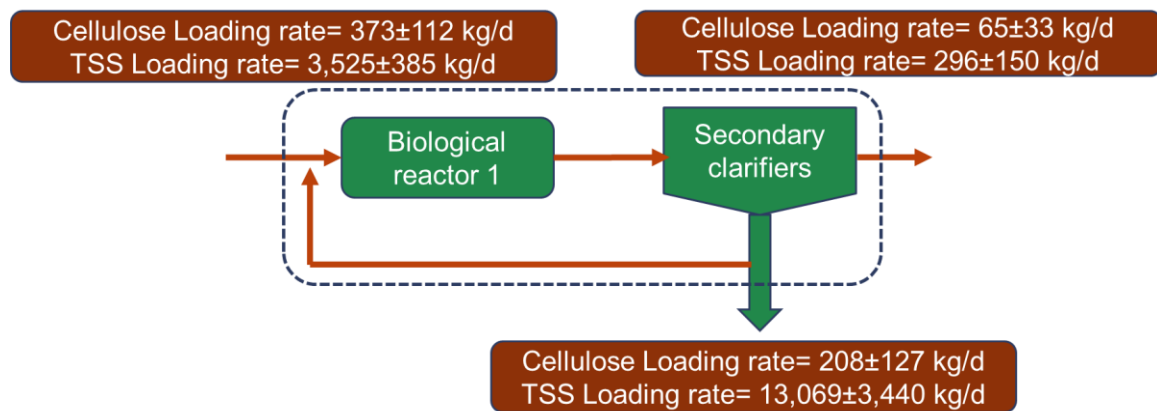


Figure 3-6. Cellulose mass balance around the secondary treatment of Train 1

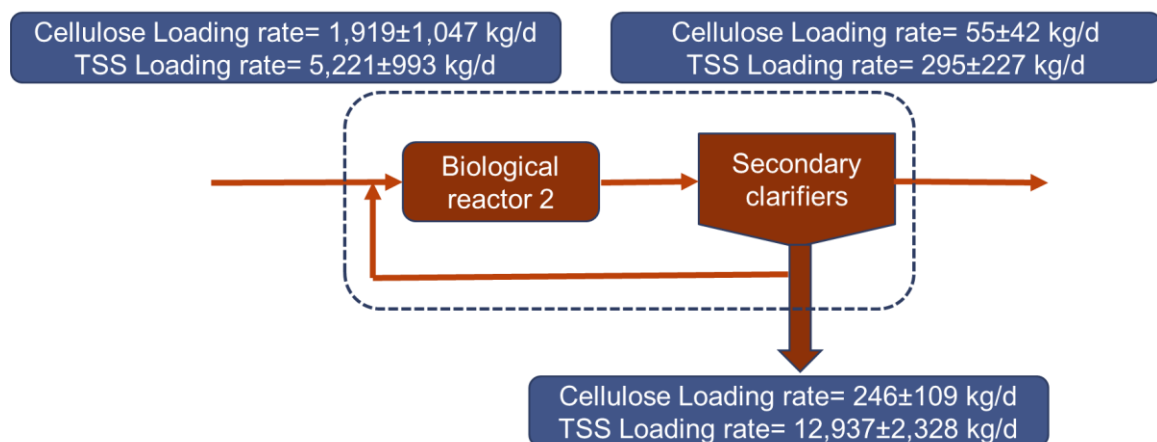


Figure 3-7. Cellulose mass balance around the secondary treatment of Train 2

For train 2 (train with no primary treatment), the cellulose influent loading rate to the biological system was estimated at $1,919 \pm 1,047$ kg of cellulose per day, while the one exiting from the system (i.e., obtained by summation of the two loads associated with secondary effluent and waste activated sludge) was 301 ± 133 kg of cellulose per day. This implies that $1,619 \pm 1,012$ kg/d of cellulose was biodegraded through the secondary treatment (corresponding in percentage to $82 \pm 10\%$ cellulose degradation efficiency). This value is confirmed by the alternate calculation for estimating biodegradability (i.e., a method based on accumulation ratio as a function of SRT/HRT). Indeed, for an SRT of 14 days and the HRT of 18 hours, the cellulose biodegradation efficiency was found to be $89 \pm 6\%$.

For train 1 (the train with RBF as primary treatment process), the mass-balance method reflected cellulose biodegradability of $27\% \pm 19\%$, based on cellulose load entering the secondary treatment of 373 ± 112 kg of cellulose per day and a combined (secondary effluent and waste activated sludge) cellulose load exiting the biological system of 273 ± 119 kg cellulose per day. It should be noted that this value is considerably lower than the one estimated using the accumulation method, which indicated an estimated cellulose biodegradability of approximately $65\% \pm 13\%$. As discussed in the laboratory results, this apparent drop in cellulose degradation efficiency observed in the case with RBF could be due to a combination of three factors, namely: (a) a low cellulose loading entering the secondary system, and its impact in determining biodegradability with accuracy; (b) the presence of a non-biodegradable, non-settleable cellulose fraction and (c) a detection limit of the cellulose quantification method used in this study when applied to secondary effluent. This implies that the measured cellulose biodegradation efficiency (especially in with highly efficient primary treatment for cellulose) should be regarded as “apparent” rather than “intrinsic” to substrate characteristics. This could also explain the relatively wide range of biodegradation efficiencies reported in other studies (Table 3-1).

The simultaneous TSS and cellulose measurements conducted in this work allowed to establish an abundance ratio between TSS and cellulose loading rates for the raw influent, the grit chamber effluent, the RBF effluent, and the RBF sludge as revealed by linear

correlation analysis ($R^2=0.8441$, and a slope of 0.3282). The latter implies a cellulose content of 33% of the influent TSS (Fig. S2b).

3.3.4 Role of water temperature

In order to check the effect of temperature on cellulose biodegradation efficiency, a second sampling event was organized at the end of the winter season for the North American plant located in London Ontario, Canada. TSS, cellulose measurements, flow rates, and loading rates for the two sets of winter samples are shown in Tables 3-6 and 3-7. It must be mentioned that the estimated primary sludge flow rates were confirmed by a total phosphorus (TP) mass balance around primary clarification.

TSS removal efficiencies in the primary treatment ranged from 69% to 77% while cellulose removal efficiencies were in the 87%-92% range. The cellulose content of the primary sludge was comprised between 10%-17% of the TSS, which was in line with the summer samples, and the lack of selectivity for cellulose was already observed for the primary clarifier (Table 3-4). During this sampling event, the ratio between cellulose and TSS concentration in the influent dropped to 20%, indicating a dilution effect associated with higher plant flow rates recorded for the winter sampling.

Cellulose biodegradability for the winter samples was estimated using the two aforementioned calculation approaches (mass balance and accumulation method). Using mass balances, the influent to the secondary treatment was estimated to be 377 kg/day, while the combined cellulose loading leaving the secondary process (effluent+WAS) was 91 kg/day (Table 3-6). This implies that 76% of the primary effluent cellulose was degraded through secondary treatment. Similar biodegradation efficiencies were observed for the second set of samples collected during the winter experiment showing a 65% degradation efficiency (Table 3-7). Using the accumulation method with an SRT of 6 days and HRT of 8.3 hrs for the first set of samples, the estimated theoretical concentration of the cellulose in the aeration tank is 312 mg/L, reflecting 90% degradation efficiency when compared to the cellulose concentration in the mixed liquor (32 mg/L). For the second set

of samples, using an SRT of 4.6 days and an HRT of 6 hrs, the estimated degradation efficiency was 92%.

Table 3-6. TSS and cellulose concentrations, loading rates, and flow rates for the North American case study (Winter samples a)

Sample locations	TSS concentration	Cellulose concentration	Flow ^a	TSS loading rates	TP loading rates	Cellulose loading rates
Unit	mg/L	mg/L	m³/day	kg/day	kg/day	kg/day
Influent	445	134	21719	9665	259	2910
Primary Effluent	101.3	17.5	21508	2178	127	377
Aeration Effluent (MLSS)	3210	32	36928	118539	–	1181
Secondary Effluent	11	2.42	20948	230	–	51
Primary sludge	35112	5833	211	7409	133	1231
Waste activated sludge (WAS)	7404	71	560	4146	–	40
Thickened activated sludge (TWAS)	51904	335	–	–	–	–

^a Influent, WAS, RAS average daily flow rates, for the measurement days, were obtained from the treatment plant flow meters. Primary sludge flow rate was calculated based on TSS mass balance for the primary clarifier.

Table 3-7. TSS and cellulose concentrations, loading rates, and flow rates for the North American case study (Winter samples b)

Sample locations	TSS concentration	Cellulose concentration	Flow ^a	TSS loading rates	TP loading rates	Cellulose loading rates
Unit	mg/L	mg/L	m³/day	kg/day	kg/day	kg/day
Influent	403	78	30168	12143	266	2346
Primary Effluent	123.7	5.9	29995	3712	152	176
Aeration Effluent (MLSS)	2750	9	45440	124959	–	407
Secondary Effluent	7.5	1.65	29365	220	–	48
Primary sludge	48645	5089	173	8430	112	882
Waste activated sludge (WAS)	7760	22.4	630	4889	14	32
Thickened activated sludge (TWAS)	44520	335	–	–	–	–

^a Influent, WAS, RAS average daily flow rates, for the measurement days, were obtained from the treatment plant flow meters. Primary sludge flow rate was calculated based on TSS mass balance for the primary clarifier.

In summary, winter measurements showed comparable cellulose removal and biodegradation efficiency to what was observed in the summer samples. This suggests that the seasonal difference in cellulose degradation efficiencies reported in previous studies may be due to several factors and not solely to water temperature.

3.3.5 Operational Cost Implications of Cellulose Removal in Primary Treatment

To evaluate the impact of cellulose recovery by primary treatment, a cost analysis was conducted based on the following assumptions: (a) cellulose removal efficiency through primary treatment is 80%, (b) cellulose degradation efficiency through biological treatment is 80% in case of biological treatment preceded by primary treatment and 85% for without primary treatment. (c) anaerobic cellulose degradation efficiency is 70% (Behera et al., 2018) and the WAS non-cellulose VSS reduction is 50% in the anaerobic digester. (d) biomass yield is 0.44 gVSS/gCOD. (e) average SRT in the secondary treatment is 10 days. (f) decay coefficient $k_d = 0.1 \text{ d}^{-1}$. (g) power consumption of 1 kWh/ kg O₂, and energy price is \$0.1 /kWh (<https://www.ontarioenergyreport.ca/>) and (h) sludge handling cost is \$684 /dry ton solids (Vasileski, 2007).

For a treatment plant receiving an influent cellulose loading rate of 1000 kg/day (80 MLD plant based on the London, ON cellulose concentration), cellulose recovered in primary treatment and WAS were calculated to be 816 kg/day and 38 kg VSS/day respectively (Figure S3a). Since more cellulose was diverted towards anaerobic digestion, energy production was 7979 MJ/day while energy consumption was 424 MJ/day, showing a net energy advantage of \$210/day. Overall sludge production of 267 kg TSS/day resulted in a sludge disposal cost of \$181/day, reflecting an overall benefit of \$29/day. For the other treatment scenario where no primary treatment (Figure S3b) cellulose recovery and biomass production were calculated to be 120 kg/day and 200 kg VSS/day, respectively. Hence, energy production was 3006 MJ/day while energy consumption was 2250 MJ/day, showing a net energy advantage of \$18/day. Sludge production rate and disposal cost were calculated to be 154 kg TSS/day and \$527/day, respectively, reflecting an overall deficit of \$509/day. Thus, cellulose diversion to anaerobic digestion through primary treatment reduced the annual operational cost by \$195,000.

3.4 Summary and Conclusions

Based on the observation reported in this paper, the following conclusions can be made:

- As confirmed by the plant surveys conducted in two full-scale water resource recovery facilities located in different geographies (Canada and The Netherlands), the influent cellulose concentration in raw municipal wastewater represents approximately one-third of the influent total suspended solids. More specifically, raw wastewater cellulose accounted for 33%, and 31% of the TSS of the North American (Canada) and European (The Netherlands) water resource recovery facility, respectively.
- Both primary processes (gravity settling and micro-sieving) investigated in this study at full scale showed similar and very high cellulose capture rates (>80%). However, micro screening operated by RBF was able to selectively capture cellulose over TSS, the latter representing a considerable advantage for water resource recovery facilities aiming at cellulose recovery. As a result of this cellulose enrichment in the solid stream, cellulose content in the RBF sludge was almost twofold higher than primary clarifier sludge (RBF sludge was 35% by weight of TSS while that cellulose in primary sludge was 17% of the TSS).
- Laboratory study conducted in SBRs was found to be in good agreement with full-scale treatment plants observations. Specifically, both studies indicated a secondary effluent cellulose concentration of approximately 2%-5% of the raw wastewater cellulose, indicating the presence of a non-settleable non-biodegradable fraction of the influent cellulose.
- At the investigated conditions and within the temperature range spanning from 13.7 °C-24.8 °C, cellulose was efficiently biodegraded during biological treatment irrespective of the biological process configuration (i.e. CAS vs. MUCT) and SRT (7 to 14 days), with all systems tested in this study achieving effluent cellulose concentrations of 2-3 mg/L.

References

- Alvarez, J. V. L., Larrucea, M. A., Bermúdez, P. A., & Chicote, B. L. (2009). Biodegradation of paper waste under controlled composting conditions. *Waste Management*, 29(5), 1514–1519. <https://doi.org/10.1016/j.wasman.2008.11.025>
- American Public Health Association. (2005). *Standard Methods for the Examination of Water & Wastewater*. American Public Health Association.
- Behera, C. R., Santoro, D., Gernaey, K. V., & Sin, G. (2018). Organic carbon recovery modeling for a rotating belt filter and its impact assessment on a plant-wide scale. *Chemical Engineering Journal*, 334, 1965–1976. <https://doi.org/10.1016/j.cej.2017.11.091>
- Boztas, S. (2017, July 27). The ick factor: Dutch project making bike lanes and bottles from used loo roll. *The Guardian*. Retrieved from <http://www.theguardian.com/sustainable-business/2017/jul/27/-ick-factor-dutch-bike-lanes-bottles-used-loo-roll-recycled-toilet-paper>
- DuBois, Michel., Gilles, K. A., Hamilton, J. K., Rebers, P. A., & Smith, Fred. (1956). Colorimetric Method for Determination of Sugars and Related Substances. *Analytical Chemistry*, 28(3), 350–356. <https://doi.org/10.1021/ac60111a017>
- Edberg, N., & Hofsten, B. v. (1975). Cellulose Degradation in Wastewater Treatment. *Journal (Water Pollution Control Federation)*, 47(5), 1012–1020.
- Franchi, A., Williams, K., Lyng, T. O., Lem, W., & Santoro, D. (2015). Rotating Belt Filters as Enabling Technology for Energy-Neutral Wastewater Treatment Plants: Current Status and Applications. *Proceedings of the Water Environment Federation*, 2015(13), 1743–1749. <https://doi.org/10.2175/193864715819540847>
- Ghasimi, D. S. M., Zandvoort, M. H., Adriaanse, M., van Lier, J. B., & de Kreuk, M. (2016). Comparative analysis of the digestibility of sewage fine sieved fraction

- and hygiene paper produced from virgin fibers and recycled fibers. *Waste Management*, 53, 156–164. <https://doi.org/10.1016/j.wasman.2016.04.034>
- Gupta, M., Ho, D., Santoro, D., Torfs, E., Doucet, J., Vanrolleghem, P. A., & Nakhla, G. (2018). Experimental assessment and validation of quantification methods for cellulose content in municipal wastewater and sludge. *Environmental Science and Pollution Research*. <https://doi.org/10.1007/s11356-018-1807-7>
- Hofsten, B. V., & Edberg, N. (1972). Estimating the Rate of Degradation of Cellulose Fibers in Water. *Oikos*, 23(1), 29. <https://doi.org/10.2307/3543924>
- Honda, S., Miyata, N., & Iwahori, K. (2000). A Survey of Cellulose Profiles in Actual Wastewater Treatment Plants. *Japanese Journal of Water Treatment Biology*, 36(1), 9–14. <https://doi.org/10.2521/jswtb.36.9>
- Honda, S., Miyata, N., & Iwahori, K. (2002). Recovery of biomass cellulose from waste sewage sludge. *Journal of Material Cycles and Waste Management*, 4(1), 46–50.
- Hurwitz, E., Beck, A. J., Sakellariou, E., & Krup, M. (1961). Degradation of Cellulose by Activated Sludge Treatment. *Journal (Water Pollution Control Federation)*, 33(10), 1070–1075.
- Metcalf & Eddy, Tchobanoglous, G., Burton, F., & Stensel, H. D. (2002). *Wastewater Engineering: Treatment and Reuse*. McGraw-Hill Education.
- Ramasamy, K., Meyers, M., Bevers, J., & Verachtert, H. (1981). Isolation and characterization of cellulolytic bacteria from activated sludge. *Journal of Applied Microbiology*, 51(3), 475–481.
- Reijken, C., Giorgi, S., Hurkmans, C., Pérez, J., & van Loosdrecht, M. C. M. (2018). Incorporating the influent cellulose fraction in activated sludge modelling. *Water Research*, 144, 104–111. <https://doi.org/10.1016/j.watres.2018.07.013>

- Ruiken, C. J., Breuer, G., Klaversma, E., Santiago, T., & van Loosdrecht, M. C. M. (2013). Sieving wastewater – Cellulose recovery, economic and energy evaluation. *Water Research*, 47(1), 43–48.
<https://doi.org/10.1016/j.watres.2012.08.023>
- Vasileski, G. (2007). *Beneficial Uses of Municipal Wastewater Residuals (Biosolids) - Final Report*. Canadian Water and Wastewater Association.
- Verachtert, H., Ramasamy, K., Meyers, M., & Bevers, J. (1982). Investigations on cellulose biodegradation in activated sludge plants. *Journal of Applied Microbiology*, 52(2), 185–190.

Chapter 4

4 Dynamic Impact of Cellulose and Readily Biodegradable Substrate on Oxygen Transfer Efficiency in Sequencing Batch Reactors.

4.1 Introduction

Energy demand for biological wastewater treatment plants varies between 0.2 to 2.0 kWh m⁻³ and might reach up to 8.33 kWh m⁻³ depending on influent wastewater characteristics, treatment plant capacity, used technology, and disposal methods (Gude, 2015; Singh et al., 2016; Tao and Chengwen, 2012). In general, more than half of the treatment plant's net energy consumption is attributed to aeration, except for site-specific pumping (Reardon, 1995; Rosso et al., 2011; Rosso and Stenstrom, 2006). Thus, to optimize the aeration energy, it is important to precisely quantify the oxygen transfer efficiency (OTE) and understand the main factors that influence the OTE.

The oxygen transfer rate in wastewater is commonly evaluated using the α -factor. The α -factor for fine bubble diffusers varies between 0.25 to 0.65 (*inter alia*, Baquero-Rodríguez et al., 2018). Several design factors have been reported to impact the aeration efficiency, including diffuser type, distribution, and depth, airflow rate, as well as aerobic reactor design. In addition, other operational factors were reported to impact the aeration efficiency such as influent wastewater characteristics, solids retention time (SRT), nutrient removal processes, and temperature (Baquero-Rodríguez et al., 2018; Gillot and Héduit, 2008; Leu et al., 2009; Rosso et al., 2011; Wagner and Pöpel, 1998).

Cellulose from toilet paper is one of the particulate organic substrates in raw municipal wastewater that can be efficiently removed by primary treatment processes, such as primary clarification (PC) and the RBF (Ahmed et al., 2019; Ruiken et al., 2013). The RBF removes total suspended solids (TSS) and biochemical oxygen demand (BOD) by up to 80%, and 20% respectively (Chakraborty, 2015; Franchi et al., 2015). In addition, the RBF has been demonstrated to selectively remove cellulose, which represents 35% of the raw

municipal wastewater suspended solids, producing cellulose-rich sludge (Ahmed et al., 2019; Ruiken et al., 2013).

Readily biodegradable substrates, which include surface-active agents, dramatically reduce oxygen transfer efficiency due to their rapid accumulation on the bubble surface (Rosso et al., 2008; Wagner and Pöpel, 1996). Thus, the use of a pre-denitrification stage is often advantageous (Rosso and Stenstrom, 2005; Rosso and Stenstrom, 2007). Fine bubbles have a rise velocity of $\sim 10^{-1}$ m s⁻¹ and a higher specific surface area when compared to coarse bubbles with a velocity of $\sim 10^0$ m s⁻¹, hence fine bubbles are prone to higher surfactant accumulation (Rosso et al., 2006). Previous results showed that OTE was reduced by 30%-70% of the clean water value because of the accumulation of surfactants on the bubble interface reducing surface tension, internal gas circulation and resulting gas-liquid interfacial renewal, as well as gas diffusivity into the liquid (Eckenfelder et al., 1956; Rosso et al., 2005; Wagner and Pöpel, 1998).

Mixed liquor suspended solids (MLSS) concentrations inversely correlate with the α -factor in membrane bioreactors (MBR) where MLSS concentrations vary between 8 g l⁻¹ to 30 g l⁻¹ (Cornel et al., 2003; Krampe and Krauth, 2003). Henkel et al., 2011 developed an inverse correlation between MLSS and α -factor in activated sludge systems from five studies where MLSS concentrations ranged between 2 g l⁻¹ and 14 g l⁻¹. Rosso et al., 2005, using off-gas transfer efficiency measurements from 26 treatment plants over fifteen years, showed that α -factor increases with the SRT increase, due to a combination of MLSS concentration and sludge characteristics. Their findings were confirmed by Gillot and Héduit, 2008. Baquero-Rodríguez et al., 2018 combined the data from the aforementioned studies and concluded that MLSS concentrations below 6 g l⁻¹ impacted the α -factor beneficially, due to the increased biosorption provided by the biomass. However, MLSS concentrations more than 7 g l⁻¹ are associated with a dramatic decrease in α -factor due to the substantially different rheology of the thick sludge, i.e. the shear-thinning nature of the solid suspension increases bubble coalescence and decreases the gas transfer interfacial area when compared to clean water (Baquero-Rodríguez et al., 2018). Apparently, except for the cases with high MLSS concentrations (> 7 g l⁻¹), there is no robust relationship

between α -factor and MLSS since at the same MLSS concentration a wide spread of α -factors was observed.

Process models for activated sludge systems have historically relied upon constant inputs for the α -factor (Henze et al., 1987; Jiang et al., 2017; Metcalf & Eddy et al., 2002; Henze et al., 2000). The use of constant values to characterize the α -factor conflicts with the now known change of the oxygen transfer efficiency due to the dynamic influent wastewater characteristics (Leu et al., 2009), and operating conditions (e.g., SRT, and real-time concentrations of different parameters inside the reactor due to biodegradation). Assuming a constant α -factor, as commonly practiced, leads to overestimation or underestimation of air requirements.

Several research contributions were established to improve aeration modeling. Wagner and Pöpel, 1998 correlated oxygen transfer efficiency parameters including standard oxygen transfer rates (SOTR) and oxygen mass transfer coefficient (k_{La}) to airflow rate, and diffusers submergence. Rosso et al., 2005 normalized the SRT, air flow rate, diffuser, and tank geometry, to reduce process data and create empirical correlations for standard oxygen transfer efficiency in process water (α_{SOTE}) and α -factors. However, the correlations are marred by the variability inherent in full-scale measurements, usually reported as daily averages. Gillot et al., 2005 and Rosso et al., 2006 attempted to reduce the variability in process data by performing dimensional analysis and producing correlations that relied on different entities, such as the superficial gas velocity and the dynamic surface tension, respectively. Gillot and Héduit, 2008 defined a new composite variable (Equivalent Contact Time) which is a function of SRT, k_{La} , and airflow rates to predict the α -factor in fine pore aeration systems. Pittoors et al., 2014 developed a mathematical model for the oxygen transfer efficiency in clean water and activated sludge that correlates k_{La} to nine operating variables including reactor volume, height, diameter, surface area, airflow rate, diffusers surface area and depth, bubble size, and dynamic viscosity. The model was validated using experimental measurements from a cylindrical batch reactor (2.7-9.3 l).

The aforementioned studies successfully provided relationships to predict α -factor from other aeration parameters; however, none of them were able to truly address the dynamic

behavior of the oxygen transfer efficiency and hence the α -factor. Most recently, Jiang, Garrido-Baserba et al., 2017 developed a dynamic aeration model that described the change in oxygen transfer efficiency as a function of the influent COD. Their results showed that the α -factor decreased exponentially with the total COD applied to secondary treatment. However, their work did not distinguish between the COD fractions involved in affecting the α -factor.

The impact of influent organic loading rates on aeration efficiency has been addressed experimentally in several studies (e.g., Gori et al., 2011; Jiang et al., 2017; Leu et al., 2009; Rosso et al., 2005). However, the real-time impact of biodegradation of these organics during the aeration process is a clear knowledge gap. In addition, the impact of cellulose on aeration efficiency has never been studied before. Furthermore, the role of biomass in oxygen transfer is not completely understood (Campbell et al., 2019; Cornel et al., 2003; Germain et al., 2007; Henkel et al., 2011; Krampe and Krauth, 2003; Rosso et al., 2005).

.Therefore, the two goals of this study are: i) to evaluate the impact of cellulose, organic loading rates, and biomass on the oxygen transfer efficiency; ii) to develop a dynamic aeration model incorporating α -factor and SOTR as a function of readily and slowly biodegradable substrates. The aeration model developed by Jiang, Garrido-Baserba et al., 2017 was combined with the ASM1CL model developed by Reijken et al. (2018) to estimate the real-time airflow rate due to biodegradation of the organics while satisfying the SOTR required for treatment.

4.2 Methodology

4.2.1 Sequencing batch pilot reactors design

Two identical pilot sequencing batch reactors (SBRs), with an operating volume of 850 l (diameter of 0.6 m and depth of 3.0 m), were built in a wastewater treatment plant in London, ON, Canada (Fig. 4-1). Each reactor was equipped with a 7" EPDM fine pore membrane diffuser disc mounted on the floor. One reactor was fed with raw wastewater and the other was fed with the RBF (SALSNES SF2000 - mesh opening = 0.158 mm) screened wastewater. Both reactors were operated two cycles per day (12 hrs per cycle).

Each cycle consisted of 15 min filling; 4.5 h anoxic; 5 h aerobic; 2 h settling; 15 min decanting. Process variables were monitored online through two sets of sensors installed in each reactor including pH (YSI Digital SensoLyt® pH), ORP (YSI Digital SensoLyt® ORP), DO (YSI TriOxmatic 700 IQ Electrochemical DO Sensor), and ammonia (HORIBA HC-200NH, Japan). Both reactors were operated at an SRT of 10 days. In addition, the air delivery was controlled in both reactors using an electric on/off valve that intermittently released a constant air flow. The electric valve was programmed to operate within a DO setpoint of $1.5 \pm 0.5 \text{ mg l}^{-1}$. To monitor the SBRs performance, the influent and effluent samples from both reactors were collected and analyzed weekly. Additionally, the reactors' MLSS and MLVSS concentrations were measured weekly.

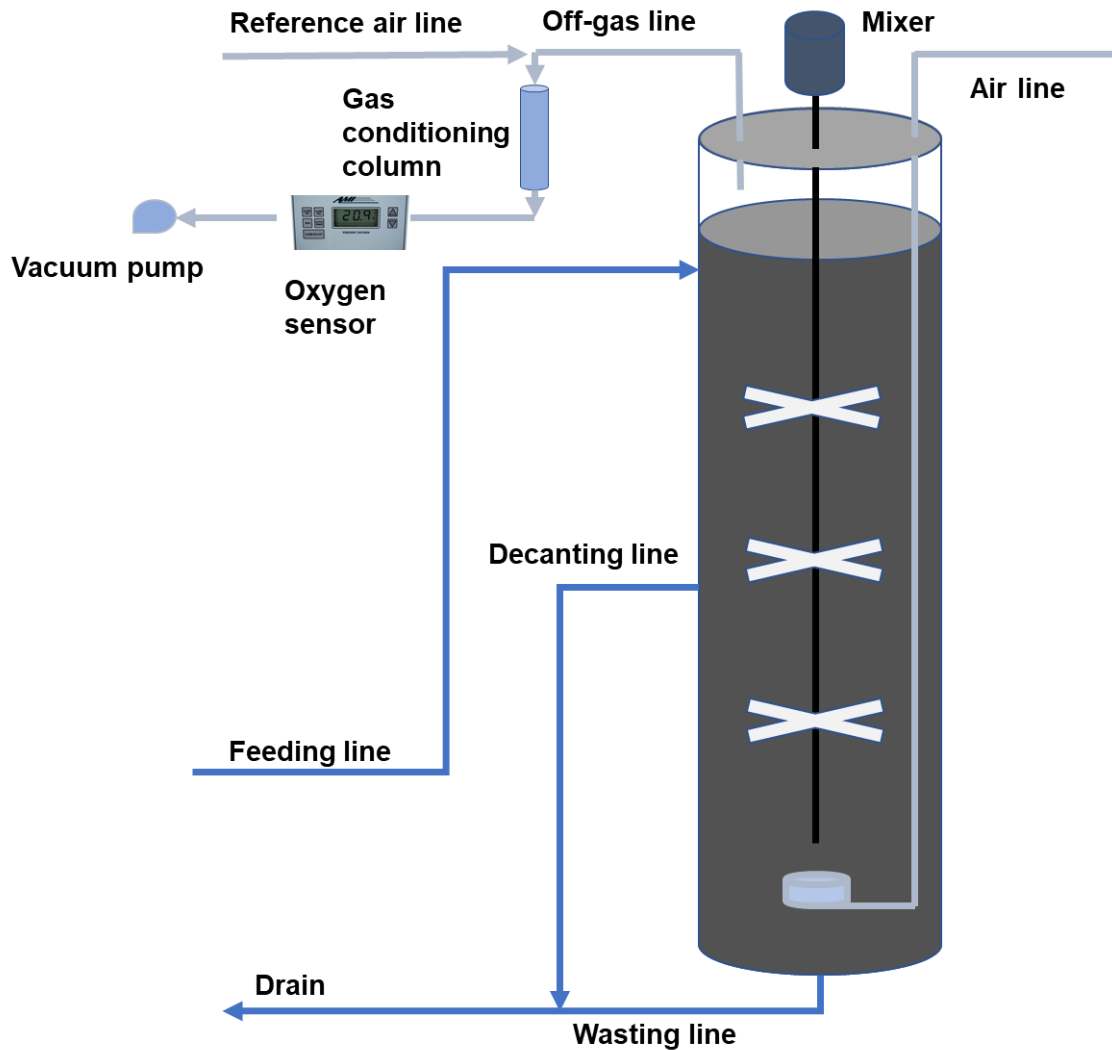


Figure 4-1. Schematic representation of one of the two identical SBRs.

4.2.2 Oxygen transfer efficiency testing

The SBR fed with the RBF-screened wastewater was tested for oxygen transfer efficiency at two different fill ratios of 60% and 80% while maintaining the same SRT of 10 days (Fig. 4-2a, and 4-2b). Since the RBF removes cellulose efficiently, selecting the SBR fed by the RBF effluent was beneficial to distinguish the impact of cellulose. Additional experiments were conducted by adding sodium acetate to increase the sCOD concentration inside the SBR by $100 \text{ mg}_{\text{COD}} \text{ l}^{-1}$ and $200 \text{ mg}_{\text{COD}} \text{ l}^{-1}$. Alpha cellulose was added to increase the cellulose content of the reactor by $100 \text{ mg}_{\text{Cellulose}} \text{ l}^{-1}$ and $200 \text{ mg}_{\text{Cellulose}} \text{ l}^{-1}$. Moreover, to

assess the effects of dissolved contaminants on oxygen transfer, and to subsequently verify the hypothesis that the activated sludge biomass adsorbs the contaminants and alleviates the effects of organics on oxygen transfer, tests using the RBF effluent without active biomass at the same cellulose and acetate concentrations were performed (Fig. 4-2c). For the tests without active biomass, the biomass was removed from the system and transferred to a storage tank for the duration of the test and then returned to the SBR. Furthermore, the oxygen transfer efficiency in the secondary effluent only was also measured at the end of the treatment cycle after removing the settled active biomass (Fig. 4-2d).

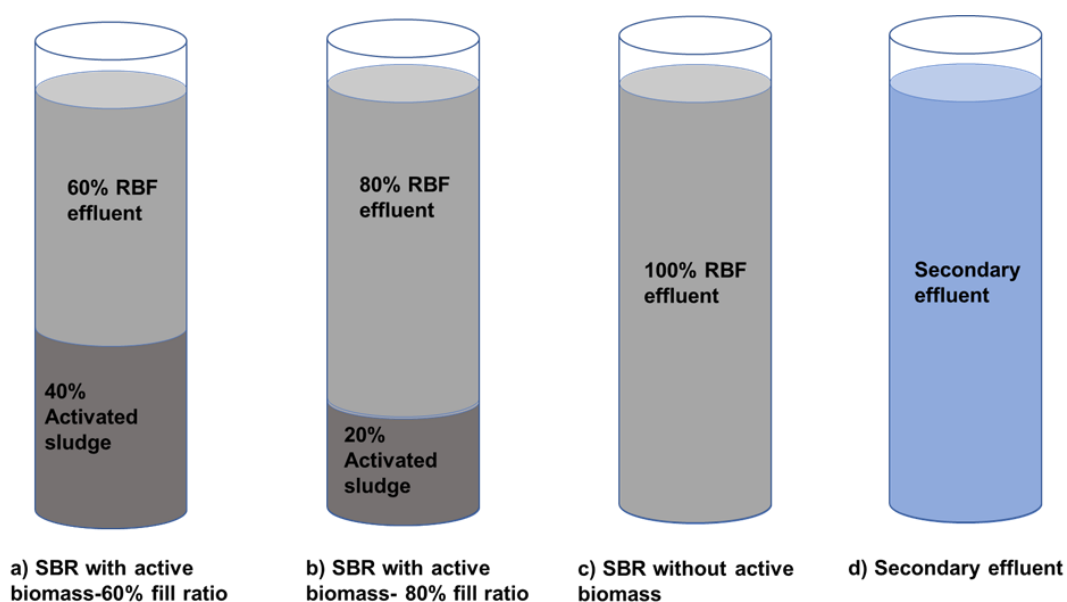


Figure 4-2. Testing scenarios for the aeration efficiency with and without active biomass

Two control strategies were applied to all testing scenarios; a relatively high airflow of $1.7 \text{ m}^3 \text{ h}^{-1}$ (1 SCFM) to maintain an average DO of 4.0 mg l^{-1} and a low airflow of $1.02 \text{ m}^3 \text{ h}^{-1}$ (0.6 SCFM) to maintain an average DO of 2 mg l^{-1} . Table 4-1 summarizes the testing scenarios.

Table 4-1. Aeration testing scenarios

Testing conditions	Testing scenarios	
	Added alpha cellulose mg _{CELLULOSE} l ⁻¹	Added acetate mg _{COD} l ⁻¹
	<i>High airflow (1.7 m³ h⁻¹) and high DO (4 mg l⁻¹)</i>	
With active biomass (60% RBF+ 40% active sludge)	0 (control)	0 (control)
	100	100
With active biomass (80% RBF+ 20% active sludge)	100	100
Without active biomass (100% RBF)	0 (control)	0 (control)
	100	100
	<i>Low airflow (1.02 m³ h⁻¹) and normal DO (2 mg l⁻¹)</i>	
With active biomass (60% RBF+ 40% active sludge)	0 (control)	0 (control)
	100	100
	200	200
With active biomass (80% RBF+ 20% active sludge)	100	100
Without active biomass (100% RBF)	0 (control)	0 (control)
	100	100
	200	200

4.2.3 Oxygen transfer efficiency measurements

Oxygen transfer was measured in clean water and secondary effluent using the unsteady-state method (ASCE, 2007). Oxygen transfer under process conditions was measured via off-gas measurements (Redmon et al., 1983; ASCE, 1996) as oxygen transfer efficiency (OTE, %; eq. 4-1) and oxygen uptake rate (OUR, mg l⁻¹ h⁻¹; eq. 4-2).

$$OTE = \frac{\text{mass } O_2 \text{ in} - \text{mass } O_2 \text{ out}}{\text{mass } O_2 \text{ in}} \times 100 \quad (4-1)$$

The airflow rate was measured using a hot-wire anemometer to measure air velocity, which was used to calculate the airflow rate given the cross-sectional area of the airflow pipe. The product of the airflow rate and the gas transfer efficiency yields the oxygen transfer rate (OTR). The OUR based on the off-gas measurement was then calculated by dividing the OTR by the volume of the water column below the hood (Eq. 2). Although the air on/off approach was used to control the DO inside the reactor, all OTE and OUR measurements were taken only when the DO, air flow, and gas sensor readings were steady (i.e., not varying by more than 5% within the time of measurement):

$$\text{OUR} = \frac{q_o \times \rho \times \text{OTE}}{V \times 100} = \frac{\text{OTR}}{V} \quad (4-2)$$

Where: ρ = Oxygen density (M L^{-3}), q_o = air flow rate ($\text{L}^3 \text{ t}^{-1}$), and V = reactor volume (L^3). Since the clean water efficiency was measured as SOTE (%), the α -factor could be calculated as:

$$\alpha = \frac{\alpha \text{SOTE}}{\text{SOTE}} \quad (4-3)$$

4.2.4 Wastewater characterization

Total suspended solids (TSS), volatile suspended solids (VSS) were measured following standard methods (American Public Health Association, 2005). Chemical oxygen demand (COD), ammonia, nitrate, total and soluble nitrogen (TN and sN), total and soluble phosphorus (TP and sP), and anionic surfactants were measured following Hach Methods. All soluble substrates were measured after filtering the collected samples through sterile 0.45- μm membrane filter papers (VWR International, Canada). Cellulose was measured following the method established by Hurwitz et al., 1961 and validated by Gupta et al., 2018. In addition, ammonia concentrations were tracked online using HORIBA HC-200NH ammonia sensors.

4.2.5 Model structure

Figure 4-3 shows the model structure developed by combining ASM1CL (Reijken et al., 2018) and the first module of the aeration model developed by (Jiang et al., 2017). ASM1CL is a development of ASM1 (Henze, 1992) incorporating the first-order hydrolysis of cellulose. The model was used to estimate the real-time airflow required due to the biodegradation of the influent substrates for both SBRs as well as other scenarios with the addition of cellulose and acetate.

The hydrolysis of slowly biodegradable substrates in ASM1 is impacted by the oxygen and nitrate concentrations, as well as the ratio of slowly biodegradable substrate to heterotrophic biomass. In fact, this process represents a variety of interconnected processes, including hydrolysis, and microorganisms lysis (Henze et al., 2000). For simplicity and to avoid the impact of oxygen as well as the denitrification process, the hydrolysis rate of cellulose was modeled using ASM 3 kinetics as shown in equation 4-4 below. Since the default value of ASM3 half-saturation coefficient of hydrolysis of X_s (K_X) at 20°C of 1 gCOD gCOD_{biomass}⁻¹ is significantly higher than X_{cl}/X_h in this study, which ranged from 0.03 g COD g COD_{biomass}⁻¹ in SBR2 to 0.12 g COD g COD_{biomass}⁻¹ in SBR1, the model is simplified to the first-order model shown in Equation 4-5, consistent with the observation of (Reijken et al., 2018).

$$\frac{dX_{cl}}{dt} = - \frac{k_{cl} \left(\frac{X_{cl}}{X_h} \right)}{K_X + \left(\frac{X_{cl}}{X_h} \right)} X_h \quad (4 - 4)$$

$$\frac{dX_{CL}}{dt} = - k_{CL} \cdot X_{CL} \quad (4 - 5)$$

Influent and effluent measurements of the COD, sCOD, ammonia, TN, and SN were used to estimate the inputs to ASM1CL. Soluble inerts (S_I) were assumed to be equal to the measured SBR effluent sCOD since there were no measurements for the effluent biochemical oxygen demand (BOD). This assumption is quite reasonable as from operational experience it was observed that readily biodegradable substrates were

biodegraded within two hours only. Influent readily biodegradable substrates concentration (S_s) was initially estimated to be equal to the difference between influent and effluent sCOD. Then S_I and S_s were calibrated to match the measured sCOD effluent. The S_s fraction was also verified using the OUR at high air flow rates and elevated DO concentrations to allow for respiration.

Influent cellulose (X_{cl}) in the raw wastewater was determined to be 33% of the influent TSS (Ahmed et al., 2019). Cellulose concentration in the RBF effluent was determined knowing that RBF, on average, removes 80% of the influent cellulose (Ahmed et al., 2019). Influent particulate inert COD concentration (X_I) was estimated using (Eq. 4-6) where HRT is the hydraulic retention time, MLVSS is the measured mixed liquor volatile suspended solids concentration, X_H is the heterotrophic biomass concentration, and X_A is the autotrophic biomass concentration. X_H and X_A were estimated using Equations 4-7 and 4-8, where Y_h is the heterotrophic biomass yield, Y_a is the autotrophic biomass yield, f_p is the biodegradable fraction of biomass leading to particulate materials i.e. 0.10 (Metcalf & Eddy et al., 2002), k_d is the heterotrophic decay coefficient, and k_{dn} is the autotrophic decay coefficient. Slowly biodegradable substrate concentration i.e. excluding cellulose (X_s) was calculated using (Eq. 4-9). Since X_s is a function of the $COD_{removed}$, X_s and X_I were calculated iteratively until they matched the measured MLVSS. TN, and sN were measured experimentally in both reactors. Ammonia was measured experimentally and monitored online in both reactors using ammonia probes. All differential equations associated with the model are listed in the supplementary information section. Figures S1 and S2 in the supplementary information show the input fractions of COD and nitrogen to both SBRs.

$$X_{I,Influent} = \frac{HRT}{SRT} \left(MLVSS_{reactor} \times 1.42 \frac{gCOD}{gVSS} - X_{H,reactor} - X_{A,reactor} \right) \quad (4-6)$$

$$X_{H,reactor} = \frac{SRT}{HRT} \left(1 + f_p \cdot K_d \cdot SRT \right) \left(\frac{COD_{removed} \times Y_h}{1.0 + k_d \cdot SRT} \right) \quad (4-7)$$

$$X_{A,reactor} = \frac{SRT}{HRT} \left(\frac{NO_x \times Y_a}{1.0 + k_{dn} \cdot SRT} \right) \quad (4-8)$$

$$X_{s,\text{Influent}} = \text{tCOD} - X_{\text{I,influent}} - X_{\text{CL,influent}} - S_{\text{s,influent}} - S_{\text{I,influent}} \quad (4-9)$$

NO_x is the oxidized ammonia which is the biologically removed ammonia minus the synthesized biomass nitrogen (Eq. 4-10) where $P_{x,\text{bio}}$ is the biomass synthesis which was calculated using the summation of the heterotrophic and autotrophic biomass produced $P_{x,\text{H}}$, and $P_{x,\text{A}}$ (Eq. 4-11):

$$\text{NO}_x = \text{TKN}_{\text{in}} - (\text{NH}_4 - \text{N})_{\text{eff}} - 0.12 \frac{P_{x,\text{bio}}}{(V_{\text{REACTOR}} \times 0.6 \text{ fill ratio} \times 2.0 \text{ cycles/d})} \quad (4-10)$$

$$P_{x,\text{bio}} = P_{x,\text{H}} + P_{x,\text{A}} \quad (4-11)$$

Heterotrophic and autotrophic biomass produced $P_{x,\text{H}}$, and $P_{x,\text{A}}$ were calculated using the following equations 4-12 and 4-13. Since $P_{x,\text{bio}}$ is a function of NO_x equations 4-10, 4-11, and 4-13 were solved iteratively using a closed loop with an initial assumption of ($P_{x,\text{bio}}=0$) till the right value of the NO_x was reached

$$P_{x,\text{H}} = (1 + f_p \cdot k_d \cdot \text{SRT}) \left(\frac{V_{\text{REACTOR}} \times 0.6 \text{ fill ratio} \times 2.0 \frac{\text{cycles}}{\text{day}} \times \text{COD}_{\text{removed}} \times Y_h}{1.0 + k_d \cdot \text{SRT}} \right) \quad (4-12)$$

$$P_{x,\text{A}} = \frac{V_{\text{REACTOR}} \times 0.6 \text{ fill ratio} \times 2.0 \frac{\text{cycles}}{\text{day}} \times \text{NO}_x \times Y_a}{1.0 + k_{\text{dn}} \cdot \text{SRT}} \quad (4-13)$$

ASM1CL model estimated the change in the concentration of the substrates with the time due to biodegradation, which was subsequently used to estimate the theoretical oxygen demand (ThOD) that corresponds to OTR using (Eq. 4-14). Utilized COD is the summation of the utilized S_s , X_s , and X_{cl} as kg d^{-1} . The $\text{NO}_{x,\text{oxidized}}$ is the oxidized ammonia as kg d^{-1} .

$$\text{ThOD} = \text{OTR} = \text{COD}_{\text{utilized}} + (4.57 \times \text{NO}_{x,\text{oxidized}}) - 1.42 P_{x,\text{bio}} \quad (4-14)$$

The real-time α factor was then estimated using the correlation that was defined between α and experimental sCOD. The real-time α factor was then used to estimate the real-time standard oxygen transfer rate (SOTR) following Eq. 4-15 where C_{∞}^* is the saturated

dissolved oxygen concentration, $C_{\infty,20}^*$ represents the saturated dissolved oxygen concentration at 20°C, T is the temperature, θ is the temperature correlation coefficient, DO is the dissolved oxygen concentration. Real-time airflow was calculated following Eq. 4-16 where SOTE is the standard oxygen transfer efficiency in clean water, ρ_{air} is the air density and y_{O_2} is the ponderal fraction of oxygen in air (=0.23). Since SOTE in the clean water is a function of the airflow (Fig. S3), the model calculated airflow and SOTE iteratively until they met the required SOTR corresponding to α -factor at each time step.

$$SOTR = \frac{OTR}{\alpha.F \left[\frac{\beta C_{\infty}^* - DO}{C_{\infty,20}^*} \right] \cdot \theta^{T-20}} \quad (4-15)$$

$$SOTR = SOTE \cdot \text{Air Flow Rate} \cdot \rho_{air} \cdot y_{O_2} \quad (4-16)$$

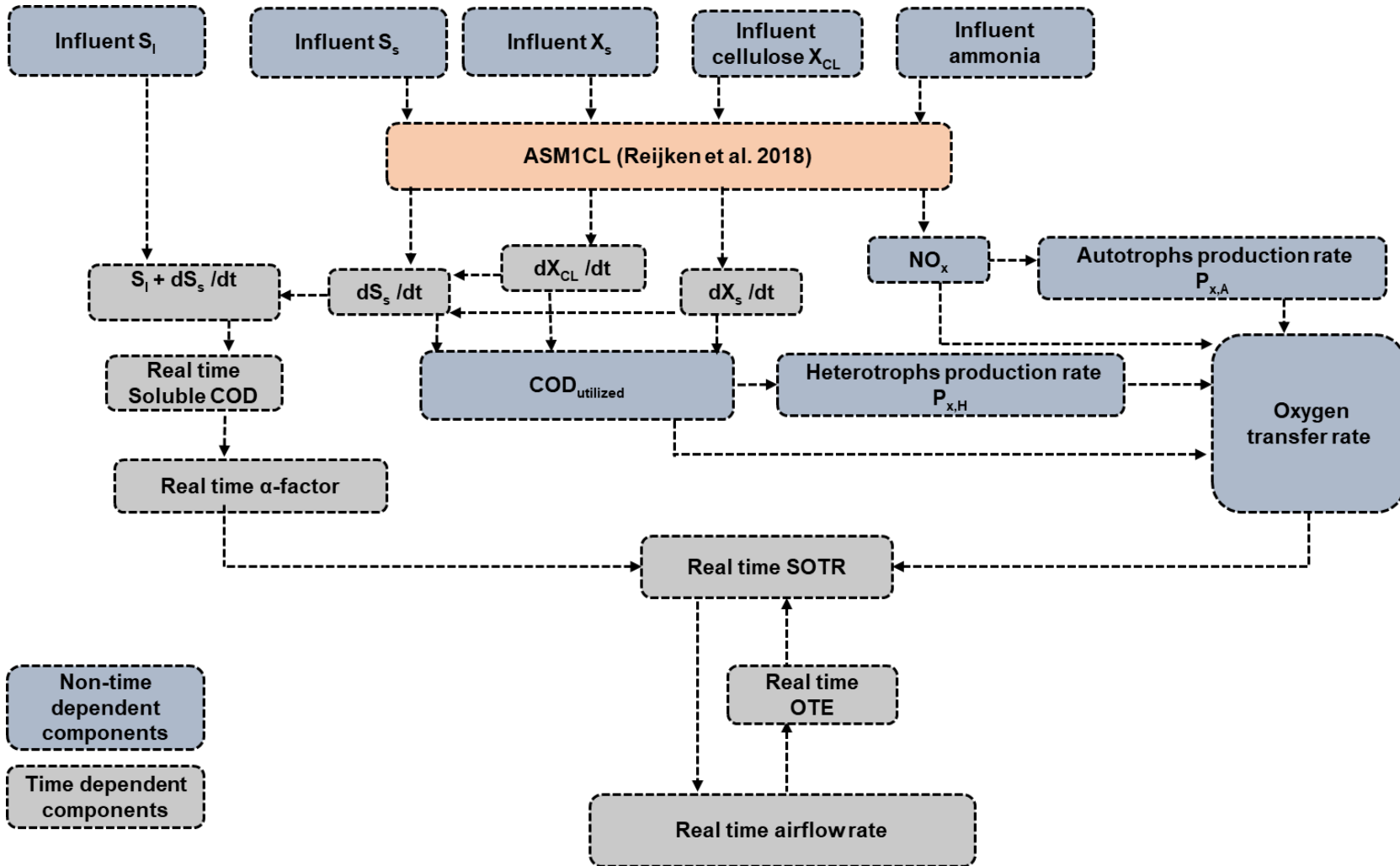


Figure 4-3. Model structure.

4.3 Results and Discussion

4.3.1 Pilot SBRs performance

The RBF showed TSS, COD, TN, and TP removal efficiencies of 39%, 28%, 4%, and 15%, respectively. Both SBRs achieved comparable COD, TN, ammonia, and TP removal efficiencies of 95%, 75%, 98%, and 92% respectively. In addition, due to the COD removal by the RBF, 30% less solids production was observed in SBR2 (fed with the RBF effluent) when compared to SBR1 (fed with the raw wastewater). Table S1 (in the supplementary information) shows the influent and effluent wastewater characteristics for both SBRs at a steady-state after being operated for one month. Figure S4 shows the effluent COD, TN, and TP for both reactors during the testing period. Both SBRs were achieving steady-state conditions and despite the variability in the influent concentrations, effluent, and biomass concentrations were at a steady state. Inert inorganic suspended solids accumulation in the sludge using the accumulation factor of (SRT / HRT) for both SBRs matched with the MLSS and MLVSS measurements. Both SBRs had a comparable observed yield of 0.4 mgVSS mgCOD⁻¹. Nitrogen mass balance showed a nitrogen content of 10% and 12% of MLVSS in SBR1 and SBR2, which matches the typical nitrogen content of biosolids. Phosphorus mass balance revealed a phosphorus content of 4% and 4.50% of MLVSS in SBR1 and SBR2, which is in close agreement with the typical phosphorus contents of biosolids in enhanced biological phosphorus removal systems (EBPR) (Zaman et al., 2019).

4.3.2 Oxygen transfer studies

Figure 4-4 shows the real-time change in α -factor, OTE, and OUR due to the addition of 100 mg_{acetate} l⁻¹ and 100 mg_{cellulose} l⁻¹. Alpha-cellulose was added after all readily biodegradable substrates (acetate) had been consumed. As expected, the α -factor, OTE, and OUR were low at the beginning of the cycle and improved with the biodegradation of the acetate and cellulose. Anionic surfactants were measured and were found to follow the sCOD, and α -factor increased with surfactants degradation (Fig. 4-5). Surfactants are characterized by their hydrophilic heads that accumulate on the gas-liquid interface and the

hydrophobic tails that remain inside the bubbles, hindering the gas-side mass transfer film renewal rate (Baquero-Rodríguez et al., 2018; Rosso and Stenstrom, 2006). Apparently, α -factor improved with the anionic surfactant biodegradation.

4.3.2.1 Acetate test

Table 4-2 shows the oxygen transfer parameters at different testing scenarios, control strategies, and acetate loading rates with active biomass. Reported values for the α SOTE, OTE, OUR from off-gas, and α -factor represent the flow weighted averages. At the high airflow and high DO, the addition of acetate did not impact the α -factor and OUR significantly. At the low air flow and DO of 2 mg l⁻¹, the addition of acetate to increase sCOD by 100 mg l⁻¹ and 200 mg l⁻¹ reduced the OUR off-gas by 49% and 57%, which, hence, reduced the α -factor by 43% and 57% respectively. It must be noted that increasing the filling ratio from 60% to 80% while maintaining the same biomass concentration did not impact oxygen transfer efficiency at both air flows and DO control strategies.

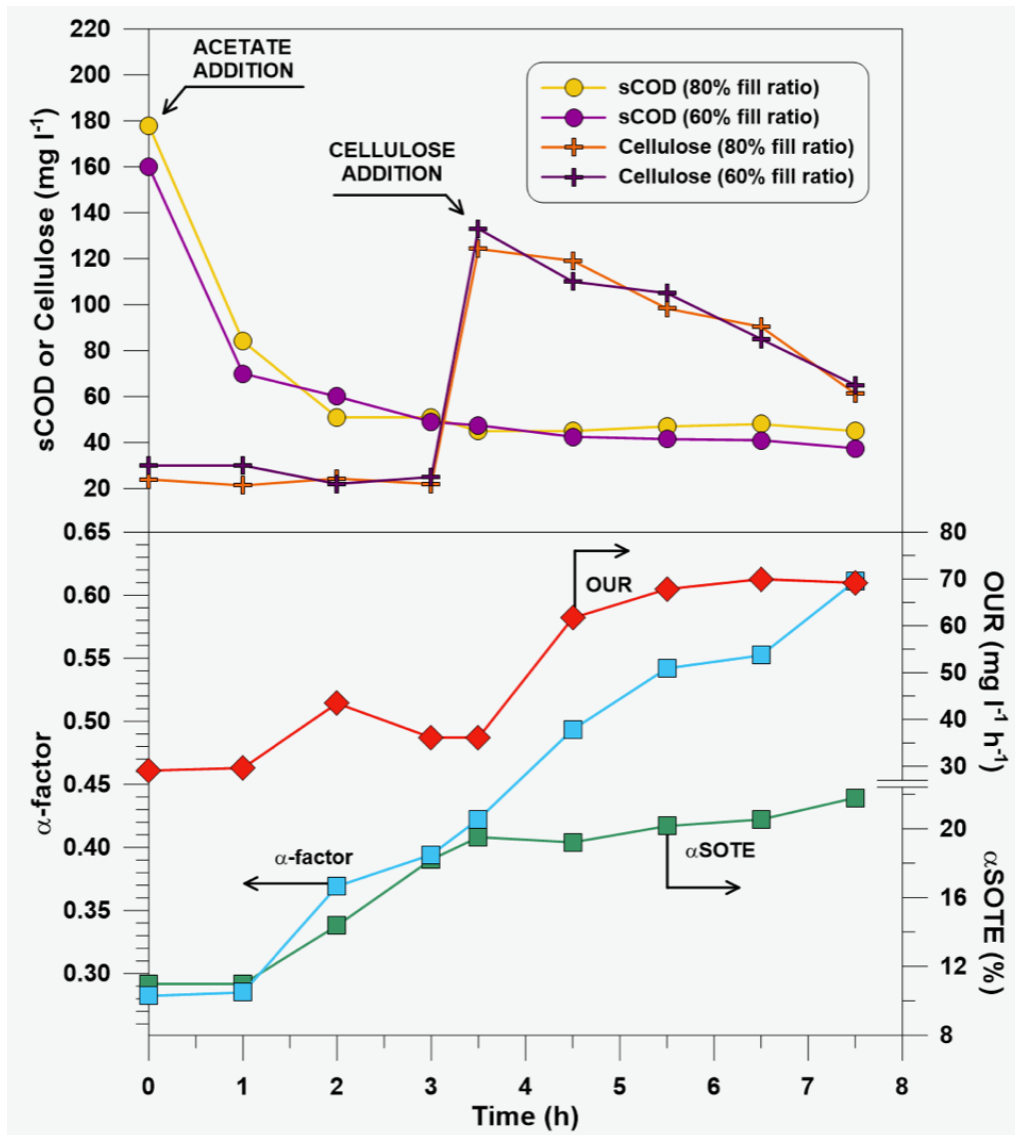


Figure 4-4. Impact of acetate and cellulose on α -factor, OUR and α SOTE. (80% fill ratio)

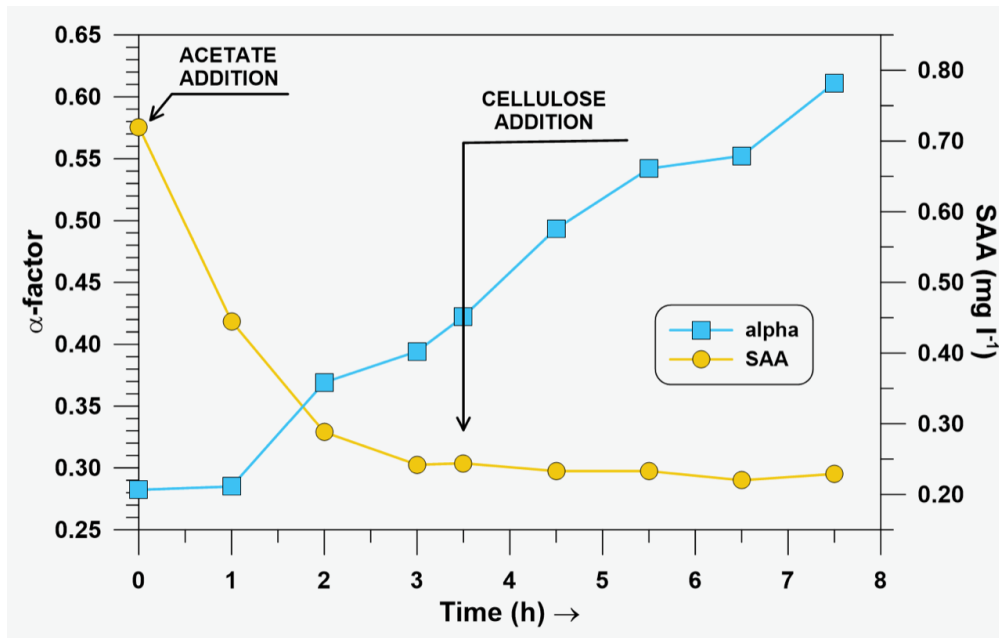


Figure 4-5. Impact of anionic surface-active agents (SAA) on the α -factor (80% fill ratio).

The OUR measured from the off-gas was then compared with the OUR measured by respiration (Table 4-2). The OUR from respiration was calculated using the rate of the change in the DO with time (i.e., dDO/dt) inside the reactor while the process air was off. The reported values in the table represent the average \pm standard deviation of OUR respiration corresponding to the off-gas measurements at different times within the treatment cycle. OUR from the off-gas measurements (gas phase) was comparable to OUR measured from the respiration (liquid phase) when acetate was added. However, for the control cases without the addition of acetate or cellulose, the measured OUR from both gas and liquid phases were not comparable. The addition of acetate as a readily biodegradable substrate hinders nitrification. This happened since high acetate concentrations were found to associate with high surfactant concentrations (Fig. 4-5) that hindered the OTE and hence nitrification. The nitrogenous OUR (NOUR) was calculated using the real-time change in ammonia (i.e., dNH_4^+/dt) multiplied by $4.57 \text{ gCOD g NH}_4\text{-N}^{-1}$. In the control cases, the summation of OUR due to carbon oxidation and NOUR was comparable to the OUR off-

gas. Since the OUR off-gas phase was measured while the air was on and the OUR respiration was measured while the air was off, the monitored ammonia and airflow rates were plotted in Fig. 4-6 considering the two phases after adding acetate and cellulose. Cellulose was added 3 h after the addition of acetate to ensure that all the acetate had been biodegraded. The addition of acetate reduced the nitrification rate and when the air was on, a very small ammonia release ($<0.5 \text{ mg l}^{-1}$) was observed (Fig. 4-6a). Once acetate and surfactants were biodegraded, nitrification started to recover. Also, nitrification was observed to be higher when the air was on than when the air was off (Fig. 4-6c) confirming that the observed difference between measured OUR from respiration and OUR from off-gas was due to nitrification. It must be asserted that in the case of the acetate, NOUR was negligible ($<10 \text{ mg l}^{-1} \text{ h}^{-1}$) due to an overall low nitrification rate, and subsequently the OUR from off-gas balanced with the OUR from respiration.

The difference between the high and low DO can be explained using OUR measurements. At the high airflow and high DO, the addition of acetate increased the OUR from respiration indicating that the high DO initiates higher substrate utilization rates when compared to the control case and therefore, the impact on the α -factor was negligible. At the low air flow and low DO, the addition of acetate to increase sCOD by 100 mg l^{-1} and 200 mg l^{-1} reduced NOUR by 61% and 74% when compared to the control case, and therefore the α -factor, on average, decreased by 48%.

Table 4-2. Oxygen transfer parameters at different testing scenarios and different acetate loading rates with active biomass

Test	α SOTE	OTE	OUR off-gas ^a	OUR respiration ^b	NOUR ^c	α - factor	DO	Airflow	MLVSS
	%	%	mg l ⁻¹ h ⁻¹	mg l ⁻¹ h ⁻¹	mg l ⁻¹ h ⁻¹		mg l ⁻¹	m ³ h ⁻¹	mg l ⁻¹
High airflow and high DO									
Control (60%RBF+40% Activated sludge)	23	14	72	37 ± 10	28	0.68	3.69 ± 0.57	1.55 ± 0.21	2,885 ± 89
Acetate test (100 mg l⁻¹) - 60% fill ratio	22	13	69	56 ± 5	27	0.65	3.84 ± 0.50	1.60 ± 0.12	1,904 ± 42
Acetate test (100 mg l⁻¹) - 80% fill ratio	21	10	53	48 ± 2	14	0.63	5.25 ± 0.25	1.69 ± 0.34	1,616 ± 55
Low airflow and normal DO									
Control (60%RBF+40% Activated sludge)	22	18	67	29 ± 4	23	0.56	1.95 ± 0.48	1.17 ± 0.07	2,138 ± 93
Acetate test (100 mg l⁻¹) - 60% fill ratio	15	12	36	24 ± 4	9	0.34	2.08 ± 0.15	0.97 ± 0.01	2,070 ± 11
Acetate test (100 mg l⁻¹) - 80% fill ratio	13	10	32	29 ± 1	9	0.30	2.13 ± 0.48	0.95 ± 0.16	1,840 ± 27
Acetate test (200 mg l⁻¹) - 60% fill ratio	10	8	29	27 ± 2	6	0.24	1.60 ± 0.00	1.06 ± 0.04	2,142 ± 116

^a OUR off-gas was calculated using the regular off-gas approach and represent flow-weighted averages (OUR=oxygen transfer rate/ reactor volume).

^b OUR respiration was calculated using the rate of change of DO with the time (dc/dt) while the air was off.

^c NOUR is the OUR due to nitrification (NOUR=4.57•dNH₄/dt).

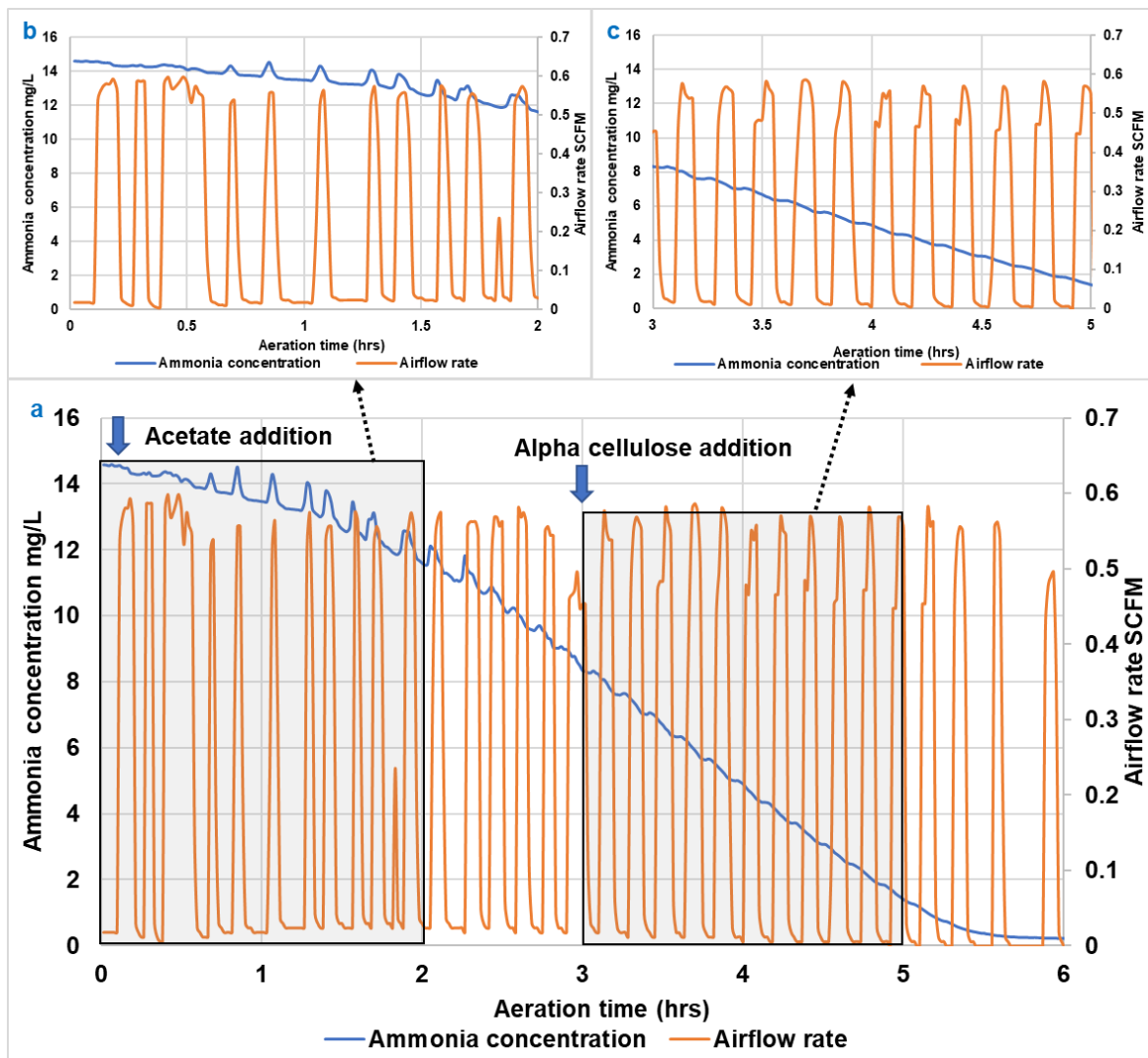


Figure 4-6. Ammonia and airflow profiles showing the nitrification rate change while controlling the airflow rates.

4.3.2.2 Cellulose test

Table 4-3 shows the oxygen transfer values for the different testing scenarios, control strategies, and cellulose loading rates with active biomass. Similar to what was observed for acetate, at the high air flow and high DO, the addition of cellulose impacted neither the α -factor nor the OUR. At the low air flow and low DO, increasing the cellulose concentrations by 100 mg l^{-1} and 200 mg l^{-1} reduced the α -factor by 16% and 25%, respectively. The addition of cellulose had a lower impact on aeration efficiency when

compared to acetate confirming the sensitivity of the aeration efficiency to acetate. The OUR measured from the gas phase (i.e., off-gas tests) was higher than the OUR in the liquid phase (i.e., respiration tests) in all cases. Analogously to the acetate cases, the NOUR was calculated, and the summation of the OUR in the liquid phase and the NOUR was comparable to the OUR in the gas phase. This happened since cellulose was added after all rbCOD was consumed. Since nitrification was confirmed to be more active when the air is on than when the air is off (Fig. 4-6), the OUR from off-gas (measured when the air was on) balanced with the summation of the OUR from respiration (measured when the air was off) and the NOUR. Similar to the tests with the acetate, at the low air flow and low DO, on average the NOUR decreased by 30%, leading to an average reduction of 19% in the α -factor due to alpha-cellulose addition.

Results obtained from the tests with the cellulose were compared with the long term off-gas measurements recorded from both SBRs, with and without primary treatment. Table 4-4 shows the impact of the RBF on oxygen transfer. The values reported for α SOTE, OTE, OUR from off-gas, and α -factor are presented as airflow-weighted averages. The influent cellulose represented on average 35% of the raw wastewater TSS, as reported in a previous study (Ahmed et al., 2019), meaning that influent cellulose in this study was 125 mg l^{-1} . The RBF removed 80% of the influent cellulose (Ahmed et al., 2019), which corresponds to $100 \text{ mg}_{\text{cellulose}} \text{ l}^{-1}$. While maintaining comparable airflow and DO in both SBRs, the SBR fed with the raw wastewater had an α -factor of 0.53 compared to 0.58 for the SBR fed by the RBF-screened wastewater (9.4% difference). In both reactors, on average, the α -factor ranged between 0.30 at the beginning of the cycle to 0.60 at the end of the cycle. The significance of the observed differences in α -factor for both SBRs was evaluated using the standard *t*-test approach at the 95% confidence level and the observed difference was insignificant since both SBRs were running at the same effluent sCOD concentrations and hence sCOD would have impacted α -factor equally. The addition of $100 \text{ mg}_{\alpha\text{-cellulose}} \text{ l}^{-1}$ to SBR2 reduced the α -factor by 16% (Table 4-3). However, in SBR1 the impact of the same concentration of cellulose on the α -factor was insignificant due to the higher biomass concentrations in SBR1 than SBR2 (2950 mg l^{-1} vs. 2055 mg l^{-1}) associated with higher biodegradation rate and hence more rapid increase in α -factor.

Table 4-3. Oxygen transfer parameters at different testing scenarios and different cellulose loading rates

Test	α SOTE	OTE	OUR off-gas ^a	OUR respiration ^b	NOUR ^c	α - factor	DO	Airflow	MLVSS
	%	%	mg l ⁻¹ h ⁻¹	mg l ⁻¹ h ⁻¹	mg l ⁻¹ h ⁻¹		mg l ⁻¹	m ³ h ⁻¹	mg l ⁻¹
High airflow and high DO									
Control (60%RBF+40%AS)	23	14	72	37 ± 10	28	0.68	3.69 ± 0.57	1.55 ± 0.21	2,885 ± 89
Cellulose test (100 mg l⁻¹) - 60% fill ratio	22	12	65	48 ± 1	27	0.66	4.24 ± 0.58	1.64 ± 0.17	2,911 ± 99
Cellulose test (100 mg l⁻¹) - 80% fill ratio	22	11	64	26 ± 1	25	0.69	4.82 ± 0.49	1.74 ± 0.23	1,775 ± 14
Low airflow and normal DO									
Control (60%RBF+40%AS)	22	18	67	29 ± 4	23	0.56	1.95 ± 0.48	1.17 ± 0.07	2,138 ± 93
Cellulose test (100 mg l⁻¹) - 60% fill ratio	19	15	48	22 ± 3	16	0.45	2.08 ± 0.13	0.99 ± 0.01	2,145 ± 44
Cellulose test (100 mg l⁻¹) - 80% fill ratio	20	17	58	26 ± 1	16	0.49	1.74 ± 0.71	1.05 ± 0.20	1,954 ± 30
Cellulose test (200 mg l⁻¹) - 60% fill ratio	17	13	49	27 ± 5	16	0.42	1.97 ± 0.72	1.14 ± 0.10	2,390 ± 88

^a OUR off-gas was calculated using the regular off-gas approach and represent flow-weighted averages (OUR=oxygen transfer rate/ reactor volume).

^b OUR respiration was calculated using the rate of change of DO with the time (dc/dt) while the air was off.

^c NOUR is the OUR due to nitrification (NOUR = 4.57 • dNH₄/dt).

Additionally, energy as kWh cycle⁻¹ and kWh kgThOD⁻¹ were calculated based on the air flow and the removed load from both SBRs, using Eq. 4-17 (Table 4-4). SBR2 showed less energy consumption per cycle than SBR1 (25%). The energy consumption per ThOD showed a saving of 6.7% compared to the 8.6% improvement in the α -factor due to the RBF (Table 4-4).

$$E = BHP \cdot \Delta t = \frac{wRT_1}{29.7 n e} \left[\left(\frac{p_2}{p_1} \right)^n - 1 \right] \cdot \Delta t \quad (4-17)$$

where: BHP = blower break horse power (kW); Δt = time on duty, i.e. aeration time – time without aeration (s); w = ponderal air flow (kg s⁻¹); R = gas constant (8.314 J mol⁻¹ K⁻¹); T_1 = absolute inlet temperature (K), p_1 = absolute inlet pressure (Pa), p_2 = absolute discharge pressure (Pa), n = 0.283 for air (-), e = blower efficiency (-).

Table 4-4. Impact of RBF screening on the oxygen transfer efficiency.

Process	DO	α SOTE	OTE	α -factor	OUR	Airflow	Energy	
	mg l ⁻¹	%	%		mg l ⁻¹ h ⁻¹	m ³ hr ⁻¹	kWh cycle ⁻¹	kWh kg _{ThOD} ⁻¹ a
SBR 1 (non-screened)	1.89±0.093	20	17	0.53	60	1.22±0.20	0.12	1.04
SBR 2 (screened)	2.73±0.76	23	17	0.58	63	1.19±0.31	0.09	0.97

^a Equal to the power required for each cycle (kWh cycle⁻¹) • 2 cycles d⁻¹ divided by the ThOD (kg_{O2} d⁻¹) estimated by the model.

4.3.2.3 Tests without active biomass

In the absence of the active biomass (Table 4-5), the impact of adding acetate and cellulose to the RBF effluent on oxygen transfer was quantified as α -factor decrease by 47% from 0.68 to 0.36 at high air flow and high DO, and by 43% from 0.56 to 0.32 at low air flow and low DO.

Similar to the case with active biomass, at the high air flow and high DO, the addition of acetate marginally impacted both OUR and α -factor relative to the case with only the RBF effluent. At the low air flow and low DO, increasing sCOD concentration by 100 mg l⁻¹ and 200 mg l⁻¹ decreased the α -factor by 25% and 44%, respectively. The presence of active biomass, which targets all biodegradable substrates, increases the OUR and improves the oxygen transfer efficiency when compared to the case without active biomass.

At the high air flow and high DO, the addition of cellulose did not impact the NOUR. However, it increased the OUR from off-gas and the OUR from respiration by 27% and

30% respectively, indicating that the addition of cellulose while maintaining high DO, enhanced the substrates utilization rate which subsequently improved aSOTE and α -factor by 25% and 23%, respectively. At the low air flow and low DO, the addition of cellulose had a negligible impact on α -factor and the OUR off-gas. This happened since in both cases i.e. the RBF effluent only and the RBF effluent with the addition of cellulose, sCOD concentrations were high due to the very low biodegradation rates, and the sCOD effect on the α -factor was more predominant than the effect of cellulose.

4.3.2.4 Oxygen transfer efficiency in secondary effluent

Oxygen transfer in the secondary effluent was measured and showed α -factors of 0.69 and 0.57 at the high and low air flows, respectively, confirming that the suppressed transfer efficiency observed at the end of the cycle was limited by the secondary effluent water quality. In fact, even though the overwhelming majority of the load was removed by the end of a secondary process (to at least meet the secondary BOD/TSS standards of 30/30 mg l⁻¹), the values of the α -factor are usually far from reaching such high levels. In fact, the residual concentration of organics in the water, not necessarily from the primary effluent but by-products of microbial metabolism (Tseng et al., 2013), still affects persistently the oxygen transfer. The attribution of this inability to recover the oxygen transfer in full should, therefore, not be placed solely on the presence of the suspended biomass (Henkel et al., 2009).

Figure 4-7 summarizes the α -factor improvement due to the biomass effect. It is interesting to note that biodegradation and biosorption increased the α -factor from 0.30 in the RBF effluent to 0.56 in the secondary effluent with biomass. The removal of biomass yielded a marginal increase in α -factor, from 0.56 to 0.60.

Table 4-5. Oxygen transfer parameters at different testing scenarios and different acetate and cellulose loading rates without active biomass.

Test	aSOTE	OTE	OUR off-gas ^a	OUR respiration ^b	NOUR ^c	α -factor	DO	Airflow	MLVSS
	%	%	mg l ⁻¹ h ⁻¹	mg l ⁻¹ h ⁻¹	mg l ⁻¹ h ⁻¹		mg l ⁻¹	m ³ h ⁻¹	mg l ⁻¹
High airflow and high DO									
Control (RBF effluent 100%)	12	5	27	17 ± 1	5	0.36	5.58 ± 0.51	1.61 ± 0.24	251 ± 14
Acetate test (100 mg/L)	10	5	26	13 ± 1	4	0.30	5.03 ± 0.78	1.74 ± 0.11	143 ± 8
Cellulose test (100 mg/L)	16	8	37	24 ± 2	5	0.47	5.06 ± 0.66	1.45 ± 0.37	313 ± 17
Low airflow and normal DO									
Control (RBF effluent 100%)	13	11	35	33 ± 1	2	0.32	2.00 ± 0.00	1.04 ± 0.06	282 ± 39
Acetate test (100 mg/L)	10	8	28	20 ± 4	3	0.24	1.64 ± 0.25	1.05 ± 0.02	134 ± 3
Acetate test (200 mg/L)	7	6	20	15 ± 2	4	0.18	2.02 ± 0.79	1.12 ± 0.11	245 ± 36
Cellulose test (100 mg/L)	12	10	35	22 ± 2	6	0.29	1.65 ± 0.30	1.07 ± 0.03	237 ± 5
Cellulose test (200 mg/L)	10	8	29	25 ± 4	7	0.25	1.83 ± 0.43	1.08 ± 0.06	460 ± 10

^a OUR off-gas was calculated using the regular off-gas approach and represent flow-weighted averages (OUR=oxygen transfer rate/ reactor volume).

^b OUR respiration was calculated using the rate of change of DO with the time (dc/dt) while the air was off.

^c NOUR is the OUR due to nitrification (NOUR=4.57*dNH₄/dt).

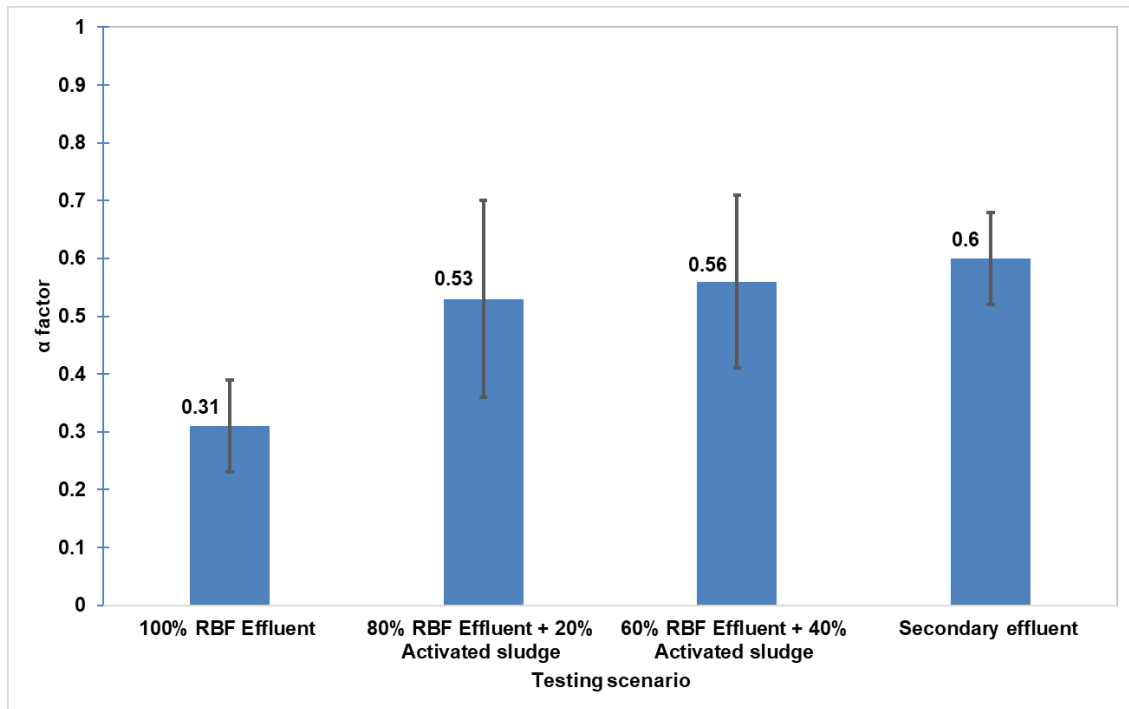


Figure 4-7. The α -factor improvement due to the biosorption impact.

4.3.3 Aeration model results

4.3.3.1 Model calibration

The kinetic coefficients were calibrated using the in-cycle measurements of MLVSS, sCOD, and ammonia in the SBR2 (Table S2). OUR respiration profiles from three different cycles were used to verify S_s and S_i fractions (Fig. S5). The concentrations of S_s were estimated using (Eq. 4-18). The tested cycles from SBR2 (filtered) had an average TCOD of 412 mg l^{-1} , sCOD of 215 mg l^{-1} and an estimated S_s of 190 mg l^{-1} , which constitutes 46% of the TCOD and 89% of the sCOD. The corresponding values in the calibrated model were 47% of TCOD and 86% of sCOD.

$$\text{Influent } S_s = \frac{\text{OUR for area A } \left(\frac{\text{mg}}{\text{L}}\right)}{(1-Y_H)} \left(\frac{V_{\text{Activated sludge(L)}} + V_{\text{Wastewater(L)}}}{V_{\text{wastewater(L)}}} \right) \quad (4 - 18)$$

The model MLVSS values were calibrated to match the MLVSS measured during the aeration cycle (Fig. S6). The heterotrophic maximum specific growth rate μ_H and the

carbonaceous substrate half-saturation constant K_s were calibrated to match the sCOD profiles (Fig. S7). The autotrophic maximum specific growth rate μ_A and the ammonium half-saturation constant $K_{\text{NH}_3\text{-N}}$ were calibrated to match ammonia profiles (Fig. S8).

The hydrolysis rate of the cellulose was calculated using the measured cellulose from both tests with the addition of 100 mg l⁻¹ and 200 mg l⁻¹ assuming first-order biodegradation kinetics and the average k_{cl} was 4.1 d⁻¹ (Fig. S9).

4.3.3.2 Experimental correlation between α -factor and sCOD

A negative correlation between α -factor and sCOD in the SBR was identified with a coefficient of determination of 0.75 (Fig. 4-8). This correlation appears to be a combination of two linear correlations. For sCOD more than 75 mg l⁻¹, the improvement of the α -factor due to the decrease in sCOD was slow due to the presence of surfactants, that negatively affected the oxygen transfer process. For sCOD less than 75 mg l⁻¹, the α -factor dramatically increased with the sCOD decrease, confirming the higher sensitivity of the α -factor to sCOD. The estimated relationship between α -factor and sCOD (Eq. 4-19) was then integrated into the model to estimate the α -factor as a function of the state variable sCOD with time. The measured dissolved anionic surfactant was added to the correlation to understand the impact of the surfactants on the α -factor. For anionic surfactants concentrations more than 0.3 mg l⁻¹, α -factor was consistently low at 0.25. With the surfactant's biodegradation, α -factor dramatically increased with the surfactant's decrease. As fine bubbles are stable at smaller diameters, their interfacial specific area is high; however, the presence of surfactants decreased k_{La} , which indicates that the k_L decrease was faster than the interfacial area (a) increases (Wagner and Pöpel, 1996; Rosso and Stenstrom, 2006). The key causes of mass transfer depression at high surfactant concentrations are molecular obstruction, which decreases the rate of interfacial regeneration and the real area covered by the surfactant molecules associated with the reduction of the available surface area for mass transfer. In addition, the presence of hydrophobic tails in the bubble decreases the internal circulation of gas, which decreases gas-side mass transfer film renewal (Rosso and Stenstrom, 2006). This indicates that hindered transfer rates were limited by the surfactants accumulation i.e. for surfactants

concentrations more than 0.3 mg l^{-1} the bubbles were colonized by surfactants and below this values α -factor improved with the accumulation decrease. This suggests that the suppressed transfer rates were restricted by the accumulation of surfactants. In the case of surfactant concentrations greater than 0.3 mg l^{-1} , the bubbles were mainly colonized by surfactants and, with biodegradation, the accumulation decreased, improving the α -factor.

$$\alpha = 4.275 \text{ sCOD}^{-0.557} \quad (4 - 19)$$

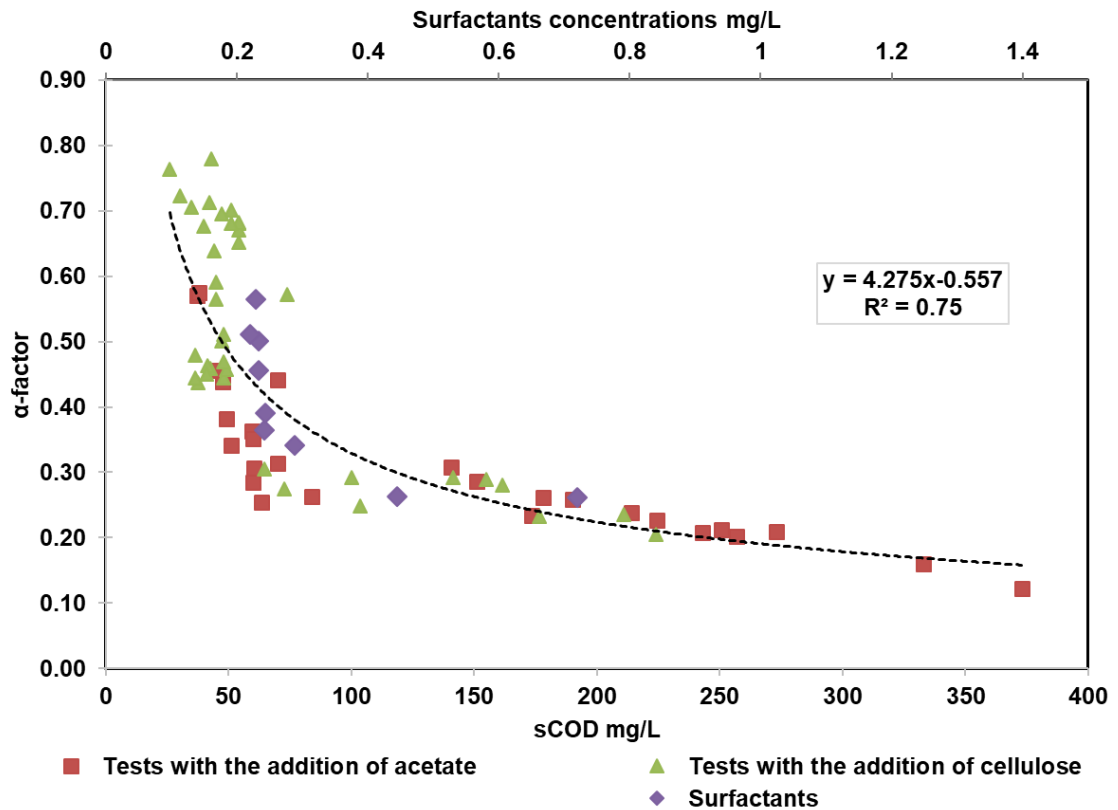


Figure 4-8. Correlation between sCOD and α -factor.

4.3.3.3 Model validation

The developed model was used as a predictive tool to quantify the air flow required to mitigate the reduction in oxygen transfer efficiency due to the organic loading. Both SBRs were modeled; SBR1 without primary treatment (influent characteristics of $\text{COD} = 643 \text{ mg l}^{-1}$, $\text{sCOD} = 255 \text{ mg l}^{-1}$, $\text{TN} = 35 \text{ mg l}^{-1}$, and $\text{NH}_4^+ = 24 \text{ mg l}^{-1}$), SBR2 with RBF treatment

(influent characteristic of COD = 465 mg l⁻¹, sCOD = 255 mg l⁻¹, TN = 34 mg l⁻¹, and NH₄⁺ = 20 mg l⁻¹). Both SBRs were modeled to target a DO set point of 2 mg l⁻¹. Initial inputs to each scenario are shown in Tables S3, S4, S5, and S6.

Figure 4-9 shows the modeled vs. measured temporal variation of the α -factor due to changes in the SBR sCOD concentrations. The measured and modeled α -factors for both reactors were comparable with an average percentage error of 4.2% and 3.7% for SBR1 and SBR2, respectively. The α -factor was very low at the beginning of the aeration cycle for both SBRs due to the high concentration of the sCOD which necessitates applying high air flow rates to mitigate the reduction in oxygen transfer efficiency. The α -factor recovered with time due to the biodegradation of the readily biodegradable substrates. As expected, the α -factor in the SBR1 recovered faster due to a higher biomass concentration of 3000 mg l⁻¹ when compared to all other modeled scenarios with an average biomass concentration of 2000 mg l⁻¹.

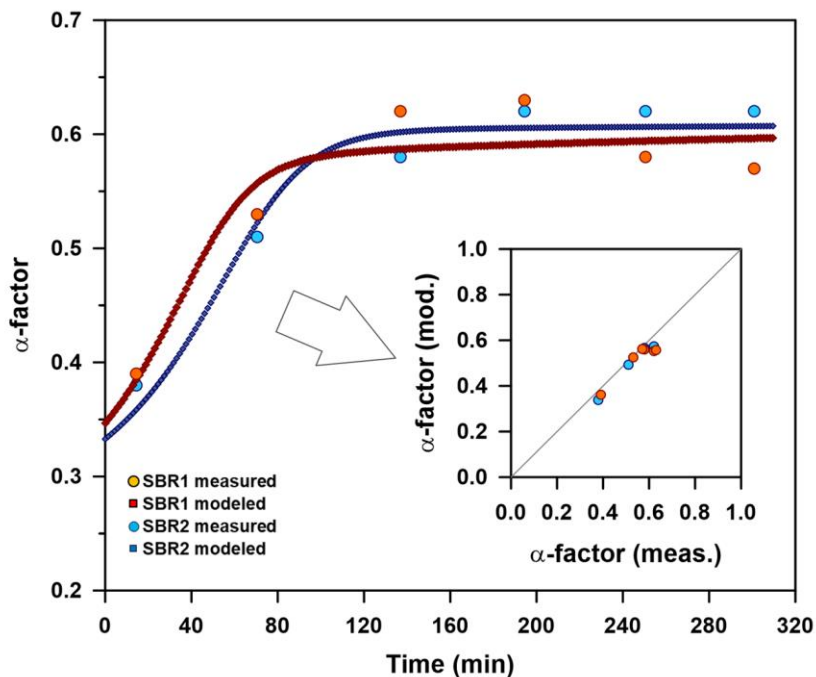


Figure 4-9. The change in the measured and modeled α -factor with the time due to the biodegradation of the organic loadings in both SBRs.

Figure 4-10 shows the temporal variation of the modeled versus measured (30-min moving average) air flow rate. The measured and modeled air flow rates for both reactors were comparable with an average percent error of 6.3% and 5.9% for SBR1 and SBR2 respectively. The moving average air flow correlates with the actual organic and nitrogen loading rates removed through the cycle. The air requirements for both reactors were high at the beginning of the cycle and decreased with the time due to the biodegradation of the organics. SBR2 had lower air flow requirements when compared to SBR 1 due to the partial removal of cellulose and slowly biodegradable substrate by the RBF. The presence of cellulose in the influent reduces the α -factor on one hand and increases the oxygen requirements on the other hand.

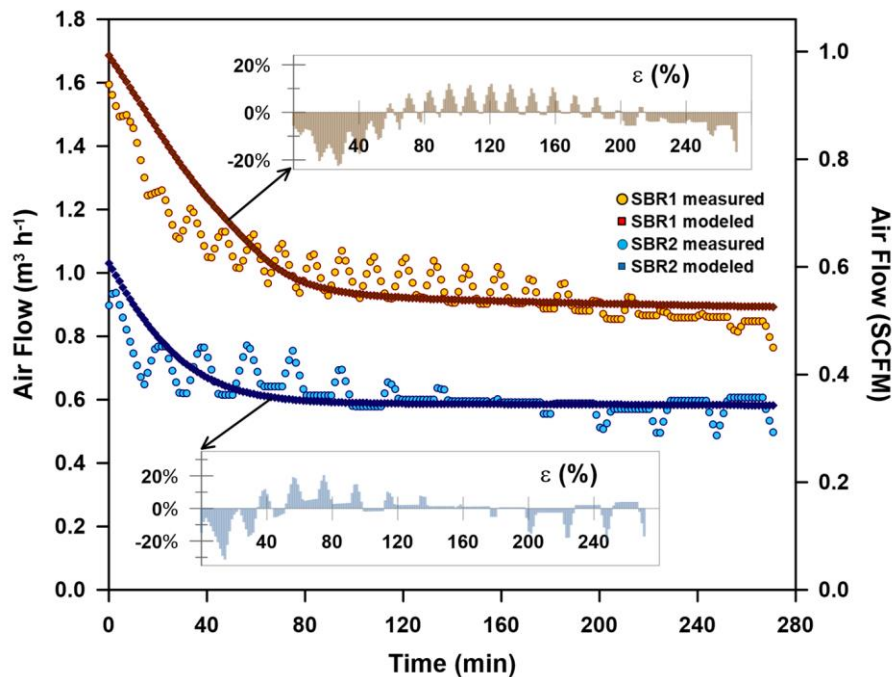


Figure 4-10. The temporal variation in the measured and modeled (30 mins moving average) air flow rates for both SBRs. ε is the percent error ((measured-modeled) *100/measured)

Additionally, SBR2 with the addition of $100 \text{ mg}_{\text{acetate}} \text{ l}^{-1}$, and SBR2 with the addition of $100 \text{ mg}_{\text{cellulose}} \text{ l}^{-1}$ were modeled. Table 4-6 summarizes the average α -factor, required air flow, and energy consumption for the four modeled scenarios. On average, SBR 2 had a

lower air flow requirement of $0.90 \text{ m}^3 \text{ hr}^{-1}$ (0.53 SCFM) when compared to SBR1 ($1.19 \text{ m}^3 \text{ hr}^{-1}$ -0.70 SCFM), leading to an overall energy saving of 25% per cycle due to the RBF, which was identical to what was observed experimentally. The energy-saving per kgO_2 consumed per day was 8.5% which was comparable to the 6.7% that was achieved experimentally. The addition of acetate required more air flow as oxygen requirements increased and more air was required to maintain the same oxygen transfer rate. The addition of acetate increased the required airflow in the SBR2 by 50%, when compared to its absence. The addition of cellulose impacted both the α -factor and the SOTR increasing the required air flow rate by 33%. SBR2 +100 $\text{mg}_{\text{cellulose}} \text{ l}^{-1}$ had a higher air flow requirement of $1.34 \text{ m}^3 \text{ h}^{-1}$ (0.79 SCFM) than SBR1 ($1.19 \text{ m}^3 \text{ h}^{-1}$ (0.7 SCFM)) due to the higher biomass concentration in SBR1 than SBR2 +100 $\text{mg}_{\text{cellulose}} \text{ l}^{-1}$. The addition of acetate required more air compared to other scenarios since all the added acetate is readily biodegradable. The addition of cellulose showed a lower impact on the α -factor, and hence, air flow since most of the added cellulose is slowly biodegradable and a reduced amount of additional air was required, when compared to the case with acetate.

The validation proved that the established correlation (Eq.19) can be used as a design tool to predict the dynamic α -factor and, subsequently, dynamic air flow rates in SBR systems. In continuous-flow systems with plug flow reactors, the α -factor change induced by biodegradation can be estimated using Eq.19 and used to design a tapered aeration system that is more efficient than uniform aeration in plug flow reactors. In continuous-flow systems with completely mixed reactors, this approach should be valid as it will estimate uniform and high α -factor throughout the whole reactor due to low sCOD concentrations. This is consistent with the literature since completely mixed reactors are characterized by their high α -factors (Gillot and Héduit, 2000; Mahendraker et al., 2005; Rieth et al., 1990) relative to plug-flow reactors.

Table 4-6. The average α -factor, required airflow, and energy consumption for the modeled scenarios

Scenario	α -factor	Energy		
		Airflow $\text{m}^3 \text{h}^{-1}$ (SCFM)	kWh cycle^{-1}	$\text{kWh kg}_{\text{ThOD}}^{-1} \text{ }^a$
SBR1	0.51	1.19 (0.70)	0.12	1.06
SBR2	0.51	0.90 (0.53)	0.09	0.97
SBR2 + 100 mg Acetate l⁻¹	0.43	1.79 (1.05)	0.18	1.41
SBR2 + 100 mg Cellulose l⁻¹	0.47	1.34 (0.79)	0.14	1.20

^a Equal to the power required for each cycle (kWh/cycle) * 2 cycles/day divided by the ThOD (kgO₂/day) estimated by the model.

4.4 Summary and Conclusions

Based on the results reported in the manuscript, the following conclusions could be drawn:

- In an SBR a regular increase in α -factor with reaction time should be expected. Hence, during SBR design, a variable α -factor should be used.
- The presence of active biomass improves the α -factor due to enhanced biodegradation. At the low air flow and low DO with active biomass, the α -factor decreased due to the presence of acetate and cellulose by 48% and 19%, respectively. At the high air flow and high DO, with active biomass, the α -factor was constant irrespective of cellulose and acetate concentrations.
- Without active biomass, the α -factor decreased due to the addition of acetate in both cases i.e. the high and low air flows. With biomass, the α -factor increased with the biodegradation of surfactants and sCOD, peaking at 0.56.
- Despite the removal of the vast majority of the organic and nitrogen load, the highest α -factor value achievable in the SBR secondary effluent without biomass was 0.60. This indicated that biomass has a marginal beneficial impact on the α -factor in secondary effluents, while the residual contaminants cause the depression of alpha.

- A dynamic model was developed to calculate the required real-time air flow rate as a function of the change in sCOD. The RBF reduced the required airflow and hence energy by 25% due to the removal of cellulose along with other slowly biodegradable substrates compared to no primary treatment. The dynamic model indicated that the addition of $100 \text{ mg}_{\text{acetate}} \text{ l}^{-1}$ to SBR2, with an initial sCOD concentration of 135 mg l^{-1} , and cellulose concentration of 25 mg l^{-1} , increased the airflow requirements by 50% to compensate for the reduction in α -factor. Similarly, the addition of $100 \text{ mg}_{\text{cellulose}} \text{ l}^{-1}$ to SBR2 increased the air requirements by 33%.

References

- Ahmed, A.S., Bahreini, G., Ho, D., Sridhar, G., Gupta, M., Wessels, C., Marcelis, P., Elbeshbishy, E., Rosso, D., Santoro, D., Nakhla, G., 2019. Fate of cellulose in primary and secondary treatment at municipal water resource recovery facilities. *Water Environ. Res.* 91, 1479–1489. <https://doi.org/10.1002/wer.1145>
- American Public Health Association, 2005. *Standard Methods for the Examination of Water & Wastewater*. American Public Health Association.
- Baquero-Rodríguez, G.A., Lara-Borrero, J.A., Nolasco, D., Rosso, D., 2018. A Critical Review of the Factors Affecting Modeling Oxygen Transfer by Fine-Pore Diffusers in Activated Sludge. *Water Environ. Res.* 90, 431–441. <https://doi.org/10.2175/106143017X15131012152988>
- Campbell, K., Wang, J., Liu, G., Daigger, G., 2019. Activated sludge morphology significantly impacts oxygen transfer at the air–liquid boundary. *Water Environ. Res.* 91, 500–509. <https://doi.org/10.1002/wer.1066>
- Chakraborty, T., 2015. *Evaluation of Filtration Performance of a Rotating Belt Filter for Different Primary Wastewater Influent*. MSc., The University of Western Ontario.
- Cornel, P., Wagner, M., Krause, S., 2003. Investigation of oxygen transfer rates in full scale membrane bioreactors. *Water Sci. Technol. J. Int. Assoc. Water Pollut. Res.* 47, 313–319.
- Eckenfelder, W.W., Raymond, L.W., Lauria, D.T., 1956. Effect of Various Organic Substances on Oxygen Absorption Efficiency. *Sew. Ind. Wastes* 28, 1357–1364.
- Franchi, A., Williams, K., Lyng, T.O., Lem, W., Santoro, D., 2015. Rotating Belt Filters as Enabling Technology for Energy-Neutral Wastewater Treatment Plants: Current Status and Applications. *Proc. Water Environ. Fed.* 2015, 1743–1749. <https://doi.org/10.2175/193864715819540847>

- Germain, E., Nelles, F., Drews, A., Pearce, P., Kraume, M., Reid, E., Judd, S.J., Stephenson, T., 2007. Biomass effects on oxygen transfer in membrane bioreactors. *Water Res.* 41, 1038–1044.
<https://doi.org/10.1016/j.watres.2006.10.020>
- Gillot, S., Héduit, A., 2008. Prediction of alpha factor values for fine pore aeration systems. *Water Sci. Technol.* 57, 1265–1269.
<https://doi.org/10.2166/wst.2008.222>
- Gillot, S., Héduit, A., 2000. Effect of air flow rate on oxygen transfer in an oxidation ditch equipped with fine bubble diffusers and slow speed mixers. *Water Res.* 34, 1756–1762. [https://doi.org/10.1016/S0043-1354\(99\)00323-1](https://doi.org/10.1016/S0043-1354(99)00323-1)
- Gillot, S., Kies, F., Amiel, C., Roustan, M., Héduit, A., 2005. Application of the off-gas method to the measurement of oxygen transfer in biofilters. *Chem. Eng. Sci.*, 7th International Conference on Gas-Liquid and Gas-Liquid-Solid Reactor Engineering 60, 6336–6345. <https://doi.org/10.1016/j.ces.2005.04.056>
- Gori, R., Jiang, L.-M., Sobhani, R., Rosso, D., 2011. Effects of soluble and particulate substrate on the carbon and energy footprint of wastewater treatment processes. *Water Res.* 45, 5858–5872. <https://doi.org/10.1016/j.watres.2011.08.036>
- Gude, V.G., 2015. Energy and water autarky of wastewater treatment and power generation systems. *Renew. Sustain. Energy Rev.* 45, 52–68.
<https://doi.org/10.1016/j.rser.2015.01.055>
- Gupta, M., Ho, D., Santoro, D., Torfs, E., Doucet, J., Vanrolleghem, P.A., Nakhla, G., 2018. Experimental assessment and validation of quantification methods for cellulose content in municipal wastewater and sludge. *Environ. Sci. Pollut. Res.*
<https://doi.org/10.1007/s11356-018-1807-7>

- Henkel, J., Cornel, P., Wagner, M., 2011. Oxygen transfer in activated sludge – new insights and potentials for cost saving. *Water Sci. Technol.* 63, 3034–3038.
<https://doi.org/10.2166/wst.2011.607>
- Henkel, J., Lemac, M., Wagner, M., Cornel, P., 2009. Oxygen transfer in membrane bioreactors treating synthetic greywater. *Water Res.* 43, 1711–1719.
<https://doi.org/10.1016/j.watres.2009.01.011>
- Henze, M., 1992. Characterization of Wastewater for Modelling of Activated Sludge Processes. *Water Sci. Technol.* 25, 1–15.
- Henze, M., Grady, C.P.L., Gujer, W., Marais, G.V.R., Matsuo, T., 1987. A general model for single-sludge wastewater treatment systems. *Water Res.* 21, 505–515.
[https://doi.org/10.1016/0043-1354\(87\)90058-3](https://doi.org/10.1016/0043-1354(87)90058-3)
- Henze, M., Gujer, W., Mino, T., Loosdrecht, M.C.M. van, 2000. Activated sludge models ASM1, ASM2, ASM2d and ASM3. IWA Publishing.
- Hurwitz, E., Beck, A.J., Sakellariou, E., Krup, M., 1961. Degradation of Cellulose by Activated Sludge Treatment. *J. Water Pollut. Control Fed.* 33, 1070–1075.
- Jiang, L., Garrido-Baserba, M., Nolasco, D., Al-Omari, A., DeClippeleir, H., Murthy, S., Rosso, D., 2017. Modelling oxygen transfer using dynamic alpha factors. *Water Res.* 124, 139–148. <https://doi.org/10.1016/j.watres.2017.07.032>
- Krampe, J., Krauth, K., 2003. Oxygen transfer into activated sludge with high MLSS concentrations. *Water Sci. Technol.* 47, 297–303.
<https://doi.org/10.2166/wst.2003.0618>
- Leu, S.Y., Rosso, D., Larson, L.E., Stenstrom, M.K., 2009. Real-Time Aeration Efficiency Monitoring in the Activated Sludge Process and Methods to Reduce Energy Consumption and Operating Costs. *Water Environ. Res.* 81, 2471–2481.
<https://doi.org/10.2175/106143009X425906>

- Mahendraker, V., Mavinic, D.S., Hall, K.J., 2005. Comparison of oxygen transfer parameters determined from the steady state oxygen uptake rate and the non-steady-state changing power level methods. *J. Environ. Eng.* 131, 692–701.
- Metcalf & Eddy, Tchobanoglous, G., Burton, F., Stensel, H.D., 2002. *Wastewater Engineering: Treatment and Reuse*. McGraw-Hill Education.
- Pittoors, E., Guo, Y., Van Hulle, S.W.H., 2014. Oxygen transfer model development based on activated sludge and clean water in diffused aerated cylindrical tanks. *Chem. Eng. J.* 243, 51–59. <https://doi.org/10.1016/j.cej.2013.12.069>
- Redmon, D., Boyle, W.C., Ewing, L., 1983. Oxygen transfer efficiency measurements in mixed liquor using off-gas techniques. *J. Water Pollut. Control Fed.* 1338–1347.
- Reijnen, C., Giorgi, S., Hurkmans, C., Pérez, J., van Loosdrecht, M.C.M., 2018. Incorporating the influent cellulose fraction in activated sludge modelling. *Water Res.* 144, 104–111. <https://doi.org/10.1016/j.watres.2018.07.013>
- Rieth, M.G., Boyle, W.C., Ewing, L., 1990. Effects of selected design parameters on the fouling characteristics of ceramic diffusers. *Res. J. Water Pollut. Control Fed.* 877–886.
- Rosso, D., Huo, D.L., Stenstrom, M.K., 2006. Effects of interfacial surfactant contamination on bubble gas transfer. *Chem. Eng. Sci.* 61, 5500–5514. <https://doi.org/10.1016/j.ces.2006.04.018>
- Rosso, D., Iranpour, R., Stenstrom, M.K., 2005. Fifteen years of offgas transfer efficiency measurements on fine-pore aerators: key role of sludge age and normalized air flux. *Water Environ. Res.* 77, 266–273.
- Rosso, D., Larson, L.E., Stenstrom, M.K., 2008. Aeration of large-scale municipal wastewater treatment plants: state of the art. *Water Sci. Technol.* 57, 973–978. <https://doi.org/10.2166/wst.2008.218>

- Rosso, D., Lothman, S.E., Jeung, M.K., Pitt, P., Gellner, W.J., Stone, A.L., Howard, D., 2011. Oxygen transfer and uptake, nutrient removal, and energy footprint of parallel full-scale IFAS and activated sludge processes. *Water Res.* 45, 5987–5996. <https://doi.org/10.1016/j.watres.2011.08.060>
- Rosso, D., Stenstrom, M.K., 2006. Surfactant effects on α -factors in aeration systems. *Water Res.* 40, 1397–1404. <https://doi.org/10.1016/j.watres.2006.01.044>
- Rosso, D., Stenstrom, M.K., 2005. Comparative economic analysis of the impacts of mean cell retention time and denitrification on aeration systems. *Water Res.* 39, 3773–3780. <https://doi.org/10.1016/j.watres.2005.07.002>
- Ruiken, C.J., Breuer, G., Klaversma, E., Santiago, T., van Loosdrecht, M.C.M., 2013. Sieving wastewater – Cellulose recovery, economic and energy evaluation. *Water Res.* 47, 43–48. <https://doi.org/10.1016/j.watres.2012.08.023>
- Singh, P., Kansal, A., Carliell-Marquet, C., 2016. Energy and carbon footprints of sewage treatment methods. *J. Environ. Manage.* 165, 22–30. <https://doi.org/10.1016/j.jenvman.2015.09.017>
- Tao, X., Chengwen, W., 2012. Energy consumption in wastewater treatment plants in China. Unpubl. Manuscr. Retrieved Httpwww Res. NetprofileTaoXie11publication266146909Energy Consum. Pdf.
- Tseng, L.Y., Gonsior, M., Schmitt-Kopplin, P., Cooper, W.J., Pitt, P., Rosso, D., 2013. Molecular Characteristics and Differences of Effluent Organic Matter from Parallel Activated Sludge and Integrated Fixed-Film Activated Sludge (IFAS) Processes. *Environ. Sci. Technol.* 130827102639005. <https://doi.org/10.1021/es4002482>
- Wagner, M., Pöpel, H.J., 1998. Oxygen transfer and aeration efficiency - influence of diffuser submergence, diffuser density, and blower type. *Water Sci. Technol.* 38, 1–6. <https://doi.org/10.2166/wst.1998.0163>

- Wagner, M., Pöpel, H.J., 1996. Surface active agents and their influence on oxygen transfer. *Water Sci. Technol., Water Quality International '96 Part 2* 34, 249–256. [https://doi.org/10.1016/0273-1223\(96\)00580-X](https://doi.org/10.1016/0273-1223(96)00580-X)
- Zaman, M., Kim, M., Nakhla, G., Singh, A., Yang, F., 2019. Enhanced biological phosphorus removal using thermal alkaline hydrolyzed municipal wastewater biosolids. *J. Environ. Sci.* 86, 164–174. <https://doi.org/10.1016/j.jes.2019.05.025>

Chapter 5

5 Influence of Bioreactor Configurations on the Dynamics of Oxygen Demand and Aeration Performance in Activated sludge Processes.

5.1 Introduction

The major contributor to the energy footprint and carbon footprint of conventional activated sludge processes is aeration, which is known to contribute more than 60% of the energy requirements (Reardon, 1995, Rosso and Stenstrom, 2005). Oxygen should be supplied efficiently to minimize the energy footprint of the WWTPs (Baquero-Rodríguez et al., 2018, Caivano et al., 2017, Rosso et al., 2005). The transfer rate of oxygen in wastewater is usually evaluated with the α -factor, i.e. the ratio of oxygen transfer in wastewater to that in clean water, which typically varies from 0.25 to 0.65 for fine-pore diffusers (Baquero-Rodríguez et al., 2018). Several design elements, including the type, distribution, and depth of the diffusers, airflow rate, and aerobic reactor design, have been shown to affect aeration efficiency (Baquero-Rodríguez et al., 2018, Garrido-Baserba et al., 2017). Besides, other operating factors have been reported to have an impact on aeration efficiency, such as influent wastewater characteristics, solids retention time (SRT), anoxic/anaerobic processes for biological nutrient removal, and temperature (Gillot and Héduit, 2008, Leu et al., 2009, Rosso et al., 2011, Wagner and Pöpel, 1998).

In activated sludge systems, aerobic reactors can be designed and built for operation as plug-flow reactors (PFR) or completely mixed stirred reactors (CSTR). Each configuration has a set of conditions that impact the treatment efficiency as well as oxygen transfer efficiency (Baquero-Rodríguez et al., 2018). In plug flow reactors, the concentrations of various contaminants and the oxygen demand change spatially (Jenkins, 2013, Rosso, 2018). In CSTR aeration tanks, COD, nitrogen, and phosphorus concentrations are high at the inlet but are more or less uniform within the tank (Jenkins, 2013). Plug flow reactors exhibit low α -factor at the inlet but α -factor increases due to biodegradation which necessitates the use of tapered aeration to supply higher air flow at the inlet (Brade and Shahid, 1993, Garrido-Baserba et al., 2020, Mueller et al., 2000). In plug flow systems, the

adoption of pre-anoxic selectors for denitrification was found to improve the α -factor and reduce the aeration energy by 12%-27% (Mueller et al., 2000, Rosso and Stenstrom, 2005). In CSTR, uniform and high α -factors were observed when compared to plug flow reactors due to the uniform distribution of the pollutants (Baquero-Rodríguez et al., 2018, Brade and Shahid, 1993, Jenkins, 2013). Practically, in CSTRs the stirrers are the main gas dispersing devices that provide mixing and aeration, and their speed and size have a detrimental effect on oxygen transfer (Garcia-Garcia et al., 2011). Zhu et al., 2001 showed that using radial flow impellers increased the oxygen mass transfer by 17% when compared to axial flow impellers. Also, Puthli et al. 2005 found that oxygen transfer efficiency and energy consumption were significantly improved with a triple impeller system.

In various applications, membrane bioreactors (MBRs) are suitable and effectively substitute secondary clarifiers. The use of MBRs is however constrained by high operating costs which is mainly due to aeration that is used for supplying dissolved oxygen (DO) and for maintaining membrane flux (Germain et al., 2007). The α -factor in MBRs was found to decrease dramatically with the MLSS increase (Baquero-Rodríguez et al., 2018, Cornel et al., 2003, Germain et al., 2007, Henkel et al., 2009, 2011a, Krampe and Krauth, 2003). This happens as with the solids concentration increase, bubble coalescing increases due to the shear-thinning nature of the solids. Coalesced bubbles (with more interfacial shear) may thin the fluid and be less resistant to rise. Indeed, such coalescing bubbles with a significantly lower "a" in their oxygen mass transfer coefficient (k_{La}) have lower α -factor (Baquero-Rodríguez et al., 2018).

Readily biodegradable substrates with surface-active agents significantly reduce the α -factor because of their fast build-up on the surface of the bubble (Rosso et al., 2006, Rosso and Stenstrom, 2006, Wagner and Pöpel, 1996). Additionally, the impact of the influent organics on the oxygen transfer efficiency has been investigated experimentally (e.g., Gori et al., 2011, Jiang et al., 2017, Leu et al., 2009, Pasini et al., 2020, Rosso et al., 2005). A significant portion of the influent slowly biodegradable substrates are cellulose resulting from toilet papers (Ahmed et al., 2019, Ruiken et al., 2013). Reijken et al., 2018 was the first to incorporate cellulose hydrolysis into ASM1 model. Ahmed et al., 2020 showed the

influence of cellulose on the oxygen transfer efficiency and reported a 19% reduction in the α -factor with the increase in influent cellulose concentration from 20 to 120 mg l⁻¹.

Most of the studies published thus far agree that low α -factors are associated with high influent loading rates. Also, their observations showed that α -factor improves due to biodegradation; however, when it comes to aeration modeling, there is a need for a dynamic mathematical relationship to correlate the α -factor with process variables.

Many research efforts to quantify α -factors have been reported. Wagner and Pöpel, 1998 were the first to correlate oxygen transfer efficiency parameters including standard oxygen transfer rate (SOTR) and $k_L a$ to air flow rates, diffusers' submergence and density, and tank geometry. Rosso et al., 2005 presented an empirical correlation for standard oxygen transfer efficiency in process water (α SOTE) and α -factors with air flow rates and SRT. These correlations were later incorporated into a model by Cierkens et al. 2012 to estimate the oxygen transfer efficiency and the model provided an accurate estimation of the dynamic DO concentrations. Amerlinck et al. 2016 calibrated the aforementioned model using off-gas measurements from a full-scale treatment plant in Eindhoven, the Netherlands. Despite the successful calibration observed for some of the measured data, the study concluded that SRT cannot be used as the only variable to predict α SOTE and α -factor recalibration was still needed, confirming the previous observations by Gillot et al. 2005 who used dimensional analysis to correlate different variables, such as the superficial gas velocity and the dynamic surface tension, respectively. Gillot and Héduit, 2008 introduced a new variable (the equivalent contact time) that is a function of SRT, $k_L a$, and airflow rate, to estimate α -factor in fine pore aeration systems. Baquero-Rodríguez et al., 2018 developed a new correlation between α -factor and MLSS using data from different studies (Cornel et al., 2003, Germain et al., 2007, Krampe and Krauth, 2003, Rosso et al., 2005) and concluded that for MLSS concentrations below 6 g l⁻¹, an MLSS increase was beneficial to the α -factor due to the biosorption effect. However, for MLSS concentrations exceeding 6 g l⁻¹, which applies to MBRs and aerobic digesters, the α -factor decreased with the MLSS increase due to the shear-thinning action of the solids. Despite the successful correlations between the α -factor and several variables, the dynamic impact of the loading

rates on the α -factor has not been considered by the aforementioned correlations and many such estimators will predict a constant and high α -factor when used in the design of activated sludge systems.

It is a challenge to estimate and integrate dynamic α -factors in aeration modeling for design purposes, as despite the limited studies demonstrating the dynamic α -factors. Verrecht et al., 2008 developed an aeration energy model for the immersed MBR. The model correlated air flux to membrane permeability using pilot plant data (Guglielmi et al., 2007, 2008). The α -factor was estimated using the exponential relationship with the MLSS published by Guender, 2001, and Krampe and Krauth 2003. The study concluded that significant energy reduction can be achieved at low levels of MLSS and by reducing the membrane air flux. Pittoors et al., (2014), using cylindrical reactor measurements (2.7-9.3 l), developed a mathematical model that correlates $k_L a$ to nine operating variables (reactor volume, height, diameter, surface area, airflow rate, diffuser area and depth, size of bubbles, and dynamic viscosity) in clean water and activated sludge. Jiang, et al., 2017 developed a dynamic aeration model that correlates the α -factor to the influent COD and that showed that α decreased exponentially with the influent COD increase. The correlation was done using data from two full-scale treatment plants with anoxic and aerobic plug flow reactors. Ahmed et al., 2020 correlated α -factor to aeration tank sCOD and incorporated this correlation into a model to estimate the dynamic change in the air flow rates due to biodegradation in SBRs.

Limited studies evaluated the impact of reactor configuration on aeration energy. Daelman et al., 2014 studied the impact of process design and operating parameters on the aerobic methane oxidation in plug flow reactors and CSTRs. The study explored the effect of the bioreactor configuration on aeration energy; however, the optimization of aeration energy was not achieved because DO concentrations were not controlled and continuous aeration was applied. It has been found that continuous air flow rates without DO control contributed to comparable power consumption for plug flow reactors and CSTRs. Siatou et al., 2020 compared energy consumption using data from 17 full-scale WWTP at similar capacities; 9 CSTRs, 3 plug flow, and 5 oxidation ditches concluded that CSTRs saved

45% of the total energy compared to plug flow reactors. All the aforementioned studies, however, did not consider the thorough impact of the tank configuration on the dynamics of α -factor and therefore aeration energy.

Therefore, the main objectives of this study were: 1- validate the dynamic air flow rates using sCOD based correlation to estimate α -factor developed by Ahmed et. al 2020 (first correlation) and compare the results with influent COD (second correlation) (Jiang et al., 2017) and MLSS (third correlation) (Baquero-Rodríguez et al., 2018) based correlations under constant and variable COD loading rates. 2. Evaluate the impact of activated sludge reactor type on aeration energy, using dynamic α -factor. 3- Assess the impact of pre-denitrification on dynamic α -factor and aeration performance. While the dynamics of α -factor variations are associated with kinetics in the first correlation and hence pertain to both steady and variable influent COD loadings, dynamic α -factors occur only under variable loadings in the second and third correlations. Furthermore, the fact that the third correlation is dependent on MLSS concentrations of up to 50 g/L, necessitated the incorporation of the high MLSS MBRs in the processes evaluated in this study. In addition to MBRs, SBR, CSTR, plug flow, and step-feed processes were also investigated. The practical significance of this work relates both to process selection and aeration design, which currently completely overlooks dynamic variations of the α -factor and aeration process control under dynamic loadings conditions.

5.2 Material and methods

5.2.1 Sequencing batch reactors pilot

Two identical pilot sequencing batch reactors (SBRs), with an operating volume of 850 l (diameter of 0.6 m and depth of 3.0 m), were operated in a wastewater treatment plant in London, ON, Canada. Each reactor was equipped with a 7" EPDM fine pore membrane diffuser disc mounted on the floor. One reactor was fed with screened raw wastewater and the other was fed with primary treated wastewater with a rotating belt filter (RBF; SALSNES SF2000 - mesh openings = 0.185 mm). Both reactors were operated three cycles per day (i.e., 8 hrs. per cycle). Each cycle consisted of 15 min filling; 1 h anoxic; 5 h

aerobic; 1.5 h settling; 15 min decanting. Each SBR has a fill ratio of 60% with a treatment capacity of 1530 L d⁻¹. Process parameters variables including pH, ORP, ammonia, and DO were monitored online through two sets of sensors installed in each reactor. Both reactors were operated at a solids retention time (SRT) of 10 days. In addition, the air delivery was controlled in both reactors using an electric on/off valve that released intermittently a constant air flow. The electric valve was programmed to operate in the DO setpoint 1.5 +/- 0.5 mg l⁻¹. To monitor the SBRs performance, samples from the influent, effluent, and mixed liquor were collected and analyzed once a week from both reactors over three months. Pilot SBRs measurements were used for model calibration.

5.2.2 Wastewater characterization

Total suspended solids (TSS), volatile suspended solids (VSS) were measured following standard methods (American Public Health Association, 2005). Chemical oxygen demand (COD), ammonia, nitrate, and total and soluble nitrogen (TN and sN) were measured using Hach methods. Ammonia concentrations were tracked online using ISE-ammonia sensors (HC-200NH, HORIBA Advanced Techno, Co. Ltd., Japan).

5.2.3 Model setup

GPS-X 7.0.1 software was used in this study. ASM1 model was developed to include the first order cellulose degradation rates (ASM1CL) (Reijnen et al., 2018). The first-order hydrolysis rate constant of the cellulose was estimated experimentally.

5.2.3.1 SBRs model

Both SBRs were modeled to calibrate the ASM1CL kinetic coefficients using the SBRs wastewater measurements over three months. Initial state variables for raw wastewater and RBF effluent were estimated using the influent and effluent concentrations of the COD, sCOD, ammonia, TN, and SN.

The soluble inerts concentration (S_I) was initially assumed to be equal to the effluent sCOD. The influent readily biodegradable substrates concentration (S_s) was the biodegraded sCOD (i.e. $sCOD_{inf.} - sCOD_{eff.}$). S_I and S_s were then calibrated to match the

measured effluent sCOD. Influent cellulose (X_{cl}) in the raw wastewater was determined to be 33% of the influent TSS as measured by Ahmed et al., 2019. Cellulose concentration in the RBF effluent was determined knowing that RBF, on average, removes 80% of the influent cellulose (Ahmed et al., 2019). Influent particulate inert concentrations (X_I) and slowly biodegradable substrate concentrations excluding cellulose (X_s) were calculated iteratively until they matched the measured MLVSS inside the SBRs. TN, sN, and ammonia measurements were used to estimate the initial concentrations of particulate N, soluble N, and ammonia. Since DO was controlled in the pilot, DO in the model was set to be 2 mg l^{-1} during the aeration cycle.

5.2.3.2 Plug flow model

A continuous-flow system with a treatment capacity of $1200 \text{ m}^3 \text{ d}^{-1}$ consisting of an aerobic plug flow reactor and a secondary clarifier was modeled (Fig. 5-1). A recirculation rate of 66% of the influent flow rate was selected to approximate the dilution factor of 60% used in the pilot SBRs. The model was designed to target an SRT of 10 days. The plug flow reactor was designed to have 12 equal compartments with a total volume of 672 m^3 (3 m depth) to match the hydraulic retention time in the SBRs. The secondary clarification was designed with a treatment volume of 162.5 m^3 and HRT of 1.9 hrs. Secondary clarifiers were modeled as a simple 1-dimension model and were calibrated to match the SBRs measured effluent TSS and VSS. Aeration was designed to be controlled using a DO setpoint of 2 mg l^{-1} . Air diffusers (7" diffusers) distribution was set to be 10% of the aeration tank surface area to match the diffuser density in the SBRs (i.e., diffuser area per SBR floor area). The standard oxygen transfer efficiency in clean water (SOTE) was defined using a correlation as a function of the airflow rates as measured in the SBRs.

To incorporate denitrification, the first two compartments were switched to anoxic whilst the remaining 10 compartments stayed aerated. Additionally, internal circulation from aeration effluent to anoxic influent was added for denitrification. The recirculation ratio was optimized to reach the lowest total nitrogen concentration in the effluent. The best recirculation ratio was 1.67 of the influent flow rate ($2000 \text{ m}^3 \text{ d}^{-1}$).

5.2.3.3 CSTR model

Similar to the plug flow model, a continuous flow system with a treatment capacity of $1200 \text{ m}^3 \text{ d}^{-1}$ was modeled while replacing the plug flow reactor with an aerobic CSTR with a volume of 672 m^3 (3 m depth) (Fig. SI-1, in the supplementary information). A similar aeration setup to the plug flow reactor was employed for the CSTR.

Similar to the plug flow reactor, another modeled scenario was done to evaluate the impact of the denitrification process on the aeration energy consisting of anaerobic CSTR (112 m^3) and aerobic CSTR (560 m^3). Similarly, internal recirculation of $2000 \text{ m}^3 \text{ d}^{-1}$ was added to enhance nitrogen removal (Fig. SI-2).

5.2.3.4 Plug flow step feed model

In this model scenario, instead of using one plug flow reactor, four plug flow reactors in series were used with a volume of 168 m^3 each (Fig.5-2). The influent, as well as return activated sludge, were divided equally to feed each reactor. Each reactor consisted of 12 equal compartments. Similar operational settings to what was used in the model with the plug flow reactor were applied to this scenario.

5.2.3.5 Membrane bioreactor (MBR) model

MBR was designed as two separate compartments (CSTRs) in series with a total volume of 672 m^3 ; one bioreactor compartment for biological reactions and the last compartment was for the MBR solids separation. The first compartments were designed to be 90% of the total volume and the MBR compartment was designed to be 10% of the total volume to minimize airflow required for membrane scouring (Fig. SI-3). The membrane was assumed to capture 99.99% of suspended solids and 10% of the soluble COD (Verrecht et al., 2008). To simulate the conditions for a typical MBR, an MLSS set point of 20 g l^{-1} was used in the MBR with a recirculated flow of $1200 \text{ m}^3 \text{ d}^{-1}$ from the MBR compartment to the first compartment to maintain an average MLSS concentration of 10 g l^{-1} inside the bioreactor. This corresponded to an SRT of 43.5 days, well within the range of typical SRTs for MBRs.

Similarly, to evaluate the impact of denitrification, another model with internal recirculation of $2000 \text{ m}^3 \text{ d}^{-1}$ was used while having anoxic compartments at the beginning. The total volume was the same as for the nitrification only to maintain the same MLSS concentrations and the volume was divided into 17% anoxic (one compartment), 73% aerobic (one compartment), and 10% for the MBR (last compartment). The anoxic volume fraction was selected to match the anoxic fraction for the plug flow and CSTR models.

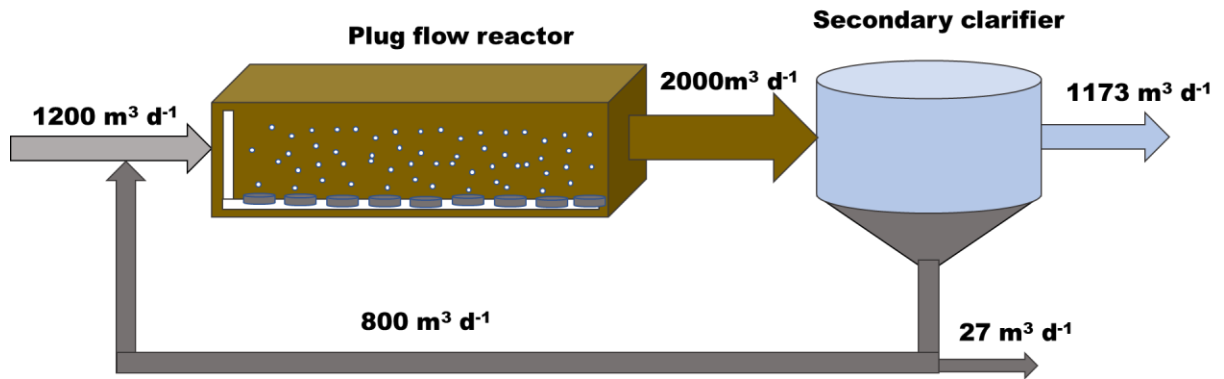


Figure 5-1. Treatment scheme for the modelled scenario with a plug flow reactor.

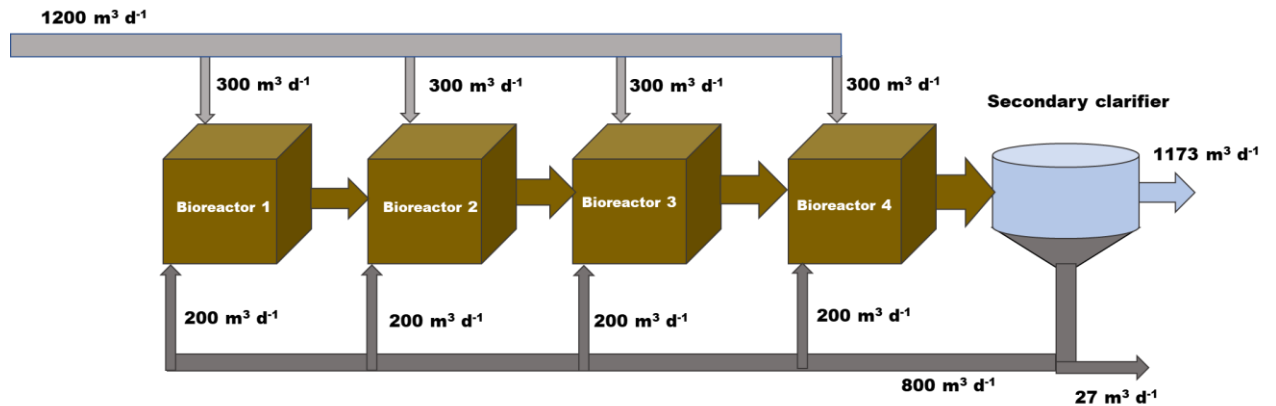


Figure 5-2. Treatment scheme for the modeled scenario with a step feed plug flow reactors.

5.2.4 Dynamic α -factor estimation

The dynamic α -factor was estimated using three different correlations;

Correlation 1: Using the correlation between sCOD (mg l^{-1}) and α -factor (Ahmed et al., 2020) following Eq. 5-1 (sCOD range 25-350 mg l^{-1})

$$\alpha = 4.275 \text{ sCOD}^{-0.557} \quad (5 - 1)$$

Correlation 2: Using the developed correlation between influent COD (mg l^{-1}) and α -factor (Jiang, Garrido-Baserba, et al., 2017) following Eq. 5-2 (COD range 200-1600 mg l^{-1})

$$\alpha = \text{Exp}(1.82 \cdot 10^{-3} \cdot \text{COD} - 0.213) \quad (5 - 2)$$

Correlation 3: Using the developed correlation between MLSS (g l^{-1}) and α -factor (Baquero-Rodríguez et al., 2018) following Eq. 5-3 (MLSS range 0.5-30 g l^{-1})

$$\alpha = \left(\frac{0.51}{0.51 - 0.1} \right) (e^{-0.1 \cdot \text{MLSS}} - e^{-0.51 \cdot \text{MLSS}}) \quad (5 - 3)$$

5.3 Results and discussion

5.3.1 SBRs performance

SBR1 with raw wastewater feed achieved on average COD, TN, ammonia, and total phosphorus removal efficiencies of 94%, 74%, 98%, and 92% respectively. SBR2 with RBF primary treated feed achieved on average COD, TN, ammonia, and total phosphorus removal efficiencies of 92%, 68%, 98%, and 92% respectively. The pre-anoxic step and high COD: N:P ratios in both reactors were beneficial for achieving high nitrogen removal

efficiency due to the pre denitrification and high phosphorus removal efficiency as it allowed for phosphorus release and subsequent uptake. Also, the high COD: N ratio was beneficial as more nitrogen was used for biomass synthesis than for nitrification. Both SBRs had a comparable observed yield of $0.35 \text{ mgVSS mgCOD}^{-1}$. On average, 71% and 60% of the influent nitrogen in SBR1 and SBR2 were used in biomass synthesis. Table SI-1 shows the influent and effluent wastewater characteristics for both SBRs at steady-state conditions.

5.3.2 Model calibration and validation

5.3.2.1 SBRs model calibration

Both SBRs were modeled and calibrated using experimental measurements over 90 days while achieving steady-state effluent characteristics. Some of the kinetic coefficients were modified while calibrating all aforementioned parameters (Table SI-2). The heterotrophic maximum specific growth rate μ_H and substrate saturation constant K_s were calibrated to match modeled and measured bioreactor MLSS and effluent COD. Figures SI-4 and SI-5 show the model MLSS and MLVSS using the dynamic wastewater characteristics for raw wastewater, and RBF effluent, respectively. For SBR receiving raw wastewater, the average absolute error between measured and modeled concentration was 3% for both MLSS and MLVSS. For the SBR receiving RBF treated wastewater, the average absolute error was 3% for MLSS and 5% for MLVSS. Figure SI-6 shows the influent and effluent COD, and sCOD with average absolute errors of 4% for the effluent COD and 7% for the effluent sCOD. Furthermore, solids' settleability was calibrated to match TSS and VSS effluents by adjusting the removal efficiency (Fig. SI-7). The average absolute error was 4% for the effluent TSS and 10% for the effluent VSS

Ammonium half-saturation constant $K_{\text{NH}_3\text{-N}}$ and ammonification rate constant k_a were calibrated to match the measured and modeled nitrogen concentrations. Figure SI-8 shows influent and model and experimental effluent TN concentrations. The average absolute error for effluent TN was 9%.

In addition, alpha-cellulose was added to the SBR receiving RBF effluent and cellulose biodegradation was tracked during the aeration time to estimate the cellulose hydrolysis constant k_{cl} (Fig. SI-9). The average k_{cl} was 4.1 d^{-1} .

5.3.2.2 SBR model validation

A cycle test was done on day 92 (Cycle 275). Initial conditions were obtained from the calibrated model for both SBRs and then validated using a batch model (ASMCL1) that was developed using MATLAB software to estimate the real-time air flow due to the dynamic change in α -factor. Figure 5-3a and 3b shows the measured and modeled sCOD and ammonia concentrations during the aeration time. Measured data in Fig. 5-3b were obtained using the calibrated ammonia sensor. The sCOD and ammonia profiles had an average percentage error of 2% and 7%, respectively. Average percentage errors were low and within the acceptable ranges which validate the calibrated kinetics for the SBRs.

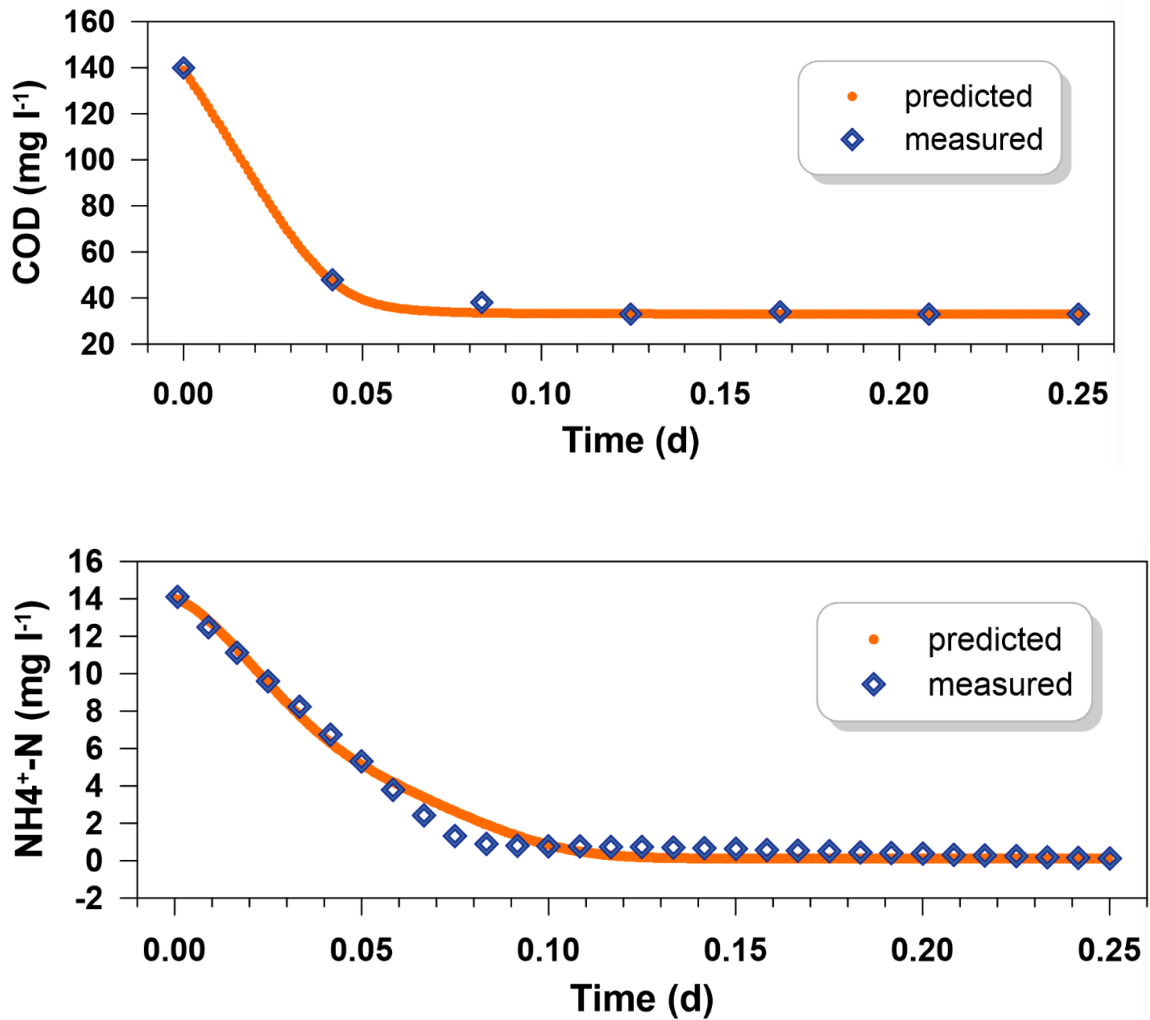


Figure 5-3. a) sCOD predicted by the model and measured sCOD after calibration.

b) Ammonia predicted by the model and measured Ammonia after calibration

Air flow rates were modeled using the three aforementioned correlations and compared with the airflow measured in both SBRs (Fig. 5-4a and 5-4b). In the SBRs, air flow was supplied using an on/off valve that was connected to a controller to maintain a DO setpoint of 2 mg l⁻¹. Since the air flow rate was constant and DO was controlled by the on/off air valve, to quantify the effect of the intermittent air supply, measured air flow rates were averaged every 30 minutes considering the on/off times i.e. the airflow is shown graphically as a step function depending on the on/off times. On the other hand, the model predicted continuous air flow rates were associated with the constant input DO of 2 mg l⁻¹.

¹. For SBR1, the first correlation had a dynamic α -factor that changed with the sCOD biodegradation. The second correlation had a constant α -factor of 0.25 which corresponds to an influent COD of 643 mg l⁻¹. The third correlation had a constant α -factor of 0.65 which corresponds to MLSS concentration of 5100 mg l⁻¹. For SBR2, the first correlation had a dynamic α - factor and hence dynamic airflow rates. The second correlation had a constant α -factor of 0.35, corresponding to an influent COD of 465 mg l⁻¹. The third correlation had a constant α -factor of 0.67, corresponding to MLSS concentrations of 3550 mg l⁻¹.

The first correlation predicted the measured airflow rates for both SBRs well with average percentage errors of 7.3% and 8.7% for both SBR1 and SBR2 respectively. The second correlation overestimated the airflow rates and the third correlation underestimated the air flow rates in both SBRs. However, at the beginning of the aeration cycle, the first and second correlations had comparable air flow rates with a percentage error of 15% and 5% for SBR1 and SBR2 respectively which suggests that by reducing the influent organic loading rates, the second correlation can be used to estimate the initial α -factor and hence air flow rates. The third correlation had comparable air flow rates to the measured air flow rates at the end of the aeration cycle with a percentage error of 8% and 6% for SBR1 and SBR2; however, it clearly overlooked the low α -factor at the beginning of the cycle.

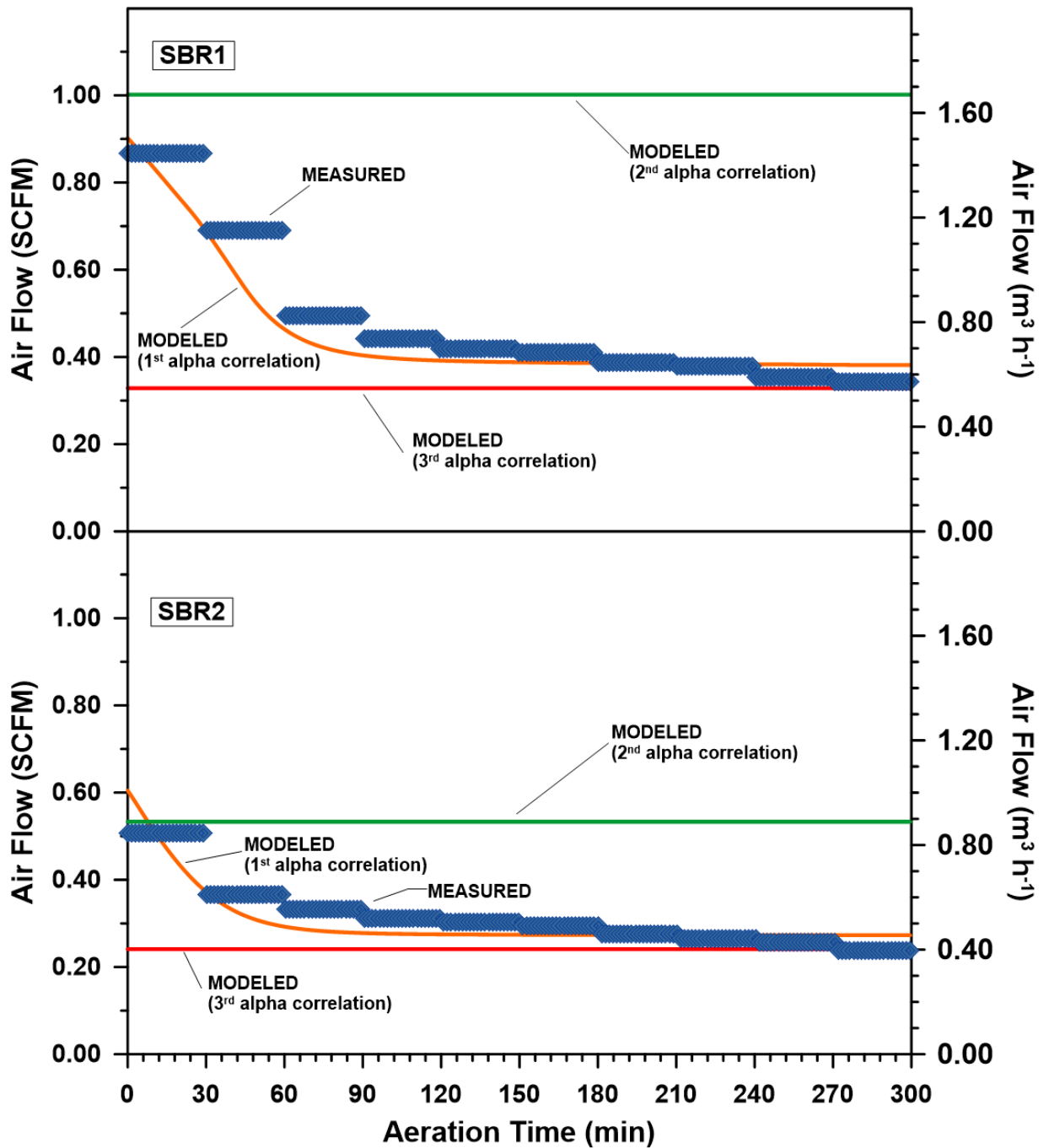


Figure 5-4. a-top) Measured and modeled air flow rates using the three different correlations to estimate α -factor (SBR1). b-bottom) Measured and modelled air flow rates using the three different correlations to estimate α -factor (SBR2).

5.3.3 Aeration Performance in Continuous-flow Activated Sludge Processes

5.3.3.1 Treatment performance

Since the wastewater characteristics used in the SBRs were atypical, exhibiting high COD, COD: N:P ratios of 100:4.6:1.5 for raw wastewater and 100:6:2 for RBF effluent, the simulations were done using typical wastewater characteristics. Plug flow and CSTR bioreactors had comparable treatment performance; however, the model with CSTR had lower biodegradation efficiency (Table SI-3). The nitrogen removal efficiency was 43% for the four modeled scenarios; plug flow, CSTR, plug flow step feed, and plug flow with MBR, while achieving full nitrification. The model with MBR had higher solids and COD removal of 99% and 94% respectively. It must be also highlighted that in all steady-state modeled scenarios the second correlation α -factor was constant at 0.37 based on an influent COD of 430 mg l⁻¹ and the third correlation had a constant α -factor of 0.65 which corresponds to MLSS concentration of 3029 mg l⁻¹

5.3.3.2 Plug flow Model

The α -factor and air flow rates were estimated using the three aforementioned correlations; using sCOD correlation (first correlation), influent COD correlation (second correlation), and MLSS correlation (third correlation). Figure 5-5a shows the estimated α -factor using the three correlations. In the first correlation, α -factor followed the sCOD biodegradation (Fig. SI-10). Figure 5-5b shows the estimated air flow rates using the three correlations. Apparently, the second correlation was consistently overestimating the air flow rates even at the beginning of the plug flow reactor. Air flow rates estimated using first and third correlations were comparable starting from compartment 4; however, the third correlation seems to neglect the impact of the organic loading rates in the first three compartments. The estimated aeration energy to treat the theoretical oxygen demand (ThOD) of 419 kgO₂ d⁻¹ for the three correlations was 108, 179, and 78 kWh d⁻¹. In the model, aeration energy was estimated using Eq.5-4 (Metcalf & Eddy et al., 2002).

$$E = BHP \cdot \Delta t = \frac{wRT_1}{29.7 n e} \left[\left(\frac{p_2}{p_1} \right)^n - 1 \right] \cdot \Delta t \quad (5-4)$$

where: BHP = blower break horsepower (kW); Δt = time on duty (hr); w = ponderal air flow (kg s^{-1}); R = gas constant ($8.314 \text{ J mol}^{-1} \text{ K}^{-1}$); T_1 = absolute inlet temperature (K), p_1 = absolute inlet pressure (Pa), p_2 = absolute discharge pressure (Pa), $n = 0.283$ for air (-), e = blower efficiency (-)

The impact of the dynamic influent concentrations over a day on the aeration energy using the three correlations was tested using the typical hourly change from (Metcalf & Eddy et al., 2002) (Fig.5-6). The peak and minimum influent concentrations were 150% and 50% of the average influent concentrations. Interestingly, at low influent organic loading rates, the three correlations estimated comparable aeration energy. At high organic loading rates, the three correlations had different aeration energy. Also, the third correlation was less sensitive to the dynamic change in loading rates as it relies on MLSS which does not change over a day.

5.3.3.3 CSTR Model

Using the first correlation, the estimated α -factor was 0.62, which corresponds to a sCOD concentration of 32 mg l^{-1} . The α -factor and energy estimated using the first and third correlations were comparable. The second correlation seems to overestimate the energy consumption. The estimated aeration energy to treat a ThOD of $412 \text{ kgO}_2 \text{ d}^{-1}$ for the three correlations was 36, 60, and 34 kWh d^{-1} , respectively. As expected, the plug flow layout exhibited slightly better biodegradation efficiency for rbCOD and slowly biodegradable substrates than the CSTR. The effluent sCOD for CSTR and plug flow was 31.2 mg l^{-1} , and 26.6 mg l^{-1} , respectively. The cellulose biodegradation efficiency in CSTR and plug flow was 98.7% and 97.6%, respectively.

Although the ThOD for both plug flow reactor and CSTR were comparable, energy savings of 66%, 67%, and 56% were achieved by the CSTR based on the first, second, and third correlations, respectively. This happens because in the plug flow reactor 57% of the influent organic loadings was removed in the first 25% of the aeration tank which necessitates applying relatively high air flow rates in the first three compartments to maintain a DO concentration of 2 mg l^{-1} resulting in high k_{la} in the first compartments and

low k_{la} in the last compartments. In the CSTR, influent organic loads were distributed equally over the total volume resulting in constant k_{la} and lower air flow rate when compared to the plug flow reactor. It must be highlighted that curbing DO at 2 mg l^{-1} is the key to achieve these energy savings in CSTRs.

The impact of the dynamic influent loading rates over a day on the aeration energy using the three correlations (Fig. 5-7) showed all three correlations with comparable aeration energy when the influent loading rate was low. Remarkably, the first (sCOD based) and third (MLSS based) correlations yielded comparable aeration energy while the second correlation estimated higher aeration energy at high organic loading rates since it depended on influent COD, a significant portion of which includes a large portion of non-biodegradable particulate that varies from plant to another. It must be asserted that the little difference observed between the first and third correlations would increase with the peak increase in the influent loading rates.

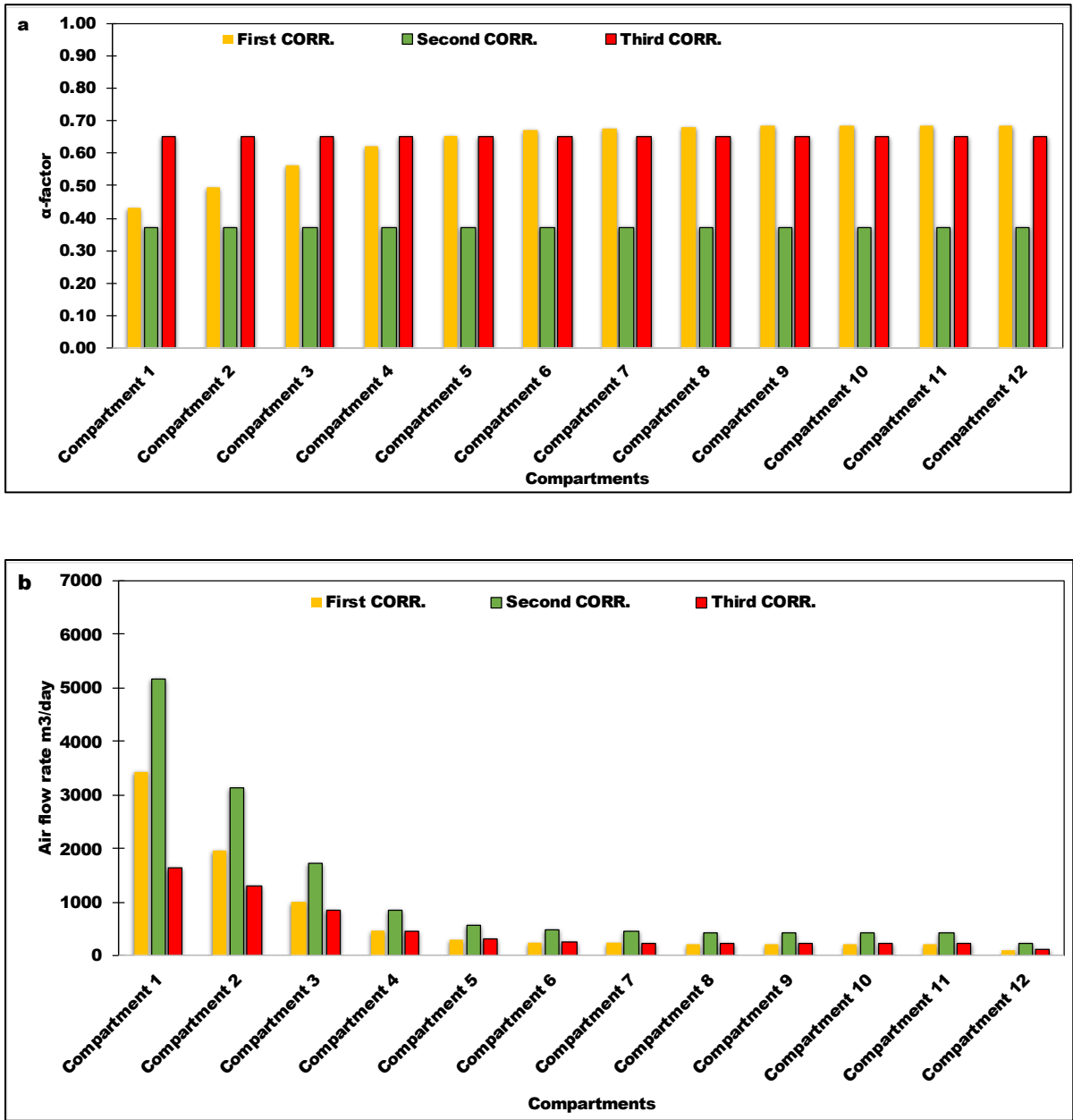


Figure 5-5. a) Estimated α -factor in each compartment using the three correlations (Nitrification only). b) Estimated air flow rates in each compartment using the three correlations (Nitrification only).

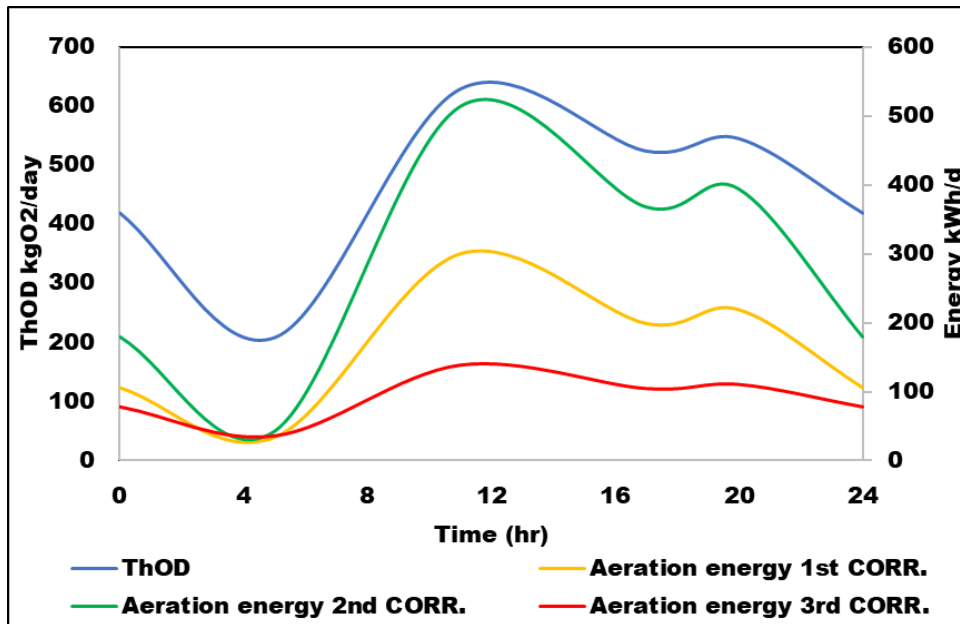


Figure 5-6. The change in aeration energy over a day due to the changes in the influent concentrations using the three correlations.

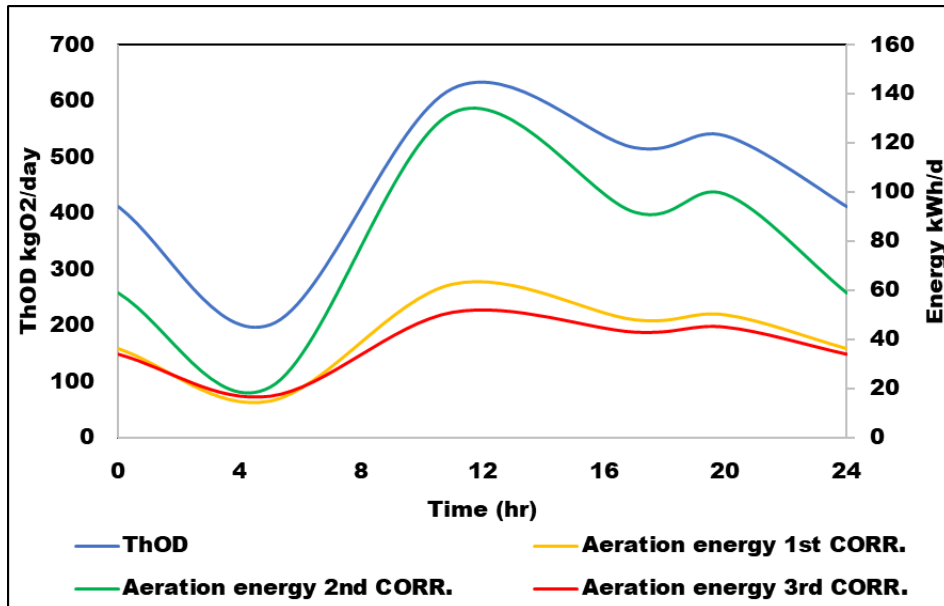


Figure 5-7. The change in aeration energy over a day due to the change in the influent concentrations using the three correlations (CSTR).

5.3.3.4 Step-feed Model

Figure 5-8 shows the average air flow rates in each plug flow reactor using the three correlations. The first correlation had an average α factor of 0.63 in all bioreactors (Fig. SI-11). MLSS concentrations in the four bioreactors were comparable and had a similar α factor of 0.65. Interestingly, the estimated α factor, as well as air flow rates using first and third correlations, were comparable in bioreactors 2, 3, and 4. The second correlation showed the highest airflow rates due to the low α -factor in all bioreactors. When compared to the case with plug flow reactor, step feed reduced the air flow rates by 16%, 12%, and 3% using first, second and third correlations respectively which were due to equal organic loadings distribution. The first reactor had a slightly higher air flow rate which is due to the longer HRT compared to other reactors. First, second, third, and fourth bioreactors had HRT of 8, 4, 2.7, and 2 hrs, respectively. The change in HRT slightly impacted the ThOD in the four bioreactors. First, second, third, and fourth bioreactors had ThOD of 105.8, 104.8, 104.3, and 103.9 kgO₂ d⁻¹. The impact of the dynamic influent loading rates over a day on the aeration energy using the three correlations (Fig. SI-12) showed comparable trends to the plug flow reactors in terms of aeration energy.

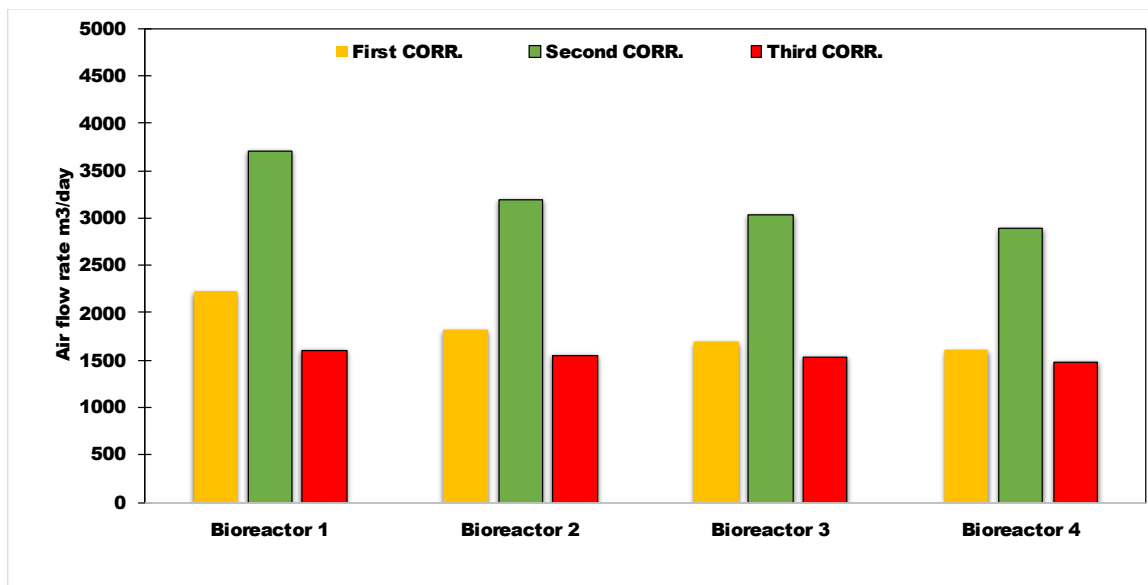


Figure 5-8. Air flow rates estimated in the four plug flow bioreactors using the three correlations.

5.3.3.5 MBR Model

The first correlation had α -factor of 0.62 in the aerobic CSTR (first compartment), increasing to 0.65 in the MBR tank due to biodegradation (Fig SI-13). The third correlation had a constant α -factor of 0.45 in the first compartment (MLSS concentration of 10800 mg l⁻¹) and α -factor of 0.17 in the MBR compartment which corresponds to the MLSS concentration of 20000 mg l⁻¹. Crossflow air flow required to scour biofilm off the membrane was calibrated for each correlation to maintain the same oxygen uptake rate (OUR) as well as oxygen transfer rate (OTR) in the MBR compartment. First, second, and third correlations had crossflow air flows of 10,000, 17,000, and 40,000 m³ d⁻¹. Those cross air flows corresponded to an average scour velocity of 0.03 m s⁻¹, 0.035 m s⁻¹, and 0.12 m s⁻¹ for first, second, and third correlations, respectively.

In the aerobic CSTR, the second correlation had the highest air flow rates as it estimated low α -factor and first correlation had the lowest air flow rates associated with high α -factor (Fig. SI-14). In the conventional model with CSTR, first and third correlations were comparable; however, in the MBR model, the third correlation was more sensitive to the MLSS increase in the aerobic CSTR as it showed a reduction in α -factor due to the MLSS increase.

In the MBR tank, the third correlation had the highest air flow rates as it considered the physical impact of the MLSS on the α -factor. Interestingly, third correlation estimated a scour velocity of 0.12 m s⁻¹ which was comparable to the practical values of 0.04-0.12 m s⁻¹ reported in the literature from different pilot studies (Verrecht et al., 2008) while other correlations estimated low scour velocities that might not be practically sufficient to scour solids off the membrane surface. The estimated total aeration energy to treat a theoretical oxygen demand (ThOD) of 489 kgO₂ d⁻¹ for the correlations 1 to 3, respectively, were 129 (38% bioreactor aeration, and 62% crossflow air in the membrane tank), 229 (37% bioreactor aeration, and 63% crossflow air), and 390 (17% bioreactor aeration, and 83% crossflow air) kWh d⁻¹.

Dynamic changes in the influent loading rates were applied daily over 8 days, to assess the impact of MLSS concentrations as well. The dynamic load was applied as shock step loads that changed every day. In the dynamic model instead of using MLSS set point, SRT was fixed at 43.5 d so that MLSS concentrations changed with the organic loads change. The peak and low concentrations were 400% and 50% of the average concentrations, respectively. The middle steps were 100% and 200% of the average concentrations. Figure 5-9 shows the daily change in the estimated aeration energy in the aerobic CSTR due to the change in the organic loading rates using the three correlations. At the peak, the first and third correlations were comparable as they had comparable α -factors of 0.33 and 0.36 while second correlation estimated very high aeration energy as it had a very low α -factor of 0.04. At the minimum, the first and second correlations were comparable as they both estimated high α -factors of 0.59 and 0.63 while the third correlation had a constant α -factor of 0.36 due to the relatively constant MLSS concentrations during the 8-day period. Running the model using the air flow rates from the first correlation and α -factors from the third correlation showed a significant reduction in DO concentrations to 0.1 mg l⁻¹ except at the peak when the DO was 2 mg l⁻¹.

5.3.4 Impact of Pre-denitrification on Aeration Performance

5.3.4.1 Treatment performance

Internal circulation was added to the previous models (plug flow reactor, CSTR, and MBR) to enhance nitrogen removal while converting the first two compartments into anoxic. Comparable treatment performance was observed for the models with the plug flow reactor, plug flow reactors with step feed and CSTR with a nitrogen removal efficiency of 75% (Table SI-4). In MBR, nitrogen removal efficiency improved to be 73%. Similar to the case with nitrification only, the second and third correlation had a constant α -factor of 0.37 based on an influent COD of 430 mg l⁻¹, and 0.65 which corresponds to MLSS concentration of 3055 mg l⁻¹.

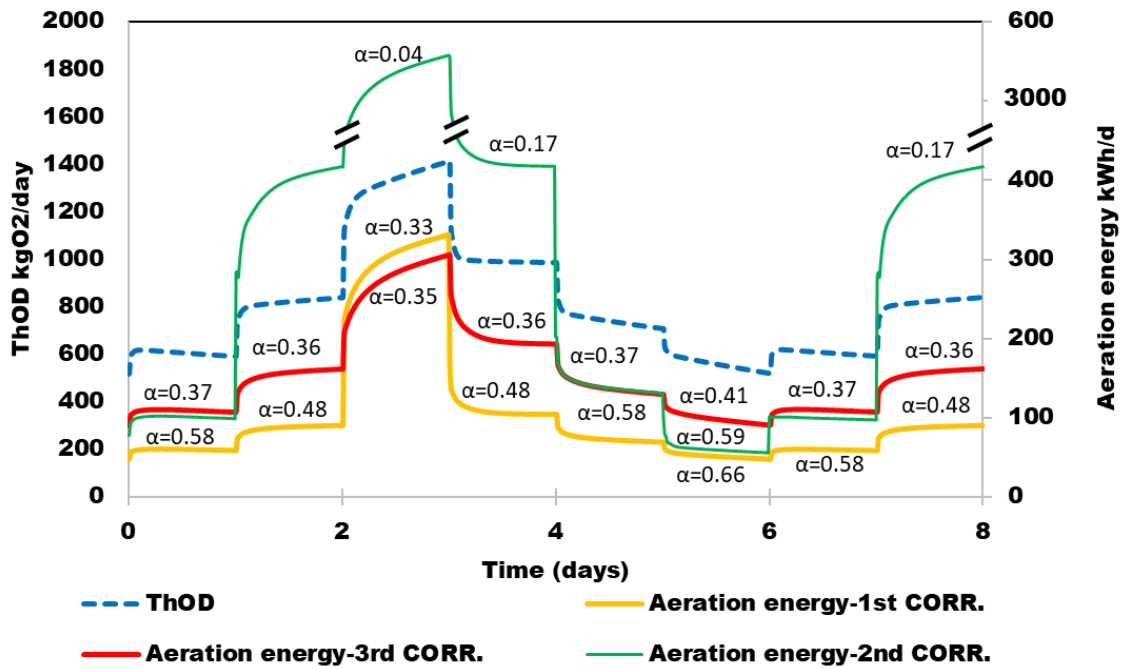


Figure 5-9. The daily change in aeration energy in the aerobic bioreactor due to the change in the influent concentrations using the three correlations (MBR-Nitrification only).

5.3.4.2 Plug flow model

When compared to the nitrification only, the overall air flow rate and hence energy decreased by 30%, 23%, and 15% using the first, second, and third correlations respectively. This is interesting as ThOD was $375 \text{ kgO}_2 \text{ d}^{-1}$ 11% lower than the nitrification only. The additional energy savings were gained due to two main reasons. First, the reduction of the organic loadings at the beginning of the plug flow reactor which reduces the initial high air flow rates in the first three compartments. This was clear in the second and third correlations when the α -factor was constant, as estimated energy savings were lower. The second reason is the removal of readily biodegradable substrates in the anoxic zone which increases the initial α -factor in the plug flow reactor, leading to more energy savings as obtained by the first correlation. The aeration energy consumption per theoretical oxygen demand showed an energy savings of 21%, 14%, and 4% for first,

second, and third correlations. The first and second correlations showed high energy savings when compared to the third correlation since they both considered the impact of loading rates on the initial α - factor.

Also, the difference between the estimated α -factor and air flow rates using the first and third correlations was lower when compared to the plug flow case with nitrification only. In the first compartment, for nitrification only, the first correlation had a 45% higher air flow than the third correlation versus 21% for nitrification and denitrification.

Similarly, dynamic hourly influent loading rates were tested using the three correlations (Fig. SI-18). Due to the anoxic removal of the readily biodegradable substrates, the difference between first and third correlations was very low when compared to the case with nitrification only.

5.3.4.3 CSTR model

Using the first correlation, α -factor was 0.62 which corresponds to sCOD concentration of 32 mg l⁻¹. The first, second, and third correlations showed aeration energy of 32, 53, and 30 kWh d⁻¹ which correspond to a ThOD of 369 kgO₂ d⁻¹. When compared to the CSTR for nitrification only, all correlations showed an energy saving of 11% which was due to the reduction in the ThOD only. In addition, when compared to the plug flow reactor, energy savings of 57%, 61%, and 55% were achieved using CSTR. Denitrification did not impact the estimated aeration energy consumption per theoretical oxygen demand since all energy reduction was due to the organic load removed anoxically. Dynamic hourly influent loading rates were simulated using the three correlations and were similar to what was observed in the case with the nitrification only (Fig. SI-19)

5.3.4.4 Step-feed model

To enhance nitrogen removal, the internal recirculation flow of 500 m³ day⁻¹ was implemented only in the first bioreactor while switching the first two compartments in all bioreactors to be anoxic. Implementing internal flow recirculation in the following bioreactors was not beneficial since most of the influent readily biodegradable carbon was

consumed to denitrify the produced nitrate in the preceding bioreactor. In fact, adding internal recirculation in all bioreactors increased the effluent nitrogen from 10 mg l⁻¹ to 11 mg l⁻¹. Internal recirculation in the first bioreactor improved the nitrogen removal efficiency by 75%. The first correlation had an average α factor of 0.63 in all bioreactors (Fig. SI-20). Interestingly, the estimated α factor, as well as air flow rates using first and third correlations, were comparable in all bioreactors. The second correlation showed the highest airflow rates due to the low α -factor in all bioreactors (Fig. SI-21). Internal recirculation flow in the first bioreactor reduced the air flow rate by 18%, 14%, and 11% using first, second and third correlations, respectively when compared to the case with nitrification only. Also, the aeration energy consumption per theoretical oxygen demand showed an energy savings of 10%, 5%, and 2% for first, second, and third correlations. Dynamic hourly influent loading rates were tested using the three correlations and showed the same trends as the plug flow reactor (Fig. SI-22).

5.3.4.5 MBR model

Similarly, the α -factor and air flow rates were estimated in each compartment following the three correlations (Figures SI-23 and SI-24). Calibrated crossflow air flow rates using first, second and third correlations were 8500, 15000, and 36000 m³ d⁻¹. The estimated aeration energy to treat a theoretical oxygen demand (ThOD) of 438 kgO₂ d⁻¹ for the three correlations was 112, 195, and 350 kWh d⁻¹. Denitrification reduced the aeration energy by 14%, 15% and 10% using first, second and third correlations, respectively. In terms of aeration energy per theoretical oxygen demand first, and second correlations showed an energy savings of 4% and 5% while the third correlation showed no impact. Dynamic daily influent loading rates were tested using the three correlations and showed similar observations to the MBR with nitrification only.

5.4 Discussion

Table 5-1 summarizes the aeration energy results from all steady-state modeled scenarios. The α -factors reported in the table represent flow weighted averages. Additionally, data were collected from the literature to be compared with the modeling results. Tables 5-2, 5-

3, and 5-4 show the measured α -factors from the published pilot and full-scale studies in plug flow reactors, CSTRs, and MBRs respectively.

In plug flow reactors the average α -factor from the reported studies was 0.50 with nitrification only and increased to 0.52 due to pre-denitrification. Only two studies by (Fisher and Boyle, 1999, and Mueller et al., 2000) investigated the impact of pre-denitrification on α -factor using similar configurations. The former reported very little impact on α -factor and the latter showed that α -factor significantly increased from 0.48 to 0.61 (27% increase) due to pre-denitrification. Interestingly, the first correlation of this study using the sCOD estimated an α -factor of 0.52 comparable to what was reported in the literature when nitrification was applied and, more importantly, it showed that α -factor improved to 0.59 due to pre-denitrification, consistent both in trend and value to Mueller et al. (2000). Both the second and third correlations predicted α -factors of 0.37 and 0.65 in plug flow reactors for both nitrification and nitrification/denitrification, not only significantly deviating from the literature average, but also overlooking the improvement due to nitrification, with the former estimates high air flow rates (wasting energy) and the latter estimates low air flow rates that significantly impact the DO concentrations. Running the model using the air flow estimated using the third correlation and α -factors estimated using first correlations as inputs showed more than 60% drop in DO concentrations in the first 4 compartments as DO concentrations varied between 0.5 and 0.8 mg l⁻¹. The reduction in DO may develop preferential growth conditions for filamentous microorganisms which reduce oxygen transfer efficiency, cause odor problems, and increase management and maintenance costs (Collivignarelli et al., 2020). Additionally, running the same model while using the second correlation air flow rates increased the average DO concentrations from 2.0 mg l⁻¹ to 5.2 mg l⁻¹ (varied between 2.7 mg l⁻¹ in the first compartment and 9.5 mg l⁻¹ in the last compartment). Since the first correlation provided the most reliable α -factor for both conditions; nitrification only and nitrification/denitrification in plug-flow reactors, it can be deduced that despite the lack of comparative literature data from full-scale step-feed plug flow, due to the similarity of plug flow and step-feed plug flow, the first correlation would also be the best for step-feed processes.

In CSTRs, based on literature, the average α -factor with nitrification only was 0.51 and increased to 0.60 due to pre-denitrification. Apparently, all reported measurements in Table 5-3 agreed that CSTRs are characterized by higher α -factors compared to the plug-flow reactor, which attests to the validity of the first and third correlations relative to the second correlation as they estimated comparable α -factors as well as comparable aeration energy. The second correlation significantly increased the aeration energy by 42% relative to the first and third correlations. Additionally, running the model using α -factors estimated by first or third correlations and using the air flow rates estimated by second correlations showed a significant increase in the DO concentration from 2.0 mg l⁻¹ to 9.5 mg l⁻¹.

In MBRs the average measured α -factor from the literature of 0.34 observed at MLSS concentrations of 10-30 g/L was comparable to α -factors estimated by second and third correlations; however, the third correlation was more sensitive to the changes in MLSS concentrations than the second correlation as it estimated different α -factors of 0.42 and 0.17 in the aerobic CSTR (before the MBR) and the MBR tank, respectively, corresponding to MLSS concentrations of 10800 mg l⁻¹ and 20000 mg l⁻¹. These values were comparable to the corresponding measurements from the literature (Table 5-4). Additionally, the third correlation was able to estimate the proper cross air flow needed to scour biofilm off the membrane surface. The second correlation estimated a constant α -factor of 0.37 in both bioreactors regardless of MLSS concentrations which makes it inappropriate for MBRs. The first correlation estimated a high α -factor of 0.63 in both reactors due to consistent low sCOD concentrations inside the MBR. Running the MBR model using α -factor from the third correlation and the air flow rates estimated by first correlation resulted in very low DO concentrations of 0.35 mg l⁻¹ which may negatively impact process performance.

The denitrification process decreased the organic loading rates to the bioreactor which reduced the aeration energy. In a plug flow reactor, the first correlation reduced the aeration energy per ThOD by 21% which was due to α -factor improvement from 0.52 to 0.59. In plug flow with step feed, the same correlation reduced the aeration energy per ThOD by only 10% which was due to the improvement in α -factor from 0.58 to 0.61. In CSTRs, aeration energy per ThOD has not been impacted since α -factor was the same under both

conditions; nitrification only, and nitrification/denitrification. Similarly, there was no effect on α -factor in MBRs as α -factor was impacted mainly by MLSS change and thus denitrification had no effect on aeration energy per ThOD.

The analysis using dynamic influent loading rates, within a 24-h period, showed that in plug flow reactor and plug flow reactors with step feed, all three correlations estimated comparable aeration energy at the minimum organic loading rate (Fig.5-6) since all of the estimated high α -factors of 0.67, 0.55, and 0.65 using first second and third correlations. At the peak organic loading rate, the three correlations showed different aeration energy as α -factors from the first and second correlations decreased to 0.44 and 0.25 respectively and the third was high (0.65) due to the constant MLSS concentrations. Interestingly, in the CSTR, the first and third correlations estimated comparable aeration energy (average percentage error of 5.0%) due to the comparable estimated α -factors (average percentage error of 5.8%) at different organic loading rates (Fig.5-7) which agreed with steady-state results. Similar to the plug flow reactor findings, all correlations estimated comparable aeration energy at the minimum loading rate in CSTRs while at the peak loading, the second correlation estimated 57% higher aeration energy compared to other two correlations.

In MBRs, dynamic analysis over 8 days (Fig. 5-9) showed that in the aerobic bioreactor, the second correlation had a high air flow rate (10 times higher than the air flow estimated by the first and third correlations) at the peak due to the very low α -factor of 0.04, which is very low compared to the literature data of Table 5-4. The first correlation estimated low air flow rates except at peak due to high α -factors (average 0.54) associated with low sCOD concentrations. The third correlation estimated an α -factor of 0.36 at the peak loading, in agreement with the average of 0.34 (Table 5-4) which makes it the most reliable correlation for MBR systems as the first correlation resulted in aeration deficiency (DO of 0.2 mg/L) and the second correlation resulted in substantial energy wastage. It must be asserted that although the model predicted a 1-fold jump in effluent ammonia to 0.27 mg l⁻¹ during the various dynamic steps, the adverse implications of the very low DO conditions for the 8-d period are not limited to nitrification but include filamentous growth and sludge bulking.

Table 5-1. Estimated α -factor and aeration energy for the modeled scenarios using typical wastewater characteristics

Treatment processes	Aeration reactor type		Correlation	α -factor	Aeration Energy	
					kWh/day	kWh/kgO ₂
Nitrification only	Plug flow		1	0.52	108	0.26
			2	0.37	179	0.43
			3	0.65	78	0.18
	CSTR		1	0.62	36	0.09
			2	0.37	60	0.14
			3	0.65	34	0.08
	Plug flow (step feed)		1	0.58	91	0.22
			2	0.37	159	0.38
			3	0.65	76	0.18
	CSTR (MBR)	Aerobic CSTR	1	0.63	49	0.09
			2	0.37	84	0.17
			3	0.42	68	0.14
		MBR tank	1	0.63	80	-
			2	0.37	145	-
			3	0.17	322	-
Nitrification and Denitrification	Plug flow		1	0.59	76	0.20
			2	0.37	138	0.37
			3	0.65	68	0.18
	CSTR		1	0.62	32	0.09
			2	0.37	53	0.14
			3	0.65	30	0.08
	Plug flow (step feed)		1	0.61	75	0.20
			2	0.37	138	0.36
			3	0.65	68	0.18
	CSTR (MBR)	Aerobic CSTR	1	0.63	43	0.09
			2	0.37	74	0.17
			3	0.42	60	0.14
		MBR tank	1	0.63	69	-
			2	0.37	121	-
			3	0.17	290	-

*flow weighted averages

Table 5-2. Measured α -factor in plug flow reactors

Plug flow			
Reference	alpha factor	influent COD	Study scale
(Fisher and Boyle, 1999)	0.33-0.53 (Nitrification only)	-	Pilot plant
	0.39-0.51 (with pre-denitrification)	-	
(Mueller et al., 2000)	0.48 (Nitrification only)	-	Fredonia Wastewater Treatment Plant (WWTP) at Fredonia, New York, (capacity 12,500 m ³ d ⁻¹)
	0.61 (with pre-denitrification)	-	
(Leu et al., 2009)	0.3-0.6 (with pre-denitrification)	250-450 mg/L	Full-scale treatment plant with the capacity of 38,000 m ³ d ⁻¹
(Zhou et al., 2013)	0.4 at the tank influent increasing to 0.8 close to the tank effluent (average 0.6) (Nitrification only)	-	The Lucun WWTP in Wuxi, China with a treatment capacity of 275,000 m ³ d ⁻¹
(Jiang et al., 2017)	0.25-0.6 (with pre-denitrification) (average 0.5)	250-450 mg/L	Two plants in southern California and one plant in the District of Columbia
Averages	0.50 (Nitrification only)		
	0.52 (with pre-denitrification)		

Table 5-3. Measured α -factor in CSTRs

CSTR			
Reference	alpha factor	influent COD	Study scale
Rieth et al., 1990)	0.53 (Nitrification only)	-	Pilot plant
(Gillot and Héduit, 2000)	0.56-0.6 (Nitrification only)	-	Milly la Foret wastewater treatment plant, France
(Mahendraker, Mavinic, and Rabinowitz, 2005)	0.41 (Nitrification only)	-	Pilot plant
	0.35-0.95 (with pre-denitrification) (average 0.6)	-	
(Mahendraker, Mavinic, and Hall, 2005)	0.6 (with pre-denitrification)	380 mg/L	Pilot plant
Averages	0.51 (Nitrification only)		
	0.60 (with pre-denitrification)		

Table 5-4. Measured α -factor in MBRs

MBR			
Reference	alpha factor	MLSS	Study scale
(Cornel et al., 2003)	0.4-0.62	10-17 g/L	Full-scale
(Krampe and Krauth, 2003)	0.1-0.45	10-30 g/L	Pilot plant
(Germain et al., 2007)	0.01- 0.5	10-30 g/L	Two pilot-scale and five full-scale plants
(Henkel et al., 2011b)	0.01-0.5	10-30 g/l	Combined and analyzed data from 7 different studies
Average	0.34		

5.5 Summary and Conclusions

Experimental data collected from pilot SBRs were used to calibrate a process model integrated with an aeration model utilizing three dynamic α -factor correlations. After model validation, various continuous-flow processes such as plug flow, CSTR, step-feed plug flow, and MBRs were assessed with respect to energy demand for nitrification and biological nitrogen removal. The following conclusions can be drawn:

Correlations impact on aeration:

- The first correlation based on reactor sCOD was validated using controlled experimental measurements from pilot SBRs and was observed to better predict diurnal and spatial variations in aeration energy in SBRs than other correlations.
- The second correlation (based on the applied or influent COD) was found to overestimate the air flow rate. However, it considered the impact of the influent loading rates on the α -factor, based on data that is more likely to be available.
- The third correlation based on MLSS correlation estimated the lowest air flow rates. However, it seems to overlook the impact of the influent loading rates on α -factor in SBRs.

Reactor configuration effect on aeration energy

- Comparing the model results with the literature revealed that the first correlation is appropriate to design SBR, plug flow, step-feed, and CSTR systems and the third correlation is appropriate to design CSTRs and MBRs while the second correlation was not valid in any of the modeled reactors.
- CSTRs reduced the aeration energy by 66% and 56% compared to the plug flow reactor for nitrification only and by 57% and 55% for denitrification using first and third correlations,
- When nitrification only was targeted, plug flow with step feed reactors reduced the aeration energy by 15% when compared to the plug flow reactor.

Denitrification impact on aeration energy

- In a plug flow reactor, internal recirculation to enhance the nitrogen removal reduced the aeration energy by 30%. The corresponding energy savings for step-feed plug flow were 18%.
- In CSTR, denitrification reduced the aeration energy by 11% whereas for MBRs energy savings were 12%.
- Denitrification reduced the aeration energy per unit kgThOD in plug flow reactor by 21%. For step-feed plug flow the corresponding energy savings were 10%.
- Denitrification did not impact the aeration energy per unit kgThOD in CSTR and MBRs.

References

- Ahmed, A.S., Bahreini, G., Ho, D., Sridhar, G., Gupta, M., Wessels, C., Marcelis, P., Elbeshbishy, E., Rosso, D., Santoro, D., Nakhla, G., 2019. Fate of cellulose in primary and secondary treatment at municipal water resource recovery facilities. *Water Environ. Res.* 91, 1479–1489. <https://doi.org/10.1002/wer.1145>
- Ahmed, A.S., Khalil, A., Ito, Y., van Loosdrecht, M.C.M., Santoro, D., Rosso, D., Nakhla, G., 2020. Dynamic Impact of Cellulose and Readily Biodegradable Substrate on Oxygen Transfer Efficiency in Sequencing Batch Reactors. *Water Res.* 116724. <https://doi.org/10.1016/j.watres.2020.116724>
- American Public Health Association, 2005. *Standard Methods for the Examination of Water & Wastewater*. American Public Health Association.
- Amerlinck, Y., Bellandi, G., Amaral, A., Weijers, S., Nopens, I., 2016. Detailed off-gas measurements for improved modelling of the aeration performance at the WWTP of Eindhoven. *Water Sci. Technol.* 74, 203–211. <https://doi.org/10.2166/wst.2016.200>
- Baquero-Rodríguez, G.A., Lara-Borrero, J.A., Nolasco, D., Rosso, D., 2018. A Critical Review of the Factors Affecting Modeling Oxygen Transfer by Fine-Pore Diffusers in Activated Sludge. *Water Environ. Res.* 90, 431–441. <https://doi.org/10.2175/106143017X15131012152988>
- Brade, C.E., Shahid, K., 1993. Advances in the Design of Fine Bubble Aeration Plants. *Water Sci. Technol.* 28, 343–350. <https://doi.org/10.2166/wst.1993.0252>
- Caivano, M., Bellandi, G., Mancini, I.M., Masi, S., Brienza, R., Panariello, S., Gori, R., Caniani, D., 2017. Monitoring the aeration efficiency and carbon footprint of a medium-sized WWTP: experimental results on oxidation tank and aerobic digester. *Environ. Technol.* 38, 629–638. <https://doi.org/10.1080/09593330.2016.1205150>

- Cierkens, K., Plano, S., Benedetti, L., Weijers, S., de Jonge, J., Nopens, I., 2012. Impact of influent data frequency and model structure on the quality of WWTP model calibration and uncertainty. *Water Sci. Technol.* 65, 233–242.
<https://doi.org/10.2166/wst.2012.081>
- Collivignarelli, M.C., Baldi, M., Abbà, A., Caccamo, F.M., Carnevale Miino, M., Rada, E.C., Torretta, V., 2020. Foams in Wastewater Treatment Plants: From Causes to Control Methods. *Appl. Sci.* 10, 2716. <https://doi.org/10.3390/app10082716>
- Cornel, P., Wagner, M., Krause, S., 2003. Investigation of oxygen transfer rates in full scale membrane bioreactors. *Water Sci. Technol. J. Int. Assoc. Water Pollut. Res.* 47, 313–319.
- Daelman, M.R.J., Van Eynde, T., van Loosdrecht, M.C.M., Volcke, E.I.P., 2014. Effect of process design and operating parameters on aerobic methane oxidation in municipal WWTPs. *Water Res.* 66, 308–319.
<https://doi.org/10.1016/j.watres.2014.07.034>
- Fisher, M.J., Boyle, W.C., 1999. Effect of anaerobic and anoxic selectors on oxygen transfer in wastewater. *Water Environ. Res.* 71, 84–93.
- Garcia-Garcia, E., Pun, J., Perez-Estrada, L.A., Din, M.G.-E., Smith, D.W., Martin, J.W., Belosevic, M., 2011. Commercial naphthenic acids and the organic fraction of oil sands process water downregulate pro-inflammatory gene expression and macrophage antimicrobial responses. *Toxicol. Lett.* 203, 62–73.
<https://doi.org/10.1016/j.toxlet.2011.03.005>
- Garrido-Baserba, M., Rosso, D., Odize, V., Rahman, A., Van Winckel, T., Novak, J.T., Al-Omari, A., Murthy, S., Stenstrom, M.K., De Clippeleir, H., 2020. Increasing oxygen transfer efficiency through sorption enhancing strategies. *Water Res.* 116086. <https://doi.org/10.1016/j.watres.2020.116086>

- Garrido-Baserba, M., Sobhani, R., Asvapathanagul, P., McCarthy, G.W., Olson, B.H., Odize, V., Al-Omari, A., Murthy, S., Nifong, A., Godwin, J., Bott, C.B., Stenstrom, M.K., Shaw, A.R., Rosso, D., 2017. Modelling the link amongst fine-pore diffuser fouling, oxygen transfer efficiency, and aeration energy intensity. *Water Res.* 111, 127–139. <https://doi.org/10.1016/j.watres.2016.12.027>
- Germain, E., Nelles, F., Drews, A., Pearce, P., Kraume, M., Reid, E., Judd, S.J., Stephenson, T., 2007. Biomass effects on oxygen transfer in membrane bioreactors. *Water Res.* 41, 1038–1044. <https://doi.org/10.1016/j.watres.2006.10.020>
- Gillot, S., Héduit, A., 2008. Prediction of alpha factor values for fine pore aeration systems. *Water Sci. Technol.* 57, 1265–1269. <https://doi.org/10.2166/wst.2008.222>
- Gillot, S., Héduit, A., 2000. Effect of air flow rate on oxygen transfer in an oxidation ditch equipped with fine bubble diffusers and slow speed mixers. *Water Res.* 34, 1756–1762. [https://doi.org/10.1016/S0043-1354\(99\)00323-1](https://doi.org/10.1016/S0043-1354(99)00323-1)
- Gillot, S., Kies, F., Amiel, C., Roustan, M., Héduit, A., 2005. Application of the off-gas method to the measurement of oxygen transfer in biofilters. *Chem. Eng. Sci.*, 7th International Conference on Gas-Liquid and Gas-Liquid-Solid Reactor Engineering 60, 6336–6345. <https://doi.org/10.1016/j.ces.2005.04.056>
- Gori, R., Jiang, L.-M., Sobhani, R., Rosso, D., 2011. Effects of soluble and particulate substrate on the carbon and energy footprint of wastewater treatment processes. *Water Res.* 45, 5858–5872. <https://doi.org/10.1016/j.watres.2011.08.036>
- Guender, B., 2001. The Membrane-Coupled Activated Sludge Process in Municipal Wastewater Treatment 49.
- Guglielmi, G., Chiarani, D., Judd, S.J., Andreottola, G., 2007. Flux criticality and sustainability in a hollow fibre submerged membrane bioreactor for municipal

wastewater treatment. *J. Membr. Sci.* 289, 241–248.

<https://doi.org/10.1016/j.memsci.2006.12.004>

Guglielmi, G., Chiarani, D., Saroj, D.P., Andreottola, G., 2008. Impact of chemical cleaning and air-sparging on the critical and sustainable flux in a flat sheet membrane bioreactor for municipal wastewater treatment. *Water Sci. Technol.* 57, 1873–1879. <https://doi.org/10.2166/wst.2008.126>

Henkel, J., Cornel, P., Wagner, M., 2011. Oxygen transfer in activated sludge – new insights and potentials for cost saving. *Water Sci. Technol.* 63, 3034–3038. <https://doi.org/10.2166/wst.2011.607>

Henkel, J., Lemac, M., Wagner, M., Cornel, P., 2009. Oxygen transfer in membrane bioreactors treating synthetic greywater. *Water Res.* 43, 1711–1719. <https://doi.org/10.1016/j.watres.2009.01.011>

Henze, M., Gujer, W., Mino, T., Loosdrecht, M.C.M. van, 2000. *Activated sludge models ASM1, ASM2, ASM2d and ASM3*. IWA Publishing.

Jenkins, T.E., 2013. *Aeration Control System Design: A Practical Guide to Energy and Process Optimization*. John Wiley & Sons, Incorporated, Somerset, UNITED STATES.

Jiang, L., Garrido-Baserba, M., Nolasco, D., Al-Omari, A., DeClippeleir, H., Murthy, S., Rosso, D., 2017. Modelling oxygen transfer using dynamic alpha factors. *Water Res.* 124, 139–148. <https://doi.org/10.1016/j.watres.2017.07.032>

Krampe, J., Krauth, K., 2003. Oxygen transfer into activated sludge with high MLSS concentrations. *Water Sci. Technol.* 47, 297–303. <https://doi.org/10.2166/wst.2003.0618>

Leu, S.Y., Rosso, D., Larson, L.E., Stenstrom, M.K., 2009. *Real-Time Aeration Efficiency Monitoring in the Activated Sludge Process and Methods to Reduce*

Energy Consumption and Operating Costs. *Water Environ. Res.* 81, 2471–2481.
<https://doi.org/10.2175/106143009X425906>

Mahendraker, V., Mavinic, D.S., Hall, K.J., 2005a. Comparison of oxygen transfer parameters determined from the steady state oxygen uptake rate and the non-steady-state changing power level methods. *J. Environ. Eng.* 131, 692–701.

Mahendraker, V., Mavinic, D.S., Rabinowitz, B., 2005b. Comparison of oxygen transfer parameters from four testing methods in three activated sludge processes. *Water Qual. Res. J. Can.* 40, 164–176.

Metcalf & Eddy, Tchobanoglous, G., Burton, F., Stensel, H.D., 2002. *Wastewater Engineering: Treatment and Reuse*. McGraw-Hill Education.

Mueller, J.A., Kim, Y.-K., Krupa, J.J., Shkreli, F., Nasr, S., Fitzpatrick, B., 2000. Full-Scale Demonstration of Improvement in Aeration Efficiency. *J. Environ. Eng.* 126, 549–555. [https://doi.org/10.1061/\(ASCE\)0733-9372\(2000\)126:6\(549\)](https://doi.org/10.1061/(ASCE)0733-9372(2000)126:6(549))

Pasini, F., Garrido-Baserba, M., Ahmed, A., Nakhla, G., Santoro, D., Rosso, D., 2020. Oxygen transfer and wide-plant energy assessment of primary screening in WRRFs. *Water Environ. Res.* n/a. <https://doi.org/10.1002/wer.1349>

Pittoors, E., Guo, Y., Van Hulle, S.W.H., 2014. Oxygen transfer model development based on activated sludge and clean water in diffused aerated cylindrical tanks. *Chem. Eng. J.* 243, 51–59. <https://doi.org/10.1016/j.cej.2013.12.069>

Puthli, M.S., Rathod, V.K., Pandit, A.B., 2005. Gas–liquid mass transfer studies with triple impeller system on a laboratory scale bioreactor. *Biochem. Eng. J.* 23, 25–30. <https://doi.org/10.1016/j.bej.2004.10.006>

Reardon, D.J., 1995. Turning down the power. *Civ. Eng.* 65, 54–56.

- Reijken, C., Giorgi, S., Hurkmans, C., Pérez, J., van Loosdrecht, M.C.M., 2018. Incorporating the influent cellulose fraction in activated sludge modelling. *Water Res.* 144, 104–111. <https://doi.org/10.1016/j.watres.2018.07.013>
- Rieth, M.G., Boyle, W.C., Ewing, L., 1990. Effects of selected design parameters on the fouling characteristics of ceramic diffusers. *Res. J. Water Pollut. Control Fed.* 877–886.
- Rosso, D., 2018. *Aeration, Mixing, and Energy: Bubbles and Sparks*. IWA Publishing. <https://doi.org/10.2166/9781780407845>
- Rosso, D., Huo, D.L., Stenstrom, M.K., 2006. Effects of interfacial surfactant contamination on bubble gas transfer. *Chem. Eng. Sci.* 61, 5500–5514. <https://doi.org/10.1016/j.ces.2006.04.018>
- Rosso, D., Iranpour, R., Stenstrom, M.K., 2005. Fifteen years of offgas transfer efficiency measurements on fine-pore aerators: key role of sludge age and normalized air flux. *Water Environ. Res.* 77, 266–273.
- Rosso, D., Lothman, S.E., Jeung, M.K., Pitt, P., Gellner, W.J., Stone, A.L., Howard, D., 2011. Oxygen transfer and uptake, nutrient removal, and energy footprint of parallel full-scale IFAS and activated sludge processes. *Water Res.* 45, 5987–5996. <https://doi.org/10.1016/j.watres.2011.08.060>
- Rosso, D., Stenstrom, M.K., 2006. Surfactant effects on α -factors in aeration systems. *Water Res.* 40, 1397–1404. <https://doi.org/10.1016/j.watres.2006.01.044>
- Rosso, D., Stenstrom, M.K., 2005. Comparative economic analysis of the impacts of mean cell retention time and denitrification on aeration systems. *Water Res.* 39, 3773–3780. <https://doi.org/10.1016/j.watres.2005.07.002>
- Ruiken, C.J., Breuer, G., Klaversma, E., Santiago, T., van Loosdrecht, M.C.M., 2013. Sieving wastewater – Cellulose recovery, economic and energy evaluation. *Water Res.* 47, 43–48. <https://doi.org/10.1016/j.watres.2012.08.023>

- Siatou, A., Manali, A., Gikas, P., 2020. Energy Consumption and Internal Distribution in Activated Sludge Wastewater Treatment Plants of Greece. *Water* 12, 1204. <https://doi.org/10.3390/w12041204>
- Verrecht, B., Judd, S., Guglielmi, G., Brepols, C., Mulder, J.W., 2008. An aeration energy model for an immersed membrane bioreactor. *Water Res.* 42, 4761–4770. <https://doi.org/10.1016/j.watres.2008.09.013>
- Wagner, M., Pöpel, H.J., 1998. Oxygen transfer and aeration efficiency - influence of diffuser submergence, diffuser density, and blower type. *Water Sci. Technol.* 38, 1–6. <https://doi.org/10.2166/wst.1998.0163>
- Wagner, M., Pöpel, H.J., 1996. Surface active agents and their influence on oxygen transfer. *Water Sci. Technol., Water Quality International '96 Part 2* 34, 249–256. [https://doi.org/10.1016/0273-1223\(96\)00580-X](https://doi.org/10.1016/0273-1223(96)00580-X)
- Zhou, X., Wu, Y., Shi, H., Song, Y., 2013. Evaluation of oxygen transfer parameters of fine-bubble aeration system in plug flow aeration tank of wastewater treatment plant. *J. Environ. Sci.* 25, 295–301. [https://doi.org/10.1016/S1001-0742\(12\)60062-X](https://doi.org/10.1016/S1001-0742(12)60062-X)
- Zhu, Y., Bandopadhyay, P.C., Wu, J., 2001. Measurement of Gas-Liquid Mass Transfer in an Agitated Vessel. A Comparison between Different Impellers. *J. Chem. Eng. Jpn.* 34, 579–584. <https://doi.org/10.1252/jcej.34.579>.

Chapter 6

6 Performance Assessment of Anoxic And Aerobic Biodegradation Of Cellulose.

6.1 Introduction

Cellulose in wastewater represents 30% to 35% of the influent particulate organics (Ahmed et al., 2019, Ruiken et al., 2013). Cellulose in wastewater treatment plants originates from the use of toilet papers (Ruiken et al., 2013). Considering that the majority of toilet paper constituents are cellulose, cellulose in the influent wastewater may contribute 20% to 30% of the influent COD (Ruiken et al., 2013). Cellulose as a particulate settleable matter can be easily recovered from primary clarification and rotating belt filter (RBF), reducing aeration energy and sludge production in secondary treatment (Ahmed et al., 2019, Reijken et al., 2018). Captured cellulose can be redirected to digesters to be converted into biogas (Ghasimi et al., 2016) or used for numerous sectors, including biofuels, construction material products, bio-plastics bottles, and asphalt (Boztas, 2017, Honda et al., 2000). Recently, Espíndola et al., 2021 recovered cellulose nanocrystals from RBF-sieved sludge, with cellulose content of 0.35-0.79 g cellulose/gTSS.

The cellulose content of waste activated sludge was between 1.4%-3.5% of the TSS (Ahmed et al., 2019, and Hurwitz et al., 1961) confirming that cellulose is biodegradable. Cellulose biodegradability under aerobic and anaerobic conditions in wastewater treatment plants has been investigated experimentally in several studies. Aerobically, the biodegradation efficiency at room temperature varied between 50% and 90% as reported by (Ahmed et al., 2019, Alvarez et al., 2009, Hurwitz et al., 1961, Verachtert et al., 1982). At cold temperatures of 12 °C to 13 °C cellulose degradation efficiency varied between 6.7% and 92% (Ahmed et al., 2019, Hurwitz et al., 1961) which suggests that cellulose degradation is temperature-dependent. Anaerobically, cellulose biodegradation efficiency varied between 50%-100% at room temperature and was 10% at a cold temperature of 9 °C.

Modeling cellulose using existing model libraries (Activated sludge models-ASM family) is difficult because they do not include cellulose as a separate state variable. Similar to other slowly biodegradable substrates, cellulose biodegradation can be modeled using either first order (Weimer, 1992), or using the surface limited reaction rate as proposed in ASM models (Henze et al., 2000). Benneouala et al., 2017 studied the role of biomass in the degradation of slowly biodegradable particles using toilet paper and pure cellulose under aerobic conditions. The study was conducted using respirometry experiments and the ASM1 model was used to better understand the role of biomass in hydrolysis. The findings revealed that the biodegradation time for toilet papers and cellulose was at least 10 days. It was also observed that a small portion of the active biomass was responsible for the hydrolysis of the slowly biodegradable substrates including toilet papers and cellulose. Behera et al., 2018 studied the effect of cellulose biodegradability and digestibility on the plant-wide energy balance using BSM2. In this study, cellulose was not modeled as a separate state variable, and instead, cellulose was assumed to account for 30% of the influent TCOD. Despite the lack of experimental cellulose measurements in this study, it was clearly shown that cellulose can play a very important role in plant-wide energy since RBF was found to reduce aeration energy by 8% and increase methane production by 10% when compared to primary clarifications. Reijken et al., 2018 were the first to integrate cellulose into the ASM1 model as a separate state variable, and cellulose was assumed to follow first-order hydrolysis kinetics. The cellulose fraction as well as cellulose hydrolysis rate were calibrated. The study clearly demonstrated that cellulose hydrolysis is not clearly understood. In addition, cellulose hydrolysis was assumed to be identical regardless of the treatment condition (i.e. aerobic and anoxic conditions).

Volatile fatty acids (VFA) generated through the fermentation of cellulose-containing primary sludge, waste activated sludge (WAS) or a mixture of both can be used as a carbon source to enhance the biological nutrient removal (BNR) process (Liu et al., 2017, Yuan et al., 2016, Zheng et al., 2010). Both primary clarification and RBF removed more than 80% of the influent cellulose with cellulose accounting for 20% and 35% of the dry solids in primary sludge and RBF sludge, respectively (Ahmed et al., 2019). Bahreini et al., 2020 compared the fermentability of the primary clarification and the RBF sludges. Results

showed that, on average, primary clarification had a higher VFA yield of 111 mg VFA/g VS than the VFA yield of the RBF sludge (70 mg VFA/g VS).

Despite the considerable experimental efforts to estimate cellulose biodegradation efficiency under aerobic and anaerobic conditions, only two studies modeled the biodegradation of cellulose (Benneouala et al., 2017, Reijken et al., 2018). Additionally, the aforementioned two modeling studies neglected the cellulose biodegradability under anoxic conditions and assumed that anoxic and aerobic hydrolysis rates of cellulose were identical. In addition, neither of the two studies mentioned above was able to calibrate their models on the basis of actual cellulose measurements. Reijken et al., 2018 calibrated their model using regular COD and solids measurements, and Benneouala et al., 2017 tested the cellulose biodegradation under controlled conditions using respirometry with the addition of pure cellulose and different types of toilet papers.

Diverting the influent cellulose from the mainstream to the biosolids stream, not only reduces aeration energy but is beneficial to enhance BNR as a result of primary sludge fermentation; however, the impact of the recovered VFA on the aeration energy as well as biosolids accumulation in the secondary treatment is a clear knowledge gap. After fermentation, the composition of the particles and flocs greatly changes to decrease their filterability and dewaterability. Mechanical centrifugation is often necessary to separate fermentation products from sludge (Liu et al., 2017). Apparently, separation is practically difficult and costly (Liu et al., 2017). Therefore, fermented primary sludge without solids separation was used in this study. The main objectives of this study were: 1- To estimate the cellulose hydrolysis rate constants under both anoxic and aerobic conditions. 2- Evaluate the impact of the fermented primary sludge on nutrients removal efficiency, solids production, and oxygen transfer efficiency in sequencing batch reactors (SBRs).

6.2 Material and methods

6.2.1 Sequencing batch reactors pilot

A pilot consisting of two parallel sequencing batch reactors (SBRs) has been built and operated at a wastewater treatment plant in London, ON, Canada. Each SBR had a total capacity of 850 liters (diameter 0.6 m, with a depth of 3.0 m) and was treating $1.5 \text{ m}^3 \text{ d}^{-1}$ with a fill ratio of 60%. One reactor was fed with raw wastewater and the other was fed with primary treated wastewater with a rotating belt filter (RBF). Both reactors were operated for three cycles a day (i.e., 8 hrs. per cycle). Each cycle consisted of 15 min filling; 1 h anoxic; 5 h aerobic; 1.5 h settling; 15 min decanting. Both reactors were operated at a solids retention time (SRT) of 10 days. Additionally, the air flow to both reactors was controlled using an electric on/off valve that released intermittently constant air flow to maintain DO of 2 mg l^{-1} .

6.2.2 Hydrolysis of cellulose

The SBR receiving raw wastewater was used due to its high influent cellulose content. Six batch cycles were tested; three anoxic and three aerobic. In addition to the raw wastewater cellulose (cellulose concentration $126 \pm 24 \text{ mg l}^{-1}$ (Ahmed et al., 2019)), pure alpha-cellulose was added at 100 and 200 mg/L to test the hydrolysis of cellulose at different concentrations.

6.2.3 Cellulose hydrolysis model development

In this study, the SBR receiving raw wastewater was modeled using GPS-X 8.0.1 software. The hydrolysis of slowly biodegradable substrates in ASM1 is directly impacted by the oxygen usage and denitrification predictions for heterotrophic species (Henze et al., 2000). For simplicity and to avoid the impact of oxygen as well as the denitrification process, the hydrolysis rate of cellulose was modeled using the surface limited reaction rate (Eq. 1) as proposed in ASM3 where heterotrophic and autotrophic decays do not impact cellulose hydrolysis.

$$\frac{dX_{cl}}{dt} = -\frac{k_{cl} \left(\frac{X_{cl}}{X_h} \right)}{K_{X_{cl}} + \left(\frac{X_{cl}}{X_h} \right)} X_h \quad (1)$$

Where; k_{cl} : is the hydrolysis rate constant of cellulose d^{-1} ; X_{cl} : is the cellulose concentration $mg\ l^{-1}$; X_h is the active heterotrophic biomass concentrations ($mg\ COD\ l^{-1}$); $K_{X_{cl}}$: half-saturation coefficient for hydrolysis of cellulose ($mgCOD\ mg\ cell\ COD^{-1}$); and t is the time.

The hydrolysis rate of cellulose was incorporated into ASM1 and a modified version ASM1CL2 was developed (Table 1). Table 1 contains only the particulate state variables and readily biodegradable substrates as they are directly influenced by the hydrolysis of cellulose. All nitrogen state variables and alkalinity remained as proposed by the original ASM1.

The SBR receiving raw wastewater was modeled using GPS-X (ASM1 model) to estimate the X_h at steady-state conditions. The average values of the experimental measurements of influent and effluent wastewater characteristics over 100 days (one sample/week) were used to calibrate the model. GPS-X optimization tool was then used to estimate k_{cl} in a batch model (ASM1CL2) using the measured values for X_{cl} over time during the batch addition of alpha cellulose. The initial concentrations during the batches were determined from the modeled SBR with an assumed constant $K_{X_{cl}}$ of $1\ gCOD/g\ cell\ COD$ in accordance with ASM3 typical values of $1\ gCOD/g\ cell\ COD$.

ASM1CL2 was then applied to the SBR model using the estimated k_{cl} to estimate cellulose concentrations as a separate state variable from the experimental measurements for MLSS, and MLVSS at steady-state conditions.

6.2.4 Pilot Fermenters

Three identical fermenters with an operating volume of 240 L were fed with primary sludge and were operated at three different SRTs of 2, 4, and 6 days (Fig. 6-1). As shown in Figure 6-1, pH and temperature were monitored using pH and temperature probes. The hot water lines were used to control the temperature inside the fermenters at $37^{\circ}C$. In this study,

primary clarification sludge was used as an alternative to the RBF sludge due to its availability.

The inocula were collected from the primary mesophilic digesters at the Guelph wastewater treatment plant (Guelph, Ontario) and were incubated in the fermenters for one week. The Guelph mesophilic anaerobic digester is a completely mixed reactor with solids retention times (SRTs) of 14–18 days achieving volatile suspended solids (VSS) destruction efficiency of 45%. Samples were collected from the fermented sludge (FS) and were analyzed for total solids (TS), volatile solids (VS), total and soluble chemical oxygen demand (TCOD and sCOD), total and soluble nitrogen (TN and sN), and total and soluble phosphorus (TP and sP).

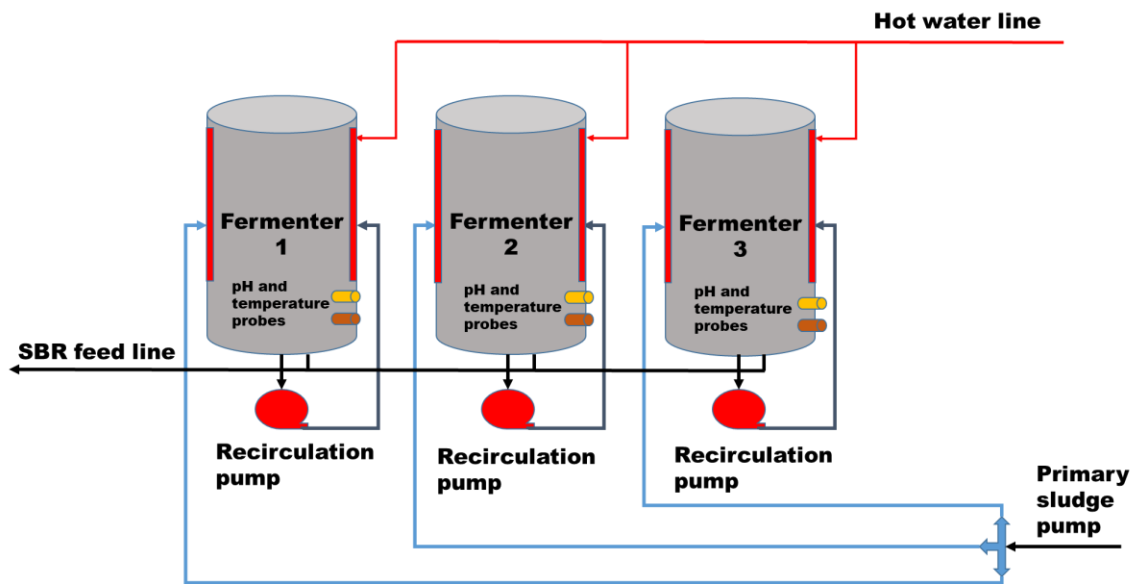


Figure 6-1. Process diagram for the three fermenters

6.2.5 Testing stages for the addition of the fermented primary sludge

Fermented primary sludge was mixed with the RBF effluent and the impact of the fermented sludge was monitored in the SBR receiving RBF effluent only. Daily waste from the fermenters was mixed with the RBF effluent in a mixing tank with a total capacity of

1230 L. Three different testing stages were applied to the SBR using the following mixtures as feeds:

First stage (8 days): mixing 1170 L of RBF effluent with 60 L of the fermented sludge at 4 d SRT.

Second stage (8 days): mixing 1190 L of RBF effluent with 40 L of the fermented sludge at 6 d SRT.

Third stage (8 days): mixing 1110 L of RBF effluent with 120 L of the fermented sludge at 2 d SRT.

6.2.6 Oxygen transfer efficiency measurements

Oxygen transfer was measured in clean water using the unsteady-state method (ASCE, 2007). Oxygen transfer efficiency under process conditions was measured using the off-gas approach (Redmon et al., 1983; ASCE, 1996). Details of the aeration efficiency measurements are presented in Chapter 4.

6.2.7 Wastewater characterization

Total suspended solids (TSS), volatile suspended solids (VSS) were measured following standard methods (American Public Health Association, 2005). The COD, ammonia, nitrate, TN, sN, TP, and sP were measured using Hach methods. Cellulose was measured following the gravimetric method developed by (Hurwitz et al., 1961) and validated by (Gupta et al., 2018).

6.3 Results and discussion

6.3.1 Anoxic and aerobic hydrolysis rate constant of cellulose

6.3.1.1 SBR performance

Table 2 shows the influent, effluent, and mixed liquor characteristics over 100 days for the SBR receiving raw wastewater. The SBR achieved TSS, COD, TN, and TP removal efficiencies of 97%, 94%, 74%, and 94% respectively. Pre-anoxic and high COD: N: P ratios were advantageous for the achievement of a high nitrogen removal efficiency. On average, 71% of influent nitrogen was used in biomass synthesis. Additionally, the high phosphorous removal efficiency was achieved since high COD: N: P allowed for phosphorus release and then uptake. The observed yield was 0.35 mgVSS mgCOD⁻¹.

Table 6-2. Influent and effluent characteristics for the SBR receiving raw wastewater.

No.	Sample name	TSS ^a	VSS ^a	COD ^a	sCOD ^a	TN ^a	sN ^a	NH ₃ ^a	NO ₃ ^a	TP ^a	sP ^a
		mg/L	mg/L	mg/L	mg/L	mg/L	mg/L	mg/L	mg/L	mg/L	mg/L
1	Influent	349 ± 48	274 ± 35	653 ± 82	246 ± 49	31 ± 2	26 ± 2	23 ± 3	0.1 ± 0.01	10 ± 3	2.4 ± 0.4
		11 ± 3	9 ± 2	39 ± 3	28 ± 2	8 ± 1	7 ± 1	0.3 ± 0.2	6 ± 1	0.61 ± 0.3	0.2 ± 0.01
2	SBR effluent	11 ± 3	9 ± 2	39 ± 3	28 ± 2	8 ± 1	7 ± 1	0.3 ± 0.2	6 ± 1	0.61 ± 0.3	0.2 ± 0.01
3	SBR Mixed liquor	5,109 ± 203	3,635 ± 182	-	-	-	-	-	-	-	-

^a Values represent the average ± standard deviation of 14 samples (1 sample/week)

6.3.1.2 Cellulose hydrolysis modeling

Experimental measurements over 100 days (Table 2) were used to calibrate the SBR model at steady-state conditions. Initial concentrations for the batch tests were obtained from the calibrated SBR model. In the batch model, several iterations for each test cycle were optimized to achieve k_{cl} that best describes the cellulose hydrolysis rate. Figures 6-2 and 6-3 show the measured versus model calibrated cellulose concentrations to estimate k_{cl} under aerobic and anoxic conditions. Table 3 shows the estimated k_{cl} for the tested cycles under aerobic and anoxic conditions. Excellent correlations were obtained between model

estimates and measured values under both aerobic and anoxic conditions which confirms the reliability of the estimated hydrolysis rate constants. On average, hydrolysis rates for cellulose under aerobic conditions were $3.74 \pm 0.33 \text{ d}^{-1}$ which was 5 times faster than hydrolysis rates under anoxic conditions ($0.7 \pm 0.31 \text{ d}^{-1}$). The ratio of X_{cl} / X_h in aerobic batches ranged from 0.05-0.18, whereas in anoxic batches it ranged from 0.07-0.18, which is significantly lower than K_{xcl} of 1 gCOD/g cell COD, indicating that cellulose hydrolysis was not limited to cellulose concentrations in all the tested batches.

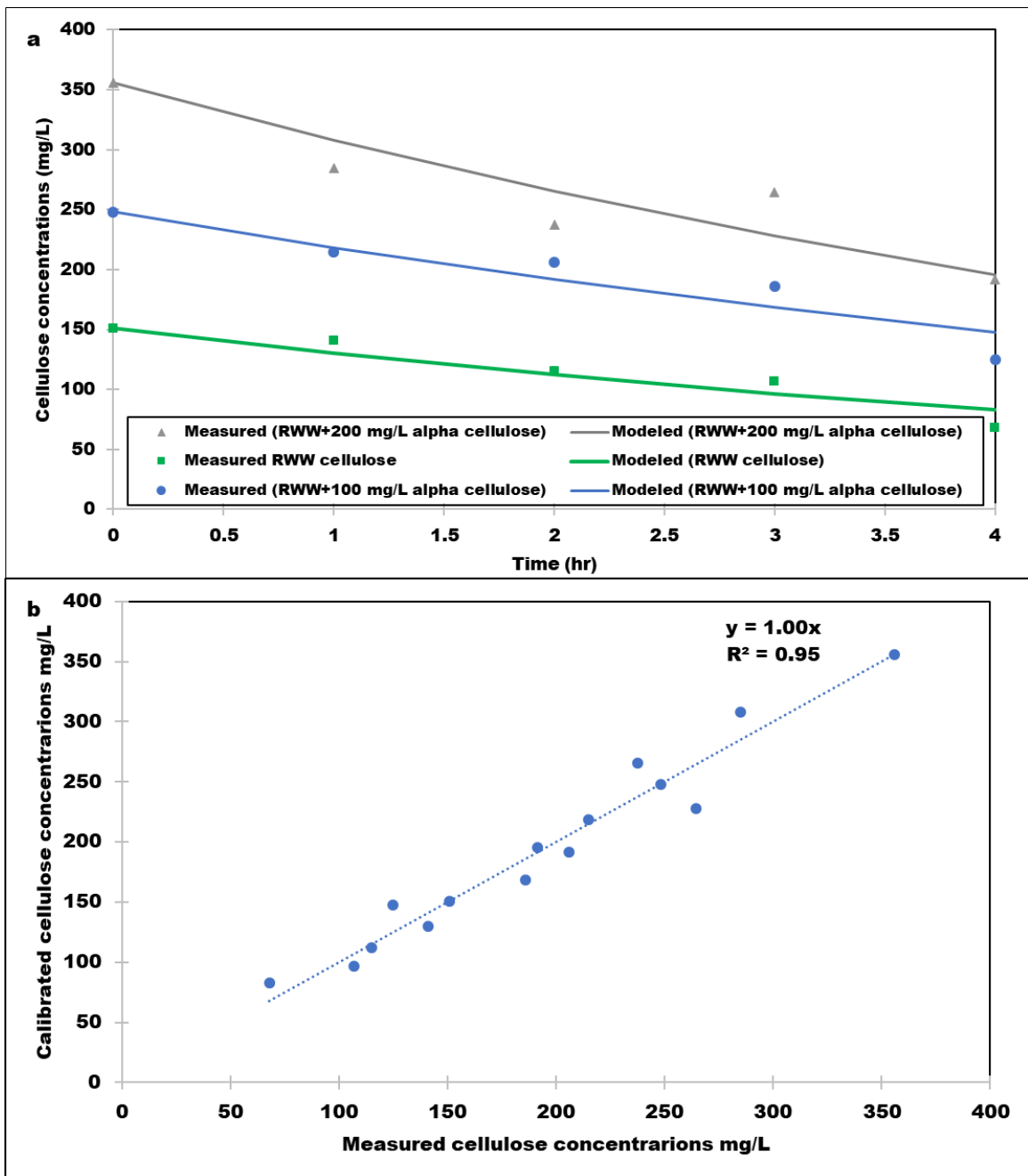


Figure 6-2. Cellulose hydrolysis rates estimated by the model to best match measured values under aerobic conditions (overall average percent error=8%).

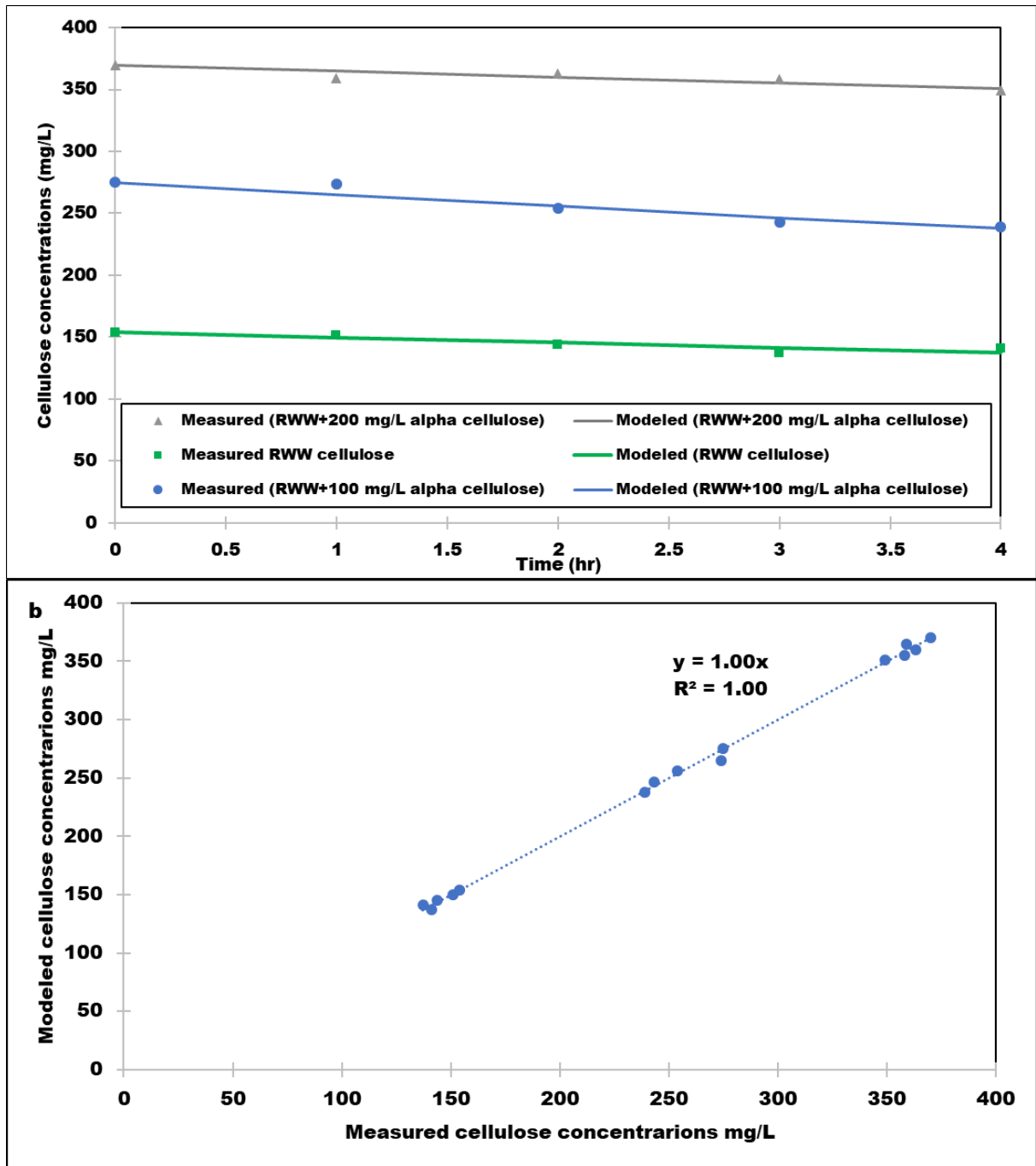


Figure 6-3. Cellulose hydrolysis rates estimated by the model to best match measured values under anoxic conditions (overall average percent error=1%).

Table 6-3. Aerobic and anoxic hydrolysis constant using surface limited reaction rate equation

Testing conditions	Aerobic	Anoxic
	$k_{cl} \text{ d}^{-1}$	$k_{cl} \text{ d}^{-1}$
Raw wastewater cellulose	3.77	0.74
Raw wastewater + 100 mg alpha-cellulose l^{-1}	3.40	0.99
Raw wastewater + 200 mg alpha-cellulose l^{-1}	4.05	0.38
AVG	3.74	0.70
STD	0.33	0.31

The developed model was then recalibrated to match experimental measurements for MLSS at steady-state conditions. Table 4 shows the calibrated influent state variables using ASM1 and ASM1CL2. Figure 6-4 shows the calibrated COD fractions as percentages using both models. Calibrated influent cellulose accounted for 21% of the total influent COD and 35% of the influent TSS, which corresponded to the cellulose content of 35% of the influent TSS estimated by (Ahmed et al., 2019, Ruiken et al., 2013). Moreover, the calibrated cellulose in the influent raw wastewater was comparable to the cellulose concentrations reported by (Ahmed et al., 2019) from the same treatment plant, London, Ontario, Canada. Prior to the addition of cellulose as a separate state variable (ASM1), X_s was 267 mg l^{-1} , which was comparable to typical wastewater characteristics where X_s varies between ($100\text{--}250 \text{ mg l}^{-1}$) (Henze et al., 2000). After including cellulose as a separate state variable (ASM1CL2), particulate inerts X_I was slightly reduced from 140 mg l^{-1} to 135 mg l^{-1} due to the cellulose accumulation.

Additionally, Table 5 shows the estimated particulate fractions inside the SBR (at the beginning of the treatment cycle after feeding and at the end of the cycle before settling) using both models; ASM1 and ASM1CL2. Interestingly, the calibrated cellulose concentrations at the beginning of the cycle (after filling) and at the end of the cycle (before settling) from the steady-state model were comparable to the measured cellulose

concentrations. Also, the calibrated MLVSS at steady-state conditions matched with measured MLVSS. The cellulose fraction in the mixed liquor varied between 2.8% of the particulate organics at the beginning of the cycle to 1.3% at the end of the cycle due to biodegradation, which again is comparable to the literature values of 1.4% - 3.5% reported by Ahmed et al.,(2019), and Hurwitz et al., (1961).

Table 6-4. Calibrated state variables for the influent using both models ASM1 and ASM1CL2

Influent state variables	ASM1	ASM1CL2	Measured
Soluble inert S_I mgCOD l^{-1}	23	23	-
Readily biodegradable substrates S_s mgCOD l^{-1}	223	223	-
Slowly biodegradable substrates X_s mgCOD l^{-1}	267	134	-
Particulate inert organic matter X_I mgCOD l^{-1}	140	135	-
Soluble nitrate nitrogen S_{NO} mgN l^{-1}	0	0	-
Soluble ammonia nitrogen S_{NH} mgN l^{-1}	23	23	23 ± 3
Soluble organic nitrogen S_{ND} mgN l^{-1}	3	3	-
Particulate organic nitrogen X_{ND} mgN l^{-1}	5	5	-
Cellulose X_{cl} mgCOD l^{-1}	0	138	126 ± 24^a
TCOD mgCOD l^{-1}	653	653	653 ± 82^b

^a Values represent the average \pm standard deviation of 6 samples reported by (Ahmed et al., 2019) using samples from the same treatment plant

^bValues represent the average \pm standard deviation of 14 samples (1 sample/week)

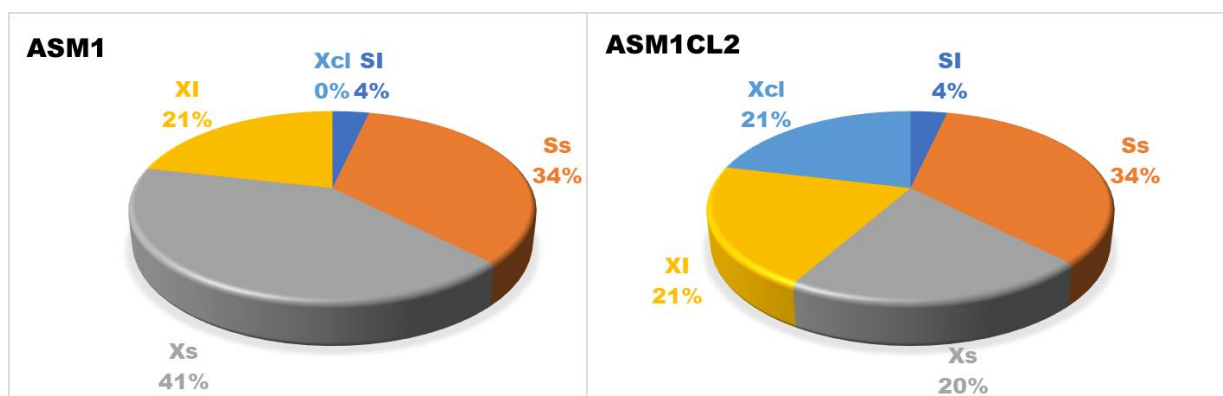


Figure 6-4. COD fractions in the influent raw wastewater using both models; ASM1 and ASM1CL2

Table 6-5. Calibration results of the particulate COD fractions in the SBR using both models ASM1 and ASM1CL2

Particulate fractions	At the beginning of the SBR cycle (after filling)			At the end of the SBR cycle (before settling)		
	ASM1	ASM1CL2	Measured	ASM1	ASM1CL2	Measured
$X_{B,H}$ mgCOD l ⁻¹	1987	1996	-	2057	2066	-
X_i mgCOD l ⁻¹	2473	2387	-	2473	2387	-
$X_{B,A}$ mgCOD l ⁻¹	49	50	-	51	52	-
X_S mgCOD l ⁻¹	176	96	-	16	16	-
X_{cl} mgCOD l ⁻¹	0	153	159 ± 11 ^a	0	72	67 ± 6 ^b
X_p mgCOD l ⁻¹	725	729	-	751	755	-
Total particulate organic mgCOD l⁻¹	5410	5412	-	5348	5348	-
MLVSS mg l⁻¹	3644	3647	3635 ± 182 ^c	3614	3613	3635 ± 182 ^c

^a Values represent the average ±standard deviation of 6 samples

^b Values represent the average ±standard deviation of 3 samples

^c Values represent the average ±standard deviation of 14 samples (1 sample/week)

6.3.1.3 Model validation

The estimated fractions from the calibrated model ASM1CL2 were then used to validate the model using dynamic influent over the 100 days of operation using the experimental MLSS and MLVSS (Fig. 6-5). Both the measured and modeled MLSS and MLVSS were evidently comparable with comparatively very low average percent errors of 3.6% for the MLSS and 5.5% for the MLVSS, confirming the reliability of the calculated fractions even after cellulose was introduced as a separate state variable. This is interesting because it is now possible to determine the influent cellulose fraction using regular influent COD, solids measurements, and the known hydrolysis rate constants of cellulose under both aerobic and anoxic conditions.

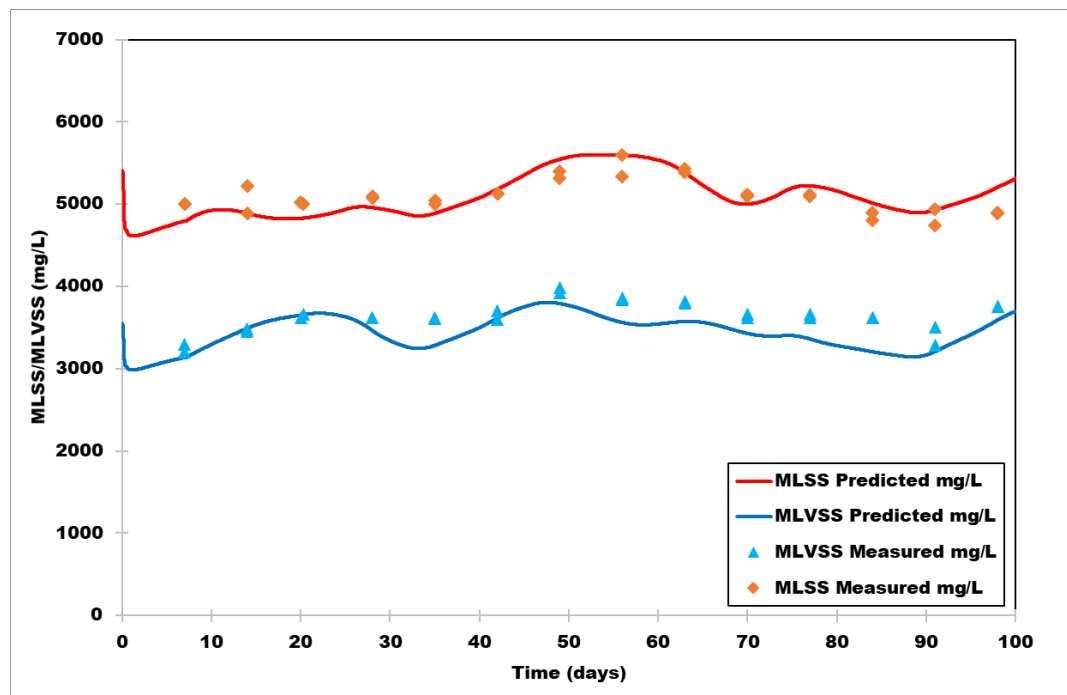


Figure 6-5. Calibrated MLSS and MLVSS for the modeled SBR using ASM1CL2 model (average absolute error for MLSS was 3.6% and for MLVSS was 5.5%)

Figure 6-6 shows the modeled cellulose concentration change with the time during the SBR cycle. On average, 95% of the biodegraded cellulose was biodegraded aerobically while

only 5% was biodegraded anoxically. The results were used to calculate the overall cellulose biodegradation using mass balances. The influent mass of cellulose from the calibrated model was 208 g day^{-1} and the mass of the wasted cellulose was 6 g day^{-1} reflecting a biodegradation efficiency of 97%, which indicates that all influent cellulose is biodegradable. Using experimental measurements of cellulose, the influent mass of cellulose is 193 g day^{-1} and the mass of the wasted cellulose was 6 g day^{-1} reflecting a biodegradation efficiency of 97%, which was identical to the model results.

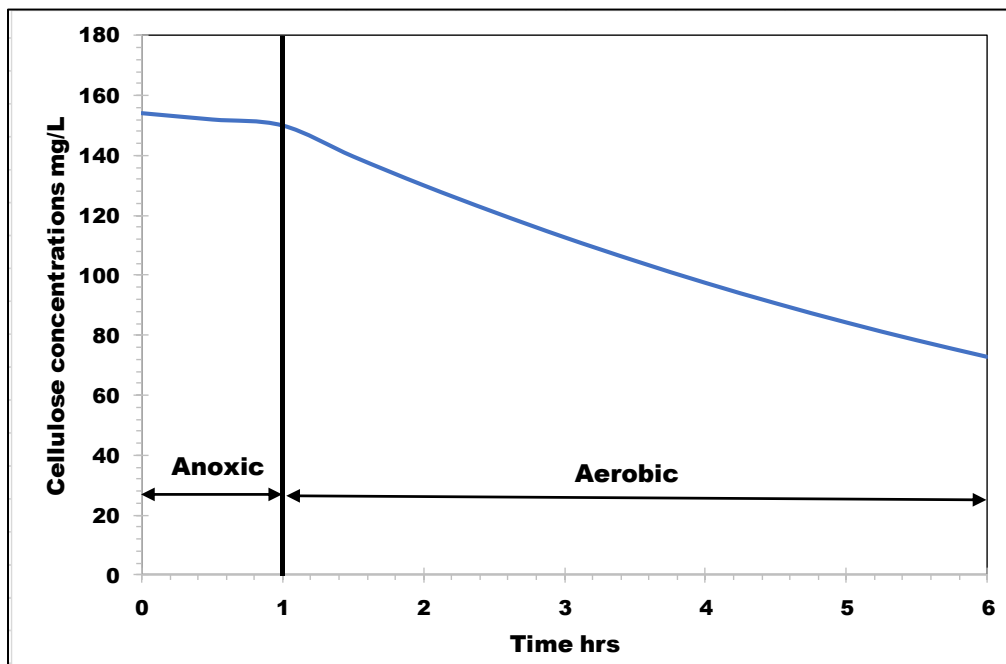


Figure 6-6. Cellulose concentration change with the time

6.3.2 Impact of the fermented primary sludge on the SBR performance

6.3.2.1 Fermented primary sludge characteristics

Table 6 shows the fermented primary sludge (FS) characteristics. Apparently, the three fermented primary sludges had comparable characteristics, although the 6d-SRT had relatively high sCOD concentrations when compared to the other SRTs. Also, all the fermented sludges had higher fractions of particulates than soluble. On average, particulate fractions represented 80%, 67%, and 77% of TCOD, TN, and TP.

Table 6-6. Fermented primary sludge characteristics

SRT	TSS* (mg/L)	VSS* (mg/L)	TCOD* (mg/L)	sCOD* (mg/L)	TN* (mg/L)	SN* (mg/L)	TP* (mg/L)	SP* (mg/L)
4d	4901 ± 1027	4045 ± 720	8,398 ± 1,260	1,603 ± 240	510 ± 76	128 ± 19	182 ± 27	45 ± 7
6d	7436 ± 1557	6297 ± 1080	11,022 ± 1,653	2,471 ± 371	346 ± 52	157 ± 24	181 ± 27	35 ± 5
2d	8622 ± 615	6731 ± 364	11,099 ± 1,665	1,759 ± 264	348 ± 52	111 ± 17	130 ± 19	33 ± 5

*Values represent average±STD of three samples

6.3.2.2 SBR treatment performance with the addition of the fermented sludge

Table 7 shows the influent, effluent, and mixed liquor characteristics during the different stages. Mixing RBF effluent with the FS at 4d (mixing ratio 19:1) and 6d (mixing ratio 30:1) had comparable influent characteristics and, on average, both increased TSS, VSS, TCOD, TN, and TP of the RBF effluent by 188%, 226%, 183%, 166%, and 188%. Additionally, they increased sCOD, sN and sP by 123%, 116%, and 167%. Mixing RBF effluent with the fermented primary sludge at 2d (mixing ratio 9:1) had a higher impact on TSS, VSS, TCOD, TN, and TP concentrations, increasing by 429%, 513%, 358%, 229%, and 263%, as compared to sCOD, sN and sP which increased by 186%, 119%, 230%. Apparently, in all stages, the impact on the particulate organics was much higher than the impact on the soluble organics which was expected due to the high particulate fractions in the FS.

Table 6-7. Influent, effluent and mixed liquor characteristics at each stage

Stages	Stage name	TSS	VSS	COD	sCOD	TN	sN	NH3	TP	sP
		mg/L	mg/L	mg/L	mg/L	mg/L	mg/L	mg/L	mg/L	mg/L
Influent Characteristics										
	RBF effluent without fermented sludge	222 ± 49	157 ± 34	440 ± 120	197 ± 33	28 ± 2	27 ± 2	23 ± 2	8 ± 3	2.7 ± 0.8
1	RBF effluent+ fermented sludge 4d SRT	445 ± 67	350 ± 45	805 ± 112	264 ± 73	52 ± 10	32 ± 1	28 ± 1	16 ± 5	4.9 ± 1.2
2	RBF effluent+ fermented sludge 6d SRT	464 ± 61	360 ± 45	807 ± 51	216 ± 42	41 ± 5	33 ± 2	29 ± 2	14 ± 3	4.1 ± 0.6
3	RBF effluent+ fermented sludge 2d SRT	1,039 ± 131	805 ± 110	1,574 ± 144	367 ± 56	64 ± 8	32 ± 3	29 ± 3	21 ± 1	6.2 ± 1.7
Effluent Characteristics										
	SBR2 effluent (filtered) without fermented sludge	10 ± 4	6 ± 2	31 ± 1	29 ± 2	9 ± 1	8 ± 1	0.2 ± 0.3	0.34 ± 0.2	0.20 ± 0.05
1	SBR2 effluent (filtered) + fermented sludge 4d SRT	13 ± 7	10 ± 7	39 ± 11	33 ± 9	15 ± 2	14 ± 2	0.4 ± 0.2	0.49 ± 0.2	0.22 ± 0.06
2	SBR2 effluent (filtered) + fermented sludge 6d SRT	10 ± 2	6 ± 2	27 ± 2	27 ± 3	8 ± 3	8 ± 3	0.3 ± 0.1	0.34 ± 0.2	0.21 ± 0.11
3	SBR2 effluent (filtered) + fermented sludge 2d SRT	11 ± 3	7 ± 2	41 ± 3	32 ± 8	8 ± 3	6 ± 2	0.3 ± 0.1	0.29 ± 0.1	0.21 ± 0.07
Mixed liquor Characteristics										
	SBR2 ML without fermented sludge	3360 ± 157	2300 ± 224	-	-	-	-	-	-	-
1	SBR2 ML + fermented sludge 4d SRT	3595 ± 424	2530 ± 285	-	-	-	-	-	-	-
2	SBR2 ML + fermented sludge 4d SRT	4857 ± 484	3707 ± 356	-	-	-	-	-	-	-
3	SBR2 ML + fermented sludge 4d SRT	6928 ± 514	5438 ± 469	-	-	-	-	-	-	-

Figures 6-7, 6-8, and 6-9 show the influent and effluent TCOD, TN, and TP for the different stages of fermented primary sludge additions. The operation with the RBF effluent only exhibited COD, TN, and TP removal efficiencies of 92%, 68%, and 94%. In stage 1, mixing RBF effluent with the FS at 4d SRT showed COD, TN, and TP removal efficiencies of 95%, 71%, and 97%. Stage 2 with the addition of the 6d-FS had comparable performance to the first stage in terms of COD and TP removal efficiencies and higher TN removal efficiency of 80%. Stage 3 with the 2d-FS maintained comparable effluent concentrations to the second stage with removal efficiencies of 97%, 92%, and 98% for COD, TN, and TP. The observed increase in the COD and TP removal efficiencies were associated with the high influent concentrations since both conditions (before and after adding the FS) had comparable effluent concentrations. The sCOD concentrations in the effluent were comparable in all stages, indicating that potentially the non-biodegradable sCOD (nbsCOD) in the fermented sludge was the same as nbsCOD in the RBF effluent. The significance of the observed differences in the sCOD effluent concentrations before and after the addition of the FS was evaluated using the standard *t*-test approach at the 95% confidence level and the observed difference was insignificant. Similarly, the significance of the observed differences in the TN, sN, TP, and sP effluent concentrations before and after the addition of the FS was evaluated using the standard *t*-test approach at the 95% confidence level. The observed differences for the TN and sN were significant; however, for TP and sP the differences were insignificant.

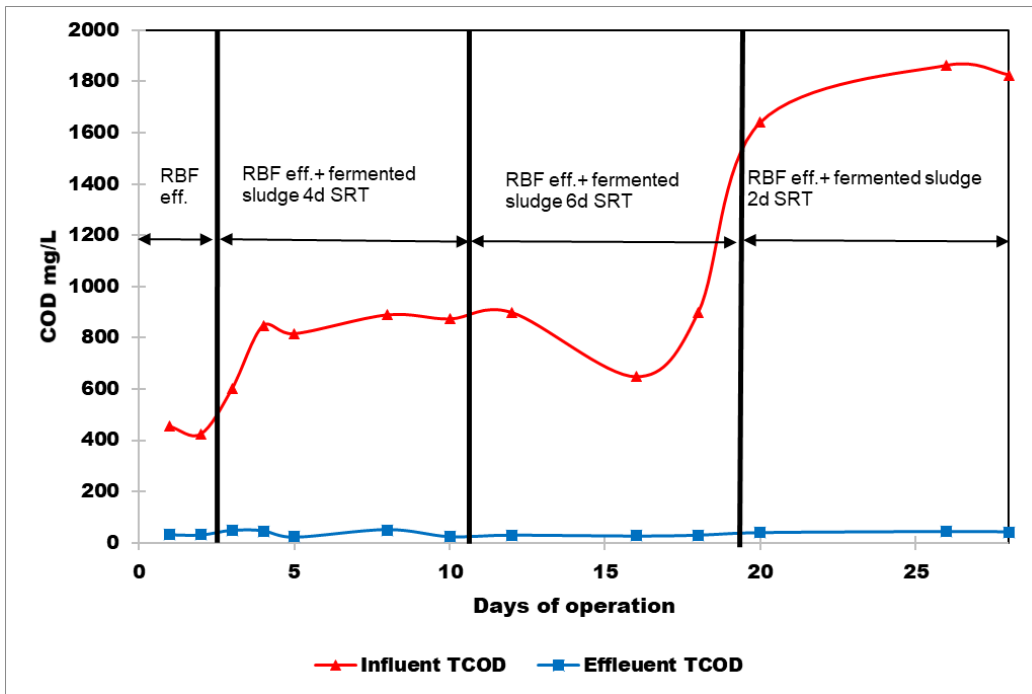


Figure 6-7. Influent and effluent COD during the different stages

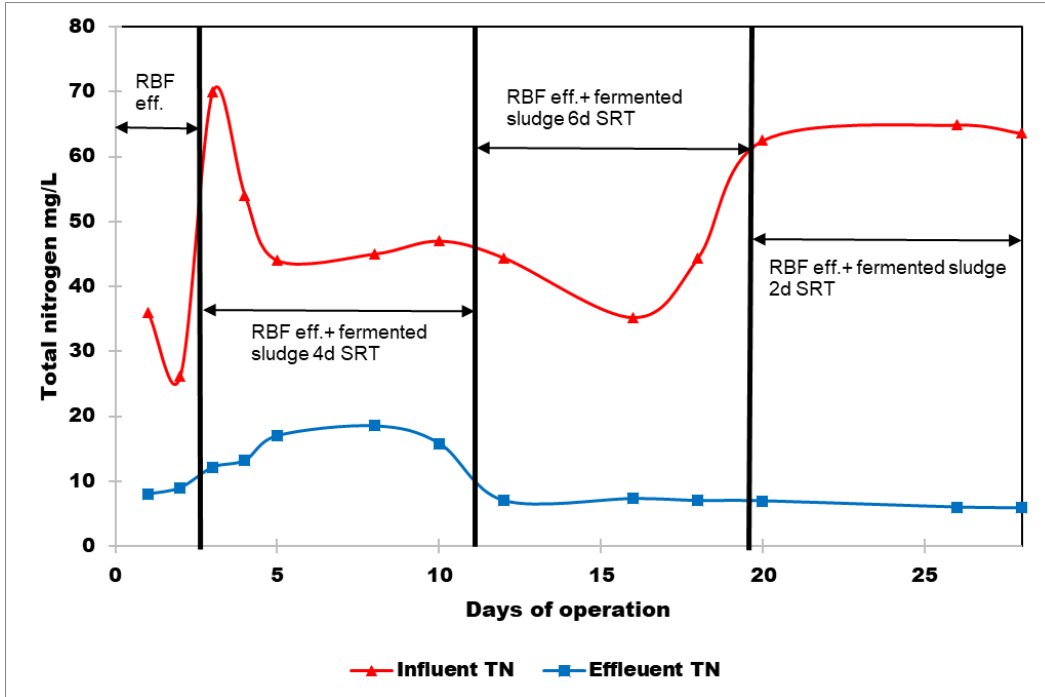


Figure 6-8. Influent and effluent TN during the different stages

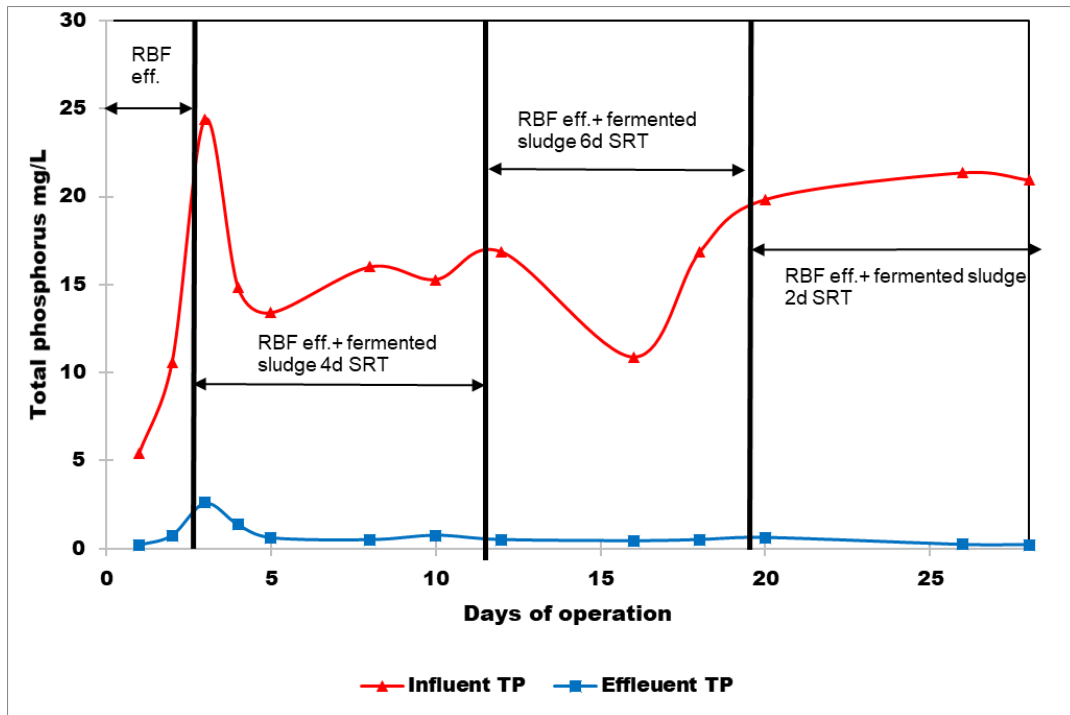


Figure 6-9. Influent and effluent TP during the different stages

Table 8 shows the COD/N and COD/P ratios during the different stages. After mixing with the 4d- FS, effluent TN increased from 9 to 15 mg l⁻¹ due to the increase in the influent TN. Stage 1 had a comparable nitrogen removal efficiency to the case with RBF effluent only as they both had comparable COD: N ratio of 16:1. The rise in the effluent nitrogen also indicated that the influent biodegradable COD: N ratio in stage 1 was lower than the biodegradable COD: N ratio in the RBF effluent. In stage 2, COD: N ratio increased to 20:1, increasing the nitrogen removal efficiency to 80%. In stage 3, COD: N ratio further increased to 25:1, increasing the nitrogen removal to 88%. In all 3 stages, the COD: P ratios were high leading to high biological phosphorus removal.

Additionally, the addition of the FS increased the MLSS concentrations due to solids production as well as solids accumulation. The observed yield was estimated before and after the addition of the FS by plotting cumulative MLVSS produced versus cumulative COD removed and both cases had an identical observed yield of 0.35 gVSS gCOD⁻¹ (Fig. 6-10). This indicates that after the addition of the fermented primary sludge, the

nonbiodegradable particulate COD: biodegradable COD ratio did not change when compared to the RBF effluent only.

Table 6-8. COD/N and COD/P ratios at the different stages

Stage	COD/N	COD/P
RBF effluent without fermented sludge	16	55
RBF effluent+ fermented sludge 4d SRT	16	50
RBF effluent+ fermented sludge 6d SRT	20	58
RBF effluent+ fermented sludge 2d SRT	25	75

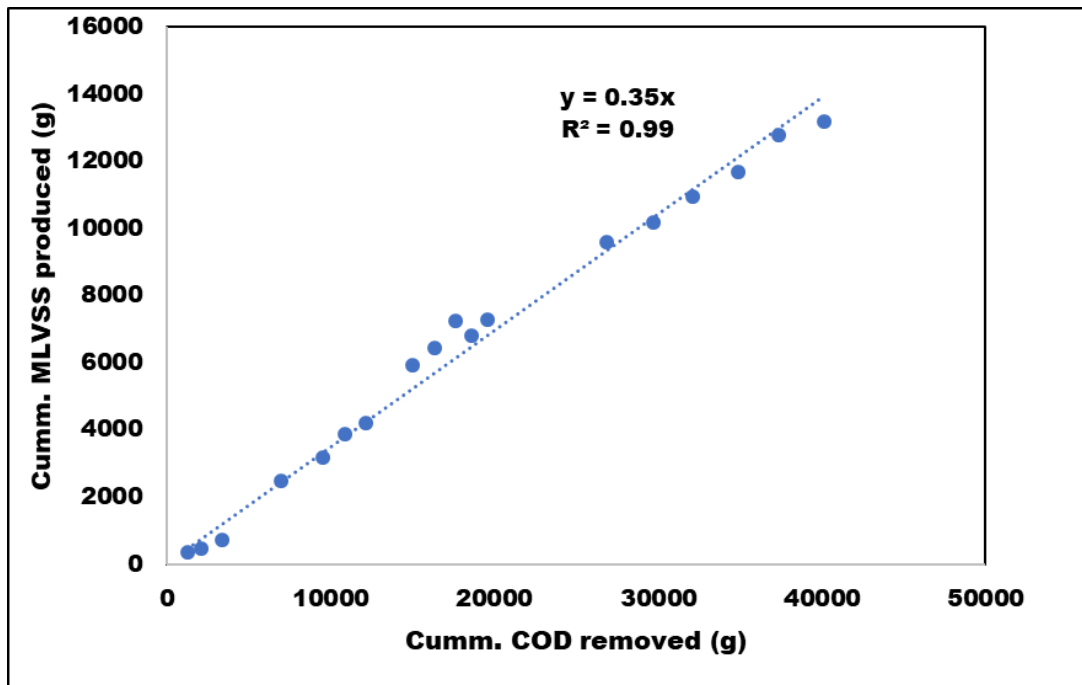


Figure 6-10. The cumulative MLVSS production and cumulative COD removed to estimate the observed yield after mixing the RBF effluent with the fermented primary sludge

6.3.2.3 Oxygen transfer efficiency measurements

Table 9 shows the measured oxygen transfer parameters including standard oxygen transfer efficiency (α SOTE), oxygen transfer efficiency (OTE), oxygen uptake rate (OUR), and α -factor as well as aeration energy in both SBRs and with the addition of the fermented sludge. Aeration energy was estimated using Eq.2 (Metcalf & Eddy et al., 2002).

$$E = BHP \cdot \Delta t = \frac{wRT_1}{29.7 n e} \left[\left(\frac{p_2}{p_1} \right)^n - 1 \right] \cdot \Delta t \quad (2)$$

Where: BHP = blower break horsepower (kW); Δt = time on duty (hr); w = ponderal air flow (kg s^{-1}); R = gas constant ($8.314 \text{ J mol}^{-1} \text{ K}^{-1}$); T_1 = absolute inlet temperature (K), p_1 = absolute inlet pressure (Pa), p_2 = absolute discharge pressure (Pa), $n = 0.283$ for air (-), e = blower efficiency (-)

The reported values for the α SOTE, OTE, OUR, α -factor, and aeration energy represent the flow weighted averages. RBF reduced aeration energy by 25% when compared to raw wastewater. While maintaining comparable air flow rates and DO concentrations in all 3 stages with the addition of the fermented sludge, the addition of 4d-FS (stage 1) reduced the α -factor, and α SOTE by 9% and increased aeration energy by 31%. Interestingly, in stage 1, the α -factor, as well as aeration energy, were comparable to the case with raw wastewater feed which indicates that the combined influent biodegradable COD concentrations in stage 1 and raw wastewater were comparable. This is confirmed by the high effluent nitrogen concentrations of 15 mg l^{-1} observed in stage 1.

In stage 2, with the addition of the 6 d-FS, MLVSS increased and the α -factor recovered. In stage 2, α -factor, and α SOTE, improved by 9%, and OUR increased by 5% when compared to stage 1; however, aeration energy was not impacted since both stages had similar organic loading rates. In stage 3 and the case with RBF effluent only, α -factor, α SOTE, and OUR were comparable indicating that the increase of the active biomass concentrations recovered α -factor due to the increase in the substrates utilization rates and hence OUR. In stage 3, MLVSS increased by 38% compared to the case of RBF effluent

while the impact on α -factor was only 9%, indicating that a significant change in MLSS is needed in order to have an impact on α -factor.

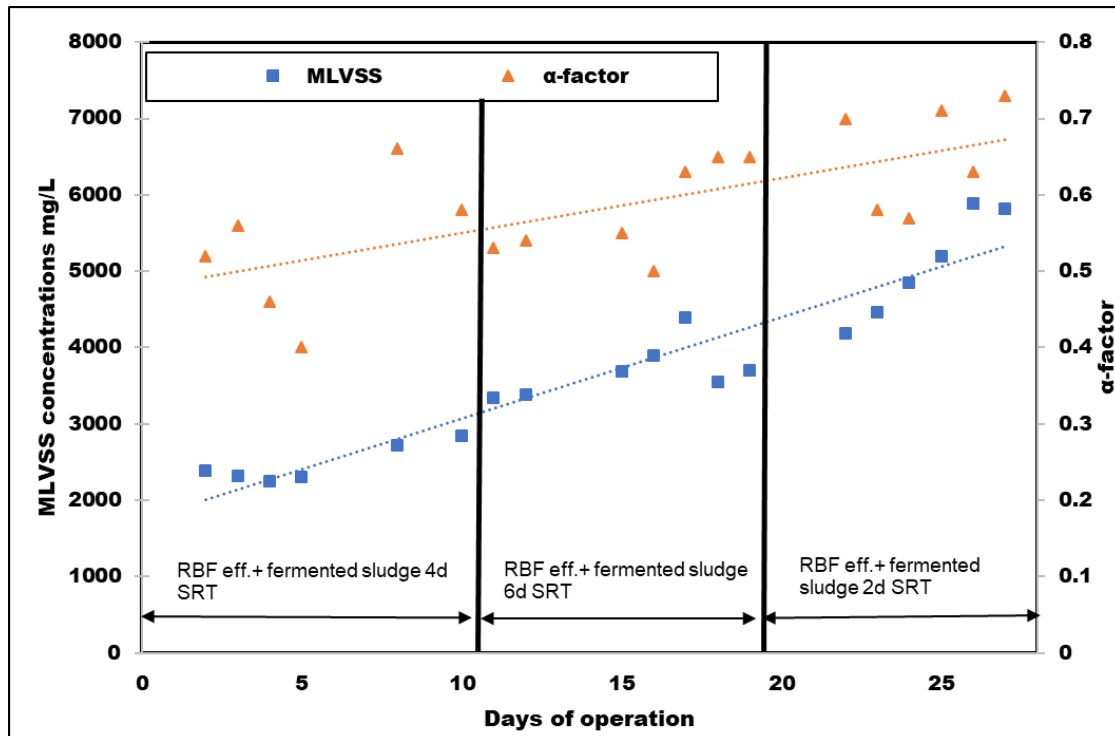
In stage 3, the α -factor, and α SOTE, improved by 8% and OUR increased by 11%, respectively, relative to stage 2. When compared to the RBF effluent only, MLSS increased by 58%; however, α -factor and OUR improved only by 8% and 6%. Aeration energy increased by 14% when compared to stage 2 and by 36% when compared to RBF effluent only.

Figure 6-11 shows the changes in the α -factor due to the MLVSS increase in the three stages. Both trendlines confirmed that α -factor improved with the MLVSS increase. Interestingly, looking at the whole testing period, MLVSS increased by 3900 mg l^{-1} (152% increase when compared to the case with RBF effluent only) while the α -factor only increased by 0.1, indicating that increasing MLVSS to improve α -factor is not practically significant unless MLVSS is very low to perform biodegradation. Figure 6-12 shows the temporal change in α -factor from three different cycles in the three stages. Apparently, in all stages, α -factor was low at the beginning of the cycle due to the presence of the surfactants and rbCOD and increased with time due to biodegradation. As expected, stage 3, recovered α -factor quicker than other stages due to higher active biomass concentrations relative to the other stages.

Removing cellulose by RBF reduced the aeration energy while reusing the fermented sludge to enhance BNR increased the aeration energy to be comparable to the case without primary treatment.

Table 6-9. Impact of the fermented primary sludge on the oxygen transfer efficiency

Process	α SOTE	OTE	OUR	α -factor	DO	Airflow	Energy
	%	%	mg/L/hr		mg/L	SCFM	kWh/cycle
SBR 1 (Raw wastewater influent)	20	17	60	0.53	1.89 ± 0.93	0.72 ± 0.12	0.12
SBR 2 (filtered)	23	17	63	0.58	2.73 ± 0.76	0.70 ± 0.18	0.09
SBR2 with the addition of FS 4d SRT	21	14	56	0.53	1.74 ± 0.81	0.70 ± 0.10	0.13
SBR2 with the addition of FS 6d SRT	23	15	59	0.58	1.91 ± 0.96	0.68 ± 0.17	0.12
SBR2 with the addition of FS 2d SRT	25	19	67	0.63	1.67 ± 0.95	0.71 ± 0.12	0.14

**Figure 6-11. α -factor improvement due to the MLVSS increase**

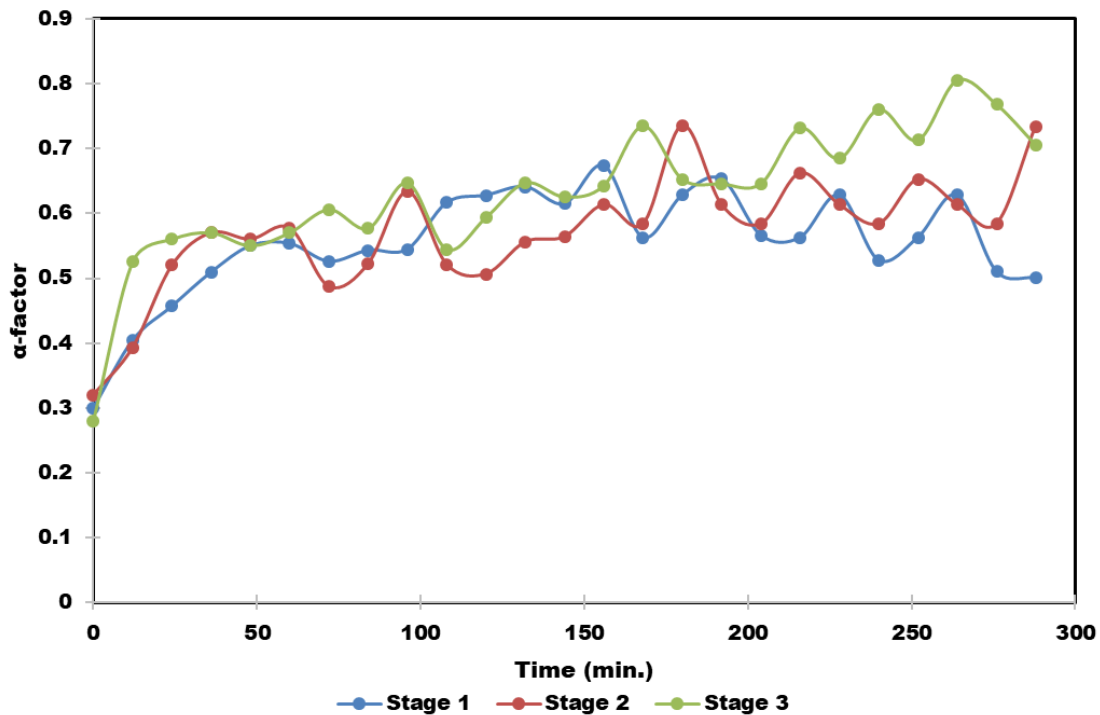


Figure 6-12. α -factor change during the aeration cycle for the three different stages

6.4 Summary and Conclusions

- The calibrated SBR model using experimental cellulose measurements showed that influent cellulose accounted for 21% of influent total COD and 35% of the influent TSS.
- The aerobic cellulose hydrolysis rate constant was $3.74 \pm 0.33 \text{ d}^{-1}$, 5 times higher than the anoxic hydrolysis rate ($0.7 \pm 0.31 \text{ d}^{-1}$).
- On average, 95% of the biodegraded cellulose was biodegraded aerobically, while 5% was biodegraded anoxically.
- Overall cellulose biodegradation efficiency was 97% for an SRT of 10 days.
- The addition of the fermented primary sludge to the SBR enhanced nitrogen and phosphorus removal efficiency by up to 92% and 98%.

- The fermented primary sludge marginally impacted α -factor, α SOTE, and OUR when compared to the feed with RBF effluent only.
- The addition of fermented primary sludge increases aeration energy by 25%-36% as compared to the case of RBF effluent.

References

- Ahmed, A. S.; Bahreini, G.; Ho, D.; Sridhar, G.; Gupta, M.; Wessels, C.; Marcelis, P.; et al. (2019) Fate of cellulose in primary and secondary treatment at municipal water resource recovery facilities. *Water Environ. Res.*, **91** (11), 1479–1489.
- Alvarez, J. V. L.; Larrucea, M. A.; Bermúdez, P. A.; Chicote, B. L. (2009) Biodegradation of paper waste under controlled composting conditions. *Waste Manag.* First international conference on environmental management, engineering, planning and economics, **29** (5), 1514–1519.
- American Public Health Association. (2005) *Standard Methods for the Examination of Water & Wastewater*; American Public Health Association.
- Bahreini, G.; Elbeshbishy, E.; Jimenez, J.; Santoro, D.; Nakhla, G. (2020) Integrated fermentation and anaerobic digestion of primary sludges for simultaneous resource and energy recovery: Impact of volatile fatty acids recovery. *Waste Manag.*, **118**, 341–349.
- Behera, C. R.; Santoro, D.; Gernaey, K. V.; Sin, G. (2018) Organic carbon recovery modeling for a rotating belt filter and its impact assessment on a plant-wide scale. *Chem. Eng. J.*, **334**, 1965–1976.
- Benneouala, M.; Bareha, Y.; Mengelle, E.; Bounouba, M.; Sperandio, M.; Bessiere, Y.; Paul, E. (2017) Hydrolysis of particulate settleable solids (PSS) in activated sludge is determined by the bacteria initially adsorbed in the sewage. *Water Res.*, **125**, 400–409.
- Boztas, S. (2017, July 27) The ick factor: Dutch project making bike lanes and bottles from used loo roll. *The Guardian*. Retrieved from <http://www.theguardian.com/sustainable-business/2017/jul/27/-ick-factor-dutch-bike-lanes-bottles-used-loo-roll-recycled-toilet-paper>

- Espíndola, S. P.; Pronk, M.; Zlopasa, J.; Picken, S. J.; Loosdrecht, M. C. M. van. (2021) Nanocellulose recovery from domestic wastewater. *J. Clean. Prod.*, **280**, 124507.
- Ghasimi, D. S. M.; Zandvoort, M. H.; Adriaanse, M.; Lier, J. B. van; Kreuk, M. de. (2016) Comparative analysis of the digestibility of sewage fine sieved fraction and hygiene paper produced from virgin fibers and recycled fibers. *Waste Manag.*, **53**, 156–164.
- Gupta, M.; Ho, D.; Santoro, D.; Torfs, E.; Doucet, J.; Vanrolleghem, P. A.; Nakhla, G. (2018) Experimental assessment and validation of quantification methods for cellulose content in municipal wastewater and sludge. *Environ. Sci. Pollut. Res.* Retrieved from <http://link.springer.com/10.1007/s11356-018-1807-7>
- Henze, M.; Gujer, W.; Mino, T.; Loosdrecht, M. C. M. van. (2000) *Activated sludge models ASM1, ASM2, ASM2d and ASM3*; IWA Publishing. Retrieved from <https://orbit.dtu.dk/en/publications/activated-sludge-models-asm1-asm2-asm2d-and-asm3-2>
- Honda, S.; Miyata, N.; Iwahori, K. (2000) A Survey of Cellulose Profiles in Actual Wastewater Treatment Plants. *Jpn. J. Water Treat. Biol.*, **36** (1), 9–14.
- Hurwitz, E.; Beck, A. J.; Sakellariou, E.; Krup, M. (1961) Degradation of Cellulose by Activated Sludge Treatment. *J. Water Pollut. Control Fed.*, **33** (10), 1070–1075.
- Liu, J.; Yuan, Y.; Li, B.; Zhang, Q.; Wu, L.; Li, X.; Peng, Y. (2017) Enhanced nitrogen and phosphorus removal from municipal wastewater in an anaerobic-aerobic-anoxic sequencing batch reactor with sludge fermentation products as carbon source. *Bioresour. Technol.*, **244**, 1158–1165.
- Metcalf & Eddy; Tchobanoglous, G.; Burton, F.; Stensel, H. D. (2002) *Wastewater Engineering: Treatment and Reuse*; McGraw-Hill Education.

- Redmon, D.; Boyle, W. C.; Ewing, L. (1983) Oxygen transfer efficiency measurements in mixed liquor using off-gas techniques. *J. Water Pollut. Control Fed.*, 1338–1347.
- Reijken, C.; Giorgi, S.; Hurkmans, C.; Pérez, J.; Loosdrecht, M. C. M. van. (2018) Incorporating the influent cellulose fraction in activated sludge modelling. *Water Res.*, **144**, 104–111.
- Ruiken, C. J.; Breuer, G.; Klaversma, E.; Santiago, T.; Loosdrecht, M. C. M. van. (2013) Sieving wastewater – Cellulose recovery, economic and energy evaluation. *Water Res.*, **47** (1), 43–48.
- Verachtert, H.; Ramasamy, K.; Meyers, M.; Bevers, J. (1982) Investigations on cellulose biodegradation in activated sludge plants. *J. Appl. Microbiol.*, **52** (2), 185–190.
- Weimer, P. J. (1992) Cellulose Degradation by Ruminant Microorganisms. *Crit. Rev. Biotechnol.*, **12** (3), 189–223.
- Yuan, Y.; Liu, J.; Ma, B.; Liu, Y.; Wang, B.; Peng, Y. (2016) Improving municipal wastewater nitrogen and phosphorous removal by feeding sludge fermentation products to sequencing batch reactor (SBR). *Bioresour. Technol.*, **222**, 326–334.
- Zheng, X.; Yinguang, C.; Chenchen, L. (2010) Waste activated sludge alkaline fermentation liquid as carbon source for biological nutrients removal in anaerobic followed by alternating aerobic-anoxic sequencing batch reactors. *Chin. J. Chem. Eng.*, **18** (3), 478–485.

Chapter 7

7 Conclusions and recommendations for future work.

7.1 Conclusions

The influent cellulose concentration in raw municipal wastewater represents approximately one-third of the influent total suspended solids, as confirmed by the plant surveys conducted in two full-scale water resource recovery facilities in Canada and the Netherlands. Similar and very high cellulose capture rates (>80 %) have been shown by both primary clarification and RBF, highlighting a significant advantage for water resource recovery facilities targeting cellulose recovery. Results from laboratory SBRs were in good agreement with full-scale observations of treatment plants. Specifically, both studies indicated a secondary effluent cellulose concentration of approximately 2%-5% of the raw wastewater cellulose concentration, suggesting the presence of non-settleable non-biodegradable cellulose in the raw wastewater. Cellulose was efficiently biodegraded during biological treatment under the investigated conditions and within the temperature range of 13.7 °C-24.8 °C, irrespective of the biological process configuration (i.e. CAS vs. MUCT) and SRT (7 to 14 days), with all systems tested in this study achieving secondary effluent cellulose concentrations of 2-3 mg / L.

A regular rise in the α -factor with reaction time was observed in the SBR due to the biodegradation of organic pollutants. The presence of organics such as acetate as a readily biodegradable substrate and cellulose as a slowly biodegradable substrate increased the oxygen demand and negatively impacted OTE. The presence of active biomass improved the α -factor due to enhanced biodegradation. At low air flow of 0.6 SCFM and low DO of 2 mg l⁻¹ with active biomass, the α -factor decreased by 48% and 19%, respectively, due to the presence of acetate and cellulose. At the high air flow of 1 SCFM and high DO of 4 mg l⁻¹, with active biomass, the α -factor was constant irrespective of cellulose and acetate concentrations. The α -factor decreased without active biomass due to the addition of acetate in both cases i.e. high and low air flow rates. With active biomass, the α -factor increased with the biodegradation of surfactants and sCOD. The highest α -factor value

achieved in the SBR secondary effluent without biomass was 0.60 despite the removal of the vast majority of the organic and nitrogen load. This showed that biomass in secondary effluents has a marginal beneficial effect on the α -factor, whereas the residual contaminants depress the α -factor. A negative power correlation between α -factor and soluble COD was developed and incorporated into a dynamic model to estimate the real-time air flow rate as a function of the change in sCOD concentrations. Despite the significant improvement in activated sludge modeling, current commercial software has allowed the incorporation of dynamic changes in α -factor but has not correlated the dynamics with any process variables. The correlation developed in this study between the alpha and reactor sCOD can be incorporated into current commercial software to enhance aeration modeling. Thus, in accordance with the dynamic alpha correlation of this study, primary treatment irrespective of whether it is gravity or microsieving (RBF) not only reduces oxygen demand but also improves oxygen transfer efficiency..

Experimental data collected from pilot SBRs were used to calibrate a process model integrated with an aeration model utilizing three dynamic α -factor correlations. After model validation, various continuous-flow processes such as plug flow, CSTR, step-feed plug flow, and MBRs were assessed with respect to energy demand for nitrification and biological nitrogen removal. Using controlled experimental measurements from pilot SBRs, the first correlation based on reactor sCOD was validated and was observed to better predict diurnal and spatial variations in aeration energy in SBRs than other correlations, based on influent COD and reactor biomass. The air flow rates were overestimated by the second correlation (based on the influent COD). The third correlation (based on the MLSS) estimated the lowest air flow rates. Comparing the results of the model with the literature showed that the first correlation is suitable for designing SBR, plug flow, step-feed, and CSTR systems, and the third correlation is suitable for designing CSTRs and MBRs, while the second correlation was not valid in any of the reactors modeled. CSTRs reduced aeration energy by 66% and 56% compared to the nitrification plug-flow reactor and by 57% and 55% for denitrification using the first and third correlations. In comparison to the plug flow reactor, when the only nitrification was targeted, plug flow with step feed reactors reduced the aeration energy by 15%. Internal recirculation in a plug flow reactor

to improve the removal of nitrogen reduced the aeration energy by 30%. The corresponding energy savings for the step-feed plug flow were 18%. In CSTR, denitrification reduced aeration energy by 11%, while for MBRs, energy savings were 12%. In the plug flow reactor, denitrification reduced the aeration energy per unit kgThOD by 21 %. The corresponding energy savings for step-feed plug flow were 10%. In CSTR and MBRs, denitrification did not impact the aeration energy per unit kgThOD.

Cellulose can be either removed through secondary treatment utilizing oxygen or diverted through primary treatment to the sludge stream to provide the VFA required to improve the BNR process through the primary sludge fermentation process. SBR modeling incorporating cellulose as a separate state variable indicated that the aerobic cellulose hydrolysis rate constant was $3.74 \pm 0.33 \text{ d}^{-1}$, 5 times higher than the anoxic hydrolysis rate ($0.7 \pm 0.31 \text{ d}^{-1}$). On average, 95% of the biodegraded cellulose was biodegraded aerobically, while 5% was biodegraded anoxically. For a 10-day SRT, the total efficiency of cellulose biodegradation was 97%. The addition of fermented primary sludge to SBR increased the efficiency of nitrogen and phosphorus removal by up to 92% and 98%. The biomass yields with and without fermentates at the same SRT were in close agreements, clearly indicating that the inert fraction of solids in the fermentate is the same as in the primary effluent. When compared to the feed with RBF effluent only, the fermented primary sludge had a marginal impact on α -factor, α SOTE, and OUR. As compared to the case of RBF effluent, the addition of fermented primary sludge increases aeration energy by 25%-36%. It must be asserted that given that the inert suspended solids accumulation in the bioreactor with fermentate supplementation increases, the potential for long-term fouling and reduction of oxygen transfer may be significant.

7.2 Recommendations for future research

Based on this Ph.D. research findings, the following topics are recommended for future research:

- The hydrolysis rate of cellulose at different SRTs, DO concentrations (and oxidation-reduction potentials) and different temperatures needs further investigation.
- Further investigations are required to determine the effect of non-biodegradable cellulose on sludge settleability and secondary treatment efficiency.
- Whole-plant modeling incorporating both the effect of cellulose into different ASM models as well as dynamic alpha factors would be beneficial to determine the cellulose diversion rate from biological treatment that would simultaneously optimize energy and disposal costs.
- The long-term effect of the addition of fermented RBF sludge on OTE and BNR in SBRs should be investigated since this study investigated only the short-term impacts. The work should also be extended to other processes.
- Fermented sludge fractionation is yet to be analyzed to understand the impact of fermented sludge solids on OTE.
- Assessing the impact of the fermentation SRT on VFA production as well as the impact of the produced VFAs, on dynamic α -factor.

Appendices

Appendix A: Supplementary information for Chapter 3

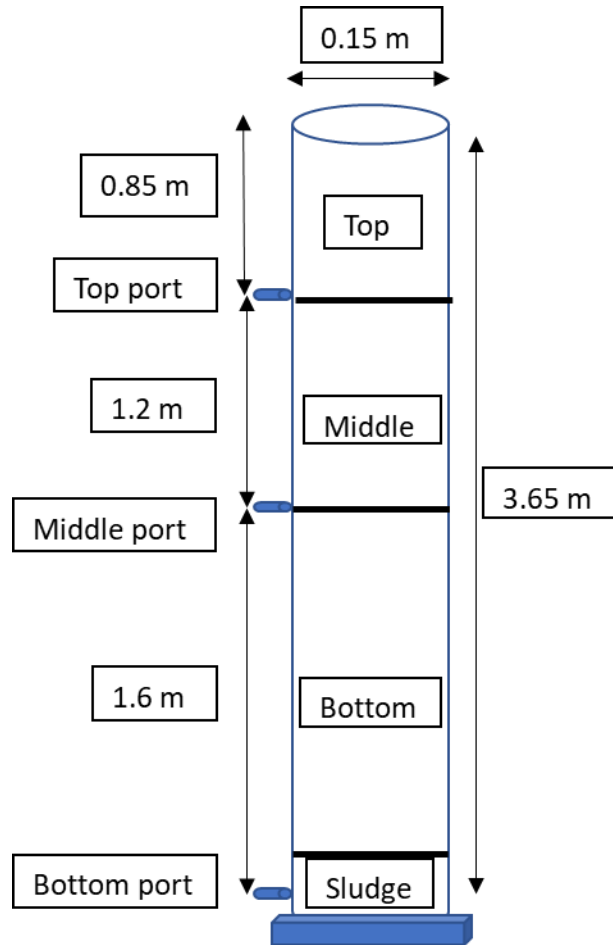


Figure S1. Column test design

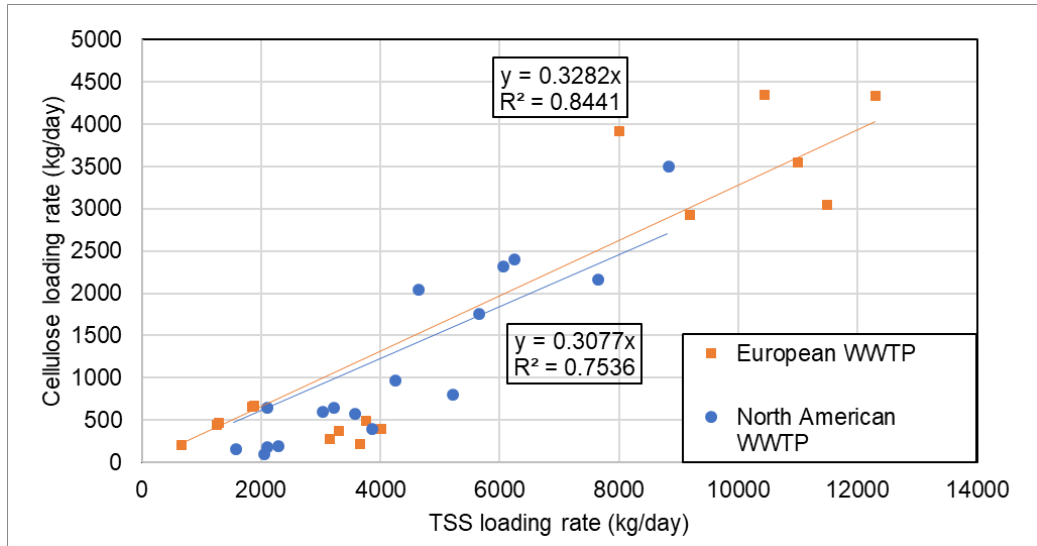


Figure S2a. Statistical correlation between TSS and cellulose loading rates for influent, primary effluent, and primary sludge (North American, and European WRRFs)

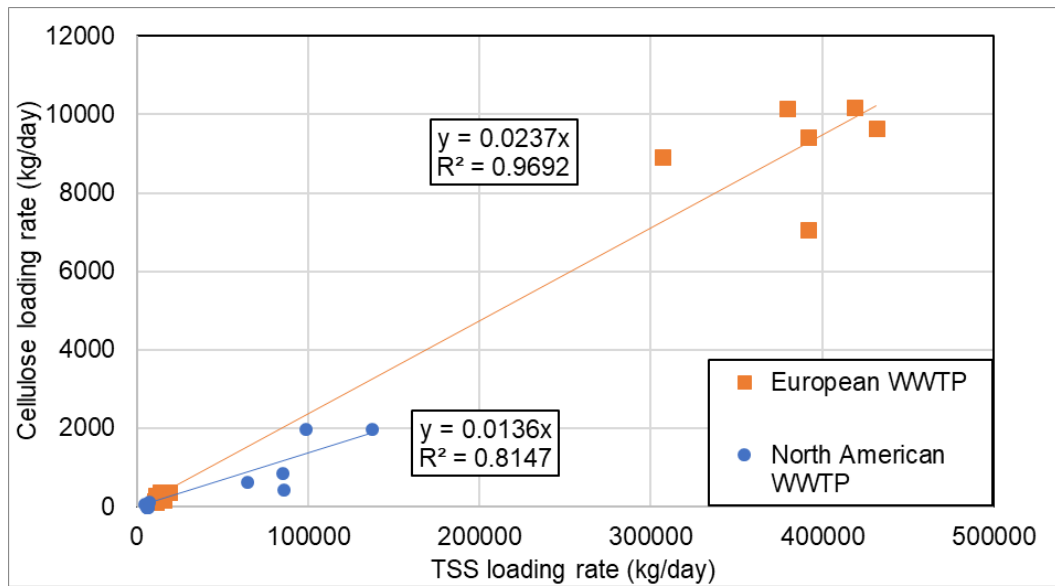


Figure S2b. Statistical correlation between TSS and cellulose loading rates for the MLSS, and WAS (North American, and European WRRFs)

Table S1a: Influent wastewater characteristics to both SBRs

Parameters	Unit	RWW-SBR	RBF-SBR
TSS	mg/L	147 ± 3	95 ± 3
VSS	mg/L	115 ± 2	75 ± 2
TCOD	mg/L	313 ± 8	220 ± 6
SCOD	mg/L	96 ± 4	86 ± 4
TN	mg/L	50 ± 2	46 ± 2
NH ₄ ⁺ -N	mg/L	27 ± 2	27 ± 1.5
TP	mg/L	4.7 ± 0.2	3.9 ± 0.3
TCOD/TN	--	6.4 ± 0.3	4.8 ± 0.2
SCOD/TN	--	1.9 ± 0.1	1.9 ± 0.1

Table S1b: Effluent wastewater characteristics from both SBRs

Parameters	Unit	RWW-SBR	RBF-SBR
TSS	mg/L	9 ± 2	9 ± 2
VSS	mg/L	6 ± 1	6 ± 1
TCOD	mg/L	27 ± 3	30 ± 3
SCOD	mg/L	19 ± 4	21 ± 3
TN	mg/L	22 ± 1	24 ± 1
NO ₃ -N	mg/L	18 ± 1	20 ± 2
NH ₄ ⁺ -N	mg/L	1.9 ± 0.3	1.7 ± 0.2
TP	mg/L	0.97 ± 0.02	0.97 ± 0.02
MLSS	mg/L	2410 ± 58	2120 ± 17
MLVSS	mg/L	1340 ± 14	1250 ± 20
MLVSS/MLSS	--	0.56	0.59
*Biomass yield	mg VSS/ mg COD	0.35	0.28

*The observed biomass yields are derived from the linear fits of cumulative VSS wasted versus cumulative COD removed.

Table S2: Results from the raw wastewater column settling test

No	Medium	TSS (mg/L) ^a	VSS (mg/L) ^a	COD (mg/L) ^a	Cellulose (mg/L) ^a	Volume (m ³)	TSS mass (g)	VSS mass (g)	CO D mass (g)	Cellulose mass (g)
1	Raw wastewater	285 ±14(2)	210 ±7(2)	626 ±93(2)	77 ±2(3)	0.064 5	18.4 ±0.9	13.6 ±0.5	40.4 ±6.0	4.94 ±0.11
2	Primary sludge	29,805 ±939(2)	22,354 ±704 (2)	38,320 ±1,018(2)	6,494 ±683(4)	0.000 4	12.6 ±0.4	9.5 ±0.3	16.3 ±0.4	2.76 ±0.29
3	Top	84 ±6(2)	65 ±7(2)	338 ±4(2)	3 ±2(2)	0.015 0	1.3 ±0.1	1.0 ±0.1	5.1 ±0.1	0.04 ±0.04
4	Middle	89 ±1(2)	64 ±1(2)	337 ±2(2)	22 ±12(2)	0.021 2	1.9 ±0.0	1.4 ±0.0	7.2 ±0.0	0.48 ±0.26
5	Bottom	94 ±3(2)	63 ±4(2)	336 ±1(2)	42 ±23(2)	0.027 9	2.6 ±0.1	1.8 ±0.1	9.4 ±0.0	1.17 ±0.63
6	Floatables	-	-	-	-	-	1.20	-	-	0.05 ±0.01
	Closure (%)	-	-	-	-	-	106	101	94	91

^a Values represent average ±standard deviation, and numbers within parenthesis are the number of measurements.

Cost analysis calculations:

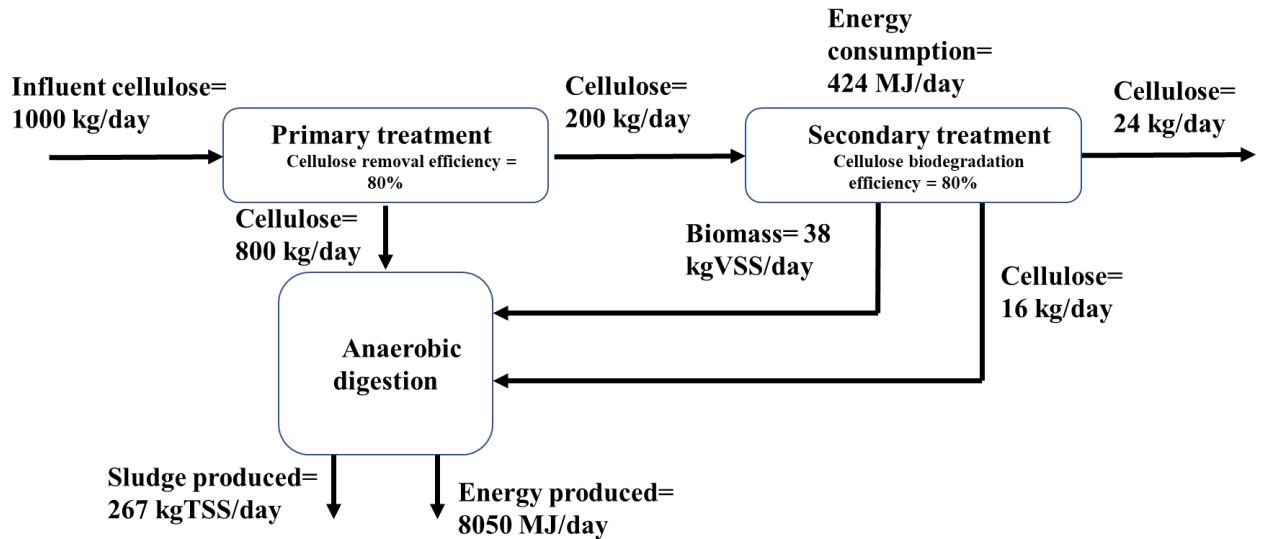


Figure S3a: Impact of cellulose on sludge production rates and energy balance (case with primary treatment)

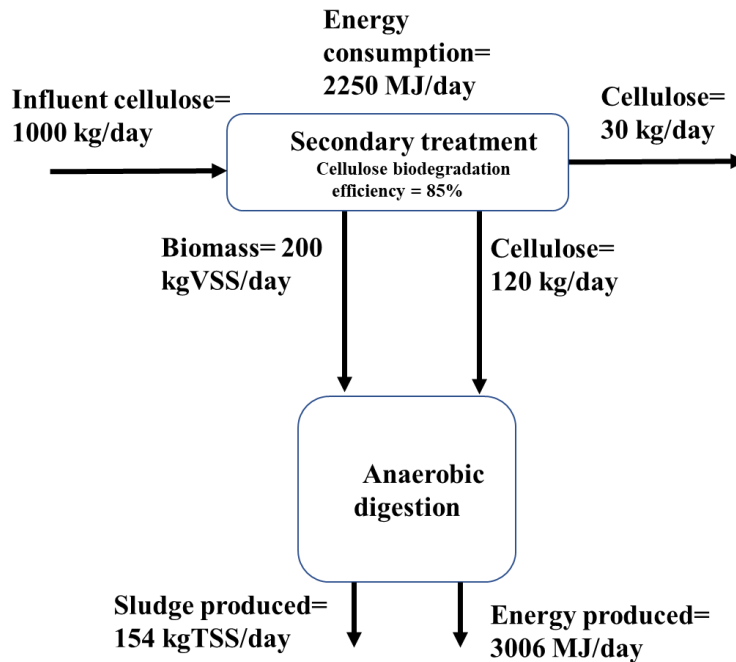


Figure S3b: Impact of cellulose on sludge production rates and energy balance (case without primary treatment)

Case I: with primary treatment

Influent cellulose=1000 kg/day

Primary treatment removal efficiency= 80%

Primary sludge loading rate= 800 kg/day

Primary effluent loading rate= 200 kg/day

Cellulose aerobic biodegradation efficiency= 80%

Cellulose converted to biomass= 160 kg/day

Total non-biodegradable cellulose= 40 kg/day

Non-biodegradable cellulose in the secondary effluent (60% of the non-biodegradable cellulose) = 24 kg/day

Non-biodegradable cellulose in the WAS= 16 kg/day

Cellulose biodegradation efficiency in the anaerobic digestion is assumed 70% according to the literature.

Biomass yield was assumed = 0.44 gVSS/gCOD

SRT=10 days

$k_d=0.1 \text{ d}^{-1}$

Biomass disintegration efficiency in the anaerobic digestion is assumed=50%

$$\begin{aligned} \text{Biomass produced} &= 160 \frac{\text{kg cellulose}}{\text{day}} \times 1.07 \frac{\text{kg COD}}{\text{kg cellulose}} \times \frac{0.44 \text{ gVSS/gCOD}}{1 + 0.1 * 10} \\ &= 38 \text{ kgVSS/day} \end{aligned}$$

Methane production

$$\begin{aligned} &= \left[\left(800 + 16 \text{ kg} \frac{\text{cellulose}}{\text{day}} \right) \times \frac{70}{100} \times 1.07 \frac{\text{kgCOD}}{\text{kgcellulose}} \right. \\ &\quad \left. + \left(38 \frac{\text{kgVSS}}{\text{day}} \times \frac{50}{100} \times 1.42 \frac{\text{kgCOD}}{\text{kgVSS}} \right) \right] \times 0.35 \frac{\text{m}^3\text{CH}_4}{\text{kgCOD}} = 223 \frac{\text{m}^3\text{CH}_4}{\text{day}} \\ &= 7979 \frac{\text{MJ}}{\text{day}} \end{aligned}$$

$$\begin{aligned}
 \text{Oxygen demand} &= 160 \frac{\text{kg cellulose}}{\text{day}} \times 1.07 \frac{\text{kg COD}}{\text{kg cellulose}} \times \left(1 - \frac{1.42 \times 0.44 \frac{\text{gVSS}}{\text{gCOD}}}{1 + 0.1 \times 10} \right) \\
 &= 118 \frac{\text{kgO}_2}{\text{day}} = 118 \frac{\text{kwh}}{\text{day}} = 424 \frac{\text{MJ}}{\text{day}} \\
 \text{Net energy} &= 8015 - 424 = 7555 \frac{\text{MJ}}{\text{day}}
 \end{aligned}$$

Assuming that energy price is 0.1 \$/kwh

$$\text{Net energy advantage} = \frac{7555 \text{ kwh}}{3.6 \text{ day}} \times 0.1 \frac{\$}{\text{kwh}} = 210 \frac{\$}{\text{day}}$$

Assuming sludge handling cost is 684 \$/ton

Total sludge production

$$\begin{aligned}
 &= \left(800 + 16 \text{ kg} \frac{\text{cellulose (TSS)}}{\text{day}} \right) \times \frac{30}{100} \\
 &+ 38 \frac{\text{kgVSS}}{\text{day}} \times \frac{50}{100} \times \frac{1 \text{gTSS}}{0.85 \text{ g VSS}} = 267 \frac{\text{kgTSS}}{\text{day}}
 \end{aligned}$$

Sludge handling cost = 181 \$/day

Overall net benefit = 210 – 181 = 29 \$/day

Case II: without primary treatment

Influent cellulose=1000 kg/day

Cellulose biodegradation efficiency= 85%

Cellulose converted to biomass= 850 kg/day

Total non-biodegradable cellulose= 150 kg/day

Non-biodegradable cellulose in the secondary effluent (20% of the non-biodegradable cellulose) = 30 kg/day

Non-biodegradable cellulose in the WAS= 120 kg/day

Cellulose biodegradation efficiency in the anaerobic digestion is assumed 70% according to the literature.

Biomass yield was assumed =0.44 gVSS/gCOD

SRT=10 days

$k_d=0.1 \text{ d}^{-1}$

Biomass disintegration efficiency in the anaerobic digestion is assumed=50%

$$\begin{aligned} \text{Biomass produced} &= 850 \frac{\text{kg cellulose}}{\text{day}} \times 1.07 \frac{\text{kg COD}}{\text{kg cellulose}} \times \frac{0.44 \text{ gVSS/gCOD}}{1 + 0.1 * 10} \\ &= 200 \text{ kgVSS/day} \end{aligned}$$

Methane production

$$\begin{aligned} &= \left[\left(120 \frac{\text{kg cellulose}}{\text{day}} \right) \times \frac{70}{100} \times 1.07 \frac{\text{kg COD}}{\text{kg cellulose}} \right. \\ &\quad \left. + \left(200 \frac{\text{kgVSS}}{\text{day}} \times \frac{50}{100} \times 1.42 \frac{\text{kg COD}}{\text{kgVSS}} \right) \right] \times 0.35 \frac{\text{m}^3 \text{CH}_4}{\text{kg COD}} = 81 \frac{\text{m}^3 \text{CH}_4}{\text{day}} \\ &= 2899 \frac{\text{MJ}}{\text{day}} \end{aligned}$$

$$\begin{aligned} \text{Oxygen demand} &= 850 \frac{\text{kg cellulose}}{\text{day}} \times 1.07 \frac{\text{kg COD}}{\text{kg cellulose}} \times \left(1 - \frac{1.42 \times 0.44 \frac{\text{gVSS}}{\text{gCOD}}}{1 + 0.1 * 10} \right) \\ &= 625 \frac{\text{kg O}_2}{\text{day}} = 625 \frac{\text{kwh}}{\text{day}} = 2250 \frac{\text{MJ}}{\text{day}} \end{aligned}$$

$$\text{Net energy} = 2899 - 2250 = 649 \frac{\text{MJ}}{\text{day}}$$

Assuming energy price is 0.1 \$/kwh

$$\text{Net energy advantage} = \frac{649 \text{ kwh}}{3.6 \text{ day}} \times 0.1 \frac{\$}{\text{kwh}} = 18 \frac{\$}{\text{day}}$$

Assuming sludge handling cost is 684 \$/ton

Total sludge production

$$\begin{aligned} &= \left(120 \text{ kg} \frac{\text{cellulose (TSS)}}{\text{day}} \right) \times \frac{30}{100} + 200 \frac{\text{kgVSS}}{\text{day}} \times \frac{50}{100} \times \frac{1 \text{ gTSS}}{0.85 \text{ g VSS}} \\ &= 154 \frac{\text{kgTSS}}{\text{day}} \end{aligned}$$

Sludge handling cost = 527 \$/day

$$\text{Overall net benefit} = 18 - 527 = -509 \text{ \$/day}$$

Appendix B: Supplementary information for Chapter 4

Model parameters and equations

State variables

S_I ; soluble inert organic matter.

S_s ; soluble biodegradable substrate.

X_s ; slowly biodegradable substrate without cellulose.

X_I ; particulate inert organic matter.

X_{bh} ; heterotrophic biomass

X_{ba} ; autotrophic biomass.

X_p ; particulate of biomass decay.

S_{NO} ; nitrate nitrogen.

S_{NH} ; ammonium nitrogen.

S_{ND} ; soluble organic nitrogen.

X_{ND} ; particulate organic nitrogen.

S_o ; dissolved oxygen concentration

X_{cl} ; cellulose concentration

Kinetic parameters

1- Heterotrophs growth and decay

μ_h = maximum specific growth rate;

k_{no} = nitrate saturation constant;

k_{oh} = Heterotrophs oxygen concentration constant;

k_s = substrate saturation constant;

b_h = Heterotrophs specific decay rate;

2- Autotrophs growth and decay

μ_a = Autotrophs maximum specific growth rate;

k_{oa} = Autotrophs oxygen concentration constant;

k_{nh} = ammonium saturation constant;

b_a = Autotrophs specific decay rate;

3- Correction factor for anoxic growth of heterotrophs

η_g = anoxic growth correction factor;

4- Ammonification

k_a = ammonification rate constant;

5- Hydrolysis

k_h = maximum specific hydrolysis rate;

k_x = half saturation coefficient of hydrolysis of Xs;

k_{cl} = cellulose hydrolysis rate;

6- Correction factor for anoxic hydrolysis

η_h = anoxic hydrolysis correction factor;

stoichiometric Parameters

y_h = heterotroph yield;

y_a = autotrophic yield;

i_{xb} = nitrogen fraction in biomass;

i_{xp} = nitrogen fraction in endogenous mass;

f_p = fraction of biomass leading to particulate material;

Reactions rates

Heterotroph aerobic growth = $\mu_h * S_s / (k_s + S_s) * S_o / (k_{oh} + S_o) * X_{bh}$;

Heterotroph anoxic growth = $\mu_h * S_s / (k_s + S_s) * k_{oh} / (k_{oh} + S_o) * S_{NO} / (S_{NO} + k_{NO}) * \eta_g * X_{bh}$;

$$\text{Autotroph aerobic growth} = \mu_a * S_{NH}/(S_{NH}+k_{nh}) * S_o/(S_o+k_{oa}) * X_{ah} ;$$

$$\text{Heterotroph decay} = b_h * X_{bh};$$

$$\text{Autotroph decay} = b_a * X_{ah};$$

$$\text{Ammonification} = k_a * S_{ND} * X_{bh};$$

$$\text{Hydrolysis } X_s = k_h * X_s/(k_x * X_{bh} + X_s) * (S_o/(k_{oh} + S_o) + \eta_h * k_{oh}/(k_{oh} + S_o) * S_{NO}/(k_{NO} + S_{NO})) * X_{bh} ;$$

$$\text{Hydrolysis } X_N = X_{ND}/X_s * \text{hydrolysis } X_s ;$$

$$\text{Hydrolysis } X_{CL} = k_{cl} * X_{cl} ;$$

Differential equations

- 1- $dS_s/dt = - 1 / y_h * \text{Heterotroph aerobic growth} - 1 / y_h * \text{Heterotroph anoxic growth} + \text{hydrolysis } X_s + \text{hydrolysis } X_{CL};$
- 2- $dX_s/dt = (1-f_p) * \text{Heterotroph decay} + (1-f_p) * \text{Autotroph decay} - \text{hydrolysis } X_s ;$
- 3- $dX_{bh}/dt = \text{Heterotroph aerobic growth} + \text{Heterotroph anoxic growth} - \text{Heterotroph decay};$
- 4- $dX_{ah}/dt = \text{Autotroph aerobic growth} - \text{Autotroph decay};$
- 5- $dX_p/dt = f_p * \text{Heterotroph decay} + f_p * \text{Autotroph decay};$
- 6- $dS_{NO}/dt = (-1 + y_h) / (2.86 * y_h) * \text{Heterotroph anoxic growth} + 1/y_a * \text{Autotroph aerobic growth};$
- 7- $dS_{NH}/dt = -i_{xb} * \text{Heterotroph aerobic growth} - i_{xb} * \text{Heterotroph anoxic growth} - (i_{xb} + 1/y_a) * \text{Autotroph aerobic growth} + \text{ammonification} ;$
- 8- $dS_{ND}/dt = -1 * \text{ammonification} + \text{hydrolysis } X_N;$
- 9- $dX_{ND}/dt = (i_{xb} - f_p * i_{xp}) * (\text{Heterotroph decay} + \text{Autotroph decay}) - \text{hydrolysis } X_N ;$
- 10- $dS_o/dt = 0.0;$
- 11- $dX_{cl}/dt = - \text{hydrolysis } X_{CL};$

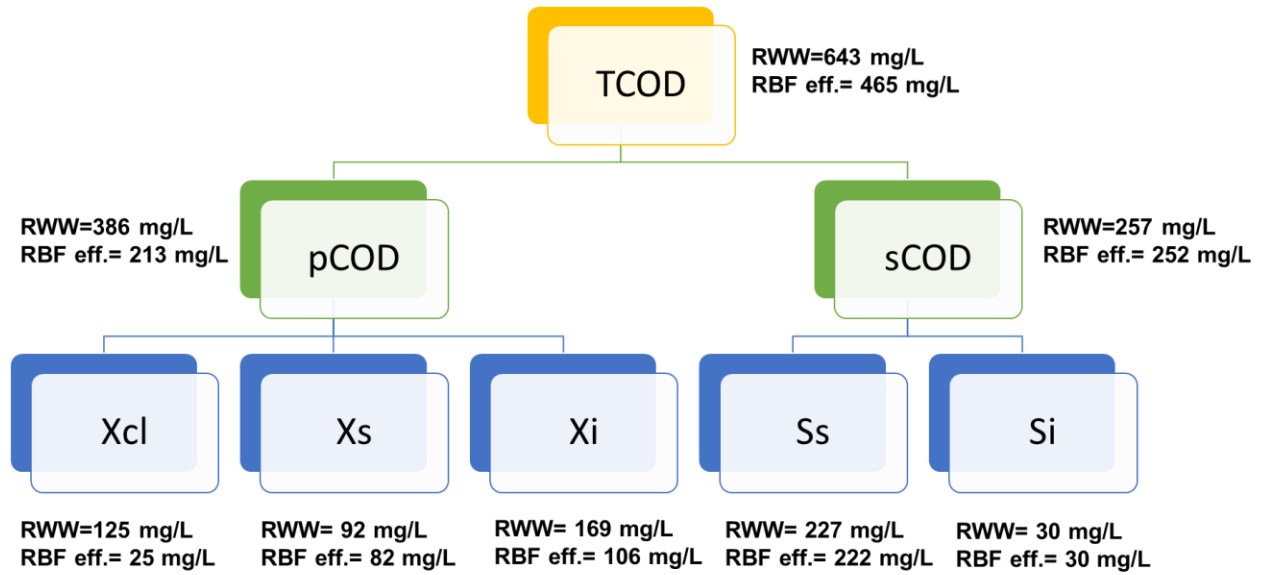


Figure S1: Input COD fractions for both SBR1 (RWW) and SBR2 (RBF)

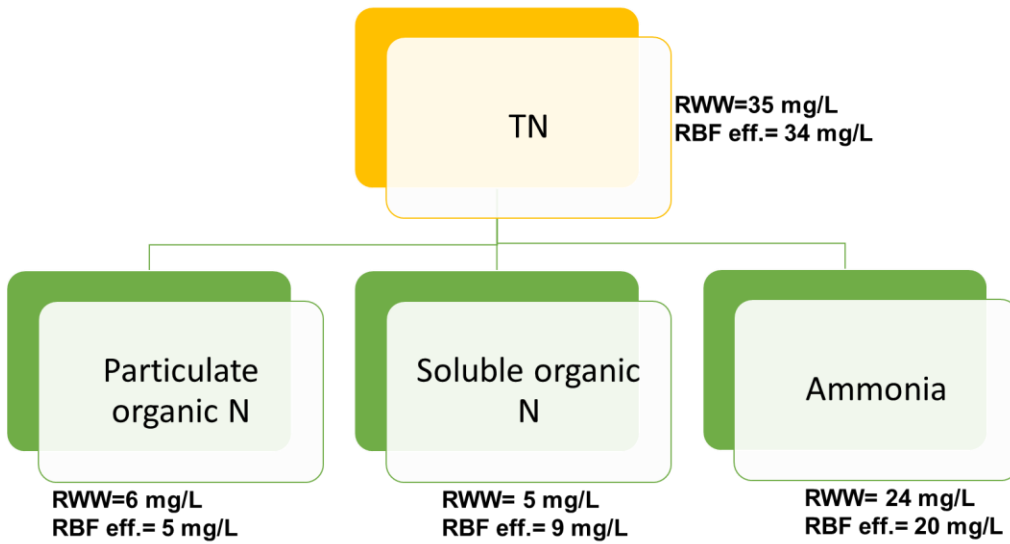


Figure S2: Input Nitrogen fractions for both SBR1 (RWW) and SBR2 (RBF)

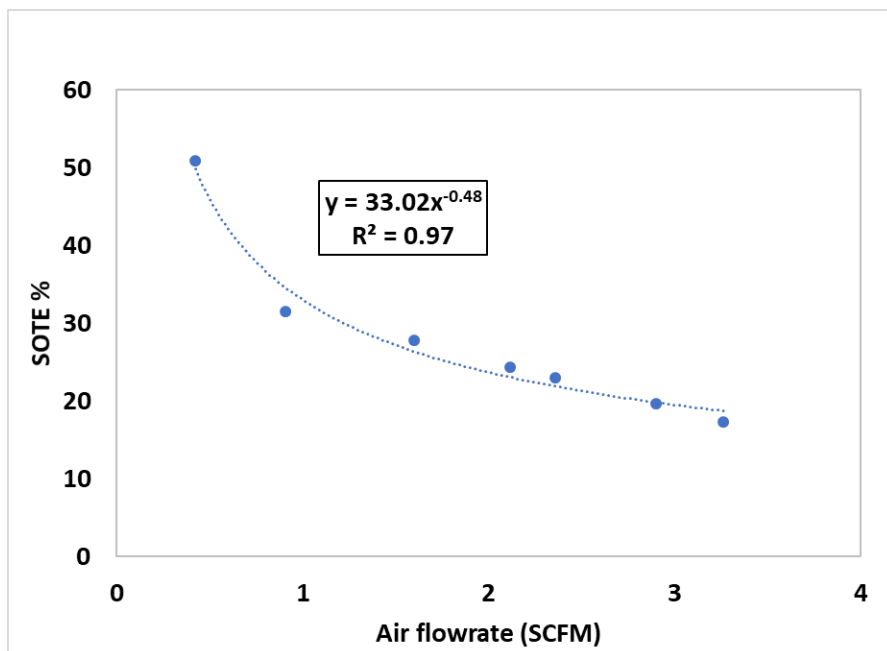


Figure S3: the correlation between SOTE and airflow rates

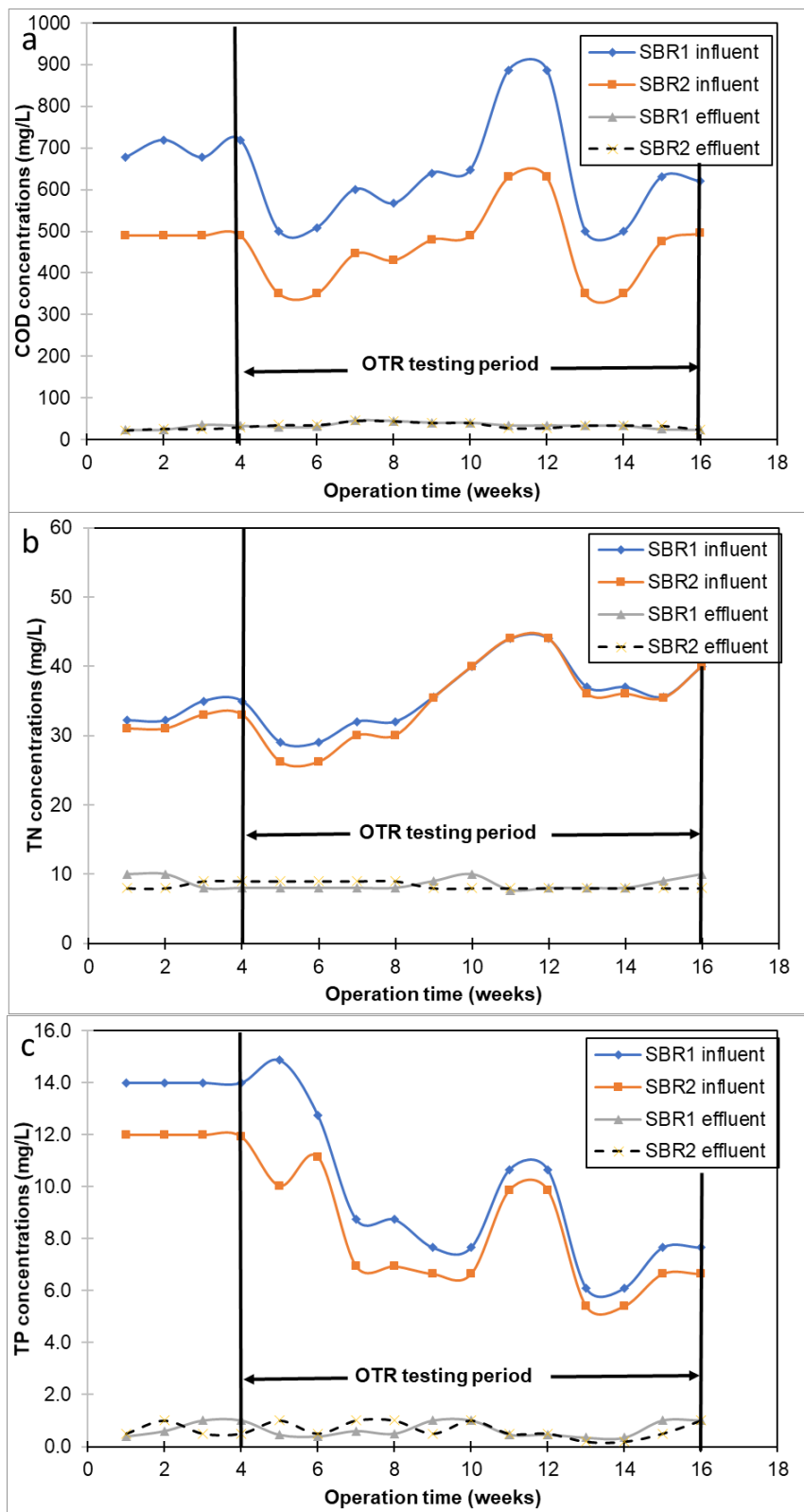


Figure S4: Effluent COD, TN, and TP for both SBRs during the period of oxygen transfer rate (OTR) testing.

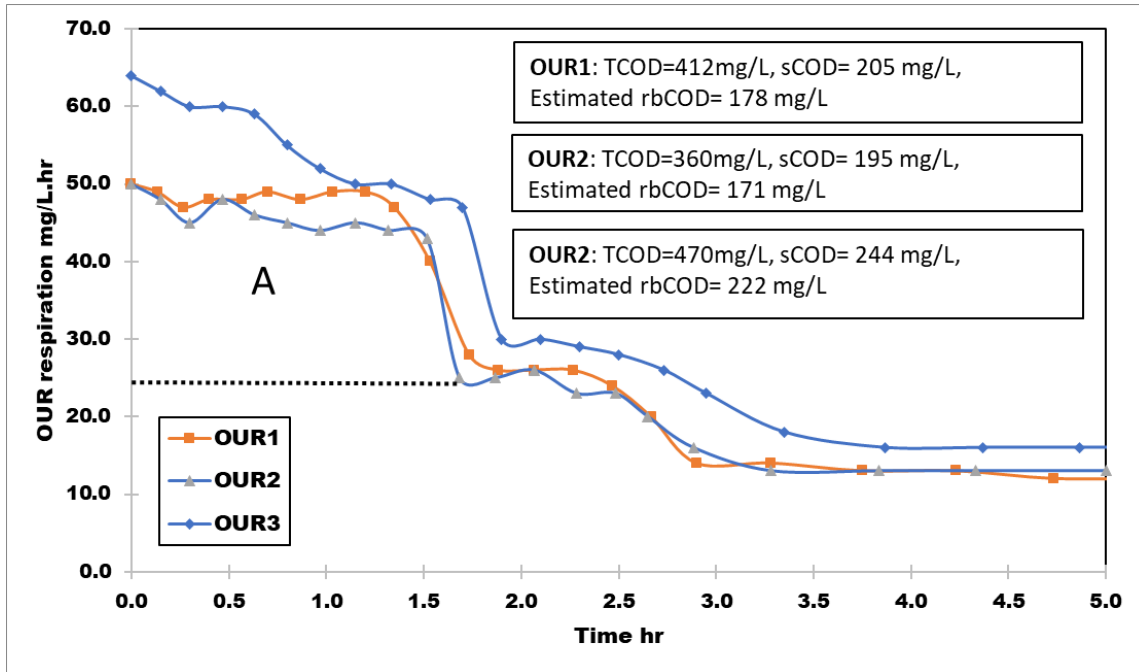


Figure S5: OUR profiles at high air flow rates and high DO

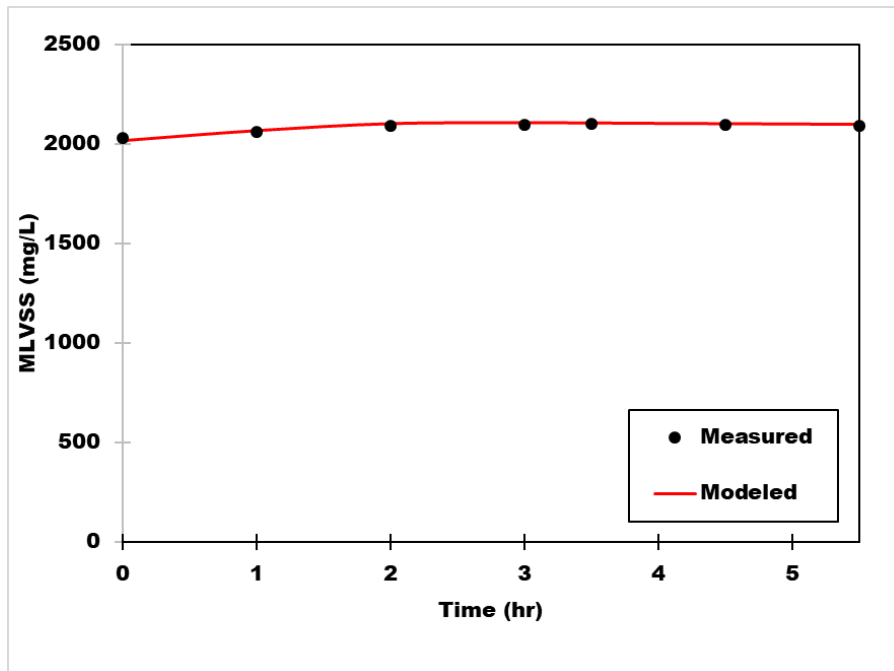


Figure S6: Calibrated MLVSS concentrations in SBR2

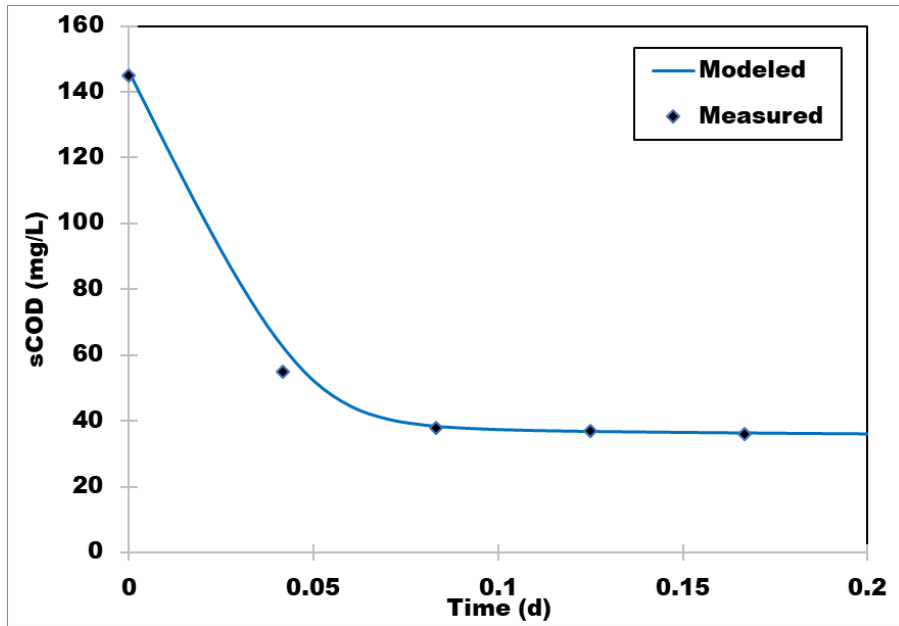


Figure S7: Calibrated sCOD concentrations in SBR2

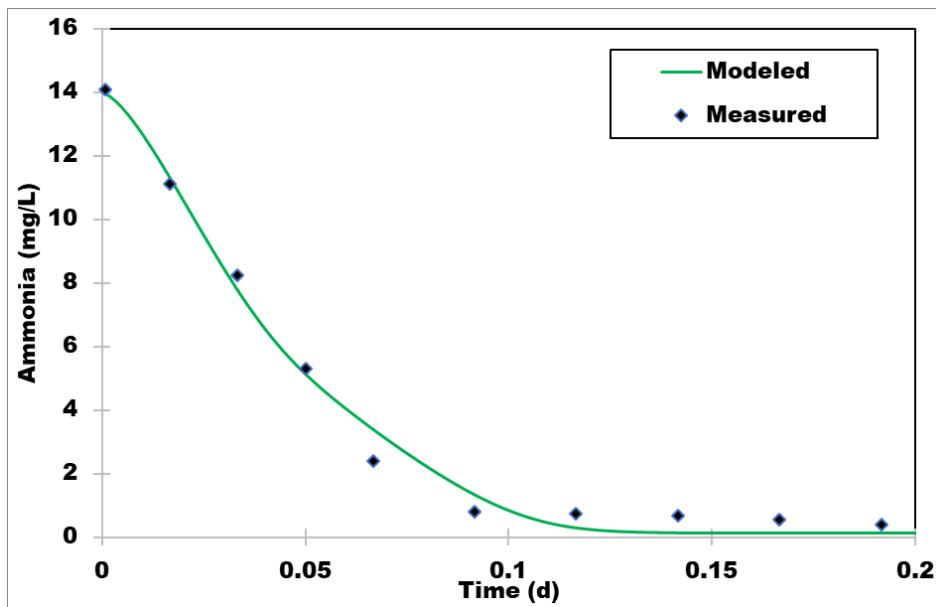


Figure S8: Calibrated ammonia concentrations in SBR2

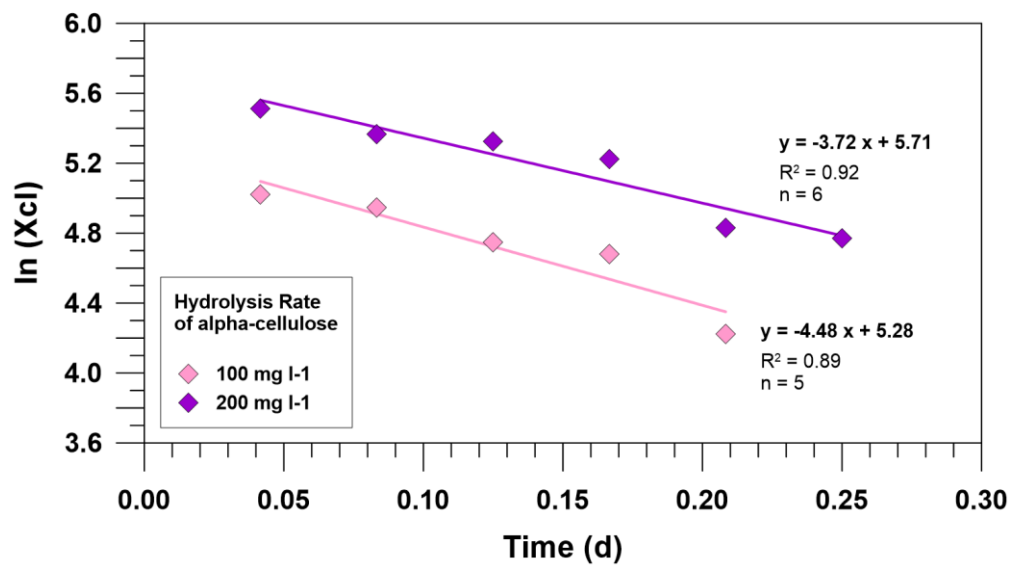


Figure S9: Hydrolysis rate of alpha-cellulose (100 mg l⁻¹, and 200 mg l⁻¹).

Table S1. Average influent and steady-state effluent wastewater characteristics for both SBRs.

No.	Sample name	TSS ^a	VSS ^a	COD ^a	sCOD ^a	TN ^a	sN ^a	NH ₃ ^a	NO ₃ ^a	TP ^a	sP ^a
		mg l ⁻¹	mg l ⁻¹	mg l ⁻¹	mg l ⁻¹	mg l ⁻¹	mg l ⁻¹	mg l ⁻¹	mg l ⁻¹	mg l ⁻¹	mg l ⁻¹
1	Influent	359±63	274±35	643±121	257±50	35±5	29±2	24±3	0.1±0	10±3	2.2±0.1
2	RBF effluent	218±48	147±22	465±87	252±58	34±6	29±2	20±2	0.1±0	8±2	2.2±0.1
3	SBR1 effluent (non-screened)	12±3	8±2	34±6	30±5	9±1	-	0.4±0.1	8±1	0.66±0.3	0.2±0.0
4	SBR2 effluent (RBF screened)	10±4	7±3	34±7	31±6	8±1	-	0.3±0.1	8±1	0.65±0.3	0.2±0.0
5	SBR1 Mixed liquor	3,957±806	2,951±560	-	-	-	-	-	-	-	-
6	SBR2 Mixed liquor	2,818±454	2,054±380	-	-	-	-	-	-	-	-

^a Values represent the average ±standard deviation of 16 samples

Table S2: Kinetic coefficients validated for the modeled SBR (Henze et al., 2000)

Coefficient	Value	Typical ASM1 values	Unit
Heterotrophic maximum specific growth rate μ_H	3 ^a	6	d ⁻¹
Specific decay rate b_H	0.62	0.2-0.62	d ⁻¹
Heterotrophic oxygen concentration constant $K_{O,H}$	0.2	0.2	gO ₂ /m ³
Substrat saturation constant K_s	20.0 ^b	20	gCOD/m ³
Nitrate half-saturation constant K_{NO}	0.5	0.5	gNO ₃ -N/m ³
Autotrophic maximum specific growth factor μ_A	0.8 ^a	0.8	Day ⁻¹
Autotrophic oxygen concentration constant $K_{O,A}$	0.4	0.4	gO ₂ /m ³
Ammonium half-saturation constant K_{NH3-N}	1.0 ^c	1	gNH ₃ -N/m ³
Autotrophic specific decay rate	0.2	0.2	Day ⁻¹
Anoxic growth correction factor	0.8	0.8	
Ammonification rate constant k_a	0.08	0.08	m ³ .COD/g.day
Maximum specific hydrolysis rate K_H	3	1-3	Day ⁻¹
Half saturation coefficient of hydrolysis of X_s (K_x)	0.03	0.01-0.03 ^d	gCOD/g cell COD.
Cellulose hydrolysis rate K_{CL}	4.1 ^e	-	Day ⁻¹
Heterotrophic yield Y_h	0.67	0.67	gcell COD/gCOD _{oxidized}
Autotrophic yield Y_A	0.24	0.24	gcell COD/gN _{oxidized}

^a μ_H and μ_A were calibrated to match the heterotrophic biomass production rate with the measured MLVSS in the SBR 2. μ_h of 3 d⁻¹ is comparable to the reported μ_h of 3.5 d⁻¹ by (Ekama, 2009; Mathieu and Etienne, 2000) at COD to MLVSS ratio of 0.2 mgCOD/ mgVSS which is identical to the ratio reported in our study.

^b K_s was calibrated to match the substrate utilization rate with the measured values in the SBR 2.

^c K_{NH3-N} was calibrated using actual measurements of ammonia.

^d K_x for ASM 3 of 1 gCOD/g cell COD was used in the modeling of cellulose hydrolysis

^e Cellulose hydrolysis rate was estimated using actual measurements of cellulose assuming a first-order degradation rate.

Table S3. SBR1 initial inputs (60% fill +40% activated sludge).

Parameter	Value, mg/L
S_I	30
S_s	120
X_s	64
X_I	2036
X_{bh}	1062
X_{ba}	23
S_{NO}	0.1
S_{NH}	14.4
S_{ND}	3
X_{ND}	3.6
S_o	2
X_{cl}	131.6

- S_I calibrated with S_s to match the measured sCOD effluent.
- $S_s =$ [influent calibrated rbCOD (227 mg l^{-1})* 0.6 fill ratio] +[rbCOD in the sludge-estimated from the model (7 mg l^{-1})*0.4 sludge ratio]- [rbCOD used for denitrification-estimated from the model (19 mg l^{-1})]= 120 mg l^{-1}
- $X_s =$ [influent calibrated X_s (92 mg l^{-1}) * 0.6 fill ratio] + [X_s in the sludge-estimated from the model (23 mg l^{-1}) *0.4 sludge ratio] = 64 mg l^{-1}
- $X_I =$ [influent calibrated X_I (169 mg l^{-1})-estimated iteratively using Eq.6 * SRT (10 days)/HRT (0.83 day) = 2036 mg l^{-1}
- $X_{bh} =$ [SRT (10 days)/HRT (0.83 =day)] * [COD_{utilized} * $Y_h/(1+k_d.SRT)$] =
 - $X_{bh} =$ [12*[290.6 mg l^{-1} (estimated from the model) *0.67/ (1+0.12*10)] = 1062 mg l^{-1}
- $X_{ah} =$ [SRT (10 days)/HRT (0.83 =day)] * [NO_x * $Y_a/(1+k_{dn}.SRT)$] =
 - $X_{ah} =$ [12*[14.4 mg l^{-1} (estimated from the model) *0.24/ (1+0.08*10)]= 23 mg l^{-1}
- $S_{NH} = 24 \text{ mg l}^{-1} * 0.6 = 14.4 \text{ mg l}^{-1}$
- $S_{ND} = 5 \text{ mg l}^{-1} * 0.6 = 3 \text{ mg l}^{-1}$

- $X_{ND} = 6 \text{ mg l}^{-1} * 0.6 = 3.6 \text{ mg l}^{-1}$
- $X_{CL} = [\text{influent calibrated } X_s (125 \text{ mg l}^{-1}) * 0.6 \text{ fill ratio}] + [X_s \text{ in the sludge-estimated from the model } (141.6 \text{ mg l}^{-1}) * 0.4 \text{ sludge ratio}] = 64 \text{ mg l}^{-1}$

Table S4. SBR2 initial inputs (60% fill +40% activated sludge).

Parameter	Value, mg/L
S_I	30
S_s	109
X_s	56
X_I	1272
X_{bh}	875
X_{ba}	27
S_{NO}	0.1
S_{NH}	12
S_{ND}	5.4
X_{ND}	3
S_o	2
X_{cl}	26

Table S5: SBR2+ 100 mg cellulose/L initial inputs (60% fill +40% activated sludge).

Parameter	Value, mg/L
S_I	30
S_s	109
X_s	56
X_I	1272
X_{bh}	875
X_{ba}	27
S_{NO}	0.1
S_{NH}	12
S_{ND}	5.4
X_{ND}	3
S_o	2
X_{cl}	126

Table S6: SBR2+ 100 mg acetate/L initial inputs (60% fill +40% activated sludge).

Parameter	Value, mg/L
S_I	30
S_s	209
X_s	56
X_I	1272
X_{bh}	875
X_{ba}	27
S_{NO}	0.1
S_{NH}	12
S_{ND}	5.4
X_{ND}	3
S_o	2
X_{cl}	26

Appendix C: Supplementary information for Chapter 5

Table SI-1. influent and effluent characteristics for both SBRs

No.	Sample name	TSS ^a	VSS ^a	COD ^a	sCOD ^a	TN ^a	sN ^a	NH ₃ ^a	NO ₃ ^a	TP ^a	sP ^a
		mg/L	mg/L	mg/L	mg/L	mg/L	mg/L	mg/L	mg/L	mg/L	mg/L
1	Influent	349 ± 48	274 ± 35	653 ± 82	246 ± 49	31 ± 2	26 ± 2	23 ± 3	0.1 ± 0.01	10 ± 3	2.4 ± 0.4
		222 ± 46	147 ± 22	464 ± 68	242 ± 56	28 ± 3	25 ± 2	21 ± 2	0.1 ± 0.01	9 ± 2	2.3 ± 0.4
3	SBR1 effluent (non-filtered)	11 ± 3	9 ± 2	39 ± 3	28 ± 2	8 ± 1	-	0.3 ± 0.2	6 ± 1	0.61 ± 0.3	0.2 ± 0.01
4	SBR2 effluent (filtered)	10 ± 2	6 ± 2	37 ± 3	26 ± 2	9 ± 1	-	0.3 ± 0.2	7 ± 1	0.65 ± 0.3	0.2 ± 0.01
5	SBR1 ML	5,109 ± 203	3,635 ± 182	-	-	-	-	-	-	-	-
6	SBR2 ML	3,554 ± 378	2,545 ± 152	-	-	-	-	-	-	-	-

^a Values represent the average ± standard deviation of 14 samples

Table SI-2: Kinetic coefficients validated for the modelled SBR (Henze et al., 2000)

Coefficient	Value	Typical ASM1 values	Unit
Heterotrophic maximum specific growth rate μ_H	3 ^a	3-6	d ⁻¹
Specific decay rate b_H	0.62	0.2-0.62	d ⁻¹
Heterotrophic oxygen concentration constant $K_{O,H}$	0.2	0.2	gO ₂ /m ³
Substrat saturation constant K_s	30.0 ^a	20	gCOD/m ³
Nitrate half-saturation constant K_{NO}	0.5	0.5	gNO ₃ -N/m ³
Autotrophic maximum specific growth factor μ_A	0.7 ^b	0.8	Day ⁻¹
Autotrophic oxygen concentration constant $K_{O,A}$	0.4	0.4	gO ₂ /m ³
Ammonium half-saturation constant K_{NH3-N}	0.7 ^b	1	gNH ₃ -N/m ³

Autotrophic specific decay rate	0.2	0.2	Day ⁻¹
Anoxic growth correction factor	0.8	0.8	
Ammonification rate constant k_a	0.08 ^b	0.08	m ³ .COD/g.day
Maximum specific hydrolysis rate K_H	3	1-3	Day ⁻¹
Half saturation coefficient of hydrolysis of X_s (K_x)	0.03	0.01-0.03	gCOD/g cell COD.day
Cellulose hydrolysis rate K_{CL}	4.1 ^c	-	Day ⁻¹
Heterotrophic yield Y_h	0.67	0.67	gcellCOD/gCOD _{oxidized}
Autotrophic yield Y_A	0.24	0.24	gcell COD/gN _{oxidized}

^a K_s and μ_H were calibrated to match the substrate utilization rate with the measured values in the SBR 2.

^b K_{NH_3-N} and μ_A were calibrated using actual measurements of ammonia.

^c Cellulose hydrolysis rate was estimated using actual measurements of cellulose assuming a first-order degradation rate.

Table SI-3: Influent and effluent wastewater characteristics for both modelled scenarios

Item	Unit	Influent (Henze et al., 2000)	Effluent (Plug flow)	Effluent (CSTR)	Effluent (Plug flow- step feed)	Effluent (MBR)
Flow	m ³ /d	1200	1174	1174	1174	1173
TSS	mg/L	239	9	9	9	0.8
VSS	mg/L	179	6	6	6	0.5
Soluble cBOD5	mgO ₂ /L	57	3	6	4	3
cBOD5	mgO ₂ /L	231	6	9	7	3
Soluble COD	mgCOD/L	108	27	31	27	26
COD	mgCOD/L	430	36	40	37	27
Ammonia Nitrogen	mgN/L	25	0.1	0.3	0.1	0.1
Nitrite and Nitrate	mgN/L	0.0	21	21	21	22
Soluble TKN	mgN/L	28	0.7	1.1	0.8	0.7
TKN	mgN/L	40	1.4	1.8	1.4	0.8
TN	mgN/L	40	23	23	23	23
Dissolved Oxygen	mgO ₂ /L	0.0	2.0	2.0	2.0	6.5
Alkalinity	mgCaCO ₃ /L	350	185	186	185	182

Table SI-3: Influent and effluent wastewater characteristics for both modelled scenarios

	Unit	Influent	Effluent (Plug flow)	Effluent (CSTR)	Effluent (Plug flow-step feed)	Effluent (MBR)
Flow	m ³ /d	1200	1173	1173	1174	1173
TSS	mg/L	239	10	10	9	0.8
VSS	mg/L	179	6	6	6	0.5
Soluble cBOD5	mgO ₂ /L	57	3	7	3	3
cBOD5	mgO ₂ /L	231	7	10	6	3
Soluble COD	mgCOD/L	108	27	32	26	26
COD	mgCOD/L	430	36	41	36	27
Ammonia Nitrogen	mgN/L	25.0	0.1	0.6	0.1	0.1
Nitrite and Nitrate	mgN/L	0.0	9	8	8	10
Soluble TKN	mgN/L	27.8	0.8	1.4	0.8	0.7
TKN	mgN/L	40.0	2	2	1.4	1
TN	mgN/L	40.0	10	10	10	11
Dissolved Oxygen	mgO ₂ /L	0.0	2	2	2	6
Alkalinity	mgCaCO ₃ /L	350.0	229	233	231	226

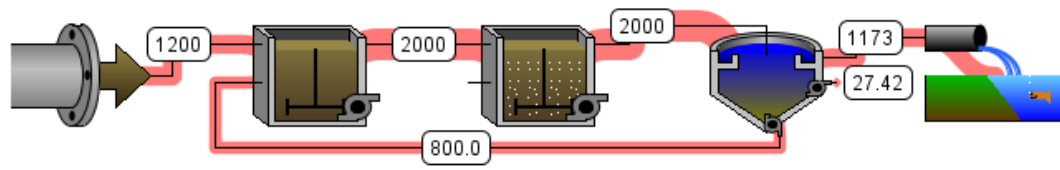


Figure SI-1. Treatment scheme for the modelled scenario with CSTR aeration reactor. Numbers represent the wastewater flow rates in $\text{m}^3 \text{d}^{-1}$

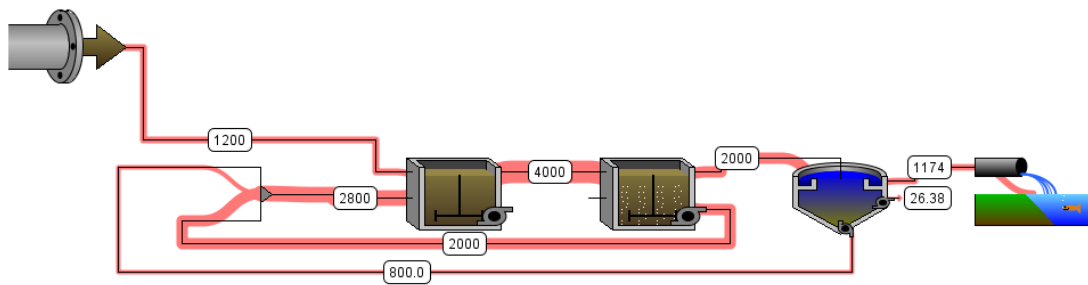


Figure SI-2. Treatment scheme for the modelled scenario with CSTR and internal recirculation to enhance nitrogen removal. Numbers represent the wastewater flow rates in $\text{m}^3 \text{d}^{-1}$

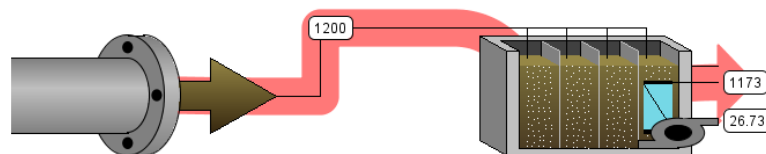


Figure SI-3. Treatment scheme for the modelled scenario with membrane bioreactor (MBR). Numbers represent the wastewater flow rates in $\text{m}^3 \text{d}^{-1}$

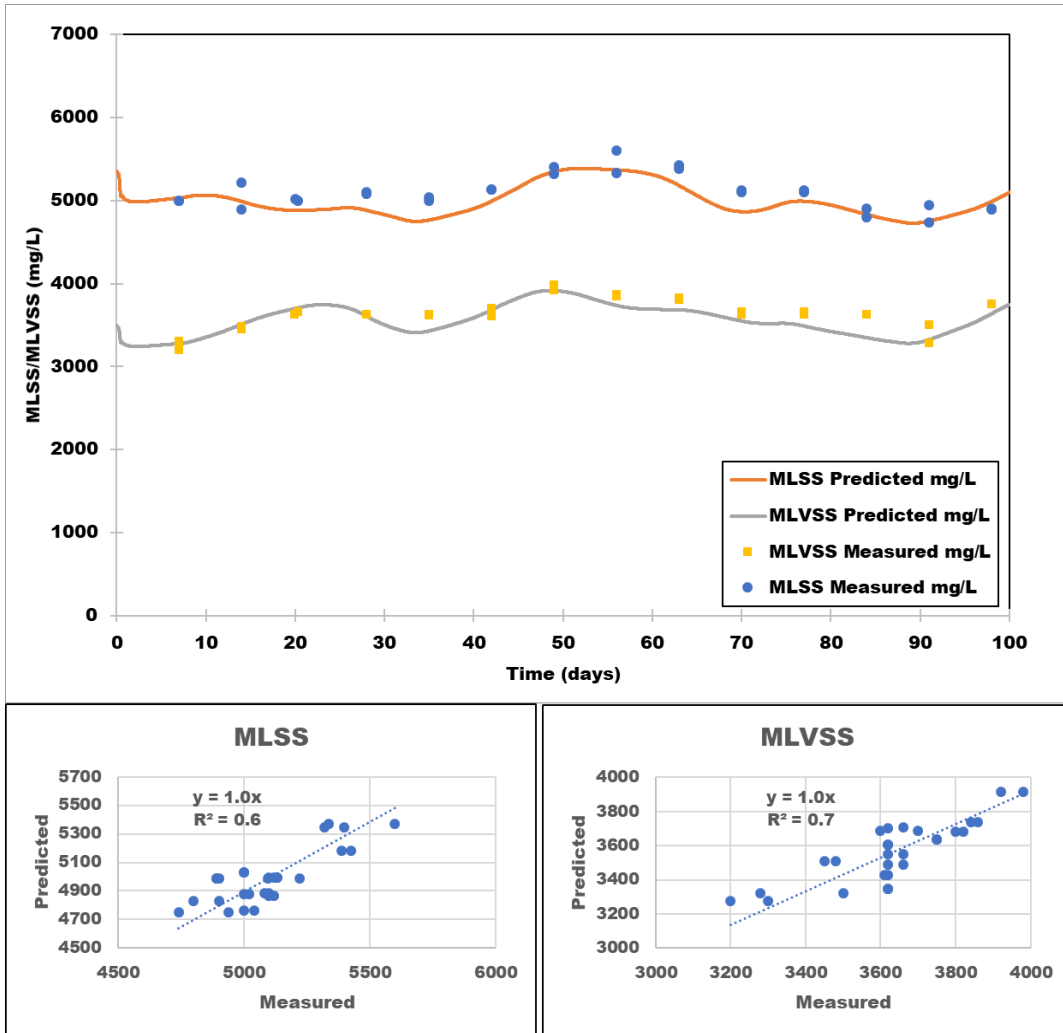


Figure SI-4: Calibrated MLSS and MLVSS for the SBR receiving raw wastewater (average absolute error for both MLSS and MLVSS was 3%)

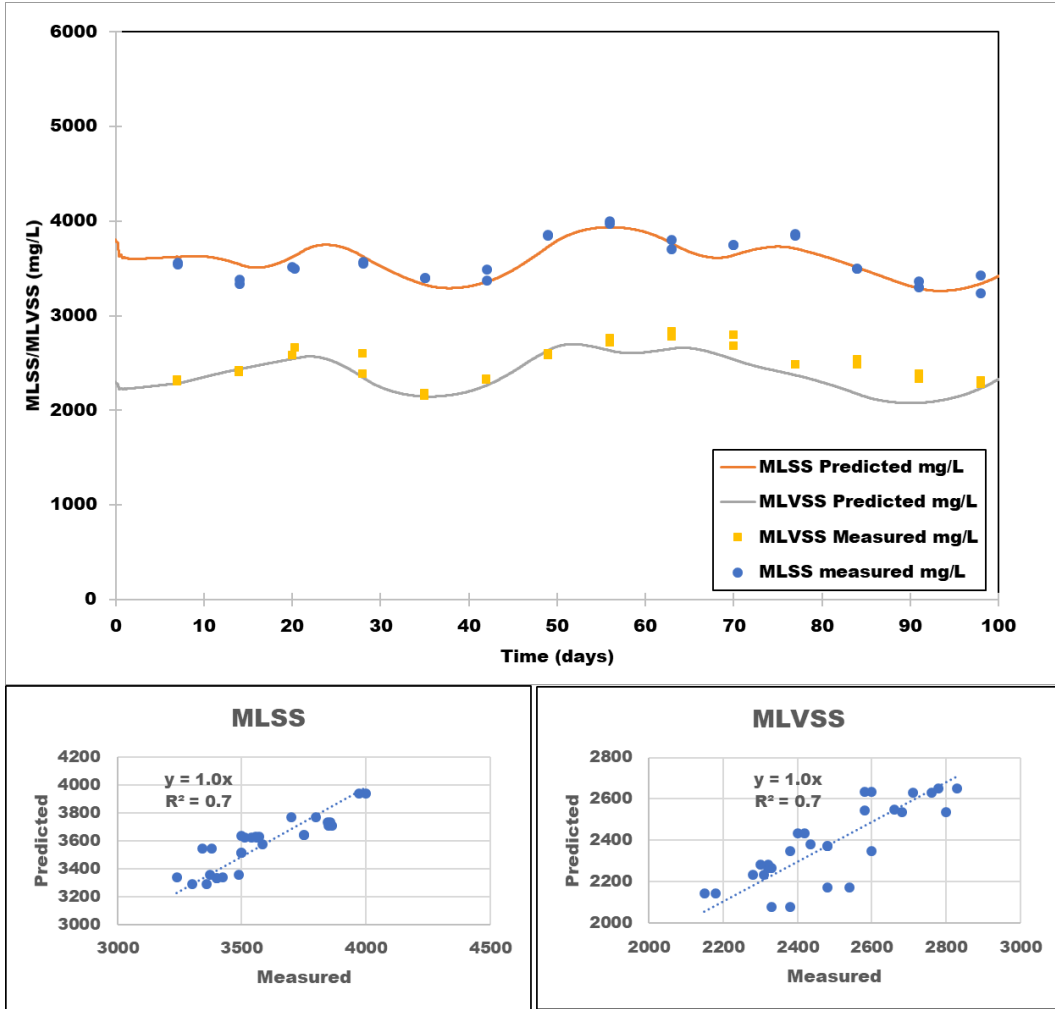


Figure SI-5: Calibrated MLSS and MLVSS for the SBR model receiving RBF treated wastewater (average absolute error was 3% for MLSS and 5% for MLVSS)

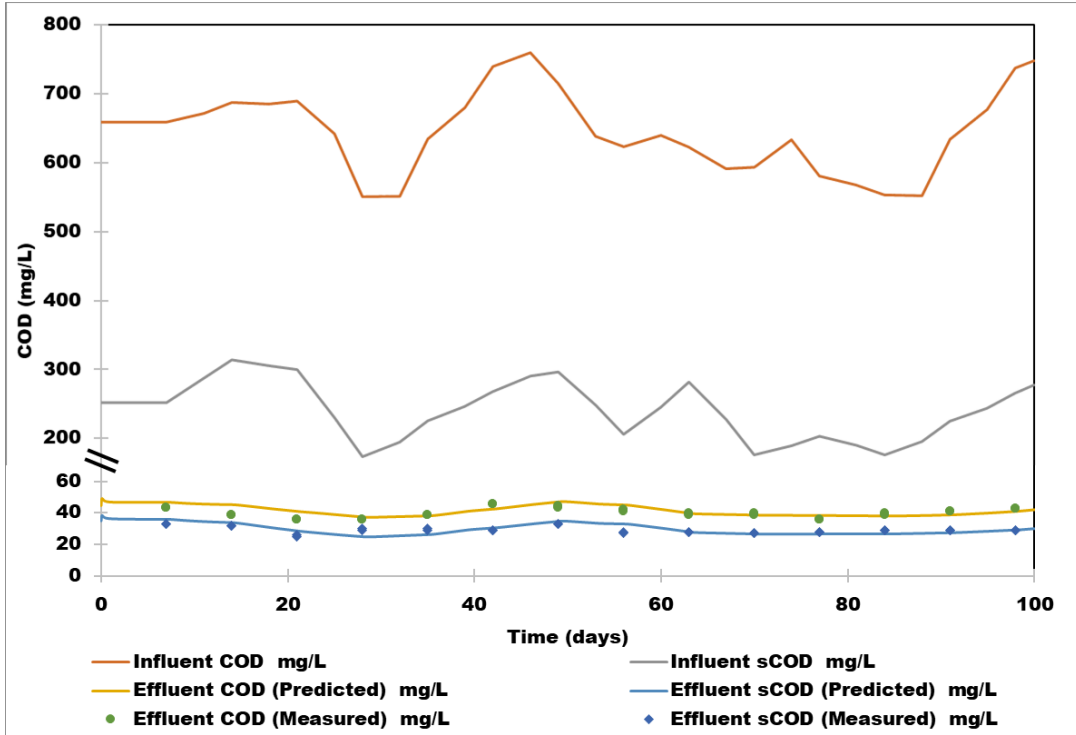


Figure SI-6: Influent and calibrated effluent COD and sCOD for the SBR receiving raw wastewater (average absolute error was 4% for the effluent COD and 7% for the effluent sCOD)

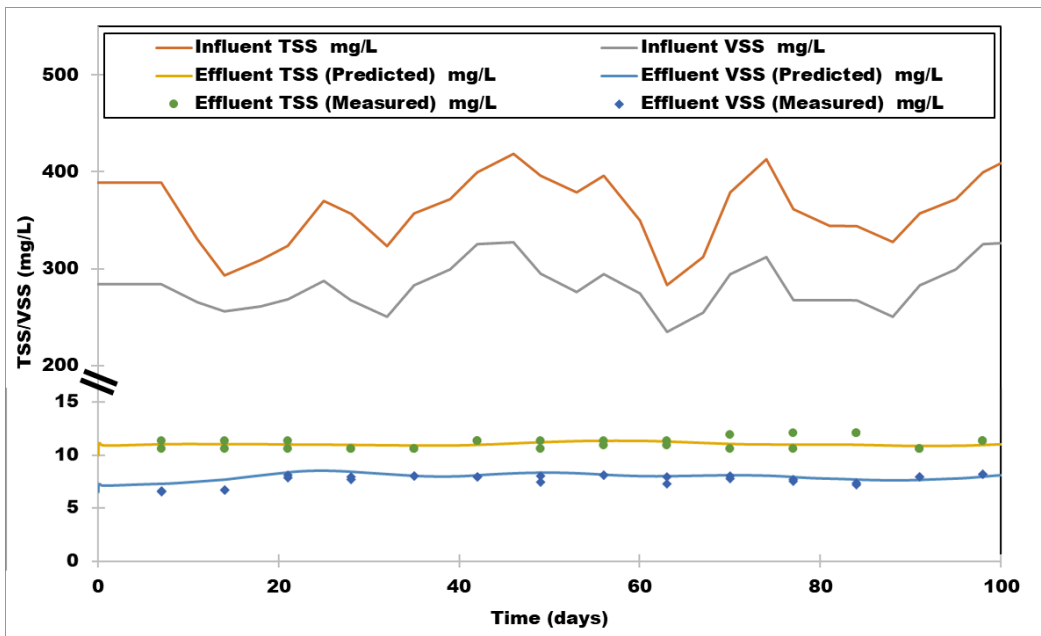


Figure SI-7: Influent and calibrated effluent TSS and VSS for the SBR receiving raw wastewater (average absolute error was 4% for the effluent TSS and 10% for the effluent VSS)

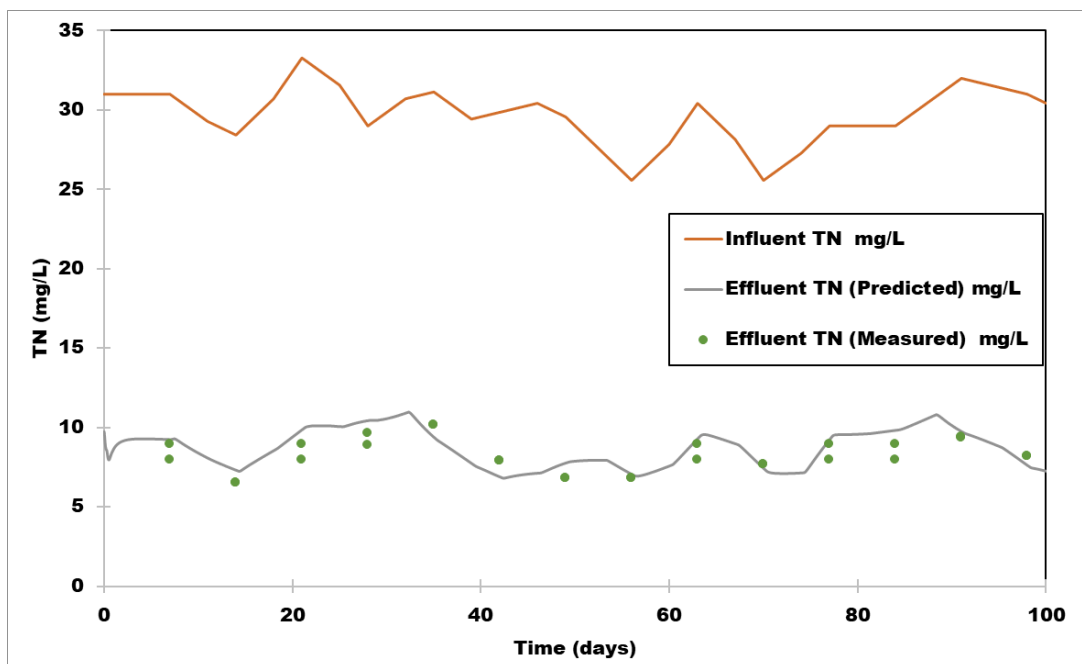


Figure SI-8: Influent and calibrated effluent TN for the SBR receiving raw wastewater (average absolute error for effluent TN was 9%).

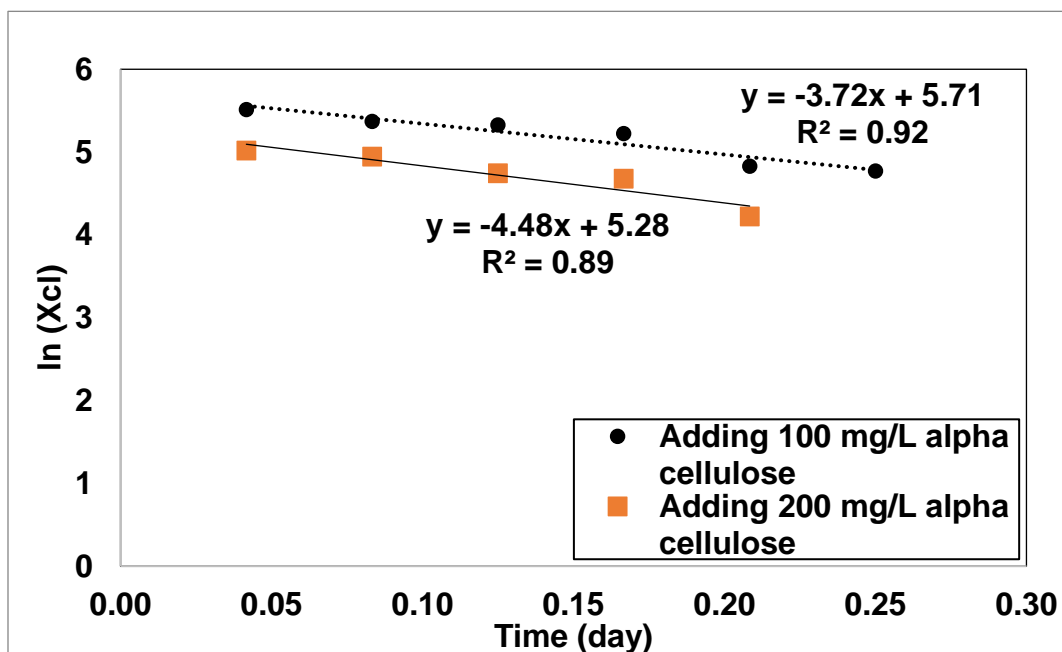


Figure SI-9: Hydrolysis rate of cellulose (100 mg l^{-1} , and 200 mg l^{-1}).

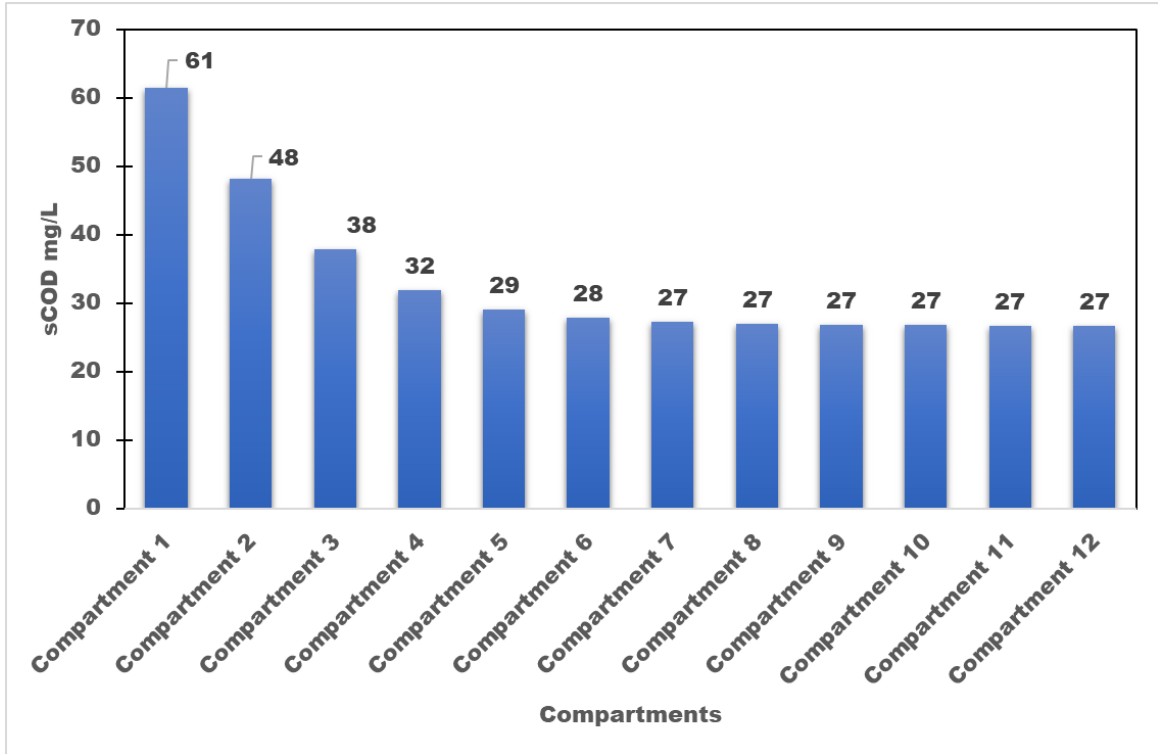


Figure SI-10: sCOD concentrations in each compartment (plug flow-Nitrification only)

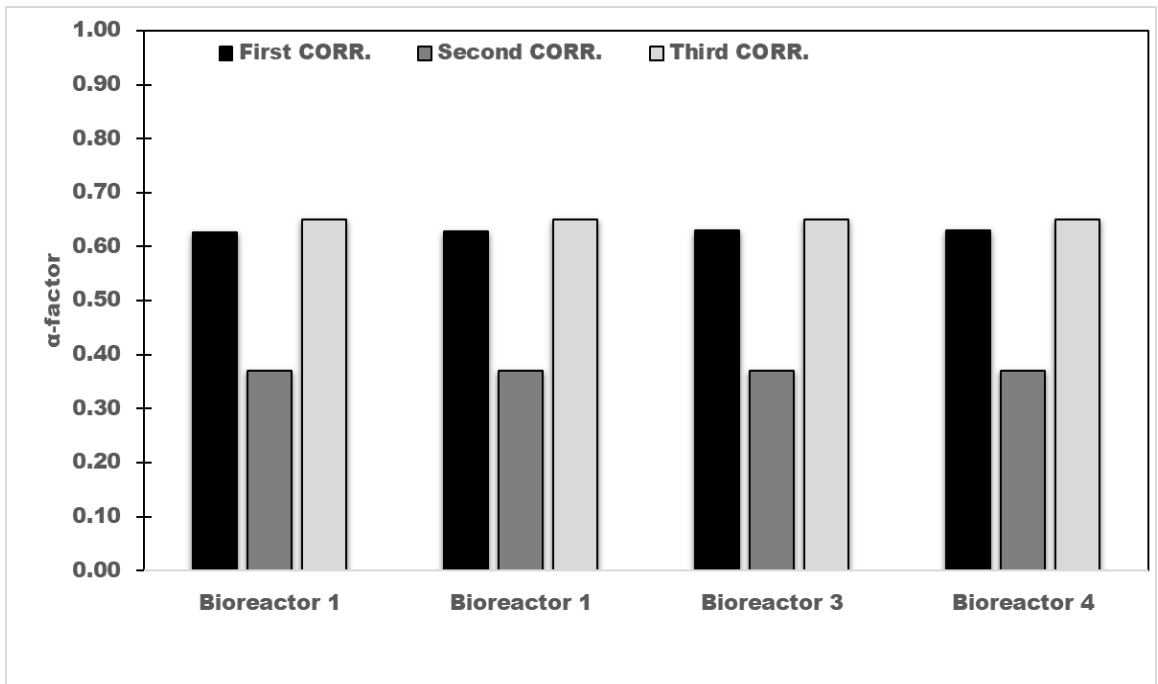


Figure SI-11: α -factor estimated in the four plug flow bioreactors using the three correlations (step feed-Nitrification only)

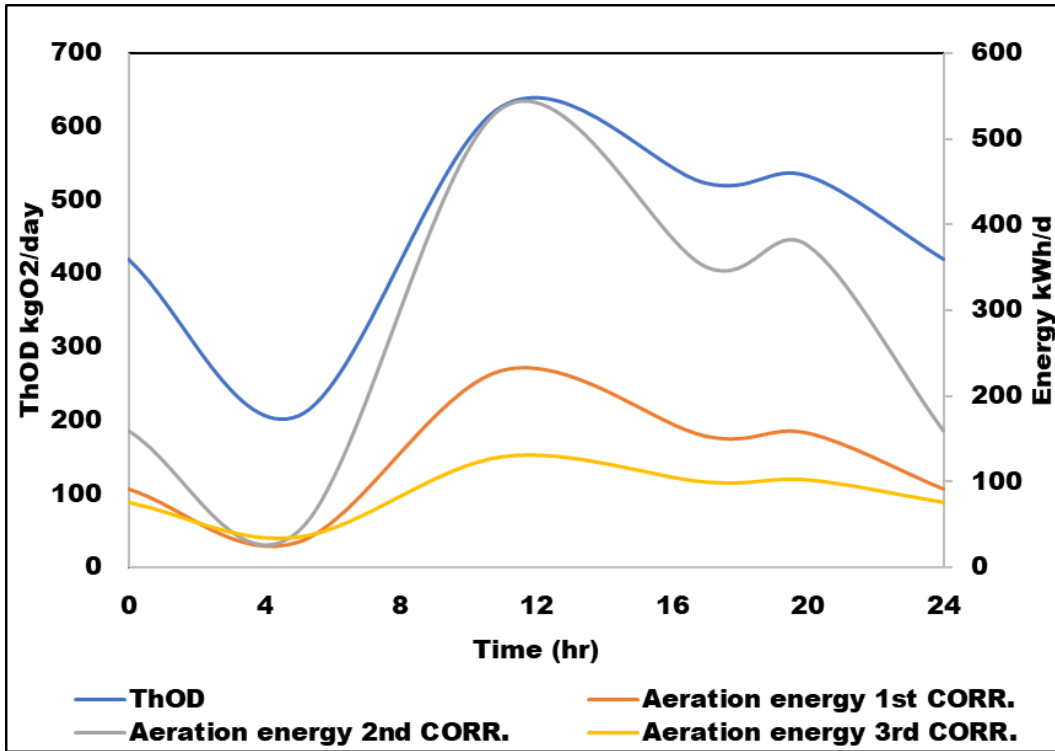


Figure SI-12: The change in aeration energy over a day due to the change in the influent concentrations using the three correlations (step-feed)

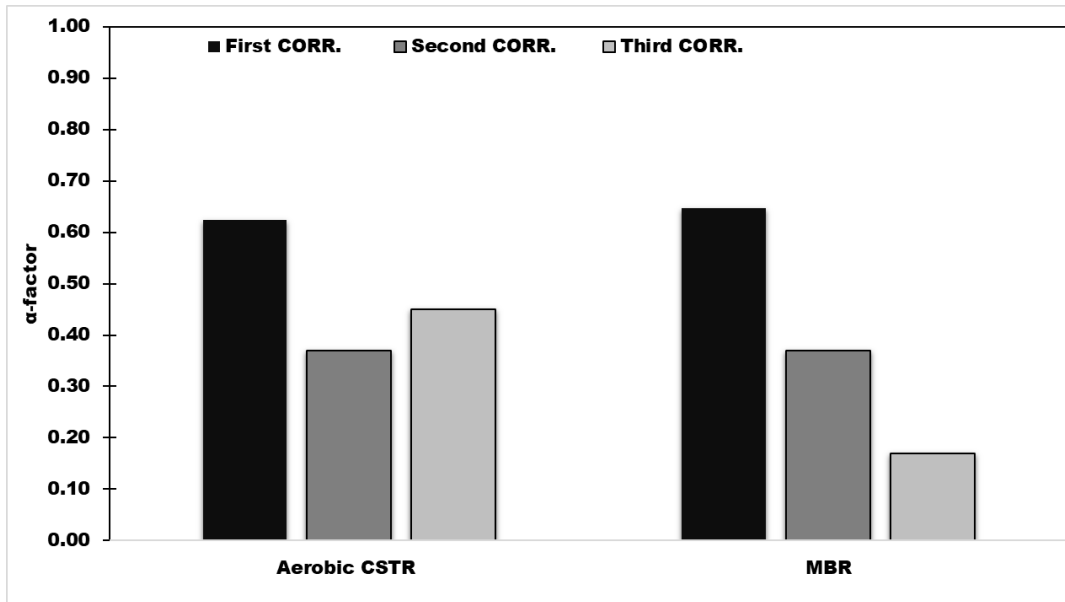


Figure SI-13. α -factor estimated in each compartment using the three correlations (MBR-Nitrification only)

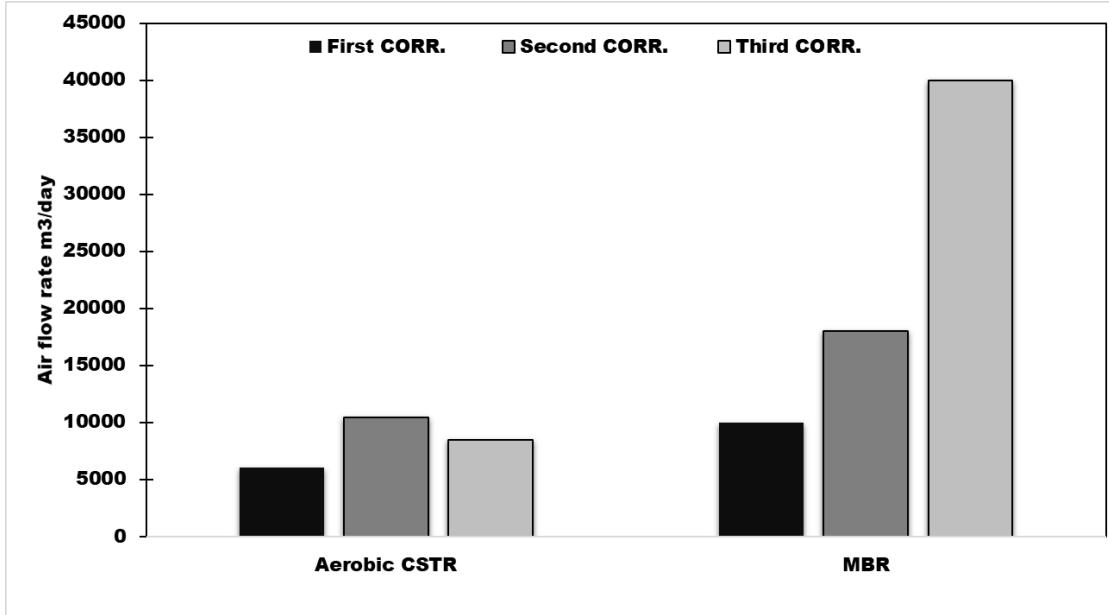


Figure SI-14. Air flow rates estimated in each compartment using the three correlations (MBR-Nitrification only)

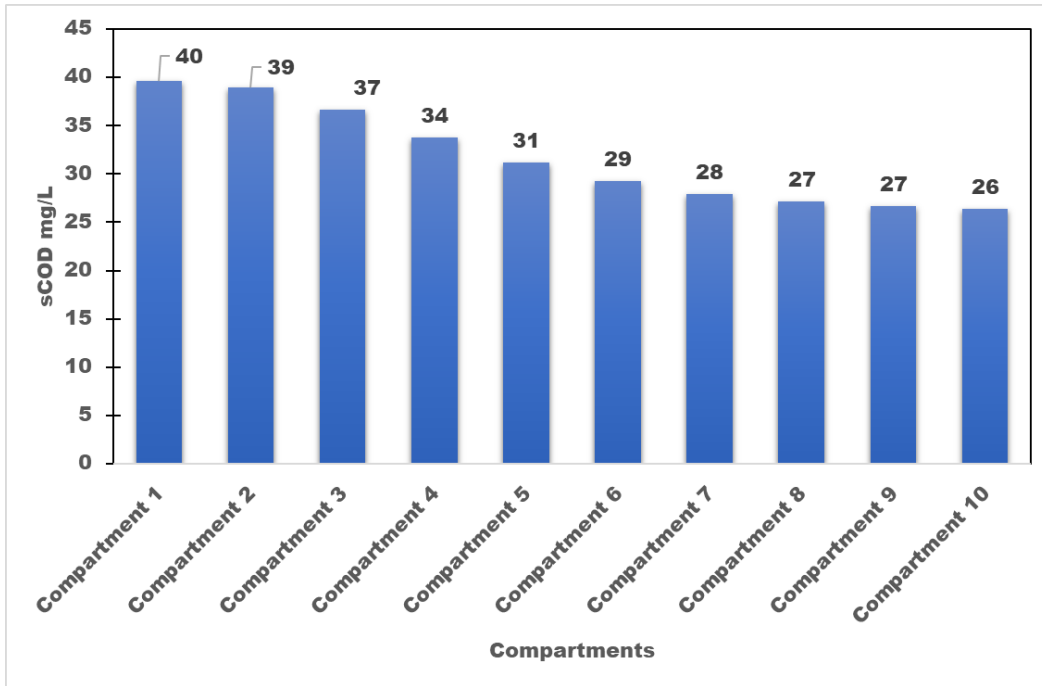


Figure SI-15: sCOD concentrations in each compartment (plug flow-Nitrification and denitrification)

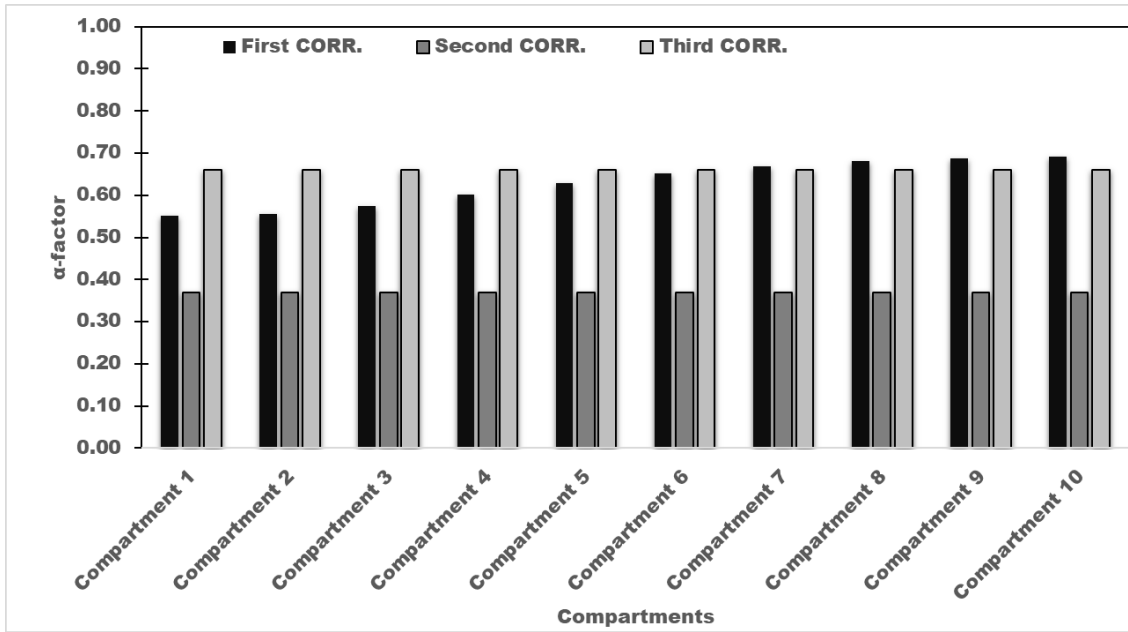


Figure SI-16: α -factor estimated in each compartment using the three correlations (plug flow -Nitrification and denitrification)

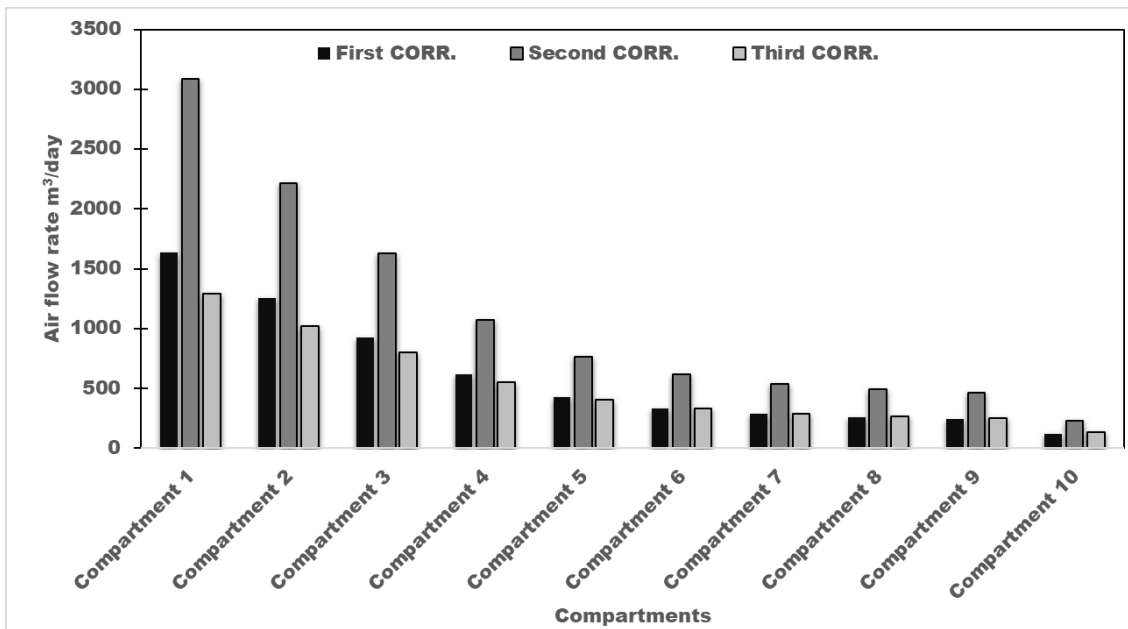


Figure SI-17: Air flow rates estimated in each compartment using the three correlations (Plug flow-Nitrification and denitrification)

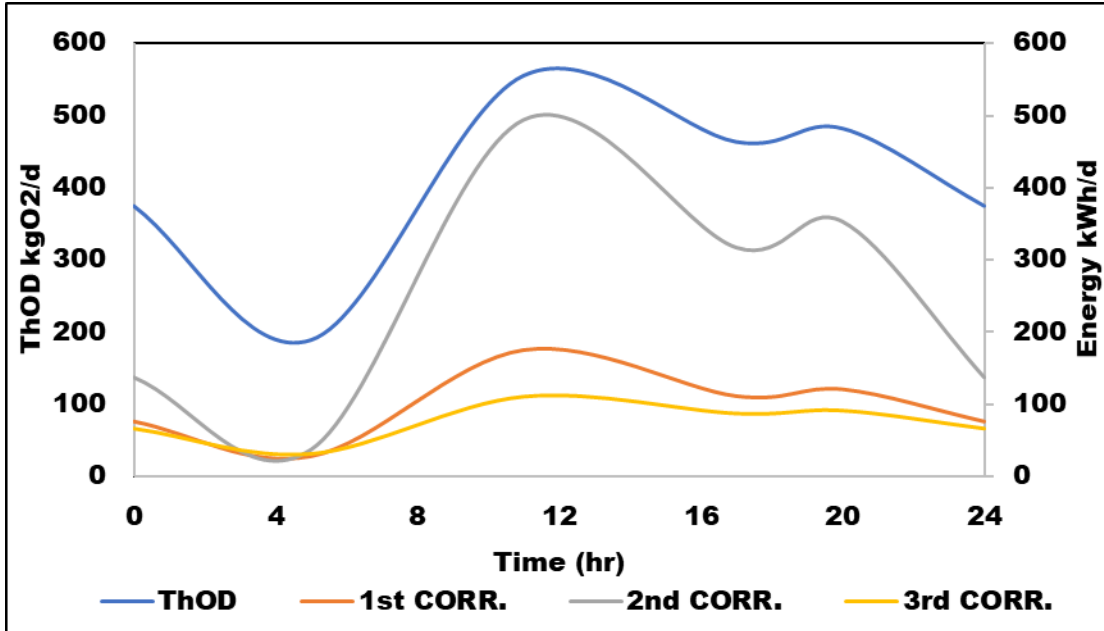


Figure SI-18: The change in aeration energy over a day due to the change in the influent concentrations using the three correlations (plug flow-nitrification and denitrification)

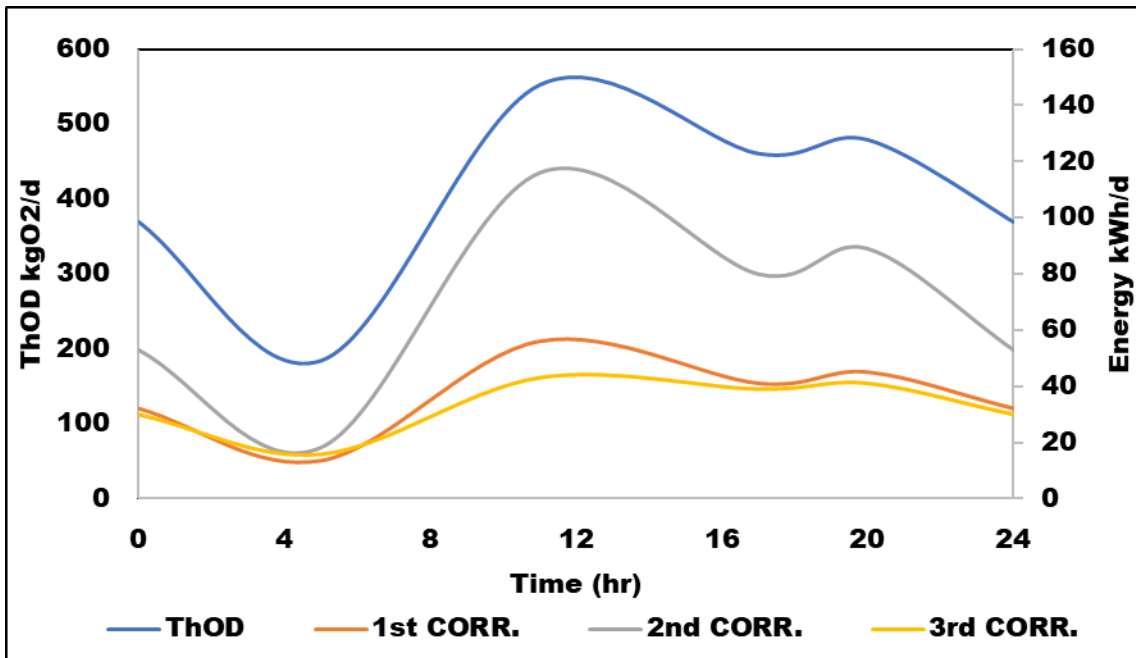


Figure SI-19: The change in aeration energy over a day due to the change in the influent concentrations using the three correlations (CSTR-nitrification and denitrification)

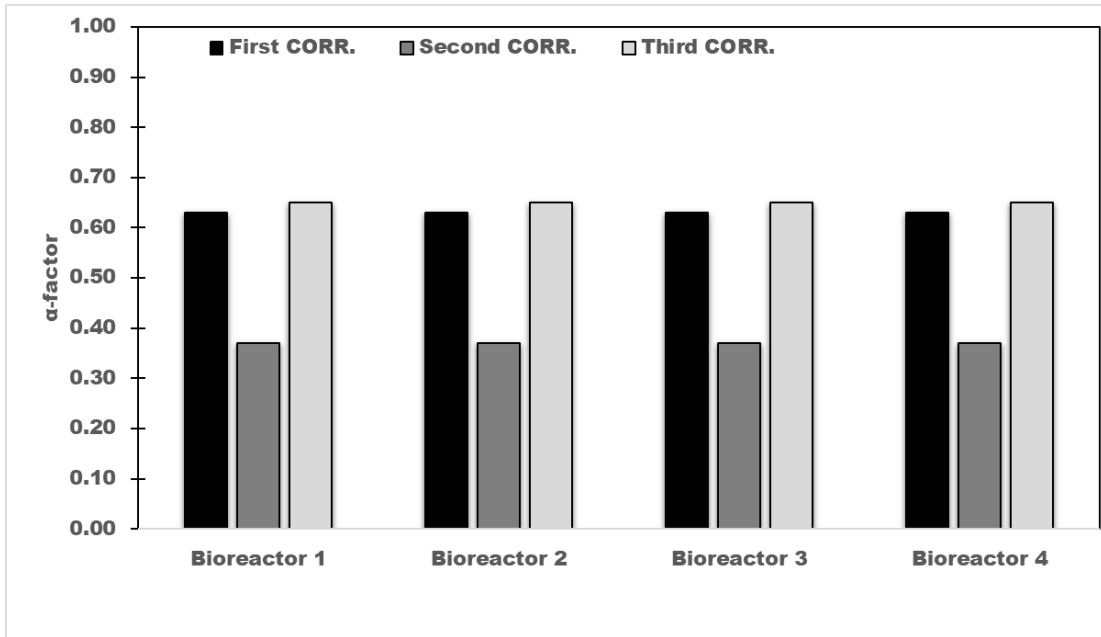


Figure SI-20: α -factor estimated in the four plug flow bioreactors using the three correlations.

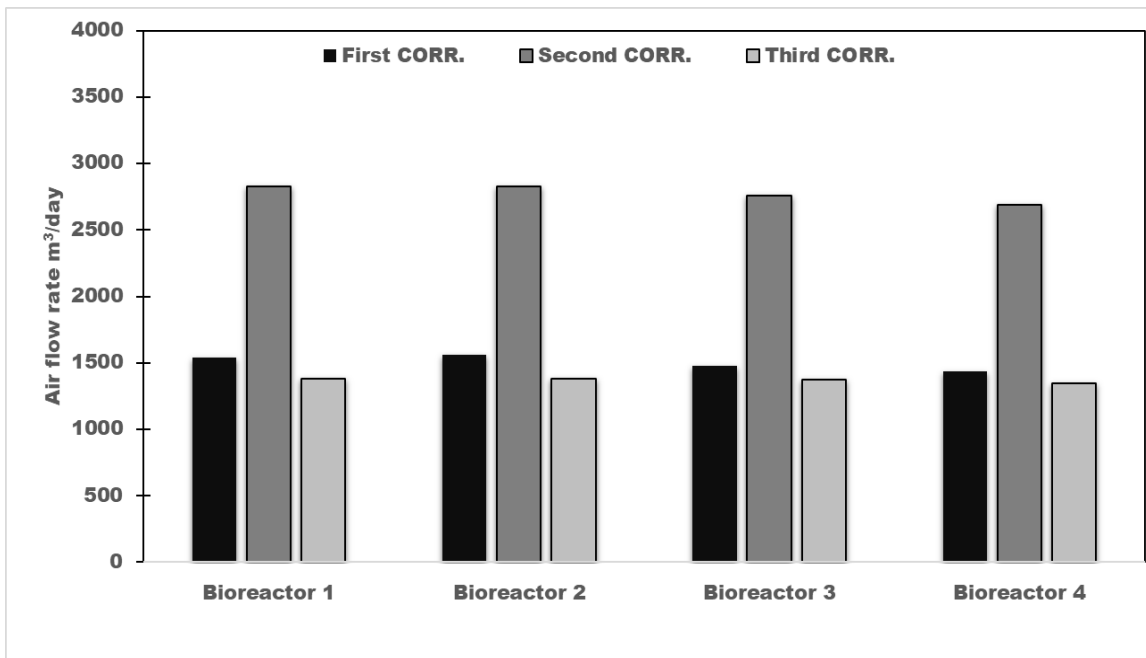


Figure SI-21. Estimated air flow rates in the four plug flow bioreactors using the three correlations.

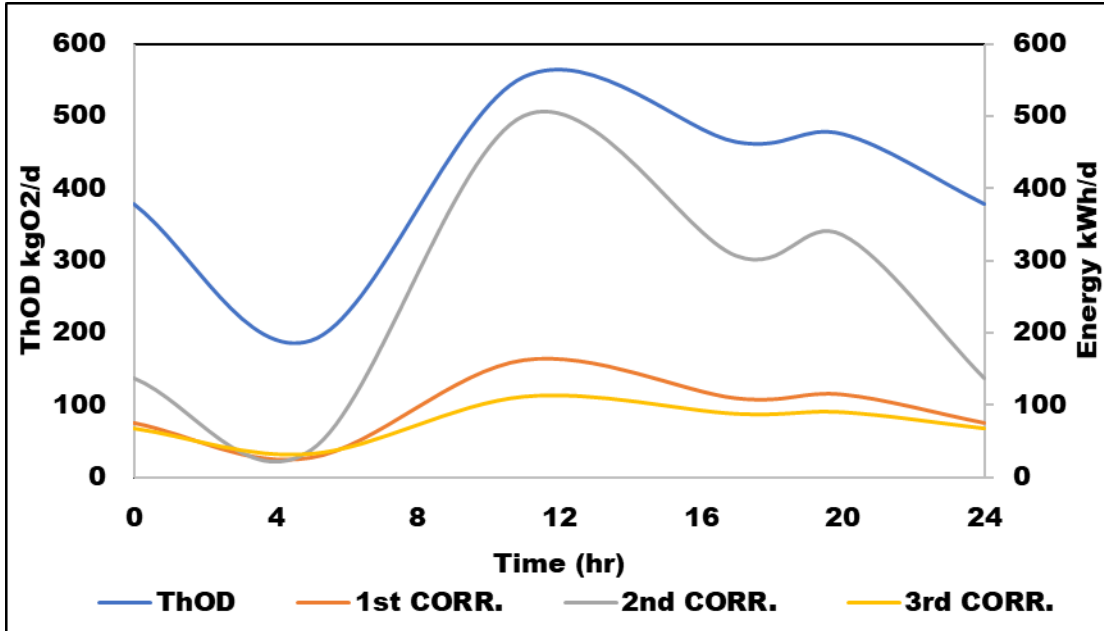


Figure SI-22: The change in aeration energy over a day due to the change in the influent concentrations using the three correlations (step feed-nitrification and denitrification)

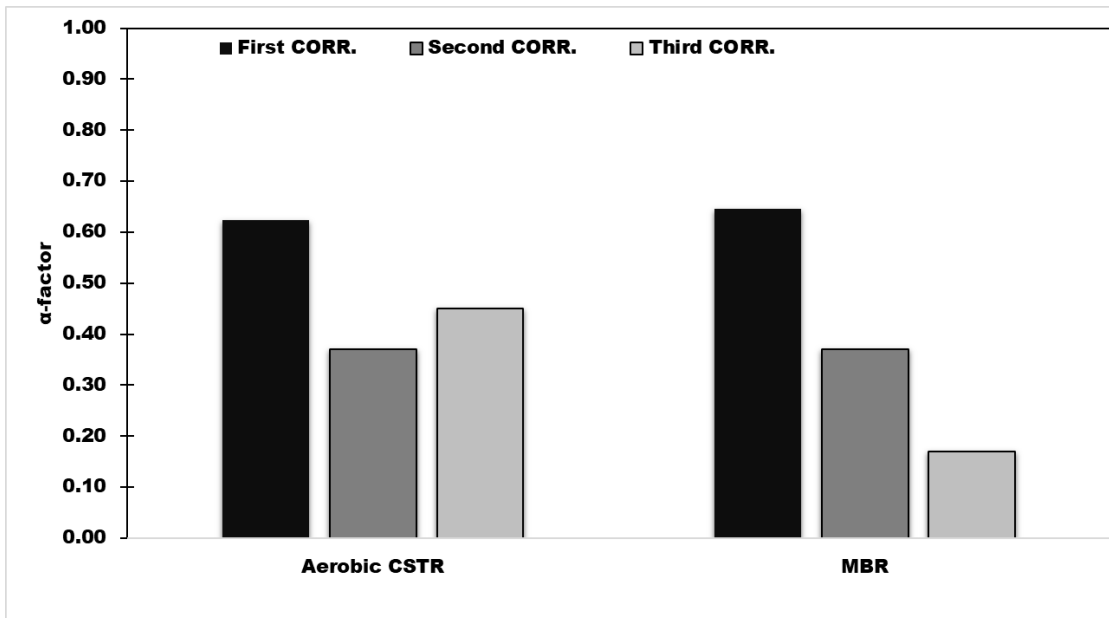


Figure SI-23: α -factor estimated in each compartment using the three correlations (MBR-Nitrification and denitrification).

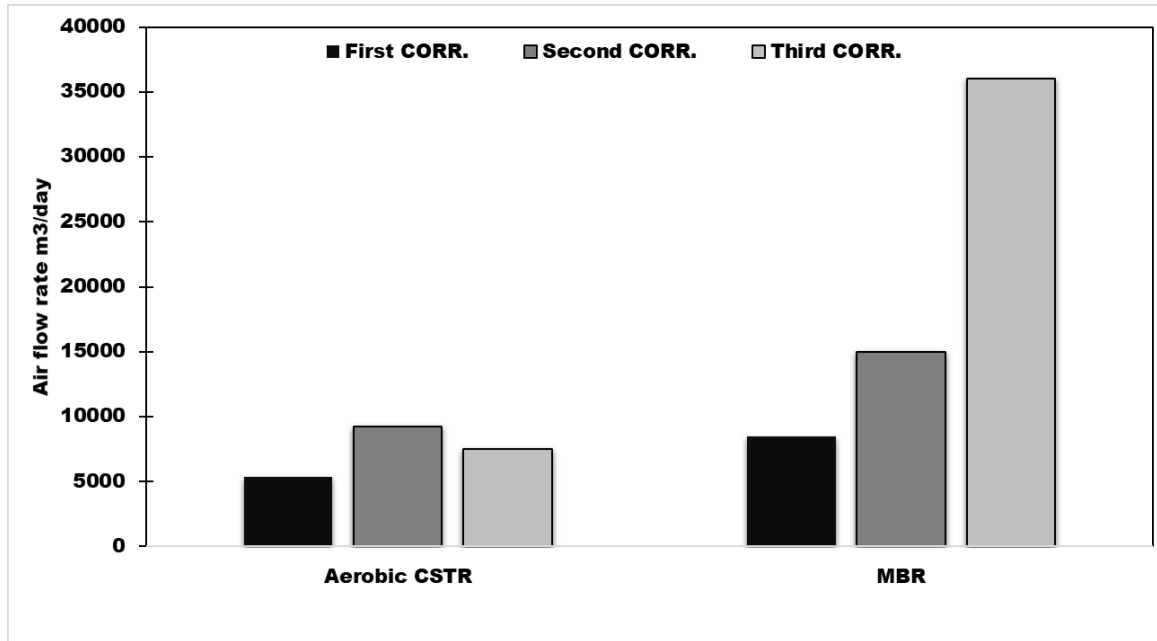


Figure SI-24: Air flow rates estimated in each compartment using the three correlations (MBR- Nitrification and denitrification)

Curriculum Vitae

Name: Ahmed Shawki Ahmed

Post-secondary Education and Degrees: The University of Western Ontario
London, ON, Canada
2017-2020 **Ph.D. in Civil and Environmental Engineering**

Cairo University
Cairo, Egypt
2011-2013 **M.A.Sc. in Environmental Engineering**

Fayoum University
Fayoum, Egypt
2006-2010 **Bachelor's degree in Civil Engineering**

Honours and Awards: Western Graduate Research Scholarship
2017-2020

MITACS Internship Grant - ACCELERATE
May 2020- October 2020

IWaTec scholarship from DAAD (German Academic Exchange Service)
October 2012- March 2013

Related Work Experience Teaching Assistant
The University of Western Ontario
2017-2020

Research Assistant
Housing and building national research center (HBRC), Egypt
March 2013- June 2014

Research Assistant
University of Duisburg-Essen, Germany
October 2012- February 2013

Teaching assistant
El Shrouk academy, Faculty of Civil Engineering, Egypt
March 2011–September 2012

Conferences (technical presentations)

1. **Ahmed, A. S.**, Santoro, D., Rosso, D., Nakhla, G., (2018). Impact of Cellulose, Organic Loading, And Operational Conditions on Oxygen Transfer Efficiency In Sequencing Batch Reactors (Sbrs). WEFTEC 2020, New Orleans, Louisiana USA
2. **Ahmed, A. S.**, Bahreini, G., Ho, D., Marcelis, P., Wessels, C., Loosdrecht, M. C., Elbeshbishy, E., et al. (2018). Mapping cellulose content and degradability in water resource recovery facilities: European and North American case studies. WEFTEC 2018, New Orleans, Louisiana USA.
3. **Ahmed, A. S.**, Pasini, F., Ho, D., Jansen, R., McKee, J., Santoro, D., Nakhla, G., et al. (2018). Impact of primary filtration on the aeration energy of wastewater treatment lagoons. ecoSTP 2018, London, Ontario, Canada.
4. Bahreini, G., **Ahmed, A. S.**, Ho, D., Marcelis, P., Wessels, C., Loosdrecht, M. C., Elbeshbishy, E., et al. (2018). Cellulose biodegradability in municipal wastewater treatment plants: European and North American case studies. ecoSTP 2018, London, Ontario, Canada.
5. Behera, C., Gupta, M., Ho, D., Daynouri-Pancino, F., **Ahmed, A. S.**, Gernaey, K. V., Santoro, D., et al. (2018). Modeling Plant-wide Effects Of Chemically enhanced Rotating Belt Filtration For Simultaneous Energy Optimization And GHGs Minimization. ecoSTP 2018, London, Ontario, Canada.
6. Giaccherini, F., **Ahmed, A. S.**, Ho, D., Pasini, F., Wessels, C., Marcelis, P., Nakhla, G., et al. (2018). Role of Primary Filtration in Plant-wide Energy Recovery. ecoSTP 2018, London, Ontario, Canada.
7. Pasini, F., **Ahmed, A. S.**, Ho, D., Nakhla, G., Giaccherini, F., Wessels, C., Marcelis, P., et al. (2018). Analysis of Activated Sludge Aeration Systems Following Primary Filtration with Microsieves. WEFTEC 2018, New Orleans, Louisiana USA.
8. **Ahmed, A. S.**, Niemann, A., & Shendi, M. (2013). Modeling the effects of different management strategies of drainage water effluent for improving the water quality of Lake Qarun. Poster SusWaTec, Cairo University, Cairo, Egypt. <http://www.suswatec.de/>

Journal technical papers

1. **Ahmed, A.S.**, Khalil, A., Ito, Y., van Loosdrecht, M.C.M., Santoro, D., Rosso, D., Nakhla, G., 2020. Dynamic Impact of Cellulose and Readily Biodegradable Substrate on Oxygen Transfer Efficiency in Sequencing Batch Reactors. Water Research 116724. <https://doi.org/10.1016/j.watres.2020.116724>
2. **Ahmed, A.S.**, Bahreini, G., Ho, D., Sridhar, G., Gupta, M., Wessels, C., Marcelis, P., Elbeshbishy, E., Rosso, D., Santoro, D., Nakhla, G., 2019. Fate of cellulose in primary and secondary treatment at municipal water resource recovery facilities. Water Environment Research 91, 1479–1489. <https://doi.org/10.1002/wer.1145>

3. Pasini, F.; Garrido_Baserba, M.; **Ahmed, A.**; Nakhla, G.; Santoro, D.; Rosso, D., 2020. Oxygen transfer and wide-plant energy assessment of primary screening in WRRFs. Water Environment Research. <https://doi.org/10.1002/wer.1349>